

**Biochemical characterization of the ChaC
family of γ -glutamyl cyclotransferases
from *Leishmania major***

Thesis submitted to Jadavpur University for the degree of
Doctor of Philosophy (Science), 2022

By

Sumit Das

CSIR-Indian Institute of Chemical Biology

4, Raja S.C. Mullick Road, Jadavpur

Kolkata-700032, India

IICB

आइ. आइ. सी. बी.



भारतीय रासायनिक जीवविज्ञान संस्थान
INDIAN INSTITUTE OF CHEMICAL BIOLOGY

(सी. एस. आइ. आर. का एक अंग)

(A Unit of C.S.I.R.)

4, राजा एस. सी. मल्लिक रोड, यादवपुर, कोलकाता -700 032

4, RAJA S.C. MULLICK ROAD, JADAVPUR, KOLKATA -700 032, INDIA

तार/ TELEGRAM : LIVINGCELL

दूरभाष : कार्यालय
PHONE : 2473 3491/0492
2473 3493/6793

फैक्स / FAX : 91 3324730284
91 3324735197

From:

Subrata Adak, Ph.D.

Chief Scientist

Structural Biology & Bio-informatics Division

e-mail : adaks@iicb.res.in

Dated: 17th Nov. 2022

Sub: Certificate from the supervisor(s)

This is to certify that the thesis entitled "Biochemical characterization of the ChaC family of γ -glutamyl cyclotransferases from *Leishmania major*" Submitted by Sri Sumit Das who got his name registered on 08.05.2017 for the award of Ph.D. (Science) degree of Jadavpur University, is absolutely based upon his own work under the supervision of Dr. Subrata Adak and that neither this thesis nor any part of it has been submitted for either any degree / diploma or any other academic award anywhere before..

(Signature of the Supervisor(s) date with official seal)

डॉ. सुब्रत अदक / Dr. Subrata Adak
मुख्य वैज्ञानिक / Chief Scientist
सीएसआईआर - भारतीय रासायनिक जीवविज्ञान संस्थान
(वैज्ञानिक तथा औद्योगिक अनुसंधान परिषद)
CSIR - Indian Institute of Chemical Biology
(Council of Scientific & Industrial Research)
४, राजा एस. सी. मल्लिक रोड / 4, Raja S. C. Mullick Road
कोलकाता-७०००३२ / Kolkata - 700032

*“Dedicated to my Parents, my
Teachers and all well-wishers....”*

Acknowledgements

Every achievement calls for the participation of numerous people and this work is not an exception. Today when I prepare my belongings and move out into the world, I genuinely feel as though I am leaving my second home- CSIR-IICB. Everything of this institute like its walls, its ground, peoples and canteen feels to my own and now feels like I am leaving my own protective shelter. I am thankful to all the teachers and mentors who have encouraged, helped and steered me in the right direction when I was overwhelmed. Therefore, I would like to express my appreciation to a number of peoples who provided numerous contributions till the end of my long journey.

First and foremost, I would like to take this opportunity to convey my sincere gratitude to **Dr. Subrata Adak**, my PhD research advisor and mentor, for his unending support and guidance throughout the years. I also want to thank him for showing me the value of patience, focus, hard work and accurate data interpretations in completing a research project. Along with being a great researcher, his straightforwardness, honesty, helpfulness, and commitment to his students' needs make him a perfect research mentor. I will always be grateful for his efforts in guiding my future career and supporting me throughout the challenging period of my doctoral studies.

Next, I would like to thank **Dr. Arun Bandyopadhyay**, the present director of CSIR-IICB and **Dr. Samit Chattopadhyay**, the former director of CSIR-IICB for providing me with all of the facilities to complete my doctorate studies. I'd also like to thank University Grants Commission (UGC) for providing me with financial assistance during my PhD tenure.

At various stages of this research, some Institute faculty members have been incredibly generous with their assistance as those of **Dr. Uday Bandyopadhyay, Dr. Siddhartha Roy, Dr. Nakul C. Maiti, Dr. Saumen Dutta, Dr. Subhas C. Biswas, Dr. Hemanta K. Majumder, Dr. Nahid Ali, Dr. Suvendranath Bhattacharyya, Dr. Krisna Das Saha, Dr. Jayati Sengupta, Dr. Debabrata Biswas, Dr. Malini Sen, Dr. Sanjay Dutta, Dr. Partha Chakrabarti, Dr. Pijush Kanti Das, Dr. Arindam Talukdar, Dr. Ranjan Jana, Dr. Indu Bhusan Deb, Dr. Samit Adhya, Dr. P. Jaisankar, Dr. Sharmila Sengupta and Dr. Rupak Bhadra.**

The people in my own lab were no less than a member of my extended family. I am extremely grateful to my seniors **Subhankar da, Moumita di, Rajesh da, Sumit da, Rina di** and **Jayasree di**. They have consistently served as my source of motivation and inspiration. I am extremely thankful to **Aditi di, Ayan da, Saroj da** and **Priya di** for being the actual bench work guide for me. I want to give a special thanks to **Swati di** for my paper modification and other very helpful suggestions from her busy schedule in daily life. **Puja, Yuthika** and **Gaurab** are the best juniors one could expect, they are always being there for me to encourage and support me. Puja, my lab junior cum friend always keeps all the lab members in a positive frame of mind and helps me a lot in HPLC, protein purification works and keeps all my cell lines alive even at the crucial situation of 1st wave of COVID pandemics; Yuthika, a very good singer and researcher keeps us always in smiling face with her funny character and helps me in experiments; Gaurab, my junior since Kalyani

ACKNOWLEDGEMENT

University always give me positive suggestions and help me a lot in my animal work. I want to thank **Sushanta da** for his incredible indulgence in preparing media, autoclaving glass wares, and animal handling, and **Khudiram da** for being my hand on trainer in the animal research.

I am extremely grateful to **Sounak da, Tanmoy da, Debalina di** and **Ramdhan da** for their technical and instrumental assistance.

I made a lot of friends in CSIR-IICB. Besides having academic discussions, we played cricket, drama, watched movies and had long interactive sessions while having tea. **Milan da, Chinmoy da, Shiladitya da, Saikat, Debanjan, Anirban da, Dushyant da, Sambit da, Sinjini, Somnath da, Shubhra da, Anand da, Sumanta da, Kamran da, Debojyoti, Dheeren da, Dipayan da, Koushik da, Snehashis da, Ritesh, Tridib da, Jeet da, Achyut, Chandrasova, Ishani, Priyanka, Shreyasi, Kajal, Sujoy, Rajeev da, Gourav da, Nanda** are few of the valuable friends.

It has been humbling to acknowledge the friends who have supported me during my PhD path and help me a lot in every situation. **Subhashis da, Vivek** and **Atanu** are those special friends.

I would also like to mention some names without them, my PhD journey was impossible. **Dr. Avinaba Mukherjee**, Assistant Professor in Zoology and **Subhradip Dey**, Assistant Professor in Botany are the unsung heroes towards my clearing NET or GATE like national examination for their guidance to concept clearance in this field. I am also wanting to thanks to Dr. Avinaba Mukherjee and **Dr. Sanchita Dutta** for guiding me to choose this lab.

I would also give a thanks to all the vendors especially **Patel da** and **Pradip da** for supplying the chemicals on before time even at the time of COVID pandemics, without them the research would be delayed.

I owe a debt of appreciation to my parents, **Bikash Chandra Das** and **Pali Das** for their love, care, prayers and huge sacrifices in educating me to this long journey. They have given me unwavering love and support, which keeps me steadfast and confident. I am grateful for them. I would like to thank **Rimita** for being with me from the beginning of my PhD career in every situation and helps me to achieve this success.

Last but not least, I want to express my heartfelt prayers and gratitude to **God**, the Almighty, for providing me the light, bravery, inspiration, positive thinking and good health.

Sumit Das

PREFACE

A sort of symbiotic interaction in which one organism or parasite is benefited at the expense of the other organism or host, is known as parasitism. Although the size of a parasite is much smaller than its host, they exhibit a high level of specialization for its way of existence and multiply more quickly than its host. Thus to circumvent the host defense mechanism, parasites evolve a biologically complex physiology. This allows them to bypass host immune system and lead to the development of drug resistance, making parasite treatment more difficult. One of the main reasons of this field's slow development is the lack of comprehensive understanding of parasite biology as a whole and as a result, the lack of therapeutic selectivity.

A protozoan parasite from the genus *Leishmania* causes the disease known as leishmaniasis, which is spread by the bite of specific sandfly species. There are three types of leishmaniasis: cutaneous, visceral and mucocutaneous. The parasite replicates and infects mammalian macrophages for effective colonization. It must withstand microbiocidal responses like oxidative burst for successful establishment within macrophages. Moreover, *Leishmania* lack enzymes like catalase and selenium containing glutathione peroxidase for rapid metabolism of reactive oxygen species. In addition, this parasite lacks genes like GSH reductase (GR) as well as thioredoxin reductase (TrxR), which are responsible for maintaining the intracellular thiol redox homeostasis in most eukaryotic organisms through the GSH/GR and thioredoxin/TrxR systems. However, a unique ROS metabolism system is present in the trypanosomatids: trypanothione/trypanothione reductase system. This trypanothione [T(SH)₂] is a GSH-spermidine conjugate; two molecules of GSH are required for its biosynthesis. Therefore, a change in GSH level can have an immediate impact on T(SH)₂ levels. Like host, GSH biosynthesis pathway is well-studied in trypanosomatids, but GSH degradation pathway is still obscure in the parasites.

Here, we found two ChaC proteins (LmChaC_{2a} and LmChaC_{2b}) in unicellular protozoan parasite *Leishmania*, which specifically degrade reduced glutathione (GSH), but no other γ -glutamyl peptides, trypanothione or oxidized glutathione. Subsequently, it inhibits the generation of intracellular T(SH)₂, which is a main player for ROS detoxification system in trypanosomatids. By using various LmChaC2 variants, in vitro and in vivo data suggest that the ChaC2 dependent GSH homeostasis is required for long-term survival in the aged culture as well as in chronic infection. Here we have discussed our research in three chapters: **Chapter 1** illustrates mainly the cloning, expression, purification and enzyme kinetics of LmChaC2 proteins from *Leishmania major*. **Chapter 2** unravels the intracellular expression and physiological significance of LmChaC2 proteins in *Leishmania major*. **Chapter 3** deals with the role of LmChaC2 proteins in GSH homeostasis and disease progression

ABBREVIATIONS

AIDS	Acquired immune deficiency syndrome
AP	Alkaline phosphatase
APX	Ascorbate peroxidase
ATP	Adenosine triphosphate
BSA	Bovine serum albumin
cDNA	Complementary DNA
CL	Cutaneous leishmaniasis
CM	LmChaC _{2a} & LmChaC _{2b} complement cells
CM _{2a}	LmChaC _{2a} complement cells
CM _{2b}	LmChaC _{2b} complement cells
CRISPR	Clustered Regularly Interspaced Short Palindromic Repeats
CT	Control cell (Genetically modified T7/Cas9 positive <i>L. major</i>)
DNA	Deoxyribonucleic acid
DEPC	Diethyl pyrocarbonate
dNTP	Deoxynucleotide triphosphate
EDTA	Ethylenediamine tetraacetic acid
ER	Endoplasmic reticulum
EtBr	Ethidium Bromide
FBS	Fetal bovine serum
GCL	Glutamate-cysteine ligase
GGT	γ -glutamyl transferase or γ -glutamyl transpeptidase
GIPL	Glycoinositol-phospholipid
GPX	Glutathione peroxidases
GSH	Glutathione
GSSG	Oxidized glutathione
GR	Glutathione reductase
HEPES	4-(2-hydroxyethyl)-1-piperazineethanesulfonic acid
HIV	Human immunodeficiency virus
HPLC	High Performance Liquid Chromatography
hr	Hour
HRP	Horseradish peroxidase
IPTG	Isopropyl β -D-1-thiogalactopyranoside
Kb	Kilo base
kDa	Kilo Dalton
KO	Knock out
Lm	<i>Leishmania major</i>
LPG	Lipophosphoglycan
M	Molar
MCL	Mucocutaneous leishmaniasis
mg	Milligram

ABBREVIATIONS

ml	Milliliter
mM	Millimolar
mRNA	Messenger ribonucleic acid
NaCl	Sodium chloride
NADH	Nicotinamide adenine dinucleotide
OD	Optical density
OE	Overexpressed cells
OE _{2a}	LmChaC _{2a} overexpressed
OE _{2b}	LmChaC _{2b} overexpressed cells
ORF	Open reading frame
PAGE	Polyacrylamide gel electrophoresis
PBS	Phosphate buffer saline
PCR	Polymerase chain reaction
PI	Propidium Iodide
PKDL	Post Kala-azar Dermal Leishmaniasis
PNA	Peanut agglutinin
PMSF	Phenylmethylsulfonyl fluoride
PRX	Peroxiredoxin
PVDF	Polyvinylidene fluoride
RNA	Ribonucleic acid
RNaseA	Ribonuclease A
ROS	Reactive oxygen species
RT-PCR	Reverse transcriptase-polymerase chain reaction
qRT-PCR	Quantitative real time-polymerase chain reaction
SDS	Sodium dodecyl sulphate
SOD	Superoxide dismutase
TAE	Tris-acetate-EDTA
TEMED	Tetramethylethylenediamine
TS ₂	Trypanothione disulphide
T(SH) ₂	Dihydrotrypanothione
TR	Trypanothione reductase
TXN	Tryparedoxin
UV	Ultra Violet
μl	Microliter
μM	Micromolar
VL	Visceral leishmaniasis
WHO	World Health Organization

CONTENTS

1. INTRODUCTION	2
1.1. Parasitism and vector borne diseases	2
1.2. Introduction of kinetoplastida	2
1.3. Introduction of <i>Leishmania</i> and leishmaniasis	4
1.3.1. Taxonomic position of <i>Leishmania</i>	4
1.3.2. Origin of <i>Leishmania</i>	5
1.3.3. Types of Leishmaniasis	5
1.3.4. Morphological feature of <i>Leishmania</i> species	7
1.3.5. Transmission	7
1.3.6. Life cycle of <i>Leishmania</i>	7
1.3.7. Pathogenicity	10
1.3.8. Treatment of leishmaniasis	11
1.4. Redox homeostasis in Trypanosomatids	12
1.5. Overview of glutathione	15
1.5.1. γ -glutamyl cycle	16
1.5.2. Enzymes involve in glutathione degradation pathways	17
1.5.3. Other enzymes involved in γ -glutamyl cycle	21
1.5.4. Newly proposed ‘Glutathione cycle’ instead of γ -glutamyl cycle	22
1.6. Glutathione degradation in <i>Leishmania</i>	23
1.7. Objectives of this present work	24
2. MATERIALS & METHODS	26
2.1. Materials	26
2.1.1. Reagents	26
2.1.2. Strains	26
2.1.3. <i>Leishmania</i> culture media	26
2.1.4. Bacterial culture media	27
2.1.5. Buffers and solutions	27
2.1.6. Cloning vectors used	29
2.1.7. Oligonucleotides used	29
2.2. Methods	30
2.2.1. Methods for cloning of LmChaC _{2a} and LmChaC _{2b}	30
2.2.1.1. Genomic DNA isolation from <i>Leishmania major</i>	30

2.2.1.2.	Polymerase Chain Reaction (PCR)	31
2.2.1.3.	Agarose gel electrophoresis	31
2.2.1.4.	Cloning of LmChaC _{2a} and LmChaC _{2b} genomic DNA	31
2.2.1.5.	Plasmid DNA isolation by using miniprep kit	31
2.2.1.6.	Restriction digestion of amplified ORF and cloning vector	32
2.2.1.7.	Recover the DNA by gel extraction kit	32
2.2.1.8.	Ligation of vector and insert DNA	32
2.2.1.9.	Transformation	33
2.2.2.	Methods for expression and purification of LmChaC _{2a} and LmChaC _{2b}	33
2.2.2.1.	Expression and purification	33
2.2.2.2.	SDS-Polyacrylamide gel electrophoresis (SDS-PAGE)	33
2.2.2.3.	Staining by using Coomassie Brilliant Blue	34
2.2.3.	Biophysical characterization of LmChaC _{2a} and LmChaC _{2b}	34
2.2.3.1.	Protein concentration determination	34
2.2.3.2.	Activity measurement assay	34
2.2.3.3.	Production of polyclonal antibodies against LmChaC _{2a} and LmChaC _{2b}	34
2.2.3.4.	Western blotting analysis	34
2.2.3.5.	Total RNA isolation from the cell by TRIzol method	35
2.2.4.	Functional characterization of LmChaC _{2a} and LmChaC _{2b}	35
2.2.4.1.	<i>Leishmania major</i> culture	35
2.2.4.2.	Construction of different types of cell lines of <i>Leishmania major</i> promastigotes	35
2.2.4.3.	Determination of physiological role of LmChaC _{2a} and LmChaC _{2b}	37
2.2.5.	Statistical analysis	40

3. RESULTS

3.1.	Chapter 1: “Cloning, expression, purification and enzyme kinetics of LmChaC2 proteins from <i>Leishmania major</i> ”	43
3.2.	Chapter 2: “Intracellular expression and physiological significance of LmChaC2 proteins in <i>Leishmania major</i> ”	52

3.3. Chapter 3:	62
“Role of LmChaC2 proteins in GSH homeostasis and disease progression”	
4. CONCLUSION AND PERSPECTIVE	68
5. BIBLIOGRAPHY	71

“Dream is not what you see in sleep, Dream is something which doesn't let you sleep”

- A.P.J. Abdul Kalam

Introduction

INTRODUCTION

1.1. Parasitism and vector borne diseases

The definition of life has been given as a systemic process that catalyzes the transformation of entropy into information. Various strategies are used by organisms to accomplish this and complete their life cycles. Parasitism is one of these strategies where symbiotic relationship exists between parasite and their respective host. Where the parasite is physiologically and ecologically dependent on the host by means of nutrients and habitat (1). Most of the parasites can be transmitted to the host through vectors and mostly by insects like mosquito, sandfly, housefly, tsetse fly etc. Some parasites undergo an obligatory life stages inside



Fig.1: *Lutzomyia longipalpis* sandfly serves as *Leishmania* vector in New World. (Adapted from <https://doi.org/10.1371/image.ppat.v05.i08.g001>)

vector's body and transmit to the host body through blood exchange at the time of biting, whereas others merely employ the vector for inoculation and transportation. Worldwide, about 17% of infections are caused by vector-borne diseases (**Fig.1**). Increased immigration, random air travel and global climate change is the main cause of spreading of these diseases (2). Treatments of these diseases include usage of chemotherapeutic drugs, which are quite expensive with many side effects and vaccines also are not available till now. Consequently, these diseases can be life-threatening and become endemic if not appropriately managed (3). List of some vector borne disease caused by parasitic protozoa and their respective arthropod vector is given below (**Table-1**).

Table-1: Some vector borne diseases caused by protozoan parasite.

Diseases	Parasites	Vectors
African trypanosomiasis	<i>Trypanosoma brucei</i>	Tsetse fly (<i>Glossina sp.</i>)
Chagas disease	<i>Trypanosoma cruzi</i>	Kissing bugs (<i>Triatoma sp.</i> , <i>Rhodnius sp.</i>)
Leishmaniasis	<i>Leishmania sp.</i>	Sandflies (<i>Phlebotomus sp.</i> , <i>Lutzomyia sp.</i>)
Malaria	<i>Plasmodium sp.</i>	Mosquito (<i>Anopheles sp.</i>)
Babesiosis	<i>Babesia sp.</i>	Ticks (<i>Ixodes sp.</i>)

1.2. Introduction of kinetoplastida

Kinetoplastida are the unicellular, flagellated protozoa belong to the class Kinetoplastea, with the distinguishable characters of large amount of DNA containing kinetoplast in the large mitochondria. Bronislaw M. Honigberg first identified in 1963 that the kinetoplastid is belongs to the members of the flagellated protozoans. All of the kinetoplastids are thought to be parasites of the human blood/tissue that are transmitted by insect vectors and are classified

as a monophyletic group. A flexible, elongated body with one or two flagella represents one stage while a typically circular body without any flagellum represents other stage in the whole life cycle of all the members of this group (4). The majority of the organelles found in eukaryotic organisms are also present in kinetoplastids, but some of these organelles are particular and unique to this group such as single mitochondrion with kinetoplast (5). The DNA-rich kinetoplast is situated in the mitochondrion, close to the flagellum's basal body and previously believed to be involved in the movement of the body (**Fig.2**). However later discovery suggests that kinetoplast is not involved in the movement of kinetoplastid (6).

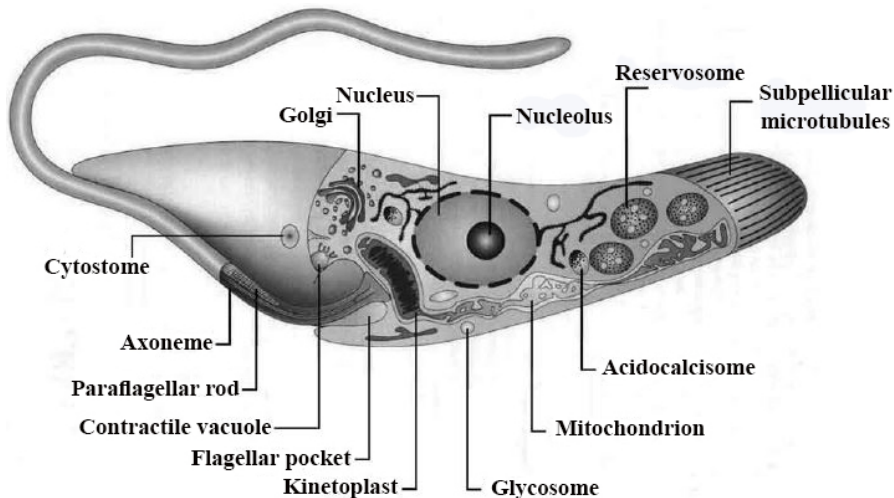


Fig.2: Schematic transmission electron microscopy (TEM) image after thin sectioning of *T. cruzi* epimastigote. (Adapted from Souza, Mem Inst Oswaldo Cruz, 2008 Jun; 103(4):313-25

Kinetoplast consists of two different types of circular DNA- numerous copies of minicircles and few copies of maxicircles, about 0.5-1 kbp and 20-40 kbp in size respectively (7). Minicircle DNA is involved in encoding small guide RNA or gRNA, which is required for specific

editing. On the other hand, maxicircles encodes ribosomal RNA or rRNA and several mitochondrial proteins (8) (**Fig.3**).

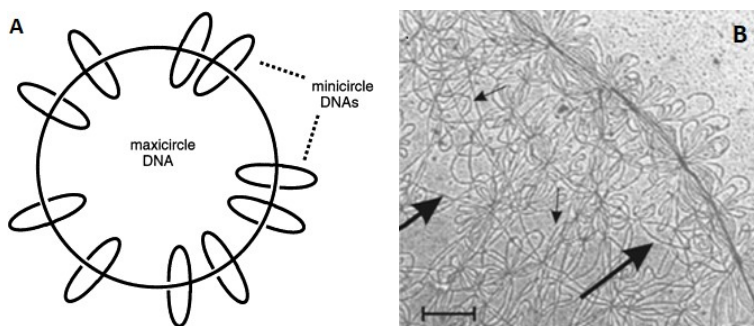


Fig.3: A) Schematic diagram and B) electron microscopy (EM) image of kinetoplastid DNA in minicircles and maxicircles. (Adapted from <https://www.sciencedirect.com/topics/pharmacology-toxicology>)

Some other remarkable features of kinetoplastid that differentiate them from higher eukaryotes are antigenic variation through gene rearrangements, polycistronic expression of proteins which are functionally unrelated, trans-splicing of nuclear RNA, glycosylphosphatidylinositol or GPI-anchored glycoproteins and glycolipids (9). The metabolic processes and regulation of these processes are quite different from other eukaryotic known concept. Most of the glycolytic enzymes are localized in glycosome, which is peroxisome-like organelle in trypanosomatids (10). Another striking features are the absence of catalase and glutathione reductase, although the presence of trypanothione (a glutathione-spermidine conjugate) and trypanothione reductase. Trypanothione plays a key role in antioxidant defense along with the glutathione in the parasites (11). De novo purine

synthesis pathways are also absent in the parasites (12). Because of their distinctiveness and uniqueness, kinetoplastid is supposed to be an attractive model for studying biochemistry, cell biology and molecular biology. An in-depth study of the kinetoplastids could offer new acumen not only for medical biology, but also in the other field of biological sciences.

1.3. Introduction of Leishmania and leishmaniasis

A group of diseases named leishmaniasis that affect human and diverse animal populations across tropics and subtropics are caused by obligatory intracellular protozoan parasite of the genus *Leishmania*. In the Old World, sandflies of the genus *Phlebotomus* and in the New World, genus *Lutzomyia* are responsible for spreading of this disease. When female sandflies feed on an infected mammalian host in quest of a blood meal, they acquire *Leishmania* parasites (13). According to WHO (World Health Organization), leishmaniasis is belongs to a serious tropical diseases that if not managed appropriately, could have very serious outcomes. Approximately 7 lakhs to 1 million new cases and 60,000 deaths are reported each year by more than 20 *Leishmania* species through more than 90 sandfly species. Leishmaniasis manifests a variety of symptoms from a localized skin ulcer to fatal infections. Leishmaniasis has an enormous historical impact because it was known thousands of years Before the Common Era (BCE). *Leishmania donovani* DNA was amplified successfully from ancient Egyptian and Christian Nubian mummies dating from 3500 to 2800 BCE. Furthermore, a skin disease known as the "Nile Pimple" that was considered to be cutaneous leishmaniasis was documented in the 1500 BC Ebers Papyrus medical manuscript (14). This group of diseases has been known by many different names such as Kala-azar, black fever, Dum-dum fever, white leprosy or espundia. However, the disease causing agent was discovered by independent research of William Boog Leishman in England and Charles Donovan in India, in 1900 and named it *Leishmania donovani* (15). Now a days, sharp increase in fatality rates in *Leishmania* and HIV coinfection because of developing immunosuppressive conditions (16).

1.3.1. Taxonomic position of Leishmania

According to Levine et al. 1980, taxonomic position of *Leishmania* is as follows:

Kingdom:	Protista
Subkingdom:	Protozoa
Phylum:	Sarcomastigophora
Class:	Zoomastigophora
Order:	Kinetoplastida
Sub order:	Trypanosomatina
Family:	Trypanosomatidae
Genus:	<i>Leishmania</i>

1.3.2. Origin of *Leishmania*

Fossil evidence: The first fossilized *Leishmania*-like organism was discovered in the alimentary canal and proboscis of a blood-filled female extinct sandfly, *Palaeomyia burmitis*. The second fossilized *Leishmania*-like creature, *Paleoleishmania neotropicum* was discovered 20-30 million years ago in the *Lutzomyia adiketis* (an extinct sandfly) (17,18). There were paramastigotes as well as promastigotes and amastigotes in the gut and proboscis of the sandfly but no evidence of vertebrate blood cells were found (19).

Geographical origin: Before the division of the supercontinent Pangaea, the genus *Leishmania* most likely evolved during the Mesozoic era. However, research on the precise geographic origin of different *Leishmania* species is currently on-going (20).

W.B. Leishman discovered *L. donovani* from the spleen sample of dum-dum fever affected soldier by using modified Romanowsky stain or Leishman's stain. A similar type of parasite was discovered about the same time by Charles Donovan at Madras University in a spleen of 'Kala-azar' patients. W.B. Leishman and C. Donovan initially named the parasite 'Leishman-Donovan bodies' and then Ronald Ross renamed it in 1903 as *Leishmania donovani*. In 1941, Adler and Ber first discovered the human transmission of *Leishmania major* by the bite of infected parasite containing *Phlebotomus papatasi*. Then in the year 1942, Swaminath, Anderson and Shortt demonstrated the Kala-azar transmission by *P. argentipes* (21).

1.3.3. Types of Leishmaniasis

On the basis of clinical symptoms, leishmaniasis may be divided into 1) Kala-azar or visceral leishmaniasis (VL); 2) Cutaneous leishmaniasis (CL); 3) Mucocutaneous leishmaniasis (MCL); 4) Post Kala-azar Dermal Leishmaniasis (PKDL) (**Fig.4**).



Fig.4: Leishmaniasis types: A) Visceral leishmaniasis (VL), B) Cutaneous leishmaniasis (CL), C) Mucocutaneous leishmaniasis (MCL), D) Post Kala-azar Dermal Leishmaniasis (PKDL). (Adapted from <https://www.jstor.org/stable/4459156>; Swain et al, Alexandria Journal of Medicine, 2019;52:343-346; Ekiz et al, Indian J Dermatol Venereol Leprol, 2017 Jan-Feb; 83(1):91-93; Zijlstra et al, The Lancet Infectious Diseases, 2003; 3(2): 87-98)

1. Visceral leishmaniasis (VL)

Kala-azar or visceral leishmaniasis is a most severe type of leishmaniasis in terms of death and outbreaks. The symptoms of kala-azar are irregular fever attacks, spleen and liver enlargement, loss of weight and anemia. If remains untreated, it can affect different organ and finally death. It predominates mostly throughout a huge portion of Asia (India, Bangladesh and Nepal), Africa, South America and southern Europe. In South America, it

is caused by *L. tropica*, *L. chagasi* and *L. amazonensis*; in eastern Africa and India by *L. donovani*; in Europe by *L. infantum* (22,23). Malnourished or immunocompromised person and children are at higher risk to get infected. More than 90% of fresh cases were reported to WHO in 2020 across 10 countries: China, India, Brazil, Kenya, Somalia, South Sudan, Yemen, Sudan, Eritrea and Ethiopia (**Fig.5**).

2. *Cutaneous leishmaniasis (CL)*

Cutaneous leishmaniasis is most common form of leishmaniasis across the globe, mainly in Pakistan, Brazil, Afghanistan, Syria, Peru and Saudi Arabia. CL can be caused by several types of *Leishmania* species, such as *L. infantum*, *L. amazonensis*, *L. major*, *L. tropica*, *L. panamensis* and *L. peruviana* (24). It primarily causes small erythema at the site of sandfly bite and finally develops ulcer on the body surface and permanent scar. According to WHO, more than 85% of new cases were reported in 2020 around 10 countries: Algeria, Pakistan, Iraq, Brazil, Tunisia, Afghanistan, Colombia, Syria, Saudi Arabia and Peru. Around 6-10 lakhs new cases are reported every year (25) (**Fig.5**).

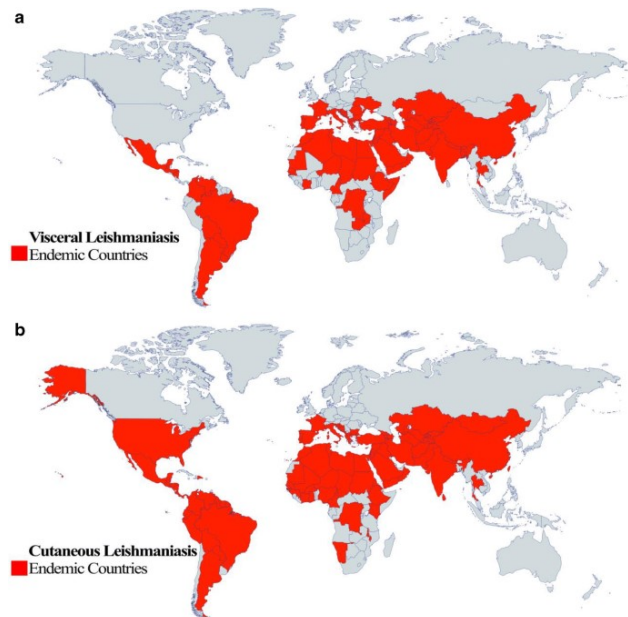


Fig.5: Epidemiology of Leishmaniasis. Red color indicates endemic countries. China, India, Brazil, Kenya, Somalia, South Sudan, Yemen, Sudan, Eritrea and Ethiopia are the endemic countries for visceral leishmaniasis. Algeria, Pakistan, Iraq, Brazil, Tunisia, Afghanistan, Colombia, Syria, Saudi Arabia and Peru are the endemic countries for cutaneous leishmaniasis. (Adapted from Sasidharan and Saudagar, Parasitol Res. 2021 May;120(5):1541-1554)

3. *Mucocutaneous leishmaniasis (MCL)*

Mucocutaneous leishmaniasis occurs often after cutaneous leishmaniasis appears to be cured (26). It is characterized by the partial or complete obliteration of mucous membrane of nose, throat and mouth. Major causative agent of this type of leishmaniasis is *L. braziliensis*, although *L. amazonensis*, *L. panamensis* and *L. guyanensis* can also cause mucocutaneous leishmaniasis (26). More than 90% of cases are reported from Brazil, Bolivia, Ethiopia and Peru (27).

4. *Post Kala-azar Dermal Leishmaniasis (PKDL)*

Around 10-20% of recovered kala-azar patient is affected with Post Kala-azar Dermal Leishmaniasis. This type complication is characterized by the formation of papulonodular or macular lesions on facial portion (28). As the parasite resides in these lesions, sandfly can easily transmit the parasite in the population. Hence, people with PKDL are thought to be an efficient source of VL infection. It mostly occurs in East Africa and Indian

subcontinent (29). Different types of leishmaniasis and its causative agents are tabulated below (**Table 2**).

Table-2: Leishmaniasis types and causative agents.

Types	Pathogen
Visceral leishmaniasis	<i>L. donovani</i> , <i>L. chagasi</i> , <i>L. infantum</i>
Cutaneous leishmaniasis	<i>L. major</i> , <i>L. tropica</i> , <i>L. aethiops</i> in Old World, <i>L. mexicana</i> in New World
Mucocutaneous leishmaniasis	<i>L. braziliensis</i>

1.3.4. Morphological feature of *Leishmania* species

Two different types of morphological form are observed in digenetic parasite *Leishmania*, 1. Extracellular flagellated promastigote forms reside in the alimentary canal of sandfly vector and 2. Non-flagellated amastigote forms in the phagolysosomal compartment of macrophage within host body (30,31). The shape of the amastigotes are typically rounded and 2-3 μm in diameter with clear nucleus and kinetoplast, whereas promastigotes are elongated and spindle shaped with around 10-20 μm in length and 1.5-3.5 μm in wide (**Fig. 6**). Surface antigens, intracellular polyamines and coat proteins are quite different in these two morphological forms (32-34).

1.3.5. Transmission

Because an animal reservoir is necessary for endemic transmission of leishmaniasis, these diseases are considered to be a zoonotic disease. Leishmaniasis is generally transmitted at the time of biting of infected female hematophagous sandflies belong to *Lutzomyia* genus (New World) and *Phlebotomus* genus (Old World) (35). Other possible and less significant ways of transmission are blood transfusion, reuse of infected needles and organ transplantation (36,37). Exchange of the infected needles is the main cause of *Leishmania*/HIV co-infection (38).

1.3.6. Life cycle of *Leishmania*

Leishmania is a digenetic parasite or life cycle of *Leishmania* has completed in two hosts: invertebrate and vertebrate host with two development stages: extracellular promastigotes and intracellular amastigotes respectively. Canids, rodents, marsupials and edentates can also act as a reservoir host along with the human (39) (**Fig. 7**).

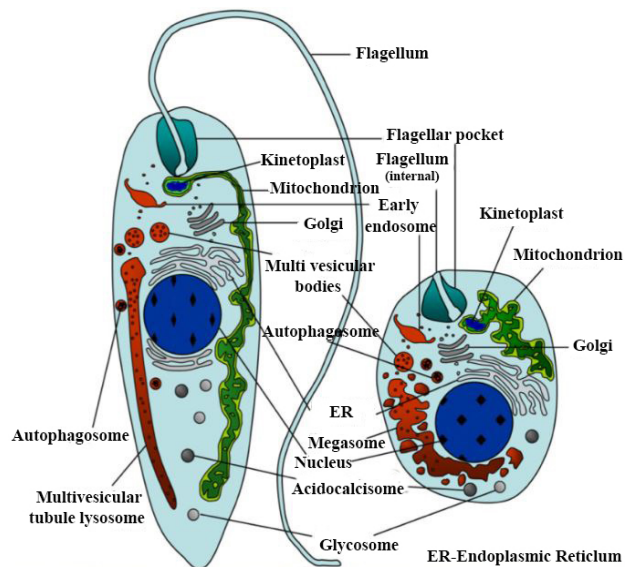


Fig.6: Schematic diagram depicts the morphological features of amastigote (right) and promastigote (left) of *Leishmania*. Different subcellular organelles are pointed in the diagram, flagellated promastigote forms are typically elongated, whereas non-flagellated amastigote forms are round in shape. (Adapted from Mansuri et al, Curr Drug Targets. 2020; 21(11):1105-1129)

Life stage in invertebrate host

After blood intake, *Leishmania* parasite multiplies within midgut of female sandfly to form procyclic promastigotes. Then it migrates into pharyngeal and buccal cavity of the flies to become infective metacyclic promastigote cell. Generally, blood meal is necessary for sandflies for the development of eggs.

Extracellular promastigote parasites are characterized by elongated, spindle shaped body and a long flagellum helps in movement of the parasites. At the time of insect biting, flagellated promastigotes is introduced into the dermal layer of

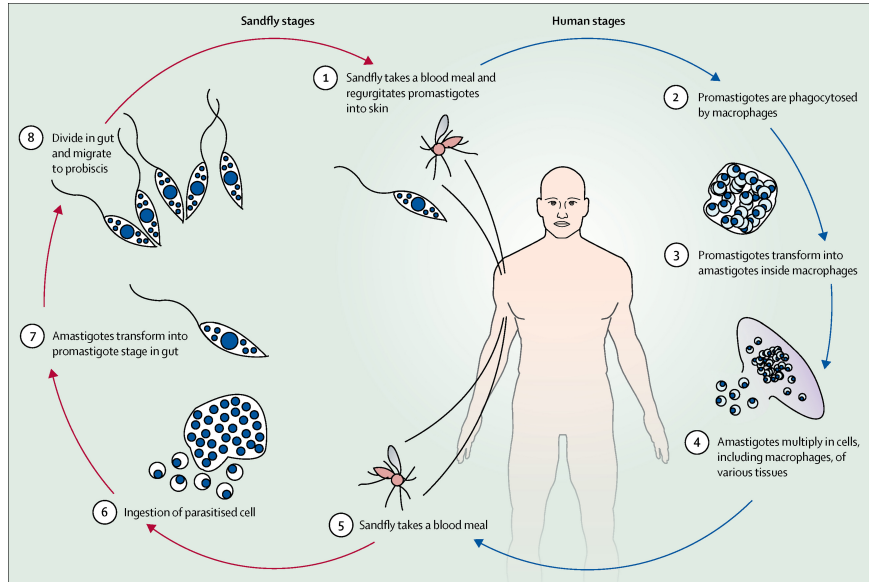


Fig.7: Life cycle of the parasite *Leishmania*. (1) During biting to the host, *Leishmania* parasites are introduced into the skin by the infected sandflies, (2) *Leishmania* then invade or phagocytosed by the host antigen presenting cells, mainly macrophages, (3) Flagellated promastigote forms then transform into non-flagellated amastigote forms inside the phagolysosome of macrophages, (4) Amastigotes multiply in the macrophages and spread to other tissues to infect additional macrophages, (5) Sandflies takes it blood meal from infected host, (6) New sandflies getting infected with the amastigote parasites, (7) Amastigote forms then transform into the flagellated promastigote forms in the gut of sandflies, (8) This promastigote parasites multiplies in the gut and migrate to the proboscis of the sandflies from where parasites moves into the host after insect biting, thus completing the life cycle. (Adapted from US Centers for Disease Control and Prevention)

vertebrate host and from where by the process of endocytosis they are engulfed into the phagocytic cells like macrophages (40).

Life stage in vertebrate host

Phagocytized metacyclic promastigotes can easily survive in the adverse environmental condition within phagolysosome and transform into non-flagellated amastigotes. Surface lipophosphoglycan or LPG is a key virulence factor which inhibits the phagosome and lysosome fusion to offer the parasite a better chance of survival inside the phagosome (41). By binary fission, amastigote parasite rapidly multiplies to lyse the macrophages and release into the circulation. Then the amastigote form eventually invades the monocyte and the macrophages of liver, spleen, lymph nodes, bone marrow and other tissues. When a female sandfly bites the infected individual, amastigotes are taken up from the circulation during the blood meal. Flagellated promastigotes are formed from the amastigote through several intermediates forms within the midgut of sandfly in 72 hours. These flagellated forms migrate to the buccal and pharyngeal cavity within 6-9 days. Finally, these infected sandflies infect

new susceptible vertebrate individuals during the blood meal to spread the diseases and thus the life-cycle is completed (42).

1.3.6.1 Vector-parasite interaction: Development inside sandflies

Phlebotomine sandflies are responsible for the transmission of the *Leishmania* parasite. More than 500 phlebotomine species of 6 genera are known, although new world flies *Lutzomyia* and old world flies *Phlebotomus* are responsible for the human infection (43). These insects are very small (~1.5-2.0 mm in body length) and resides mainly in tropical and subtropical parts. Development of the parasite begins within vector's body, when female flies take up circular, immobile amastigote (~2-3 μm) containing macrophages during blood meal (30). The changes in the condition (Temperature and pH) from vertebrate host to sandflies vector triggers the physiological and morphological changes in the parasite and can develop inside the vector. At first, amastigotes are transformed into first replicative and poorly motile procyclic promastigotes forms bearing short flagellum. After 2-3 days, by reducing the replication rate, highly motile elongated nectomonad promastigotes are developed from the parasites (44). At the anterior midgut, they differentiated into shorter nectomonad forms or leptomonads and enter into next proliferative cycle. After completing several steps like detachment, anterior migration and colonization of stomodeal valve, parasite transforms into infective

metacyclic promastigote forms (13,45-48). Following next blood meal, these infective forms are delivered to the circulation of vertebrate host (Fig.8). Life-cycle of *Leishmania* is completed in ~6-9 days within sandflies vector depending upon the species. LPG dependent attachment of nectomonad promastigotes can be seen in some specific vectors like *P. duboscqi* and *P. papatasi*. Although in case of permissive vectors, attachment is LPG independent. Several times metacyclic forms were found in the saliva and urinary discharge of the flies at the time of blood feeding (49).

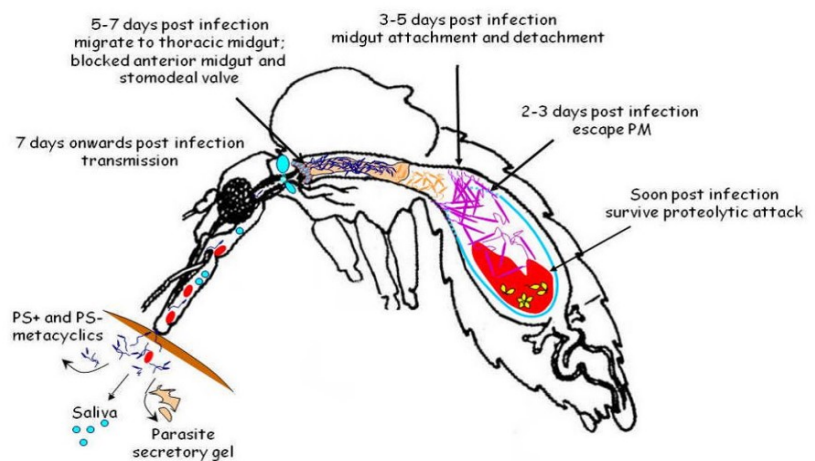


Fig.8: Leishmanial life cycle inside midgut of sandfly. Different types of barriers faced by *Leishmania* parasites during the developmental stages in sandflies. Digestive proteases mediated proteolytic attack that is produced right after a blood meal develops the initial barrier. Peritrophic matrix (PM) poses a second barrier from which *Leishmania* must escape and is thought to be achieved between 2- 3 days following infection. The third barrier is the necessary midgut attachment, which is needed to prevent the parasites from being excreted with the leftovers of the blood meal, which typically happen 3-5 days post infection (PI). In order to reach the thoracic midgut, parasites must eventually separate from the midgut. The "blocked" sand fly is produced by the secretion of parasite secretory gel (PSG) and the degradation of the stomodeal valve. Because blocked sand flies can't finish a full blood meal, they try to feed more frequently, which increases the risk of transmitting parasites. The sandfly contains metacyclic that either express phosphatidylserine (PS +) or do not express (PS-), which are injected into the mammalian host (Adapted from Ortigao et al, Open Parasitol J.2010 Jan 1; 4:195-204)

1.3.6.2 Leishmania-host interaction: Development within phagolysosome.

A very remarkable characteristic of *Leishmania* species is their capability to survive and divide inside the phagolysosomal compartment of the phagocytes. Phagocytosis of the parasites by the macrophages can occur directly or indirectly with the involvement of neutrophils (50). Promastigotes differentiated into amastigote forms inside the vacuole of the macrophages, where amastigotes further multiply by the binary fission and can evade dendritic cells and fibroblast cells. A thick coating layer of glycocalyx, which is made up of GPI-anchored proteins like phosphoglycan, glycoinositol-phospholipid (GIPL) and lipophosphoglycan (LPG) is present in the *Leishmania* promastigotes (51).

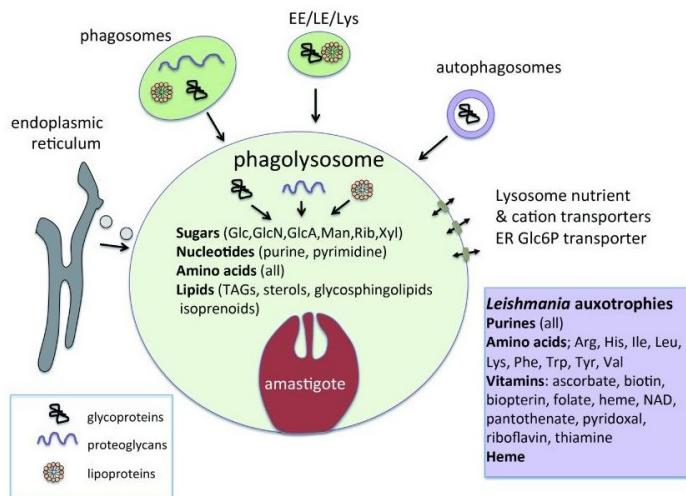


Fig.9: Multiplication of *Leishmania* inside the phagolysosome of the macrophage. Various endocytic pathways, lysosomal membrane transporters, autophagy and fusion with the ER are used to transfer various carbon sources (sugars, fatty acids and amino acids) and critical nutrients to the phagolysosome. Macromolecules supplied to this compartment are either hydrolyzed by the luminal hydrolases or absorbed by amastigotes and hydrolyzed within their own hydrolytically active lysosomes. EE, early endosome; Arg, arginine; Glc, glucose; Glc6P, glucose 6-phosphate; GlcN, glucosamine; His, histidine; GlcA, glucuronic acid; Ile, isoleucine; Leu, leucine; LE, late endosome; Lys, lysine; Man, mannose; Rib, ribose; TAG, triacylglycerol; Phe, phenylalanine; Trp, tryptophan; Xyl, xylose; Tyr, tyrosine; Val, valine. (Adapted from McConville et al, F1000Res. 2015 Oct 1; 4 (F1000 Faculty Rev):938)

lipophosphoglycan (LPG) is present in the *Leishmania* promastigotes (51). Through the mutation studies with mutant surface components, it is proved that LPG is the key component of macrophage infection and knockout of other component apparently has no impact on the pathogenicity (52,53). Macrophages are most recognizable types of cells that can be contaminated by a huge number of amastigotes that can infect single parasite containing vacuole or huge communal vacuole (*L. pifanoi*, *L. amazonensis* and *L. mexicana*) (54). The vacuole containing membrane and luminal marker enzymes (hydrolase and NADH oxidase) generate anti-microbial oxidative burst at the low pH (pH 5.4) (55). Phagolysosomal compartment can uptake various macromolecules from the host and degraded by the hydrolases (protease, glycosidase and lipase) and provide free sugar, amino acids and lipids, which is taken up by the amastigotes via membrane transporter

(56) (**Fig.9**). Phagolysosome comprises of several essential nutrients (amino acids, vitamin, purines and heme) and carbon sources to get rid of amastigotes driven degradation of host macromolecule using own lysosome (57,58). On the other hand, endolysosomal compartment may be removed from the lysosome (56).

1.3.7. Pathogenicity

One of the biggest threats of visceral leishmaniasis is the *Leishmania*/HIV co-infection. Statistical data shows that approximately 39.5 million of people are infected with HIV from

which 95% are came from developing countries (59). HIV patients are more vulnerable to *Leishmania* infection, where leishmaniasis accelerates the infection with HIV and AIDS progression. The response rate of the treatment is very low and without antiretroviral therapy (ART) patients eventually dies due to high chance of relapse.

1.3.8. Treatment of leishmaniasis

Approximately 12 million of individuals are getting infected with leishmaniasis every year worldwide. World Health Organization or WHO declares it as a major tropical disease. Although till now, no preventive medicines or vaccines are available. The only protective measure is to avoid the biting of sandflies. The commonly used drugs have several side effects; those are very much costly and become drug resistance due to frequent uses. Therefore, development of new drugs is absolutely necessary. Various fresh drugs and vaccines are now on trial and few of them show promising effects. Some commonly used drugs used to treat leishmaniasis are given in **Table-3** (60).

Table 3: Frequently used anti-leishmanial drugs.

Drugs	Properties	Mode of administration	Effectivity	Side effects
Pentavalent antimony	Polymeric organometallic complexes.	Intra-venous or intra-muscular for VL and CL.	Resistance to drugs in various parts of India, sodium stibogluconate based cheap treatment, uneven response in CL.	Pain, abdominal pain, edema, thrombocytopenia, nausea and erythema.
Amphotericin B	Polyene antibiotic, product of <i>Streptomyces nodosus</i> .	Intra-venous.	Major drug for VL in India, in Sb resistance cases. Used for VL, CL and complicated forms of CL.	Hypokalemia or infusion related anemia, azotemia.
Paromomycin	Aminoglycoside, product of <i>Streptomyces rimosus</i> . Supplied as sulphate.	Intramuscular for VL and tropical for CL.	Used for VL in India, under clinical trials for VL in East Africa. Formulation with gentamycin and surfactants in phase III trial.	Pain, erythema, edema, blister and ototoxicity.
Pentamidine	Diamidine as isethionate salt.	Intramuscular	For specific CL only in South America.	Nausea, diarrhea, vomiting, cardiotoxicity and hyperglycemia.

Always vaccines are the long term solution of any diseases, also in case of leishmaniasis. However, till now no vaccines are routinely used against *Leishmania* anywhere in the globe. Several factors like antigenic diversity, digenetic life cycle and genetic plasticity increases the difficulty of developing the effective vaccines. Over last two decades, scientists are trying

to develop new strategies for vaccines production and fewer of them are in the last stages of clinical trials (61,62) (*Table-4*).

Table 4: Status of different anti-leishmanial vaccines

Generation	Nature	Present status
First generation	Killed parasites that stimulate low immune response.	In phase III clinical trials in Asia and South America since 1940 (62).
Second generation	Genetically modified live parasites, viruses or bacteria having native or recombinant fragment of <i>Leishmania</i> genes.	Antigens like recombinant hydrophilic acrylated surface protein B1, <i>Leishmania</i> homolog of receptors for activated C-kinase, A2 protein, kinetoplastid membrane protein-11 (KMP-11), Histone H1 from <i>Leishmania</i> have been used in vaccine manufacture with considerable success (63,64).
Third generation	Composed of DNA vaccines which are highly stable, cost effective and induce durable and stronger immune responses through stimulating innate immune responses.	Still under development and standardization.

1.4. Redox homeostasis in Trypanosomatids

Reactive Oxygen Species (ROS) are produced primarily in the mitochondria as a by-product of cellular metabolism. A least amount of ROS is required for cellular signaling pathways, induce and regulate numerous cellular activities like growth, cell differentiation and gene expression (65). ROS can make a serious damage to the cells; hence cellular system possesses many antioxidant defense systems for scavenging and eliminating them. In the cellular system, there have a fine balance between formation and elimination of the ROS. Excessive ROS formation from the by-product in intracellular environment can affect the cellular redox homeostasis. Increased ROS production or impaired normal reductive mechanisms can cause oxidative stress to the cells. Low molecular weight molecules play a significant role in maintaining redox buffer (66,67). Short or long-term adaptive responses are developed by the cells depending upon the intensity of oxidative stress. The redox level of the kinetoplastid seems to be well-regulated since the parasites are able to successfully tolerate the oxidative burst and probably withstand at different environmental condition during host infection. The parasites lack glutathione reductase, catalase and selenium contained glutathione peroxide but the presence of different types of thiols, trypanredoxin, ascorbate peroxidase and trypanredoxin dependent peroxidases helps to maintain redox homeostasis. Trypanosomatids possesses four types of major low molecular weight thiols: glutathione, trypanothione, glutathionylspermidine and ovolthiol A. Only glutathione is a common low molecular mass thiol, which present also in the host. A brief description of these molecules is given below.

1. Ovothiol A:

All of the insect stages contain ovothiol A with more than 1 mM concentration in *Leishmania* and less than 0.25 mM in other trypanosomatids (68). Ovothiol A content exceeds the trypanothione in the late log or stationary phase of *Leishmania* promastigotes. Although ovothiol A is less effective than trypanothione, it can act as a non-enzymatic hydrogen peroxide scavenger (69).

2. Trypanothione and Trypanothione reductase :

A high concentration of glutathione, a sulfur-containing tripeptide makes it feasible to maintain an intracellular reducing environment in most living organisms. Generally, GSH/GR is responsible for intracellular redox homeostasis maintenance. Glutathione reductase is a very efficient enzyme that reduces the glutathione from oxidized (GSSG) to reduced form (GSH). However in case of kinetoplastida, most of the glutathione is converted into a unique thiol, trypanothione or N1,N8-bis (glutathionyl) spermidine (70) (**Fig.10**). Trypanothione is formed by the conjugation of two glutathione with one

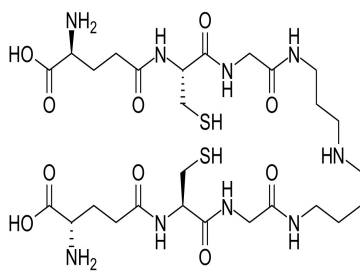


Fig.10: Trypanothione [T(SH)₂] structure (Adapted from <https://en.wikipedia.org>)

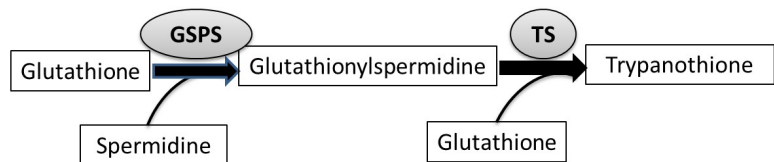


Fig.11: Trypanothione biosynthesis. One molecule of glutathione and one molecule of spermidine are attached by the glutathionylspermidine synthetase to form glutathionylspermidine, which in turn conjugated with another molecule of glutathione to form trypanothione by trypanothione synthetase; GSPS- Glutathionylspermidine synthetase, TS- Trypanothione synthetase.

molecule of Spermidine (**Fig.11**). γ -glutamyl cysteine synthetase or glutamate-cysteine ligase (GCL) and glutathione synthetase are the common enzymes present in trypanosomatids as well as in other organisms for glutathione synthesis (71,72). The biosynthesis pathway of trypanothione is unique to the trypanosomatids. The conversion of reduced form of trypanothione or dihydrotrypanothione [T(SH)₂] from the oxidized form or trypanothione disulphide (TS₂) by the unique enzyme trypanothione reductase (TR) helps to maintain redox homeostasis in all kinetoplastids (73) (**Fig.12**). Compared to

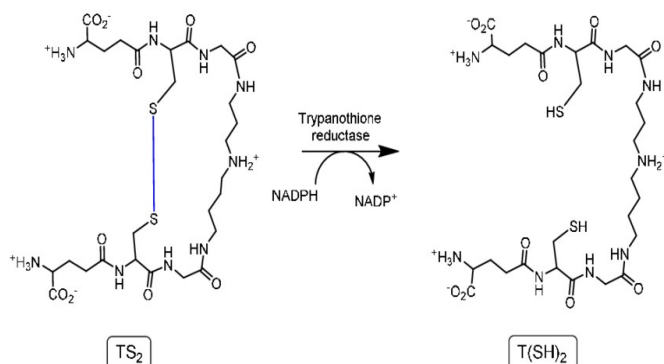


Fig.12: Conversion of TS₂ to T(SH)₂ by Trypanothione reductase. Structure of oxidised trypanothione [TS₂] and reduced trypanothione [T(SH)₂] is shown. Trypanothione reductase or TR reduces the oxidised form into the reduced form. (Adapted from Nagarajan et al, J Med Chem. 2003 Dec 18; 46(26):5712-24)

GSH, T(SH)₂ block the NO 600 times more efficiently and it is proposed that higher level of catalytic activity of could T(SH)₂ protect the parasite cells from high exposure of NO from mammalian host (74,75).

3. Tryparedoxin:

In trypanosomatids, a distinct type of oxidoreductase, named tryparedoxin (TXN) is found, which is related to thioredoxin. It is a component of detoxification pathways of hydroperoxide in kinetoplastids, where they involve in electron transfer between peroxiredoxin and trypanothione to reduce hydroperoxide as well as peroxynitrite (76). Tryparedoxin can also reduce ribonucleotide reductase and react with various tryparedoxin peroxidase and Universal minicircle sequence Binding Protein (UMSBP), in a way being involved in numerous cell functions like synthesis of DNA, regulation of mtDNA synthesis, peroxide metabolism (77,78).

4. Tryparedoxin peroxidase:

The peroxidase that uses reducing electrons from tryparedoxin to remove peroxides, is termed as “tryparedoxin peroxidase” or TXNPx. Members of peroxiredoxin and non-selenium glutathione peroxidase is belongs to this family. The first enzyme to be reported to have tryparedoxin peroxidase activity is peroxiredoxin (PRX), which is an antioxidant enzyme that can reduce hydroperoxide and peroxynitrite by using active cysteine (79).

5. Non-selenium glutathione peroxidase:

Glutathione peroxidases (GPX) are the group of antioxidant enzymes that reduce hydroperoxides at high catalytic efficiency (80). GPX has a common catalytic residue, formed by tryptophan, glutamine and selenocysteine (Se-Cys). Although some of GPXs contain Cys in place of Se-Cys residue, is named as ‘non-selenium glutathione peroxidase’ (nsGPX) (81). In *T. cruzi*, glycosomal nsGPXA1 is supposed to function in phospholipids, hydroperoxides and fatty acids metabolism (82).

6. Ascorbate peroxidase:

In 1994, ascorbate is identified in trypanosomatids and capacity of vitamin C synthesis has been identified in *T. cruzi* and *T. brucei* (83). In photosynthetic organisms, ascorbate is oxidized in a H₂O₂-dependent manner by ascorbate peroxidases (APXs) - a class-1 heme-containing peroxidase enzyme (84). In *L. major*, APX is involved in intracellular ROS detoxification by catalyzing the reduction of H₂O₂ is identified (11).

7. Glutathione:

As the tripeptide glutathione is present from prokaryotes to almost all eukaryotes, overview of this thiol molecule is discussed below.

1.5. Overview of glutathione

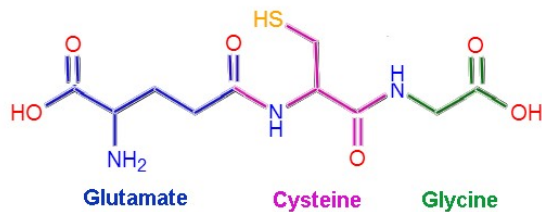


Fig.13: Structure of glutathione. Glutathione is a tripeptide thiol made up of Glutamic acid, Cysteine and Glycine. (Adapted from <https://commons.wikimedia.org>)

peptide bond linkage between glutamate and cysteine is aided by γ -carboxyl group, rather than usual α -carboxyl group. Three main reservoirs of GSH are cytosol (~90%), mitochondria (10%) and endoplasmic reticulum (ER) (<1%) in eukaryotic cells. Mitochondrial GSH has greater half-life (30 hrs) than cytosolic GSH (2-4 hrs). In mammalian cells, GSH is found in a concentration between 1-10 mM (85).

Plants and humans both experience embryonic mortality when glutathione biosynthesis is disrupted (86,87). Unicellular eukaryotes like yeast also could not able to grow in this condition (88). However, only exogenous glutathione can restore the condition (89). Glutathione still is not necessary for survival in prokaryotes like *E. coli* unless under stressful conditions (90).

Glutathione exist in two forms – reduced or GSH and oxidized or GSSG. Alteration of the balance of these two forms can affect the redox balance in the cells. Besides its role in redox buffer (91), glutathione exhibits various function in all organisms including iron-sulfur biogenesis in mitochondria (92), transport and storage of sulphur (93), ROS elimination (94), detoxification of xenobiotics and metals (91,95), protein function regulation by glutathionylation of cysteine residue (96). In addition, glutathione plays a significant role in immune system regulation like regulation of antigen-processing machinery by antigen-presenting cells (APCs) to initiate Th1 and Th2 response (97). GSH can also act as a cofactor for the antioxidant enzyme glutathione peroxidase (GPX), a selenium containing peroxidase reduces the peroxides (98) (**Fig.14**).

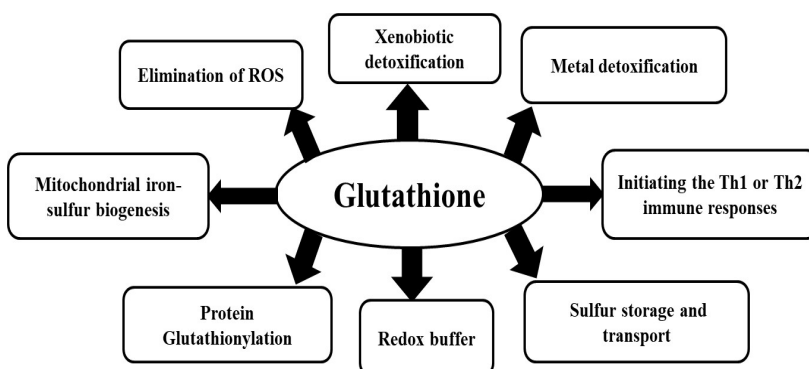


Fig.14: Graphical presentation of the functions of glutathione in the cell. Glutathione plays several roles in the intracellular milieu such as xenobiotic and metal detoxification, ROS elimination, mitochondrial iron-sulphur biogenesis, protein glutathionylation, redox buffer, sulphur transport and reservoir, regulation of immune response.

Increased oxidative stress is a direct result of the GSH deficiency, which can be associated with many diseases such as liver disease, Alzheimer's disease, Parkinson's disease,

degeneration of macular eye, cancer, aging and HIV infection (99). Moreover, GSH degradation lead to the cell apoptosis and it is act as a hallmark of apoptosis (100). On the other hand, extreme level of glutathione is also associated with the cell toxicity because of the non-specific glutathionylation and activity inhibition of the cellular protein in this elevated level of GSH (101). GSH synthesis and degradation as well as glutathione transport and efflux, also the regulating enzymes such as reductase and peroxidase play crucial role for the maintenance of glutathione homeostasis. Among these, glutathione degradation may be the least understood in terms of maintaining glutathione homeostasis. The significance of glutathione degradation is becoming better understood as a result of the recent discovery of some new glutathione degradation pathways.

1.5.1. γ -glutamyl cycle:

The γ -glutamyl cycle that is involved in the cyclic degradation and re-synthesis of GSH, is responsible for carrying out the metabolism of glutathione in cells (*Fig.15*). However, the

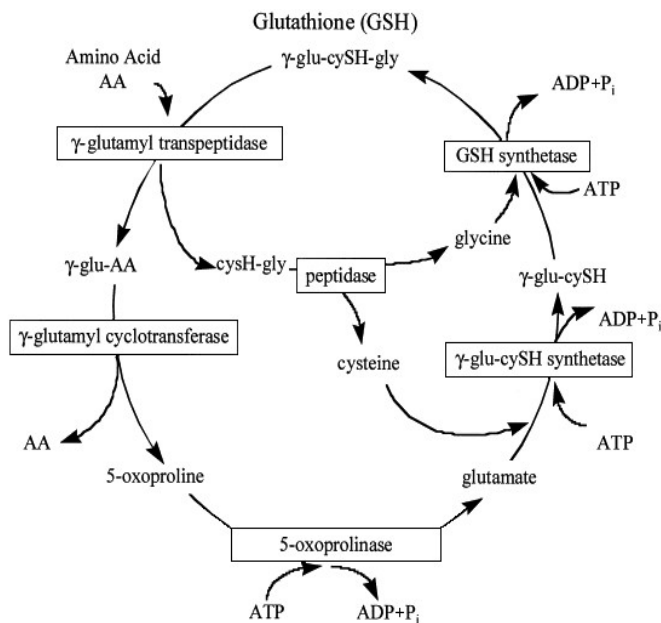


Fig.15: Schematic diagram of γ -glutamyl cycle. This cycle is essential to maintain intracellular glutathione (GSH) homeostasis. This cycle is accomplished by six enzymes found in the cytosol and plasma membrane. Glutathione is degraded by the γ -glutamyl transpeptidase to form γ -Glu-AA and Cys-Gly. Cys-Gly is then degraded by the peptidase to form free Cysteine and Glycine, whereas γ -Glu-AA is in turn degraded by γ -glutamyl cyclotransferase enzyme into free amino acid and 5-oxoproline. This 5-oxoproline is then transformed into glutamic acid by the 5-oxoprolinase. The produced glutamate and cysteine are combined to form γ -Glu-Cys by glutamate-cysteine ligase (GCL). The final step of GSH biosynthesis pathway involves the addition of Gly by ATP and Mg^{2+} dependent glutathione synthase (GS). (Adapted from <https://flipper.diff.org/app/pathways/info/8031>)

cycle does not resemble to all the organisms because some of the steps are missing in some organisms. The γ -glutamyl cycle is thoroughly studied in mammalian systems and six enzymes are involved to complete the cycle (102). Two ATP-dependent enzymes are required for the biosynthesis of GSH- γ -glutamate-cysteine ligase (GSH1) is responsible for the ligation of glutamate and cysteine via the γ carboxyl group. Later, glycine is linked to γ -Glu-Cys to form GSH by glutathione synthetase (GSH2). The rate-limiting step of GSH production is the synthesis step of γ -Glu-Cys by GSH1, which is tightly regulated at transcriptional as well as post-transcriptional levels (103,104). Initially glutathione degradation is catalyzed by γ -glutamyl transpeptidase or γ -glutamyl transferase (GGT, γ -GT) that can transfer γ -glutamyl moiety to the available amino acid to form γ -Glu-amino acid and the dipeptide Cys-Gly (105). These two degraded product were presumed to be passed through the membrane, but details of transport are not clearly depicted in the cycle. Cys-Gly dipeptide is then degraded

into Cysteine and Glycine by the peptidase, while γ -glutamyl cyclotransferase is acted upon the γ -Glu-amino acid to yield 5-oxoproline and respective amino acids (106). Then another enzyme, 5-oxoprolinase (ATP dependent) hydrolyses 5-oxoproline or pyroglutamic acid into glutamate (107).

First trace of existence of GGT independent alternate pathways was found through a genetic study in 2003 (108). Glutathione degrading enzymes have been identified in last two decades includes Dug enzyme (yeast and fungi) (109), ChaC1 enzyme (higher eukaryotes) (110), ChaC2 enzyme (bacteria to human) (111) and RipAY enzyme (few bacteria) (112). A better picture can be drawn about function of GSH degradation in GSH homeostasis, amino acids recovery and recycling with the emergence of new degradation pathways.

1.5.2. Enzymes involve in glutathione degradation pathways:

The biochemical properties and functions of glutathione degradation pathway's enzymes are briefly discussed in below.

A. γ -glutamyl transpeptidase (GGT):

GGT is an enzyme that cleaves the γ -glutamyl bond of GSH and transfer to the acceptor like peptides and amino acids by transpeptidation reaction or water by hydrolysis. Glutathione is degraded into glutamic acid and Cys-Gly through the hydrolysis reaction. The name γ -glutamyl transpeptidase is derived from the ability of the enzyme to transfer γ -glutamyl moiety to acceptor like dipeptide or amino acids forming a new γ -glutamyl molecule (90,113,114). γ -glutamyl transpeptidase is heterodimeric protein consists of two subunits - large and small subunit (**Fig.16**). The enzyme is synthesized through the

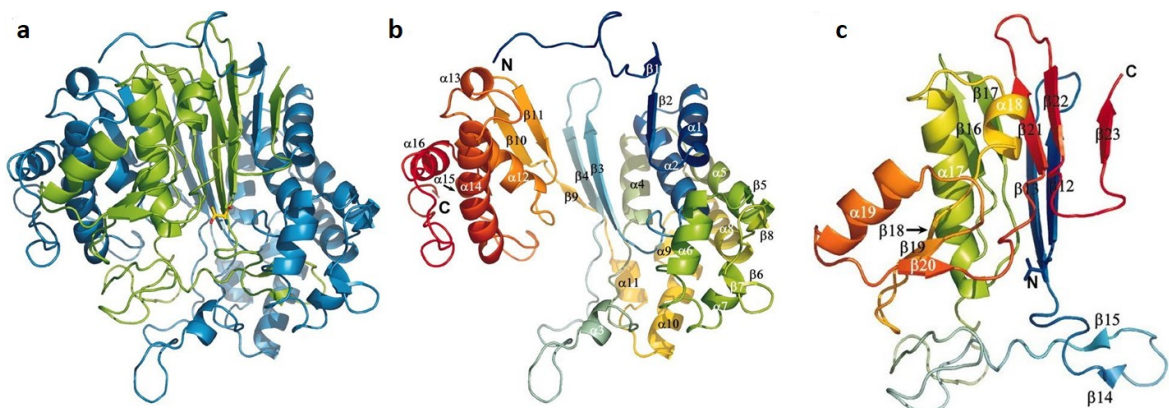


Fig.16: Crystal structure of γ -glutamyl transpeptidase of *Escherichia coli*. (a) Ribbon representation of GGT heterodimer (PDB code-2DBU). The L subunit is blue-colored and the S subunit is green-colored. (b) Ribbon representation of L subunit. (c) Ribbon representation of S subunit. α -Helices and β -strands are labelled. In each of the L and S subunits, the N terminus is colored blue and the C terminus is colored red, with intermediate colours following the distance in the sequence from the N terminus. The N-terminal residue of S subunit (Thr-391) is shown with a stick model. (Adapted from Okada et al, Proc Natl Acad Sci U S A.2006 Apr 25; [103\(17\)](#):6471-6)

autocleavage of a propeptide to form two subunits. This protein belongs to the superfamily of N-term nucleophile hydrolase (Ntn hydrolase) because conserved 'Thr' at the N-terminal is critical for the initiation of the catalysis (115-117). GGT is able to

cleave various γ -glutamyl substrates where free glutamate moiety is present such as reduced and oxidized glutathione (GSH and GSSG), γ -glutamyl compounds and GSH-S-conjugates (118).

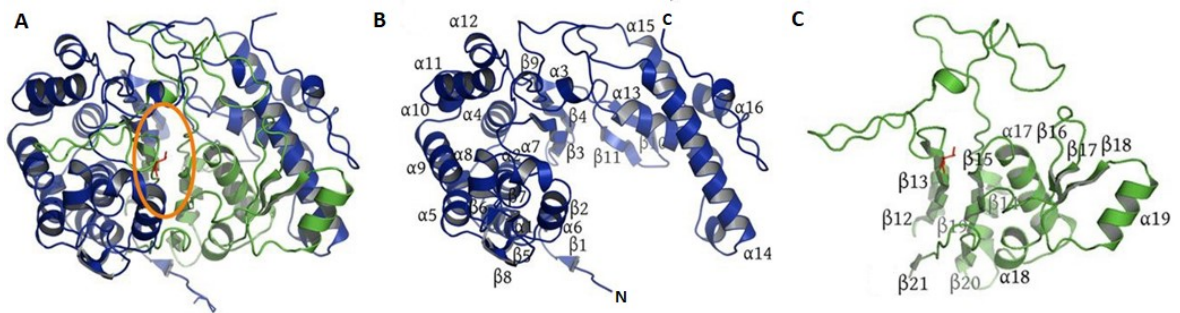


Fig.17: Crystal structure of human GGT1. (A) Ribbon representation of the hGGT1 heterodimer (PDB code- 4DGX). The large subunit is colored blue, and the small subunit is colored green. The active site Thr-381 is colored red. The orange round outlines the active site cleft. Ribbon representations of large subunit (B) and small subunits (C) of hGGT1 are shown. (Adapted from West et al, J Biol Chem.2013 Nov 1; 288(44):31902-13)

Out of 13 identified GGT homologues, only two genes (GGT1 and GGT5) are able to encode protein in human genome (119) (**Fig.17**). Both are situated on the extracellular side of plasma membrane. In case of yeast, only one GGT is found at the vacuolar membrane facing towards vacuolar lumen (120). Whereas in *Arabidopsis thaliana* plant, 4 GGTs were characterized, where GGT1 and GGT2 are supposed to be located in plasma membrane facing apoplast involved in the transport of GSH, formation of γ -glutamyl amino acid and vacuolar GGT3 and GGT4 are involved in initial GSH conjugate metabolism step and cleavage of γ -glutamyl residue from Glutathione S-bimane (GSB) as initial degradation step of glutathione S-conjugate respectively (121-123).

Although it was thought that the major activity of GGT was transpeptidation, several studies reveal that the main function of it as a hydrolase, not transpeptidase (124-126). As the active site situated towards outwards, recovering glutathione from the outside and constituents back to inside of the cells could be the main function of this enzyme (127). GGTs catalyze the degradation of different γ -glutamyl substrates to produce glutamic acid-AA conjugate and Cys-Gly. This Cys-Gly can eventually be hydrolyzed by Cys-Gly peptidases (membrane bound) to form glycine and cysteine, which can be consumed by the cells for GSH and protein synthesis. In mammals, the central role of GGT is to replenish glutathione and cysteine stores, which is expressed predominantly in proximal tubules of the kidney (128). So, GGT has a major role in the homeostasis of cysteine and protect the cells from oxidative stress related damage (90).

B. DUG enzyme:

GGT knock out *Saccharomyces cerevisiae* cells is able to grow and degrade glutathione when glutathione is used as only sulfur source that suggesting the existence of alternate pathway for glutathione degradation (108). These alternate pathway genes are identified

through genetic study and named the pathway as DUG pathway or Defective in Utilization of Glutathione pathway. Four genes are identified named DUG1, DUG2, DUG3 and DUG4. DUG1 is act as a Cys-Gly peptidase and DUG4 encodes a transporter called HGT1 or high affinity glutathione transporter (89,109,129). Remaining Dug2p and Dug3p were interacted each other to form heterodimeric (Dug2p-Dug3p)₂ complex, that is active DUG enzyme, where large Dug2p protein is consisted of two domains and Dug3p bears a glutamine aminotransferase II domain. This interaction is necessary for the enzymatic activity of this enzyme (130). This Dug pathway has found only in yeast (*Candida albicans*) and fungi (*Aspergillus nidulans*) but absent in bacteria, animals or plant, suggesting that Dug is yeast and fungi specific pathway (131,132).

Cytosolic Dug enzyme are transcriptionally activated under sulfur deprived condition and inactivated in cysteine and methionine presence (130). Hence, stress inducible Dug enzyme plays an important role in GSH homeostasis in the cell. Different studies reveal that the enzyme can cleave γ -glutamyl bond of γ -glutamyl p-nitroanilide (GPNA) suggesting that it could have broad specificity like GGT. Albeit the GSH synthesis is essential for *Candida albicans* survival in vivo, the GSH degradation is not related to their virulence (131).

C. ChaC1 enzyme:

Members of γ -glutamyl cyclotransferase family shows identical BtrG/ γ -GCT fold which is distinguished by an exclusive character of beta barrel and that is surrounded by alpha helices. The first reported enzyme of this family is BtrG protein of bacteria and γ -GCT proteins of mammals. This enzyme produces 5-oxoproline and various compounds by acting upon different γ -glutamyl substrates (133). ChaC1 belongs to this family, specifically act upon the reduced glutathione (not even oxidized glutathione) to form Cys-Gly and 5-oxoproline. The mammalian ChaC1 protein shows the K_m value between 2-3 mM and induced under ER stress or unfolded protein response (UPR) (110,134). Two alternative spliced variants of ChaC1 as isoform A and isoform B are found in the human. The nomenclature of ChaC was first described in *E. coli*, where ChaC belongs to the CHA operon. Three genes of this operon are: ChaA which encodes a transporter, ChaB encodes a regulator and ChaC encodes cation transport regulator-like protein, which is a regulator of ChaA. The presence of Ca^{+2} / H^+ antiporter in the operon along with GSH degradation enzyme suggests there have a close relationship between this two (135). ChaC1 protein homologues are present in all organisms; however functional orthologues are only present in higher eukaryotes. ChaC1 paralogues named ChaC2 also present in these organisms. Albeit ChaC2 functions as glutathione degradation like ChaC1 but in terms of kinetics and physiological role they appear to be quite different (90).

ChaC1 proteins are induced under numerous conditions includes endoplasmic reticulum stress (ER stress) (134), amino acid deprivation (136), cancer (137), viral infection, (138,139), diabetes, neurogenesis (140), atherosclerosis (141), retinal axonal damage (142) and liver metabolism (143). ChaC1 induction occurs through the PERK/ATF4/ATF3/CHOP induction under ER stress (144). Amino acid deprivation response occurs through GCN2/eIF2a/ATF4/ATF3 pathway (136). It is seems that ChaC1

is required for providing amino acids (glutamate, cysteine and glycine) to the cells in the stress condition which can be required for the cell growth. As the ChaC1 is specific towards reduced glutathione, it has the ability to change the redox potential of the cells and sudden ChaC1 induction leads to decrease of GSH/GSSG ratios to provide oxidizing environment. Higher migration and proliferation can occur in human breast and ovarian cancer cells with the overexpression of ChaC1 because of the hypoxic and ER stressed condition in the cancer cells (137). The induction of ChaC1 (Botch) is observed during neurogenesis of mouse suggests that ChaC1 has an important role in developmental processes (145).

D. ChaC2 enzyme:

ChaC2 as a member of ChaC family are found from lower prokaryotes to higher eukaryotes unlike its paralogues ChaC1 which is only restricted to higher eukaryotes. Detailed studies from human, mouse and yeast ChaC2 reveal that it is located in cytosol and specifically act on the GSH to yield Cys-Gly and 5-oxoproline (**Fig.18**). There have

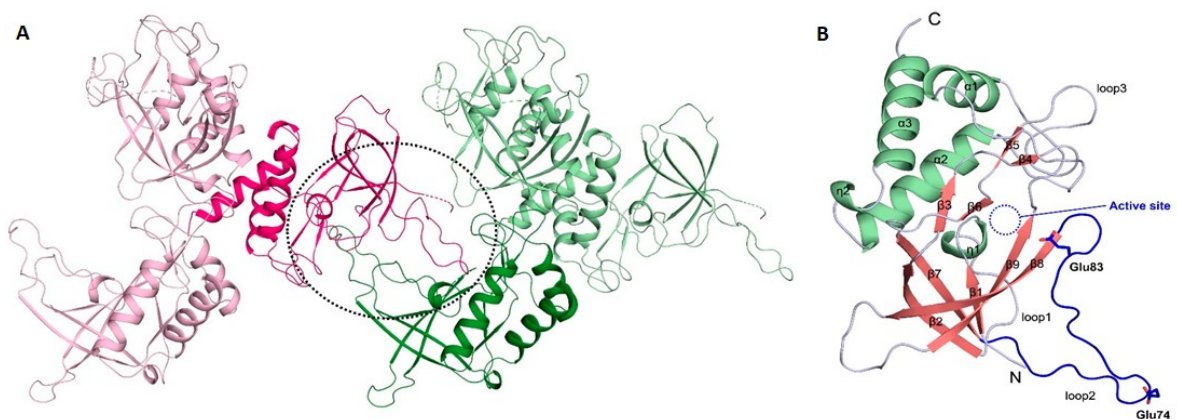


Fig.18: Structure of ChaC2 from human. (A) Schematic representation of ChaC2 in the crystal. ChaC2 of the crystallographic dimer from two nearby an asymmetric unit (ASU) are colored in pink and green, respectively. The crystallographic dimer formed by flexible loop2 is denoted with black dotted circle. (B) Structure of ChaC2 (PDB code-6K95). Helices, β -strands, and loops are colored in green, salmon, and light blue, respectively. The active site of ChaC2 is denoted with a blue dotted circle. Loop2 is colored in blue. The side chains of Glu74 and Glu83 are shown as stick models. (Adapted from Nguyen et al, Biomolecules.2019 Dec 24; [10\(1\):31](#))

60% sequence similarity between ChaC1 and ChaC2 of human and 90% similarity between mouse and human ChaC1. Thus ChaC2 is much similar to ChaC1 but differs mainly in catalytic activity. ChaC2 can degrade GSH with 10-20 folds less efficiently than ChaC1 enzyme (111). There have three homologues of ChaC2 in plant *A. thaliana*, named GGCT2:1, GGCT2:2 and GGCT2:3; all are present in cytosol and with low catalytic efficiencies (146,147).

Unlike mammalian ChaC1, ChaC2 enzymes are not induced in any condition in mammalian cells. Expression level of ChaC2 in normal or any stressed condition remains unchanged and higher than ChaC1 in human. Thus constitutively expressed ChaC2 enzymes have housekeeping role of continuous and slow turnover of glutathione (111). In case of *Arabidopsis thaliana*, only GGCT2:1 is regulated via sulfur starvation and has a

significant role in glutamic acid recycling (147,148). On the basis of regulation and catalytic efficiency, it can be concluded that ChaC2 is the earliest enzyme with housekeeping capacity but ChaC1 is thought to be evolved at later period in higher eukaryotes to response in stressed condition (90).

E. RipAY enzyme:

Recently a glutathione degradation enzyme is found in a plant pathogenic bacterium *Ralstonia solanacearum* named as RipAY and which belongs to the ChaC family. RipAY catalyzes the degradation of glutathione with exceptionally high catalytic efficiency (100-200 fold higher K_{cat} than plant and yeast ChaC2) and regulated by thioredoxin (112). During *R. solanacearum* infection, it can alter the host glutathione homeostasis (149).

1.5.3. Other enzymes involved in γ -glutamyl cycle:

A. γ -glutamyl cyclotransferase:

γ -glutamyl amino acids were produced by the transpeptidation reaction of γ -GT, which acts upon the glutathione in γ -glutamyl cycle. Then this γ -glutamyl amino acid is cyclized by the γ -glutamyl cyclotransferase (γ -GCT) to produce amino acids and 5-oxoproline. In mammals, this protein is observed to be acted with γ -glutamyl derivatives of alanine, glutamine and methionine but not with valine and leucine derivatives (133,150). This protein is completely absent in plants or yeast and is thought to be exclusively present in mammals. Crystal studies reveal that glutamate residue at 98 position (Glu98) of γ -GCT is critical for its catalytic activity (**Fig.19**). γ -glutamylamine cyclotransferase (GGACT) is a structural homologue of γ -glutamyl cyclotransferase is identified and acts solely on γ -glutamyl amines like γ -glutamyl- ϵ -lysine (151).

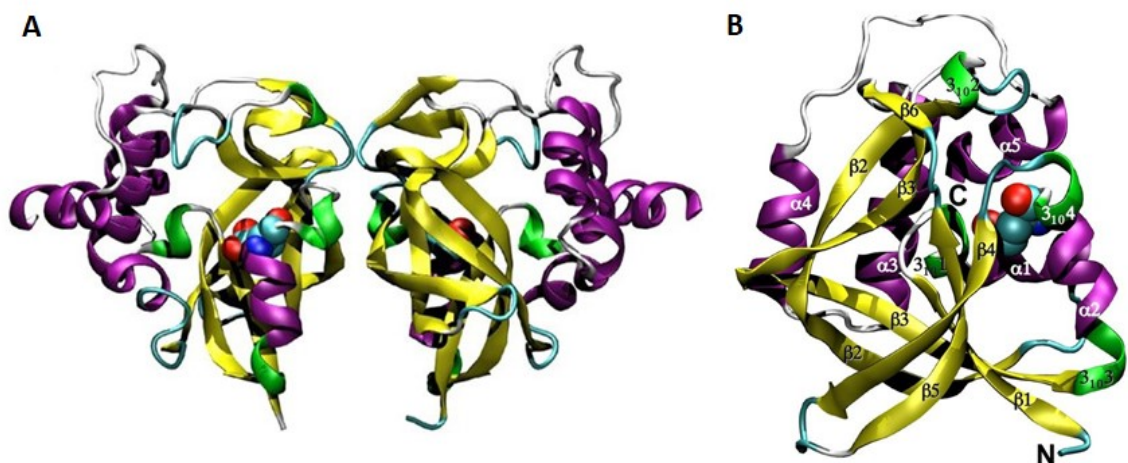


Fig.19: Crystal structure of Human γ -glutamyl cyclotransferase (GGCT). (A) Schematic representation illustrating the GGCT dimer (PDB code-3CRY). Atoms of Glu⁹⁸ are represented as spheres. β -strands are yellow, α -helices are purple and 3_{10} helices are green. (B) Schematic representation of the GGCT monomer with secondary structure elements labeled. (Adapted from Oakley et al, J Biol Chem.2008 Aug 8; [283\(32\):22031-42](#))

B. 5-oxoprolinase:

ATP-dependent enzyme 5-oxoprolinase catalyze the hydrolysis of 5-oxoproline to form glutamic acid. The cyclized form of glutamic acid or 5-oxoproline (pyrrolidone carboxylic acid or pyroglutamic acid) is produced from γ -glutamyl-AA by γ -GCT. It could also be generated from the glutathione directly by the enzyme ChaC1 or ChaC2 or through other reaction (152). Excessive level of pyroglutamate in the blood, urine or CSF can lead to various severe diseases like hemolytic anemia, severe metabolic acidosis and CNS dysfunction (153). Hence, 5-oxoprolinase plays a very important role in removing 5-oxoproline and regenerating glutamate. Structural studies from eukaryote cells reveal that this enzyme is a large homodimeric protein consists of two hydantoinase domains for each subunit. Catalytic efficiency of 5-oxoprolinase is very low (154,155). 5-oxoprolinase is found from bacteria to eukaryotes and it is also present in some organism that don't have the ability to produce glutathione, which suggest that 5-oxoproline could be produced through multiple pathways in the cells (156).

C. Cys-Gly peptidase:

Cys-Gly accumulation in the cells can leads to several toxic effects. Hence it is very important to degrade this dipeptide. Cys-Gly peptidases can breakdown Cys-Gly and recover cysteine and glycine for the cyclization of the γ -glutamyl cycle. Since GSH can be broke down both at cytosol and extra cytoplasmic spaces, Cys-Gly peptidases can also be found in cytoplasm as well as extracellular environment. M20A dipeptidase or Dug1p/CNDP2 peptidase is cytosolic homodimeric manganese or zinc dependent metallopeptidase which shows Cys-Gly peptide specific activity (129). Although this type of peptidase can be found in human and yeast but absent in plant and bacteria. M17 metallopeptidases or Leucine amino peptidases can be found in the cytosol of animals, plant, some yeast and bacteria and it is a hexameric zinc or manganese dependent peptidase that has a higher specificity towards Cys-Gly and oxidized Cys-Gly (157,158). M1 metallopeptidases or Aminopeptidase N is a membrane bound metallopeptidase which can hydrolyze Cys-Gly (159). M19 metallopeptidase is also a membranous homodimeric dipeptidase that can hydrolyze Cystinyl-bis-glycine (Cys-bis-Gly), oxidized form of Cys-Gly and leukotriene D4 (S derivative of Cys-Gly) and form leukotriene E4 by removal of glycine from Cys-Gly of leukotriene D4. By the activity of GGT on GSSG, Cystinyl-bis-glycine can also be formed (160).

1.5.4. Newly proposed 'Glutathione cycle' instead of γ -glutamyl cycle:

From about five decades, glutathione metabolism in various organisms has been presented through γ -glutamyl cycle. Since many new discoveries have been emerged in glutathione metabolism, clearly it can be concluded that γ -glutamyl cycle is not sufficient to describe the metabolism of glutathione in the cells. Newly proposed "glutathione cycle" includes all the current discoveries about glutathione metabolism such that localization and function of the enzymes, transporter of the glutathione and degradation as well as transporter of the respective amino acids (90) (*Fig.20*).

1.6. Glutathione degradation in Leishmania:

Like other eukaryotic and prokaryotic cells, GSH synthesis enzymes such as γ -glutamylcysteine ligase and glutathione synthetase are present in *Leishmania*. But no glutathione

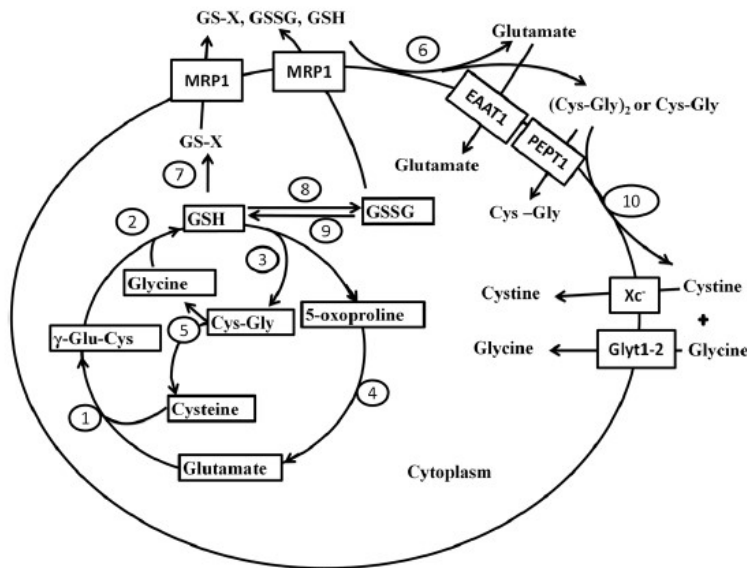


Fig.20: The glutathione cycle in the mammalian cells: 1) γ -glutamylcysteine synthetase, 2) glutathione synthetase, 3) ChaC1 & ChaC2, 4) 5-oxoprolinase, 5) Cys-Gly peptidase, 6) gamma-glutamyl transpeptidase, 7) ligandins or glutathione S-transferase, 8) dehydroascorbate reductase (DHAR) or glutathione peroxidase (GPx), 9) Glutathione reductase (GR), 10) membrane bound Cys-Gly dipeptidase. (Adapted from Bachhawat and Kaur, Antioxid Redox Signal.2017 Nov 20; 27(15):1200-1216)

degradation enzymes have been reported in any kinetoplastida. Many glutathione degradation enzymes have been reported in many organisms through decades such as GGT, DUG, ChaC1, ChaC2 and RipAY (**Fig.21**). As glutathione synthesis as well as degradation is a

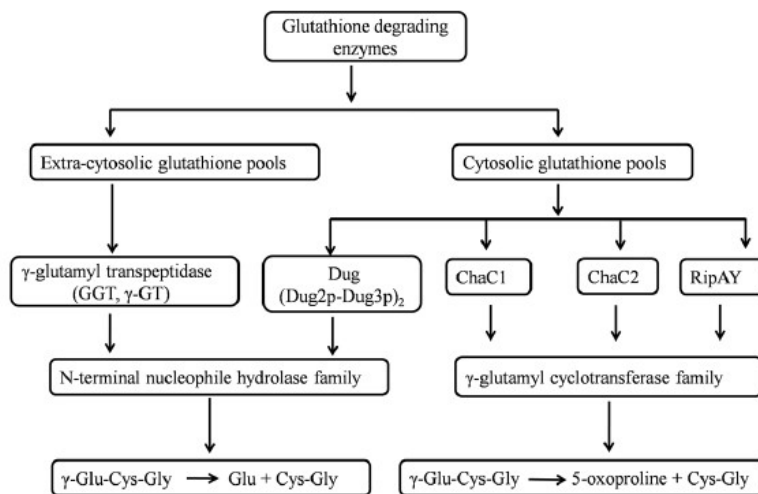


Fig.21: Enzymes involved in glutathione degradation: The different glutathione degradation enzymes are categorized according to the glutathione pools they work on and their enzymatic activities. (Adapted from Bachhawat and Kaur, Antioxid Redox Signal.2017 Nov 20; 27(15):1200-1216)

crucial factor for maintaining the glutathione homeostasis, any alteration in this homeostasis can cause a serious effect on the cellular level. Although trypanothione plays a role as a main redox molecule in the kinetoplastida, a large amount of glutathione is required for the formation of trypanothione with spermidine. So, trypanothione level will be altered with changing the glutathione level and subsequently affect the redox balance in these organisms. This work is mainly based on the finding of novel degradation pathways of glutathione in trypanosomatids like *Leishmania*.

1.7. Objectives of this present work:

Several tropical parasitic life threatening diseases such as leishmaniasis, malaria and amoebiasis continues to affect the population even today. These pathogens differ from their host through a remarkable and fascinating array of biochemical, molecular, structural and metabolic differences. Drugs can control some of these parasitic diseases to some extent but the parasites have also developed various drug resistant mechanisms that impede the development of treatment and cure. With this viewpoint, researchers are involving for searching various drug targets. Amphotericin B, pentamidines, paromomycin are widely used chemotherapeutic drugs for the treatment of leishmaniasis and those are very expensive drugs with several side effects. The necessity to create novel and cost effective leishmaniasis treatments that can be administered in a way that will be target-specific, minimizes patient compliances, prevents rapid evolution of resistance and hence need multi-domain methods. It is well observed that *Leishmania* completes its life cycle in two hosts- promastigote stages in sandflies and amastigote stages in vertebrate host and cellular environments are remarkably different in these hosts. Finding new therapeutic targets can be valuable if genes and proteins of *Leishmania* involved for pathogenesis are identified and characterized.

Glutathione degradation is equally important as the glutathione synthesis for any organism, especially in unicellular organisms for maintaining their glutathione homeostasis. As our primary focus to explore glutathione degradation pathway related enzyme, during the search in tritrypdb site on *Leishmania major* genomic database, we have found two putative ChaC-like sequences (LmjF.22.1190 and LmjF.22.1200) situated in tandem array in the 22 chromosome of the genome. The open reading frame (ORF) of 714 base pair for shorter version ChaC-like gene encodes a 237 amino acid long protein, whereas ORF of 972 base pair for longer version of ChaC-like gene translates into 323 amino acid long protein.

Thus main objectives of this work is summarized as - 1) *In vitro* characterization and comparative kinetic activity measurement of two ChaC proteins from *Leishmania major*, 2) Regulation of either LmChaC proteins expression in *Leishmania major*, 3) Functional characterization of LmChaC proteins in *Leishmania major* by constructing overexpression, knockout and complementary cell lines, 4) Deciphering the physiological role of LmChaC proteins in terms of infectivity and virulence through *in vivo* studies in macrophage and BALB/c mice.

“Experience is the only teacher we have. We may talk and reason all our lives, but we shall not understand a word of truth until we experience it ourselves.”

- Swami Vivekananda

Materials and Methods

MATERIALS & METHODS

2.1. Materials

2.1.1. Reagents

Plasmid DNA isolation for miniprep kit (QIAprep spin miniprep kit), QIAamp-DNA mini kit for the isolation of genomic DNA, DNA gel extraction kit, PCR purification kit and Ni-NTA agarose resins were purchased from 'Qiagen'. *Leishmania* culture media-M199, Raw 264.7 cell culture media-RPMI 1640, Schneider's *Drosophila* media and fetal bovine serum (FBS) were purchased from 'GIBCO'. Unstained and pre-stained protein molecular mass markers, DNA molecular weight marker, various restriction enzymes, platinum Taq DNA polymerase, platinum Taq high fidelity DNA polymerase, T4 Rapid DNA Ligation Kit, protease inhibitor cocktail were purchased from 'Thermo Scientific'. G418 solution, protease inhibitor cocktail and NBT-BCIP tablet were purchased from 'Roche'. Anti α -tubulin antibody was purchased from 'Cell signaling technology'. All the required oligonucleotides were obtained from either 'GCC Biotech Pvt. Ltd' or 'IDT'. HEPES, propidium iodide, β -Mercaptoethanol, Bromophenol Blue, Coomassie Brilliant Blue R-250, TEMED, SDS, Tris-base, Tris-Cl, glycine, NaCl, EDTA, PMSF, lysozyme, DMSO, EtBr, RNase A, anti- rabbit and anti-mouse secondary antibody, perchloric acid were purchased from 'Sigma-Aldrich'. Protein estimation reagent (Bradford reagent) was obtained from 'Bio-Rad Laboratories'. Glacial acetic acid, NaOH, KH_2PO_4 , K_2HPO_4 , Na_2HPO_4 , NaH_2PO_4 , APS were purchased from 'SRL'. Methanol and isopropanol was purchased from 'FINAR'. HPLC grade ethanol and nitrocellulose membrane were purchased from 'Merck-Millipore'. Yeast extract, agar-agar, tryptone, acrylamide-bis-acrylamide solution, Luria-Bertani Broth, Terrific Broth and sulfur deficient M199 media (AT1076) were purchased from 'HIMEDIA'.

2.1.2. Strains

A. *Leishmania*

Leishmania major (Strain 5ASKH)

B. Macrophage

RAW 264.7

C. Bacteria

Following Strains of *Escherichia coli* bacteria were used:

DH5 α , C41 (DE3) and BL21 (DE3)

D. Mice

BALB/c

2.1.3. *Leishmania* culture media

A. Preparation of sulphur containing M199 media:

M199 powder	13.2 gm.
HEPES	6.12 gm.
Adenine	200 µM
Folic acid	150 µg/ml
Haemin	10 µg/ml
Gentamycin	50 µg/ml
Penicillin-streptomycin	1%

Media pH was adjusted to 7.4 with HCl and volume was made up to 1000 ml with glass distilled water. Finally media was filtered by using 0.22 µm radiation sterilized stericup and stored at 4°C.

B. Preparation of sulphur deficient M199 media:

M199 powder(AT1076)	9.5 g
NaHCO ₃	2.2 g
Adenine	200 µM
Folic acid	150 µg/ml
Haemin	10 µg/ml
Gentamycin	50 µg/ml
Penicillin-streptomycin	1%

Media volume was adjusted up to 1 L and pH was set to 7.4 and then filtered through 0.22 µm sterilized stericup and stored at 4°C.

2.1.4. Bacterial culture media

A. Luria-Bertani Broth (LB), pH 7.5

Yeast extract	5 g/litre
Bacto Tryptone	10 g/litre
Sodium chloride	10 g/litre

B. Terrific broth (TB), pH 7.5

Yeast extract	24 g/litre
Bacto Tryptone	12 g/litre
Glycerol	4 ml/litre

2.1.5 Buffers and solutions

A. Phosphate buffered saline, pH 7.4

Na ₂ HPO ₄	14.4 g/L
KH ₂ PO ₄	2.4 g/L
NaCl	80 g/L

MATERIALS & METHODS

KCl 2 g/L

B. Potassium phosphate buffer

KH₂PO₄ 170 mM

K₂HPO₄ 720 mM

C. 50X TAE buffer

Tris base 242 g/L

Glacial acetic acid 57.1 ml/L

EDTA(0.5 M, pH 8) 100 ml/L

D. SDS-PAGE running buffer

Glycine 14.4 g/L

Tris-base 3 g/L

SDS 1 g/L

E. Electroporation buffer for L. major

HEPES, pH 7.4 21 mM

NaCl 137 mM

NaH₂PO₄ 0.7 mM

D-Glucose 6 mM

F. Equilibrium buffer for protein purification

Phosphate buffer, pH 7.0 50 mM

NaCl 150 mM

Glycerol 10%

Imidazole, pH 7.5 20 mM

PMSF 1 mM

G. Bacterial cell lysis buffer

Phosphate buffer, pH 6.0 50 mM

NaCl 150 mM

Glycerol 10%

Imidazole, pH 7.5 20 mM

PMSF 1 mM

Protease inhibitor (without EDTA) 0.5 tablet

β-Mercaptoethanol 0.05%

Lysozyme 1 mg/ml

H. Protein elution buffer

Phosphate buffer, pH 7.0	50 mM
NaCl	150 mM
Glycerol	10%
Imidazole, pH 7.5	250 mM
PMSF	1 mM

2.1.6. Cloning vectors used (Table-5)

Purpose	Name of the vector
For cloning the ORF	pET28a and pET16b (Novagen)
For overexpression leishmanial cells	pXG-B2863
For leishmanial null mutants generation	pTPuro_v1 and pTBlast_v1
For generation of Cas9 expression leishmanial cell-lines	PTB007
For leishmanial complement cells generation	pXG-PHLEO and pXG-B2863

2.1.7. Oligonucleotides used (Table-6)

Primer	Primer sequence (Restriction sites are underlined)	Purpose
Primer 1	5'- AAAAC <u>CATATG</u> ATGTCATCCTCATCGGAACTG -3'	Cloning of LmChaC _{2a}
Primer 2	5'- AAAA <u>GGATCCT</u> CATATCTTCTTTTCGCTACAG -3'	
Primer 3	5'- AAAAC <u>CATATG</u> ATGCCAAAAGTACCGAC -3'	Cloning of LmChaC _{2b}
Primer 4	5'- AAAA <u>GGATCCT</u> TACGCCATCGTGGCGACC -3'	
Primer 5	5'-AAAAGACAAGAAGTACAGCATCGG-3'	Confirmation of cas9 cassette
Primer 6	5'-AAAAGTCGCCTCCCAGCTGAGAC-3'	
Primer 7	5'-AAAACAAAGTCGGGAAAAGCAGTAGTAGTCgtataatgcagacctgtgc-3'	Repair cassettes
Primer 8	5'-GTGGTACAGATATTTTAGCGCACCGTGCCGccaatttgagacctgtgc-3'	
Primer 9	5'aaaagcaccgactcgggtccacttttcaagtgataacggactagccttattttaactgctatttctagctetaaac-3'	Primer G00
Primer 10	5'-gaaattaatagcactactataggTTACATATCTTCGCACATACgtttagagctagaatagc-3'	LmChaC _{2a} 5' sg RNAs primers

MATERIALS & METHODS

Primer 11	5'-gaaattaatacagactactataggTTTCTCACTTCACCTGTGTGgttttagagctagaaatagc-3'	LmChaC2b 3' sg RNAs primers
Primer 12	5'-AAAACCCGGGCGCATGTCATCCTCATCGGAACTG-3'	Cloning of OE construct for LmChaC _{2a}
Primer 13	5'-AAAAGGATCCTCATATCTTCTTTTCGCTACAG-3'	
Primer 14	5'- AAAACCCGGGCGCATGCCCAAAACTGATACCGAC -3'	Cloning of OE construct for LmChaC _{2b}
Primer 15	5'- AAAAGGATCCTTACGCCATCGTGGCGACC -3'	
Primer 16	5'-AAAAGTATAAGCTTGATGGAGAGCG-3'	Confirmation of knockout strain
Primer 17	5'-AAAACAACTTACGTGTGTGCGTG-3'	
Primer 18	5'- AAAAGGATCCCGCATGCCCAAAACTGATACCGAC-3'	Cloning of CM Construct for LmChaC _{2b}
Primer 19	5'- AAAAGGATCCTTACGCCATCGTGGCGACC -3'	
Primer 20	5'- TCGTGACCATCTACGACGCC-3'	qPCR of LmChaC _{2a}
Primer 21	5'- GTGGCAGGACCGAGGTAGTC-3'	
Primer 22	5'- CCAGCGGACCCTGAGAACT-3'	qPCR of LmChaC _{2b}
Primer 23	5'- CGGCACGTATTGTGTGGAGC-3'	

2.2. Methods

2.2.1. Methods for cloning of LmChaC_{2a} and LmChaC_{2b}

2.2.1.1. Genomic DNA isolation from *Leishmania major*:

Genomic DNA of the *Leishmania major* parasite was isolated by using 'QIAamp DNA mini kit' (Qiagen) by following steps. 1×10^8 promastigote cells were taken in 15 ml centrifuge tube and pelleted down at 3500 rpm for 7 minutes, then washed twice with the 1x PBS in 1.5 ml micro-centrifuge tube. 200 μ l 1x PBS, 200 μ l AL buffer (for cell lysis), 20 μ l proteinase K and 10 μ g/ml RNase A were added into the pellet and pulse vortexed for 30 seconds followed by pulse spin. The mixture was then incubated at 56°C for 10 minutes for complete cell lysis. Then 200 μ l of 100% ethanol was added and further vortexed and spin. After that mixture was transferred into the spin column and centrifuged at 8000 rpm for 1 minute. Bottom tube containing solution was discarded and 500 μ l AW1 buffer was then added to the column and centrifuged at 8000 rpm for 1 minute. Again bottom tube was discarded and 500 μ l of AW2 buffer was added into the column and centrifuged at 14000 rpm for 3 minutes. Then the column was placed on a fresh 1.5 ml micro-centrifuge tube and DNA was eluted with 50 μ l DNase free water by centrifuging it at 14000 rpm for 1 minute. The purity of the DNA was checked at A_{260}/A_{280} ratio (~ 1.8 indicates pure DNA) and stored at -20°C.

2.2.1.2. Polymerase Chain Reaction (PCR):

Both the ORF was amplified by using Veriti Thermal Cycler (Applied Biosystems). Each 50 μ l reaction was consisted of 50 ng template genomic DNA, 5 μ l of 10x high fidelity PCR buffer, 2 mM MgSO₄, 0.2 mM DNTP mix, 0.2 μ M each forward and reverse primer and 1 U Platinum Taq DNA polymerase high fidelity enzyme. PCR cycle consisted of i) initial denaturation at 95°C for 2 minutes, ii) denaturation at 95°C for 15 seconds, iii) annealing at 60°C for 30 seconds, iv) extension at 68°C for 1 minute, v) final extension at 68°C for 5 minutes, above mentioned ii-iv was repeated for 34 cycles. The amplified DNA product was checked by agarose gel electrophoresis.

2.2.1.3. Agarose gel electrophoresis:

1% agarose gel was run to separate DNA fragments depending on the size of the fragments. Each DNA samples were combined with the 6x loading dye (Thermo Scientific) and loaded into the wells of the gel in the negatively charged end. 1X TAE was used as running buffer to run the DNA samples at 70 V. Intercalating dye ethidium bromide (EtBr) (0.5 μ g/ml) was used for staining of the DNA and visualized under UV light.

2.2.1.4. Cloning of *LmChaC_{2a}* and *LmChaC_{2b}* genomic DNA:

LmChaC_{2a} and *LmChaC_{2b}* genes were amplified by using *Leishmania major* genomic DNA (40 ng) as a template. Primer 1 and primer 2 (**Table-6**) were utilized to amplify *LmChaC_{2a}* whereas primer 3 and primer 4 (**Table-6**) were used to amplify *LmChaC_{2b}*. The amplified *LmChaC_{2a}* ORF (714 bp) was restriction digested and cloned into pET28a vector by using NdeI and BamHI restriction sites. Similarly the amplified *LmChaC_{2b}* ORF (972 bp) was restriction digested and cloned within pET16b vector between NdeI and BamHI restriction sites. Finally, DNA sequencing was performed to confirm both the ORFs.

2.2.1.5. Plasmid DNA isolation by using miniprep kit:

5-10 ml of overnight bacteria culture containing respective plasmid was harvested in a 2 ml micro-centrifuge tube at 14000 rpm for 1 minute. 300 μ l of P1 buffer (Resuspension buffer) containing RNase A was added into the bacterial pellet and mixed well by vortexing. Then 300 μ l of P2 buffer (Lysis buffer) was added to the mixture solution and mixed gently. After that 400 μ l of N3 or neutralizing buffer was added and mixed by upside down. This final solution was centrifuged at 14000 rpm for 30 minutes for eliminating genomic DNA, cell debris and proteins. After centrifugation, supernatant was loaded into the spin column provided by the manufacturer and centrifuged at 14000 rpm for 60 sec. After that the solution which is deposited in the bottom tube was discarded and 500 μ l of PB binding buffer was added and centrifuged at same. After that 750 μ l PE wash buffer containing ethanol was added and centrifuged. The empty column and bottom tube was re-centrifuged to remove trace amount of PE buffer. Then, the column was placed onto an autoclaved fresh 1.5 ml micro-centrifuge tube and 70 μ l of nuclease free water was added in the middle bed of the column. After 5 minutes, DNA dissolve in the water was recovered by centrifuging the whole

at 14000 rpm for 1 minute. DNA concentration and quality was checked by using NanoDrop and agarose gel electrophoresis.

2.2.1.6. Restriction digestion of PCR amplified DNA and cloning plasmid:

Restriction digestion of the PCR amplified DNA product and cloning plasmid was done at 37°C for overnight according to the followings:

Sterile, nuclease free water	10 μ l
10X Tango buffer	8.0 μ l (2x)
DNA	18 μ l (2 μ g)
NdeI restriction enzyme	2 μ l
BamHI restriction enzyme	2 μ l
<i>Final volume</i>	<i>40 μl</i>

2.2.1.7. Recover the DNA from the gel by gel extraction kit:

The restriction digested DNA products were loaded and run on the 1% agarose gel, from where by using sterile blade band of interest was cut out and DNA was extracted from the gel pieces using gel extraction kit (Qiagen). The gel pieces were taken in a micro-centrifuge tube and QG buffer (300 μ l/100 mg gel) was added. After incubation for 10-15 minutes at 56°C, 350 μ l of isopropanol was added in the solution and loaded into a spin column that is provided by the manufacturer. After centrifuging at 14000 rpm for 1 minute, 500 μ l QG buffer was added into the column followed by 500 μ l PB buffer and centrifuged at the same. Finally, 750 μ l of PE buffer containing ethanol was added followed by free spin to remove trace of PE buffer. 30 μ l of nuclease free water was added in the middle bed of the column after placing the column on a fresh micro-centrifuge tube. After incubation for 5 minutes, purified DNA was obtained by centrifuging the tube at 14000 rpm for 1 minute.

2.2.1.8. Ligation of vector and insert DNA:

Ligation was performed at 22°C for 60 minutes by using Rapid DNA Ligation Kit (Thermo Scientific) in a following way:

Vector DNA	3 μ l
Insert DNA	7 μ l
5X ligation buffer	4 μ l
Nuclease free water	5 μ l
T4 ligase	1 μ l
<i>Final volume</i>	<i>20 μl</i>

2.2.1.9. Transformation:

CaCl₂ treated competent DH5α *E. coli* cells were used for the transformation. 10 μl of ligated product was mixed with the 100 μl of competent cells and kept in ice for 30 minutes. Heat shock was applied for 90 seconds at 42°C temperature and immediately placed on ice for 10 minutes. Then 1 ml of fresh sterile LB media was added to this transformation tube and kept for shaking at 37°C for 1 hr. After that, bacterial cells were pelleted by centrifuging at 14000 rpm for 1 minute, then pellet was resuspended in 100 μl of media and spread on the agar plate containing respective antibiotic by using L-shaped spreader.

2.2.2. Methods for expression and purification of LmChaC_{2a} and LmChaC_{2b}

2.2.2.1. Expression and purification

For expressing the LmChaC_{2a} and LmChaC_{2b} proteins, recombinant pET28a/LmChaC_{2a} and pET16b/LmChaC_{2b} was used to transform into *Escherichia coli* BL21 (DE3) cells and *Escherichia coli* C41 (DE3) cells, respectively. Both pET28a/LmChaC_{2a} and pET16b/LmChaC_{2b} transformed cells were separately grown overnight in 10 ml Luria-Bertani broth at 37°C in a shaker in presence of 50 μg/ml kanamycin and 200 μg/ml ampicillin, respectively, then inoculated separately in 500 ml of terrific broth in presence of respective drug. When both culture reached an O.D. of 0.5-0.8 at 600 nm, 0.5 mM isopropyl β-D-1-thiogalactopyranoside (IPTG) was added to the media and further grown for 16-18 hrs at 16°C. Then the cells were harvested by centrifuging it at 6000 rpm for 10 min and pellets were washed two times with PBS. Pellets were then resuspended in 50 mM potassium phosphate buffer, pH 6.0 (10 ml), containing 150 mM NaCl, 1.0 mM PMSF, 20 mM imidazole, and 10% glycerol, 1.0 mg/ml lysozyme and a protease inhibitor cocktail tablet without EDTA (Roche Applied Science). The resuspended solution was kept for 60 min in ice with regular vortexing, followed by a 20-sec pulse sonication (Sonicator Cell Disrupter, model no. W-220F, Heat Systems, Ultrasonics, Inc.) and 1 min of rest in ice in between. After that the lysate was centrifuged at 14,000 rpm for 60 min at 4°C temperature and immediately the pellet-free soup was loaded onto a Ni²⁺-NTA column. The column was then washed with equilibration buffer (50 mM phosphate buffer, pH 6.0, 150 mM NaCl, 10% glycerol, 1.0 mM PMSF and 20 mM imidazole). The enzyme was eluted with 50 mM phosphate buffer solution, pH 6.0, 150 mM NaCl, 10% glycerol and 250 mM imidazole and then dialyzed 3 times against 500 ml of 50 mM phosphate buffer, pH 6.0 and 100 mM NaCl having 10% glycerol. Purity and predicted molecular weight of the proteins were confirmed by 10% SDS-PAGE.

2.2.2.2. SDS-Polyacrylamide gel electrophoresis (SDS-PAGE):

All the samples were mixed with 1x Laemmli buffer and boiled for 15 minutes at 100°C followed by centrifugation at 14000 rpm for 10 min and then supernatant was loaded onto the well of SDS-Polyacrylamide gel.

2.2.2.3. Staining by using Coomassie Brilliant Blue:

The SDS-PAGE gel was incubated for 1-2 hrs in a solution containing 10% acetic acid, 45% methanol and 0.25% Coomassie Brilliant Blue R-250 for staining. After proper staining, gel was placed in a destaining solution containing 10% acetic acid and 45% methanol. The protein band was visualized under light transilluminator.

2.2.3. Biophysical characterization of LmChaC_{2a} and LmChaC_{2b}

2.2.3.1. Protein concentration determination:

Protein concentration of LmChaC_{2a} and LmChaC_{2b} proteins was determined by using Bradford reagent (Bio-Rad) in spectrophotometer. BSA protein was used as a standard.

2.2.3.2. Activity measurement assay:

To study the γ -GCT activity of the LmChaC2 proteins, 10.0 μ g of LmChaC_{2a} or 1.0 μ g of LmChaC_{2b} were mixed with 10 mM of γ -glutamyl-containing dipeptide (γ -Glu-Cys and γ -Glu- ϵ -Lys) or glutathione in a total reaction mix of 100 μ l containing 50 mM Tris-HCl buffer (pH8). Then the reaction mixture was incubated up to 60 min at 37°C. The reactions were terminated at 95°C for 5 min by the process of heat denaturation. Before HPLC (Waters) analysis, inactivated proteins were removed from the samples by centrifuging at 14000 rpm for 30 min. To product analysis of the reaction, 20 μ l of the reaction mixture were used for the HPLC analysis using C₁₈ HPLC column (Sunfire™ C18, 5 μ m, 4.6 x 250 mm Column, Waters) with a 2% (v/v) aqueous solution of perchlorate used as the mobile phase at 1 ml/min flow rate. Peaks of glutathione, Cys-Gly and 5-oxoproline were monitored in UV-Vis detector at 210 nm. With the help of authentic standards, substrate and products were identified. Peak of the reaction product corresponding to Cysteinyl-Glycine (Cys-Gly) and 5-oxoproline appeared at 7.1 min and 9.9 min, respectively. A third peak (between 5-oxoproline and Cys-Gly peaks) of oxidized Cys-Gly at 8.2 min appeared in reaction mix, which is derived from Cys-Gly.

2.2.3.3. Polyclonal antibodies production against LmChaC_{2a} and LmChaC_{2b}:

Polyclonal antibodies against the purified recombinant LmChaC_{2a} or LmChaC_{2b} was raised by subcutaneous injection of LmChaC_{2a} or LmChaC_{2b} (20 mg) respectively in almost 6-month old rabbit (female) using Freund's complete adjuvant (Sigma). This was followed by three booster doses of recombinant LmChaC_{2a} or LmChaC_{2b} (15 mg) at 15 days' intervals with incomplete adjuvant (Sigma). The rabbit was bled after 2 weeks of last booster dose and sera were isolated from the blood and used for western blot analysis.

2.2.3.4. Western blotting analysis:

Proteins were run on 10% SDS-PAGE and transferred to the nitrocellulose membrane (Merck) for 1 hour at 90 V by TE series transphor electrophoresis unit from Hoefer at 4°C. After 3 hrs of blocking in milk or 5% BSA at 37°C, the membrane was incubated with antisera against recombinant LmChaC_{2a} or LmChaC_{2b} protein at the dilution of 1:100 at 4°C

overnight. The membrane was washed for 3 times with the 1× TBS containing 0.1% Tween20 (TBS-T) for 5 minutes and finally incubated in alkaline phosphatase (AP)-conjugated anti-rabbit secondary antibody (1:15000) of Sigma or HRP-conjugated secondary antibody (1:10000) of Merck. As endogenous control α -tubulin was used and AP or HRP-conjugated anti-mouse secondary antibody (1:15000) was used against anti-mouse α -tubulin antibody. NBT/BCIP solution from Roche was used for AP conjugated antibody and Clarity Max Western ECL substrate from Bio-Rad for HRP conjugate antibody for band detection.

2.2.3.5. Total RNA isolation from the cell by TRIzol method:

To isolate total RNA from the whole cell suspension, cells were taken in centrifuge tube and centrifuged at 4000 rpm for 6 mins at 4°C, then washed 2 times with chilled PBS. 1 ml of TRIzol solution (Invitrogen) was added into the pellet and vigorously mixed and kept for 5 minutes at Room Temperature. Then, 200 μ l of chloroform was added (200 μ l/1ml TRIzol) and shake vigorously by the hand for 15 seconds. After 3 mins of incubation at RT, sample was centrifuged for 15 mins at 12000 g and 4°C. Now clear upper aqueous layer containing RNA was transferred to a new pre-chilled centrifuge tube. 500 μ l of isopropanol was added to the aqueous layer and incubated for 10 mins at 4°C. Centrifuged the sample at 12000 g for 10 mins at 4°C, pellet was resuspended in 1ml of 75% ethanol by vortexing and centrifuge for 5 mins at 7500 g and 4°C. The sample was air-dried for 5-10 mins and added 20-50 μ l of DEPC water. Samples containing RNA was then incubated at 55°-60°C for 10-15 mins and stored at -40°C.

2.2.4. Functional characterization of LmChaC_{2a} and LmChaC_{2b}

2.2.4.1. Leishmania major culture:

Leishmania major (Strain 5ASKH) promastigotes were regularly cultured in M199 media (Gibco) containing HEPES, adenine, penicillin-streptomycin, gentamycin and 10% fetal bovine serum. The newly cultured promastigotes were kept at 22°C for multiplication.

2.2.4.2. Construction of different types of cell lines of Leishmania major promastigotes:

A. Transfection in Leishmania major:

Respective construct was transfected in *L. major* by electroporation method. Late-log phase promastigote cells (10^8 cells) were spin down at 3000 rpm for 7 minutes (4°C) and washed two times in electroporation buffer. Then the pellet was resuspended in 300 μ l electroporation buffer and taken in a 0.2 cm chilled electroporation cuvette (Bio-Rad). Then, 20-30 μ g of DNA dissolved in 70 μ l buffer was added to the cells of the cuvette and kept for at least 10 minutes in ice. Finally, electroporation was performed at 450 V and 500 μ F by using Bio-Rad Gene Pulser apparatus. Then the electroporating cells were revived in 5 ml of Drosophila Schneider's media (Gibco) for overnight at 22°C in drug-free condition. Based on the drug-resistant cassette in respective constructs, recommended concentration of antibiotics was added in parasite containing M199 medium and kept at 22°C for another 7-10 days. Generation of different cell types was confirmed by either PCR or western blot.

B. Construction of *LmChaC* overexpression system in *L. major* (OE_{2a} and OE_{2b}):

Amplification of *LmChaC*_{2a} open reading frame was performed by using the primer 12 and 13 (**Table-6**). The entire ORF of *LmChaC*_{2b} was amplified by PCR using primers 14 and 15 (**Table-6**). The amplified products were separately cloned in pXG-B2863 plasmid between *Sma*I and *Bam*HI sites to generate full length *LmChaC*_{2a} and *LmChaC*_{2b}. Then recombinant pXG-B2863 plasmid containing *LmChaC*_{2a} or *LmChaC*_{2b} was transfected separately in *Leishmania major* by electroporation process and all the transfected cells were maintained in 200 µg/ml G418 solutions. Overexpressed clones were confirmed by Western blot analysis with rabbit anti-*LmChaC*_{2a} antibody or rabbit anti-*LmChaC*_{2b} antibody (1:100).

C. Construction of genetically modified T7/Cas9 expressing *L. major*:

Genetically modified T7/Cas9 expressing *L. major* was generated by transfecting *Pac*I digested linear pTB007 (Flag::NLS::Cas9::NLSNLS::T7 RNAP) fragment into the WT *L. major* cells. Cells were revived and maintained in M199 media (Gibco) supplemented with 10% FBS and hygromycin B (100 µg/ml) (Roche). *Pac*I digested pTB007 fragment was readily integrated in β-tubulin locus of the *L. major* for the stable expression of the T7 RNA polymerase as well as Cas9 proteins. Genetically modified *Leishmania major* cell line was identified by PCR technique by using Cas9 gene specific primer 5 and primer 6 (**Table-6**) (161,162).

D. Generation of stable knockout strain (*LmChaC*_{2a} + *LmChaC*_{2b})^{-/-} for both *LmChaC*_{2a} and *LmChaC*_{2b} alleles by CRISPR/Cas9 based editing:

CRISPR-Cas9 based gene editing was performed for knocking out both *LmChaC*_{2a} and *LmChaC*_{2b} genes in Cas9 expressing *L. major* (strain 5ASKH) promastigotes cells (**Fig.22**). By using LeishGEdit server (<http://leishgedit.net/>), primer sequences of both *LmChaC*_{2a} (LmjF.22.1190) and *LmChaC*_{2b} (LmjF.22.1200) genes were designed for knockout cell generation. Two repair cassettes containing the antibiotic puromycin-resistance genes and the blasticidin-resistance genes were amplified by PCR from pTPuro_v1 and pTBlast_v1 plasmid, respectively using 3% (v/v) DMSO, 15 ng pT plasmids, 0.2 mM dNTPs, 2 µM of primers 7 and primer 8 (**Table-6**), 1X High Fidelity reaction buffer and 1 unit Platinum[®] Taq DNA Polymerase High Fidelity (Invitrogen) in total 40 µl reaction mixture. PCR steps were initial denaturation at 98°C for 5 min then 40 cycles of 30 s at 98°C, 30 s at 65°C, and 2 min 15 s at 72°C and ultimately a final elongation step at 72°C for 7 min. Two sgRNA cassettes targeting 5' end of *LmChaC*_{2a} and 3' end of *LmChaC*_{2b} (5' and 3' sgRNAs templates) were amplified using 2 µM each of primer 9 (primer G00, sgRNA scaffold) (**Table-6**), 0.2 mM dNTPs, 2 µM of primer 10 (5' sgRNA primer of *LmChaC*_{2a}) or primer 11 (3' sgRNA primer of *LmChaC*_{2b}) (**Table-6**) and 1 unit Platinum[®] Taq DNA

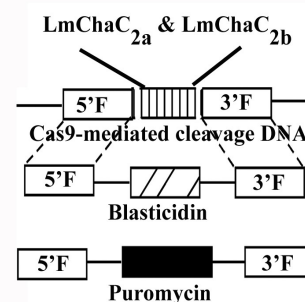


Fig.22: Schematic diagram showing CRISPR/Cas9 based *LmChaC*2 gene knock out technique and the plasmid constructs used for gene replacement. (Adapted from Das et al, J Biol Chem.2022 Sep 17; 298(11):102510)

Polymerase High Fidelity. PCR steps were initial denaturation at 98°C for 30 s followed by 35 cycles of 10 s at 98°C, 30 s at 60°C, and 15 s at 72°C and final elongation step at 72°C for 10 min. Molecular weight and purity of the PCR products were confirmed by using 1% agarose gel. Two PCR purified 5' and 3' sgRNAs templates and two drug cassettes were co-transfected at a time in a healthy log phase T7/Cas9 expressing *L. major* cells by electroporation technique. Bio-Rad Gene Pulsar apparatus were used for the electroporation at 450 V and 500 µF capacitance. Schneider's Drosophila Insect media (Gibco) were used to revive the transfected cell and kept at 22°C for 24 hrs. Then the revived cells were cultured in M199 media (Gibco) containing 15% FBS, 20 µg/ml puromycin dihydrochloride (Sigma-Aldrich), 100 µg/ml hygromycin B and 5 µg/ml blasticidin (Invitrogen) at 22°C (161,162).

E. Complementation of LmChaC_{2a} gene in KO mutant (CM_{2a}):

LmChaC_{2a} ORF was amplified by PCR using the forward primers 12 and reverse primer 13 (**Table-6**). The amplified product was cloned at the SmaI and BamHI site of pXG-B2863 plasmid and this recombinant plasmid was transfected into the LmChaC2 knockout cells. Transfected promastigotes were maintained in the presence of 200 µg/ml neomycin, 20 µg/ml puromycin and 5 µg/ml blasticidin at 22°C. CM_{2a} complementation was confirmed by measuring LmChaC_{2a} protein expression in Western blotting technique with rabbit anti-LmChaC_{2a} antibody.

F. Complementation of LmChaC_{2b} in knock out mutant (CM_{2b}):

LmChaC_{2b} ORF was amplified by PCR using primer 18 and primer 19 (**Table-6**). The amplified PCR product was cloned at BamHI site of pXG-PHLEO plasmid and this recombinant DNA was transfected into the null mutant cells. Transfected promastigotes were revived in Schneider's Drosophila Insect media and finally maintained in the M199 media containing FBS, 10 µg/ml phleomycin, 5 µg/ml blasticidin and 20 µg/ml puromycin at 22°C. CM_{2b} cell generation was confirmed by Western blot analysis with rabbit anti-LmChaC_{2b} antibody.

G. Complementation of both LmChaC_{2a} and LmChaC_{2b} genes in KO mutant (CM):

LmChaC_{2b}/pXG-PHLEO recombinant plasmids were transfected into the CM_{2a} cells. Transfected promastigotes were finally maintained in M199 media supplemented with FBS, 200 µg/ml neomycin, 10 µg/ml phleomycin, 5 µg/ml blasticidin and 20 µg/ml puromycin at 22°C. Western blot technique was performed for the confirmation of the generation of CM cells by measuring LmChaC_{2a} and LmChaC_{2b} expression.

2.2.4.3. Determination of physiological role of LmChaC_{2a} and LmChaC_{2b}:

A. Measurement of intracellular ROS:

Reactive oxygen species or ROS production was measured using CM-H2DCFDA (Invitrogen) by Flow cytometric analysis. CT, OE_{2a}, OE_{2b}, KO, CM_{2a}, CM_{2b} and CM cells (1 x 10⁷ promastigotes/ml) were washed two times with 1x PBS at 1200 g for 6 minutes. Then the cells were incubated with 6 µM of CM-H2DCFDA for 30 minutes in dark at 26°C with

mild shaking. The fluorescent intensity was measured immediately in the flow cytometer (BD LSR Fortessa) (Ex_λ-493nm; Em_λ-527nm for CM-H2DCFDA).

B. Measurement of intracellular calcium (Ca²⁺) level:

Intracellular Ca²⁺ concentrations were measured using Ca²⁺-specific fluorescent probe Fluo-4, AM (Invitrogen). CT, OE_{2a}, OE_{2b}, KO, CM_{2a}, CM_{2b} and CM cells (1x10⁷ cells/ml) were taken and washed two times using 1x PBS at 1200 g for 6 minutes and then the cells were incubated with 6 μM of Fluo-4, AM at room temperature for 60 min. Then the cells were pelleted and washed with fresh serum-free M199 medium and analyzed with flow cytometer (BD LSR Fortessa) (Ex_λ-494nm; Em_λ-506nm).

C. Cell viability analysis by flow cytometry:

Cell death was determined by propidium iodide (PI) fluorescence dye, which only permeable to non-living cells. Control, OE_{2a}, OE_{2b}, knockout, CM_{2a}, CM_{2b} and CM cells (1 x 10⁷ cells/ml) were taken and washed twice with 1x PBS and resuspended in 1x PBS containing 5 μg/ml of propidium iodide (Calbiochem) and kept at room temperature in the dark for 15 min. The stained cells were analyzed using flow cytometer (Ex_λ-488nm; Em_λ-617nm).

D. Promastigotes growth profile analysis:

10⁶ mid-log phase control, overexpressed, knockout, and complement cells were cultured in 10 ml of M199 medium supplemented with 10% FBS to evaluate the growth profiles of different types of cell line. In an upgraded Neubauer chamber (hemocytometer), cell counts were performed every 24 hours to determine growth rates. On the other hand, 10⁶ mid-log phase promastigotes were inoculated in 5 ml of sulphur deficient M199 media (Himedia-AT1076) supplemented with 10% FBS in presence or absence of reduced glutathione/GSH or N-acetyl cysteine/NAC (Sigma) and determine the growth profile of different cell types in sulphur deficient media.

E. Intracellular glutathione measurement by flow cytometry:

Intracellular glutathione level was evaluated by intracellular glutathione (GSH) Detection Assay Kit (Abcam). 10⁶ different types of cells were taken and washed twice with 1x PBS at 1200 g for 6 minutes. Then add 5 μl of 200X Thiol Green Dye into the 1 ml of cell solution and incubate the cells for 15 minutes at 22°C. Excess dye was removed by centrifuging the cells at 1000 rpm for 4 minutes and then re-suspends the cells in 1ml of assay buffer. Fluorescence intensity was measured by flow cytometer (Ex_λ-490nm; Em_λ-525nm).

F. Determination of intracellular trypanothione level by HPLC:

2x10⁸ promastigotes were collected and washed twice with Dulbecco's PBS. To achieve complete cell lysis, cells were then resuspended in 200 μl of extraction buffer (100 mM HCl and 1 mM EDTA) and subjected to 5 minutes of sonication with vortexing every 30 seconds followed by freeze thaw cycle for twice. The samples were centrifuged at 13000 g for 10

mins at 4°C and then Millipore 0.22 µm filter paper was used to filter the supernatant. A 2% (v/v) aqueous solution of perchlorate was used as the mobile phase, and a 40 µl sample was injected into the HPLC analysis using a C18 HPLC column (Sunfire™ C18, 5 µm, 4.6 x 250 mm Column, Waters) with a 1 ml/min flow rate at 210 nm. Peak of trypanothione were appeared at 52 mins. Trypanothione were identified with authentic standards. The intracellular concentration of trypanothione was measured from standard curve.

G. Infection assay:

CT, OE_{2a}, OE_{2b}, KO, CM_{2a}, CM_{2b} and CM promastigotes cells were used to infect a murine macrophage cell-line RAW 264.7 as well as BALB/c mice.

i) In-vitro murine macrophage infection:

Promastigotes of different LmChaC variant cell lines were used to infect murine macrophage cell line RAW 264.7 adhered on glass coverslips (2x10⁶ macrophages/coverslip) in 0.5 ml of RPMI 1640/10% FBS at a 10:1 parasite to cell ratio for 2 hours for determination of parasite entry and more than 6 hours for the evaluation of intracellular parasite numbers. Unphagocytosed parasites were eliminated following incubation by washing with media and cells were then resuspended in RPMI 1640/10% FBS at 5% CO₂, 37°C. After 6 hours of incubation, the cultures were placed to a CO₂ incubator at 37°C for infection periods of 12, 24, and 48 hours. Then the cells were fixed in a methanol solution and stained with propidium iodide dye. Finally cells were visualized and quantified using Olympus IX81 microscope.

ii) In-vivo mice (BALB/c) infection:

For in vivo cutaneous infection analysis, 4-6 weeks old female BALB/c mice (10 mice/group) were subcutaneously injected in left hind footpad with 5 x 10⁶ stationary phase CT, OE_{2a}, OE_{2b}, KO, CM_{2a}, CM_{2b} and CM promastigotes. Daily caliper measurements of footpad swelling were used to track the development of the disease.

iii) Parasite loads in the footpad of infected mice:

Parasite loads in the left footpad of mice with different variants of LmChaC2 cell lines were measured by limiting dilution assay. Initially footpad tissue were weighted and readily immersed in a serum free M199 media. After the homogenization of the tissue in the media, cell suspension was centrifuged at 500 rpm to remove the tissue debris. Then supernatant was collected and centrifuged at 4000 rpm for 20 mins to pellet down the cells. M199 medium supplemented with 40 mM HEPES (pH 7.4, Sigma), 200 µM adenine (Sigma), 1% penicillin–streptomycin, 50 µg/ml gentamycin and 15% heat-inactivated FBS was used to dissolve the pellet. A flat-bottomed 96-well tissue culture plate was used to serially dilute each tissue homogenate in the same medium. The number of viable

parasites per mg of tissue was calculated from the highest dilution in which promastigotes could be grown after 10 to 15 days of initial incubation at 22°C.

H. Determination of LmChaC_{2a} and LmChaC_{2b} mRNA expression in promastigotes as well as amastigotes:

Semi-quantitative reverse transcriptase PCR was used to measure the LmChaC_{2a} and LmChaC_{2b} mRNA expression in promastigote and amastigote *L. major* cells. Total cellular RNA was extracted from the parasites using TRIzol reagent according to the manufacturer's protocol. cDNA synthesis from this isolated RNA was then performed using PrimeScript 1st cDNA Synthesis Kit (Takara). LmChaC_{2a} was amplified by PCR using primers 1 and primer 2 (**Table-6**) to get a 714-bp fragment. The entire ORF of LmChaC_{2b} was amplified by PCR analysis using primers 3 and primer 4 (**Table-6**) to get a 972-bp fragment.

I. Measuring LmChaC_{2a} and LmChaC_{2b} mRNA level in presence of H₂O₂ and tunicamycin:

Real time PCR was used to determine the LmChaC_{2a} and LmChaC_{2b} expression in promastigote after treatment of H₂O₂ and tunicamycin. Isolation of total RNA and cDNA synthesis were performed using TRIzol reagent (Invitrogen) and PrimeScript 1st cDNA Synthesis Kit (Takara), respectively. Real-time quantitative PCR was performed on the StepOne™ Real-Time PCR system (ABI) using Power SYBR™ Green PCR Master Mix (ABI) and primers 20 and 21 or primer 22 and 23 (**Table-6**). By employing 18S rRNA as the endogenous control, the comparable CT method was used to quantify the mRNA.

2.2.5. Statistical analysis:

All the results were verified by at least three independent experiments and expressed as mean ± SD. By using Student's t test or analysis of variance (ANOVA) parametric data was statistically analyzed with the help of Origin 7.0 software (Microcal software, Inc. Northampton, MA, USA). The ANOVA was followed by the evaluation of the difference between individual groups using post hoc analysis (multiple comparison t test). A p value of < 0.05 was considered statistically significant.

*“Even if the open windows of science at first
make us shiver...in the end, the fresh air brings
vigor and the great spaces have a splendor of
their own.”*

- Bertrand Russell

Results

CHAPTER 1

“Cloning, expression, purification and enzyme kinetics of LmChaC2 proteins from *Leishmania major*”

RESULTS (Chapter 1)

“Cloning, expression, purification and enzyme kinetics of LmChaC2 proteins from *Leishmania major*”

<i>3.1.1. Background</i>	44
<i>3.1.2. Sequence alignment and nomenclature of LmChaC proteins</i>	44
<i>3.1.3. Expression of LmChaC_{2a} and LmChaC_{2b} protein in E. coli</i>	45
<i>3.1.4. Analysis of enzyme kinetics by HPLC</i>	46
<i>3.1.5. Substrate specificity of LmChaC2</i>	47
<i>3.1.6. Discussion</i>	47

3.1.1. Background

32.8 Mb genomic data of *Leishmania major* Friedlin was fully sequenced and published in 'Science' journal in the year 2005. The complete genome sequence of *L. major* is now widely available and creating new possibilities to uncover as well as thorough functional investigation of several genes that encode important proteins (163). Almost all the higher eukaryotes maintain the redox homeostasis by controlled synthesis and degradation of glutathione, so glutathione plays a vital role in this condition. However in trypanosomatids, a unique redox molecule named trypanothione plays the main function of redox balance instead of glutathione. This may be due to the lack of selenium-containing glutathione peroxidase, catalase and glutathione reductase in these parasites (70). The presence of trypanothione reductase(TR)/trypanothione system in kinetoplastids provides them a unique oxidative stress removing pathways even in the oxidative burst during the infection to the host (164). Although trypanothione plays the main role of redox balance, glutathione is a very important player in this pathway because two molecules of glutathione are necessary for the formation of one molecule of trypanothione. Enzymes related to glutathione synthesis pathway are well studied in many organisms such as γ -glutamylcysteine synthetase and glutathione synthetase which are ubiquitous to the entire kingdom for the synthesis of glutathione (165). Similarly, different types of glutathione degradation enzymes are reported in many organisms such as γ -glutamyl transpeptidase, DUG enzyme, ChaC1 and ChaC2 enzyme and highly catalytic RipAY enzyme (90). Until now, no glutathione degradation enzymes have been described in the literature in any trypanosomatids. In the genomic database of *Leishmania major*, we found two putative ChaC-like proteins in the tandem array related to glutathione degradation pathway. Enzymes related to degradation of glutathione might play an important role in maintaining the trypanothione level as well as the redox balance, which could be vital for the cell survivability. Therefore, having a better grasp of biochemical and physiological significance of this gene product would be enlightening the whole glutathione metabolism as well as redox system in the trypanosomatids parasite. These genes were selected for the present research keeping this background in mind.

3.1.2. Sequence alignment and nomenclature of LmChaC proteins:

In the *Leishmania major* genome database (<https://tritrypdb.org>), two tandem array of putative LmChaC sequences have been identified as open reading frames. Systemic name of these ORFs are LmjF.22.1190 and LmjF.22.1200 with 714 bp and 972 bp gene sequence respectively. 714 bp DNA sequence has the potential to encode comparatively shorter 237 amino acids residue ChaC-like protein, whereas 972 bp DNA sequence can encode comparatively longer 323 amino acids residue ChaC-like protein. Multiple sequence alignment with human ChaC1 and ChaC2 proteins reveals that comparatively shorter version of 237 amino acids ChaC-like sequence bears 32% and 40% identity with human ChaC1 (HsChaC1) and ChaC2 (HsChaC2) respectively, whereas longer version of 323 amino acids ChaC-like sequence have 35% and 45% sequence homology with human ChaC1 and human ChaC2 amino acids sequences respectively. Moreover, the presence of YGSL/I signature motif and catalytic glutamic acid (E) residue in both the *Leishmania major* ChaC-like

proteins indicating that both the proteins are the members of ChaC family of γ -glutamyl cyclotransferase (**Fig.23**). As we found more sequence identity with the human ChaC2 (40% for shorter and 45% for longer amino acids sequence), the shorter variant of 237 amino acids sequence protein is referred as LmChaC_{2a} and longer version of 323 amino acids sequence is named as LmChaC_{2b}.

3.1.3. Expression of LmChaC_{2a} and LmChaC_{2b} protein in E. coli:

In order to identify the biochemical characteristics of both leishmanial ChaC2 proteins, LmChaC_{2a} and LmChaC_{2b} proteins were expressed in BL21 *E. coli* cells and C41 *E. coli* (generally used to express toxic protein) cells, respectively. Using Ni²⁺-NTA column,

```

LmChaC2a -----MSSSS 5
LmChaC2b -----MPKTDTDVSAHHHYGTHQPPTGGSTPASHVAASLPKLLPAQPELPHQH 48
HsChaC1 MGGAQLELPSGARPGVCVRRSFRAHAGDQPRRPPGPIPVPG----TMKQESAAPNTPPTS 56
HsChaC2 -----0

LmChaC2a ELVTRATHYHEQFGLPSFDDRVFVVFYGSILWKQNFEDAEYEAYIKGYKRVFYQGSRD 65
LmChaC2b STETASTRYHEQFGLPSFDDHVFVVFYGSILWKQNFEDAEYEAYIKGYKRVFYQGSRH 108
HsChaC1 QS----PTPSAQFPRNDGDPQALWIFGYGSLVWRPDFAYSDSRVGFVRGYSRRRFWQGDTF 112
HsChaC2 -----MWVFGYGSILWKVDFPYQDKLVGYITNYSRRRFWQGSTD 38
          : :*****: : * : . . . : : . * * : ** .

LmChaC2a HRGVDPKPGRVVTLTLLPSEDKEQRVYKAYQLPADPEKLNRI FQALDVRE--KGGYERL FV 123
LmChaC2b HRGVDPKPGRVVTLTLLPSEDKEQRVYKAYQLPADPEKLNRI FQALDVRE---GGYDRVQL 165
HsChaC1 HRGSDKMPGRVVTLL--EDHEGCTWGVAYQVQGEQVSKA--LKYLNVREAVLGGYDTKEV 168
HsChaC2 HRGVDPKPGRVVTLV--EDPAGCVWGVAYRLPVGKEEEV--KAYLDFRE--KGGYRTTIV 92
          ***      *****: **      . : * * * : : . * : * * * : * * * :

LmChaC2a TIYDAHPSFATDGEDRP-----LRLA 144
LmChaC2b TLFNAHPTTGNLTTT PMLPAPMSKSFKIESSTQYVPPPRQNSSDVEAGVAEKVLDIFSHP 225
HsChaC1 TFYPQDAP-----176
HsChaC2 IFYPKDPT-----100
          : :

LmChaC2a DKGTGTPGKAMVCLCYNATEDNADYLGPATMEAMARQILSSTGLSGPNREYLYNLDRLR 204
LmChaC2b NAPAVQPRKNVYLCYIATEQNEGYVGEASMEEMAAEILSCAGVSGSNREYLFLLADCLR 285
HsChaC1 -----DQPLKALAYVATPQNPGYLGPAPEEAIATQILACRGFSGHNLEYLLRLADFMQ 229
HsChaC2 -----TKPFSVLLYIGTCDNPDYLGPALEDIAEQIFNAAGPSGRNTEYLFELANSIR 153
          : . * * . * : * . * * * * * : * : * : . * * * * * * * : :

LmChaC2a DMGA--ADPHVFELAALARQLEVECPA VIC--SEKK-I---- 237
LmChaC2b AMGA--TDPHVFELDAVAKRILRGREAEFA--AGAKRVATMA 323
HsChaC1 LCGPQAQDEHLAAI VDAVGTM-----LPCFCPTEQALALV- 264
HsChaC2 NLVPEEAEHLFALEKLVKERLEGGKQNLNCI-----184
          * * : : .

```

Fig.23: Sequence analysis of ChaC family of γ -glutamyl cyclotransferases from *Leishmania major*. Amino acid sequence of LmChaC_{2a} and LmChaC_{2b} were aligned with human ChaC1 and ChaC2. * indicates identical residue. Dashes indicate variations in sequence length among aligned proteins. Underline denotes active site residues. (Adapted from Das et al, J Biol Chem.2022 Sep 17; 298(11):102510)

recombinant LmChaC_{2a} and LmChaC_{2b} proteins with six-histidine tag at C and N- terminal respectively was purified. As 250 mM imidazole was used to elute the purified protein, this high concentration of imidazole was eliminated by overnight dialysis process. Lastly gel

filtration chromatography was performed to remove any contamination like degraded protein or bacteria derived protein. Purified recombinant LmChaC_{2a} and LmChaC_{2b} protein migrated to the position of 28 kDa and 38 kDa respectively in the SDS-PAGE as expected from theoretical molecular weight (**Fig.24**).

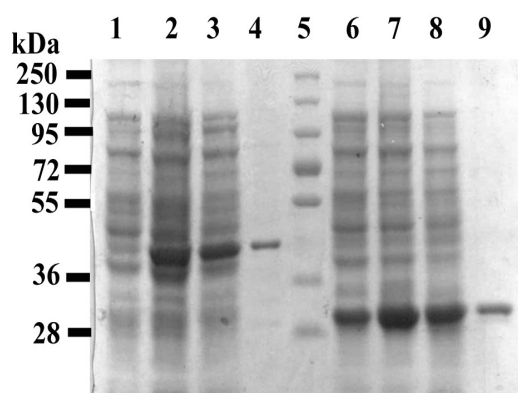


Fig.24: Purification of LmChaC_{2a} and LmChaC_{2b} protein. (A) SDS-PAGE. Lanes: 1, -isopropyl β -D-1-thiogalactopyranoside (without IPTG) (LmChaC_{2b}); 2, with IPTG (LmChaC_{2b}); 3, lysate (LmChaC_{2b}); 4, LmChaC_{2b} purified protein; 5, molecular weight marker; 6, without IPTG (LmChaC_{2a}); 7, with IPTG (LmChaC_{2a}); 8, lysate (LmChaC_{2a}); and 9, purified (LmChaC_{2a}). (Adapted from Das et al, J Biol Chem.2022 Sep 17; 298(11):102510)

3.1.4. Analysis of enzyme kinetics by HPLC:

High performance liquid chromatography (HPLC) was used to evaluate the enzymatic activity of LmChaC2 proteins after the injection of assay mixture. The assay mixture contained 50 mM Tris-HCl (pH 8), substrate (different γ -Glu-dipeptides, GSH, GSSG or T(SH)₂) and enzyme (LmChaC_{2a} or LmChaC_{2b}). This assay mixture was incubated at various time points till 60 min with different substrate concentration at 37°C. Presence of an active enzyme in the assay mixture was determined by the disappearance of substrate peak and appearance of new product peaks. γ -glutamyl cyclotransferase enzymes catalyze the degradation of γ -glutamyl amino acid to produce 5-oxoproline and amino acid (133). HPLC data showed the degradation of GSH by LmChaC family proteins to produce 5-oxoproline, which confirms the γ -glutamyl cyclotransferase activity of these proteins. Their γ -glutamyl cyclotransferase activity was determined by quantifying the concentration of 5-oxoproline (**Fig.25A**). LmChaC mediated GSH degradation also produces Cys-Gly dipeptide along with 5-oxoproline. The kinetic analysis of LmChaC_{2a} or LmChaC_{2b} proteins showed that both the proteins followed the typical Michaelis-Menten enzyme kinetics toward the substrate (GSH). The initial velocity of LmChaC_{2a} or LmChaC_{2b} was evaluated at 5 min or 2 min of incubation period, respectively (**Fig.25, B and C**). The Michaelis-Menten constant (K_m) and turnover number (k_{cat}) was calculated from different time dependent and substrate dependent kinetics measurements. K_m values of LmChaC_{2a} protein (1.75 ± 0.08) were similar to LmChaC_{2b} (2.0 ± 0.15 mM) for GSH, which were comparable to mouse as well as human ChaC proteins (111). Albeit the K_m value of LmChaC_{2a} is very similar to LmChaC_{2b}, catalytic efficiency of the former is ~ 17 -fold lower than the latter, as $k_{cat} = 0.9 \pm 0.1$ s⁻¹ for LmChaC_{2a} and $k_{cat} = 15 \pm 1.8$ s⁻¹ for LmChaC_{2b}.

3.1.5. Substrate specificity of LmChaC2:

To assess the substrate specificity of both LmChaC2 proteins towards different γ -Glutamyl-dipeptides, GSSG, GSH and T(SH)₂; we measured the 5-oxoproline concentration for estimation of γ -glutamyl cyclotransferase activity (Fig.26). HPLC data suggested that both the LmChaC2 proteins actively cleaved reduced glutathione (GSH), but they showed no such activity toward any γ -glutamyl peptides includes γ -Glu-amino acids (γ -Glu-Cys, γ -Glu- ϵ -Lys etc.), oxidized glutathione (GSSG) or T(SH)₂ (Fig.27).

3.1.6. Discussion

This chapter illustrates two putative ChaC family of γ -glutamyl cyclotransferase proteins, which are the first reported enzymes in glutathione degradation pathway from entire trypanosomatids group. Homology alignment of LmChaC_{2a} and LmChaC_{2b} with human ChaC1 and ChaC2 suggested that both proteins shared more homology with human ChaC2 enzymes compare to human ChaC1. Similar to human ChaC protein, leishmanial ChaC2 proteins contains YGSL/I motif and glutamate residue for cyclotransferase activity (111,134).

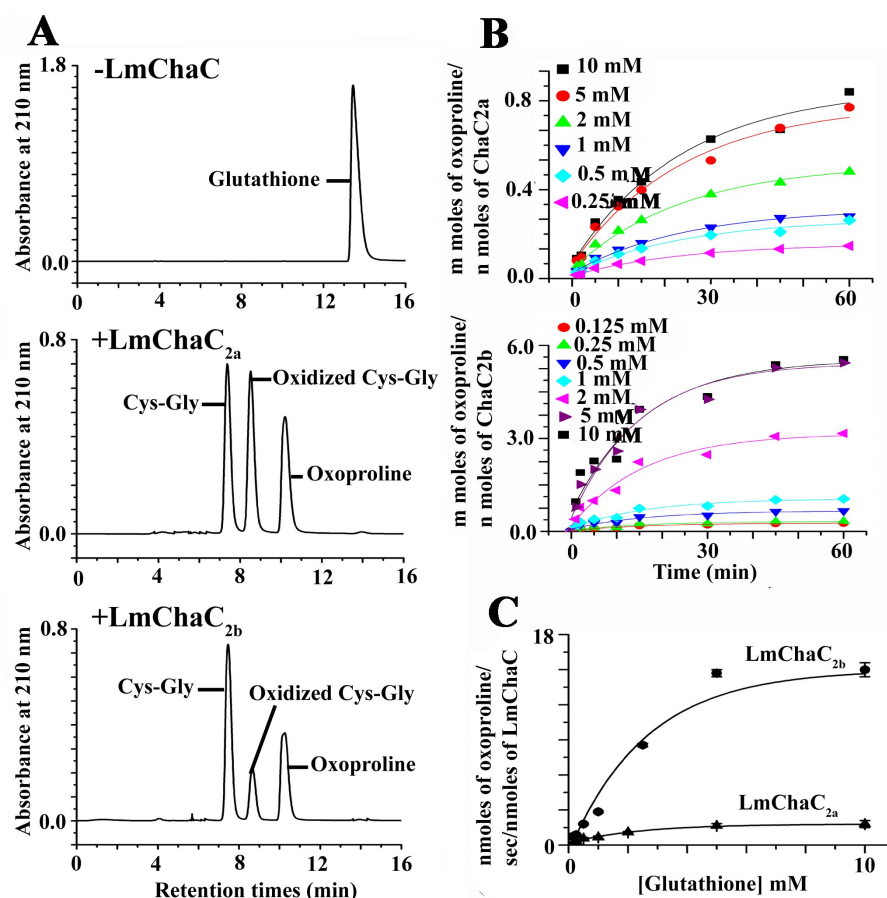


Fig.25: Biophysical characteristics of LmChaC2 proteins. A. LmChaC2 proteins show enzymatic activity specifically towards GSH to produce 5-oxoproline and Cys-Gly. Assay mixture was incubated and analyzed using HPLC on a Sunfire™ C18 column (5 μ m 4.6 x 250 mm, Waters) and a mobile phase of 2% (v/v) aqueous perchloric acid at 1.0 ml/min flow rate. B. Velocity of LmChaC2 enzyme catalyzed GSH degradation. 100 μ g of LmChaC_{2a} or 10.0 μ g of LmChaC_{2b} were incubated in 1.0 ml of 50 mM Tris-HCl buffer (pH-8) at 37°C with different concentration of glutathione. At various time points, 100 μ l aliquots were taken up from the assay mixture and were deactivated by heat denaturation at 95°C for 5 mins. Samples were centrifuged for 30 min at 14000 rpm to remove inactivated proteins before HPLC (Waters) analysis. All data are fitted to a hyperbolic curve. C. Oxoproline production dependent on the substrate GSH. All values were derived from time dependent oxoproline production curve at different concentration of GSH. The initial velocity of LmChaC_{2a} and LmChaC_{2b} was evaluated within 5 mins and 2 mins of incubation period, respectively. (Adapted from Das et al, J Biol Chem. 2022 Sep 17; 298(11):102510)

Enzyme kinetics indicates that both ChaC-family of γ -GCT enzymes are GSH specific and could not able to degrade other γ -glutamyl peptides like human ChaC protein. Kinetic studies also suggested that LmChaC_{2b} protein degrade the GSH \sim 17 fold more efficiently than

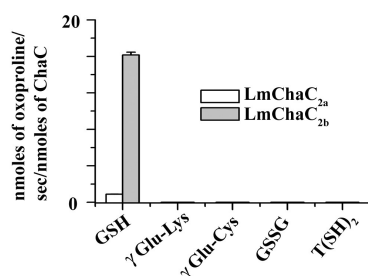


Fig.26: LmChaC activity in the presence of different γ -glutamyl dipeptides, GSSG and T(SH)₂. 5-oxoproline production indicates the breakdown of the substrate due to the γ -glutamyl cyclotransferase activity of these proteins. The concentrations of GSSG, T(SH)₂, γ -Glu- Cys, γ -Glu- Lys, LmChaC_{2a} and LmChaC_{2b} used were 10 mM, 10 mM, 10 mM, 10 mM, 10 μ g, and 1.0 μ g, respectively. (Adapted from Das et al, J Biol Chem. 2022 Sep 17; 298(11):102510)

LmChaC_{2a} and on the other hand, in case of human, ChaC1 shows \sim 10-20 fold high catalytic efficiency than ChaC2 (110). The Km values of *Leishmania* ChaC2 proteins for glutathione are comparable with mammalian ChaC protein. With respect to the intracellular GSH concentrations (0.39 mM in amastigotes stage and 0.21 mM in promastigotes), our experiment derived Km values for recombinant LmChaC2 proteins are high (166). The possible explanation is that either the Km values of the LmChaC2 proteins in the intracellular milieu may be lower than the experimental values or the previous determinations of intracellular glutathione concentrations may not be sufficiently reliable. In case of eukaryotic cells, the main GSH reservoir is cytoplasm (\sim 90%) whereas mitochondria (10%) and

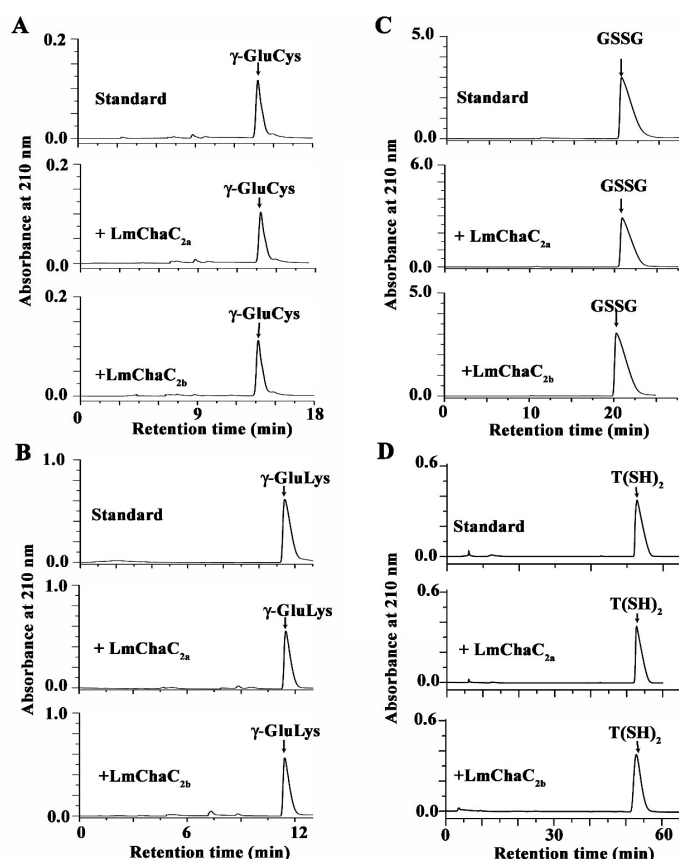


Fig.27: LmChaC2-catalyzed γ -glutamyl cyclotransferase activity for γ -Glu-Cys (A), γ -Glu- ϵ -Lys (B), GSSG (C) or T(SH)₂ (D). The mixture was incubated at 37°C for 1 hr. Then the reactions were deactivated by heat denaturation at 95°C for 5 min. Samples were centrifuged for 30 min at 14000 rpm to remove all the inactivated proteins before HPLC (Waters) analysis. 20 μ l samples were injected to the HPLC system on a SunfireTM C₁₈ column (5 μ m 4.6 x 250 mm, Waters) and a mobile phase of 2% (v/v) aqueous perchlorate at 1.0 ml/min. (Adapted from Das et al, J Biol Chem. 2022 Sep 17; 298(11): 102510)

endoplasmic reticulum (ER) also serves as a minor reservoir. This could be the main reason behind the presence of mammalian ChaC protein (GSH specific γ -glutamyl cyclotransferase) in the cytosol (85).

Two products - cysteinyl-glycine and 5-oxoproline are created by the ChaC mediated degradation of GSH; in case of the host this product may be further degraded to yield free amino acids by 5-oxoprolinase and Cys-Gly peptidase. Two such enzymes are also found in *Leishmania* genome, a) putative 5-oxoprolinase (LmjF.18.1040) that transforms the cyclic form of glutamate or 5-oxoproline to glutamate and b) leishmanial putative M20/M25/M40 family di-peptidase (LmjF.33.1610) that cleaves cysteinyl-glycine to form free cysteine and glycine.

Since not any GSH degradation enzyme has been characterized in trypanosomatids, after physical characterization we were focused to explore the physiological importance of LmChaC2 proteins in *Leishmania major*. We uncovered the expression pattern of either LmChaC2 proteins for physiological characterization as well as in which condition these proteins are expressed within the parasites. Then in order to further characterization, we generated overexpressed, knockout and complement construct of LmChaC2 in vivo. The functional characterization of LmChaC_{2a} or LmChaC_{2b} proteins for understanding physiological relevance is discussed in the next chapter.

CHAPTER 2

**“Intracellular Expression and
physiological significance of
LmChaC2 proteins in *Leishmania
major*”**

RESULTS (Chapter 2)

“Intracellular expression and physiological significance of LmChaC2 proteins in *Leishmania major*”

3.2.1. Background	52
3.2.2. Expression of LmChaC2 at different life stages	53
3.2.3. Expression of LmChaC2 under different stressed condition	53
3.2.4. CRISPR/Cas9 mediated gene replacement of LmChaC2 alleles	55
3.2.5. Variation in LmChaC2 expression in various cell lines	55
3.2.6. Comparative analysis of intracellular GSH and T(SH)₂ content	55
3.2.7. Comparative study of oxidative stress among different cell lines	56
3.2.8. Cell viability in late log phase cell lines	57
3.2.9. Comparative studies of metacyclogenesis among cell lines	58
3.2.10. Variation in the expression of antioxidant gene LmAPX in different cell lines	58
3.2.11. Discussion	59

3.2.1. Background

In the eukaryotic system, GSH plays numerous functions to maintain cell integrity. Although glutathione plays all these important physiological roles, excessive level of GSH can also have detrimental effect on the cells. So redox balance should be maintained for the survival of a cell which could be achieved by means of glutathione synthetase, glutathione reductase, glutathione peroxidase, thioredoxin reductase and different GSH degradation enzymes in the higher eukaryotic cells. γ -glutamyl transpeptidase is a major glutathione degradation enzyme in eukaryotic system through its transpeptidation activity transfer the γ -glutamyl group to amino acid to yield γ -glutamyl amino acids and cysteinyl-glycine. Moreover, γ -GCT reacts with several γ -glutamyl amino acids to form amino acids and 5-oxoproline whereas γ -glutamylamine cyclotransferase (GGACT) reacts with the γ -glutamyl amine to yield amines and 5-oxoproline (133,167). Recently identified ChaC1 and ChaC2 proteins in mammals also have a major role in the breakdown of GSH and direct production of 5-oxoproline and Cys-Gly. In the mammalian host cells, ChaC2 protein is expressed in a constitutive manner whereas ChaC1 protein expression is depend on the endoplasmic reticulum (ER) stress or sulfur limitation conditions (110,111,134).

In the trypanosomal parasites, although major eukaryotic thiol redox homeostasis systems (thioredoxin/TrxR and GSH/GR systems) are absent but a unique redox metabolism pathway is developed in the parasite and this is achieved by low-molecular weight di-thiol trypanothione [bis(glutathionyl) spermidine] or T(SH)₂ and trypanothione reductase (164,168,169). Albeit the GSH/glutathione reductase system is absent *Leishmania*, most of the GSH is recruited for the formation of bis(glutathionyl) spermidine or trypanothione. So affecting the GSH related enzyme could have the direct effect on the trypanothione level and subsequent redox level.

Leishmania is a digenetic parasite, with two life stages amastigote and promastigote lived in two hosts human and sandflies respectively. Amastigotes are colonized in the acidic phagolysosomal compartment (pH 5.6) of the macrophages. Again promastigote stage has two distinct morphology within the sandfly vector; one is replicating and non-infective procyclic promastigotes and second is non-replicating and highly infectious metacyclic promastigotes (48). The transformation from procyclic to metacyclic is associated with an enhanced capacity for infection and survival within the mammalian host, where the host immune system is trying to destroy the parasite (170). During this cell differentiation, several morphological as well as chemical changes are observed: long flagella, elongated shape, smaller cell size, increased expression of LPG (lipophosphoglycan) and gp63 surface protease (171,172). A greater ability to survive within the macrophage is the defining feature of this development. Albeit several genes related to this transformation have been identified, still the exact molecular regulatory mechanisms remain unclear.

Leishmanial GSH degradation enzymes LmChaC_{2a} and LmChaC_{2b} proteins were first time successfully cloned, expressed and biochemically characterized. Naturally, the next focus was on the determination of physiological significance of these proteins. In order to achieve the goal; regulation of both the proteins in the *Leishmania* parasites was observed in different condition and generated overexpressed cell line of both the proteins (OE_{2a} and OE_{2b}), double knockout cell lines (KO) and complement cell lines (CM_{2a}, CM_{2b} and CM). Regulation of

these proteins was estimated by means of different stress inducer and conditions. Additionally, comparative studies of reactive oxygen species concentration and calcium level were performed. Then cell differentiation and cell viability in different types of cells as well as expression level of the antioxidant protein in different types of *L. major* cells is discussed in this chapter.

3.2.2. Expression of *LmChaC2* at different life stages:

To determine whether either of the GSH degrading enzymes (*LmChaC2_a* or *LmChaC2_b*)

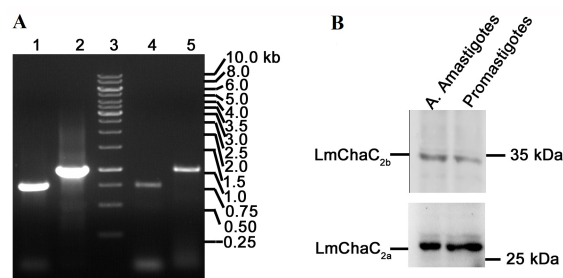


Fig.28: Expression of *LmChaC2_a* and *LmChaC2_b* in mRNA and protein level in the promastigotes as well as amastigotes stages of *Leishmania* parasite. (A) Agarose gel of PCR-amplified DNA from the cDNA of *LmChaC2_a* and *LmChaC2_b*. Lane 1 and 2, PCR amplified products of promastigote parasites with *LmChaC2_a* and *LmChaC2_b* specific primers, respectively, Lane 3 molecular marker, Lanes 4 and 5, PCR amplified products from intracellular amastigotes with *LmChaC2_a* and *LmChaC2_b* specific primers, respectively. (B) The whole cell lysate of promastigote parasites and axenic amastigotes (A. Amastigotes) stages of *Leishmania major* were used for Western blotting analysis. 200 µg of proteins was used as a sample for Western blotting analysis. Rabbit anti-*LmChaC2_a* and anti-*LmChaC2_b* antibody are used in Western blot analysis. (Adapted from Das et al, J Biol Chem.2022 Sep 17; 298(11):102510)

expression are particular life-cycle stage specific or it is expressed throughout all life stages, we performed semi-quantitative PCR and Western blot experiments. Semi-qPCR data from amastigotes derived from *Leishmania* infected mice and promastigotes reveals that the band of both the genes (*LmChaC2_a* and the *LmChaC2_b*) were appeared in the agarose gel (**Fig.28A**). Then Western blot experiments from axenic amastigotes and promastigotes confirmed that both *LmChaC2_a* and *LmChaC2_b* were expressed in both amastigotes and promastigotes stages (**Fig.28B**). Then to identify the intracellular expression profile of *LmChaC2_a* or *LmChaC2_b* throughout different phases of promastigote stages, real time quantitative PCR (qRT-PCR) and Western blot analysis was performed (**Fig.29, A and D**). These data suggested that *LmChaC2_a* expression level remains unchanged throughout all phases, whereas expression of *LmChaC2_b* was significantly increased (~1.5

fold) during stationary phases but did not changed significantly during lag and log phases of promastigote stages.

3.2.3. Expression of *LmChaC2* under different stressed condition:

In human *ChaC1* protein is induced under stress condition such as ER stress and sulfur-limited stress, whereas *ChaC2* protein is constitutively expressed (111,134). To determine the constitutive or inducible expression pattern of either *LmChaC2* proteins within parasites, different stress inducing agent such as tunicamycin, which is an ER stress inducer and H_2O_2 , which is an oxidative stress inducing agent were used to treat the *Leishmania* parasite. Unlike human, qRT-PCR and Western blot data suggested that even after the treatment of 1 mM of tunicamycin for about 1 hour could not significantly influence either *LmChaC2_a* or *LmChaC2_b* protein expression in the parasites (**Fig.29, B and D**). Even after the treatment of

maximum 2 mM H₂O₂ for 4 hrs could not still influence the expression level of either

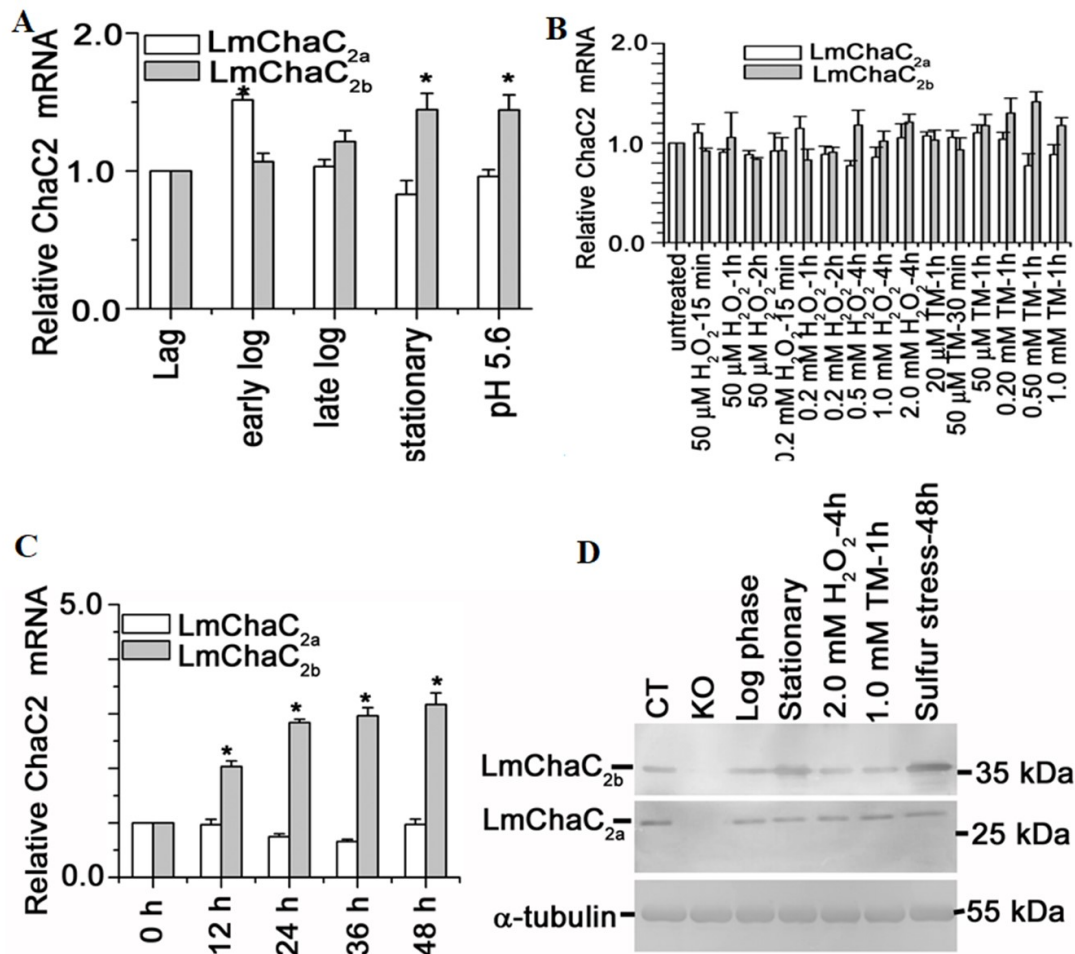


Fig.29: LmChaC2 expression under different conditions. (A) The measurement of mRNA abundance was determined using quantitative real-time PCR at different stages of growth of the promastigotes. pH 5.6 denoted that the stationary phase promastigotes those were incubated for 24 h at acidic pH 5.6 (pH of phagolysosome). (B) The quantification of mRNA abundance in the promastigote stage of parasites was determined by qRT-PCR in presence of H₂O₂ as oxidative stress inducer and ER stress inducer-tunicamycin. (C) The measurement of mRNA transcript in the promastigote stage of parasites, which were incubated at sulphur deficient media for 12, 24, 36 and 48 hrs. (D) Gene expression was determined by Western blot analysis in presence of sulfur limited media (48 h), H₂O₂ (2 mM for 4 hrs) or tunicamycin (1 mM for 1 h). All the data are representative of at least three independent experiments. (Adapted from Das et al, J Biol Chem.2022 Sep 17; [298\(11\):102510](#))

protein. GSH act as a sulfur reservoir within the cells and its degradation provides sulfur to the cells. Therefore, we investigated the impact of sulfur-deficient media upon the expression of either LmChaC2 proteins. qRT PCR data reveals that LmChaC_{2b} transcription level was significantly increased up to 3.5 folds after 48 hrs of incubation of the *Leishmania* in sulfur limited media. On the other hand, LmChaC_{2a} mRNA levels did not alter significantly (**Fig.29C**). Western blotting data confirmed that LmChaC_{2b} protein expression level was significantly elevated after 48 hrs incubation but LmChaC_{2a} expression level remains unaltered (**Fig.29D**). These findings suggest that LmChaC_{2a} expression was constitutive, whereas LmChaC_{2b} expression was sulfur stress-dependent.

3.2.4. CRISPR/Cas9 mediated gene replacement of *LmChaC2* alleles:

To investigate the precise physiological function of *LmChaC_{2a}* and *LmChaC_{2b}* in *Leishmania* parasites, CRISPR/Cas9 genome editing method was employed for knocking out the genes (**Fig.22**). *LmChaC_{2a}* and *LmChaC_{2b}* knockout strain was prepared in the previously

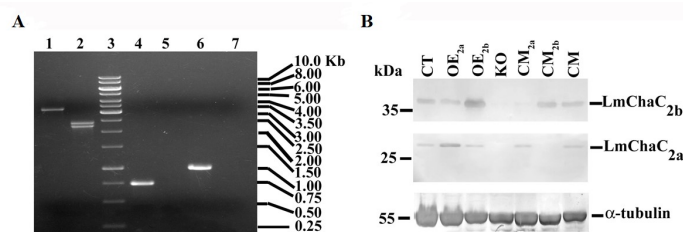


Fig.30: Generation of stable knockout parasite for both *LmChaC_{2a}* and *LmChaC_{2b}* alleles by CRISPR/Cas9 based editing. (A) Agarose gel of PCR amplified DNA for *LmChaC_{2a}* and *LmChaC_{2b}* genes. Lanes 1/4/6 and 2/5/7 represent PCR with gDNA from wild type and KO parasite respectively with external primers 16 and 17 (5' and 3' flanking region) (lanes 1-2) for both genes, with internal primer of *LmChaC_{2a}* gene (lanes 4-5) and *LmChaC_{2b}* gene (lanes 6-7). The expected size of *LmChaC_{2a}*-*LmChaC_{2b}* region, PURO and BLAST gene PCR amplified products are 3.2, 2.4 and 2.3 Kb, respectively. The expected size of PCR amplified product with internal primers of *LmChaC_{2a}* and *LmChaC_{2b}* are 714 bp and 972 bp, respectively. (B) Western blot analysis was performed for the confirmation of generated cell lines such as CT, OE_{2a}, OE_{2b}, KO, CM_{2a}, CM_{2b} and CM cell lines using anti-*LmChaC_{2a}* (Rabbit) anti-*LmChaC_{2b}* (Rabbit) and anti- α -tubulin (Mouse) primary antibody. 200 μ g of *L. major* cell lysate were used for Western blotting analysis. (Adapted from Das et al, J Biol Chem.2022 Sep 17; 298(11):102510)

constructed Cas9 protein expressing *L. major* cells. *LmChaC_{2a}* and *LmChaC_{2b}* genes were no longer expressed in null mutant cells (KO), which were confirmed by PCR analysis from genomic DNA (gDNA) and Western blotting (**Fig.30, A and B**).

and *LmChaC_{2b}* proteins, respectively. Then pXG-B2863/*LmChaC_{2a}* construct was transfected into KO cells to prepare *ChaC_{2a}* complement (CM_{2a}) cell line and pXG-PHLEO/*LmChaC_{2b}* plasmid was transfected into null mutant cells to prepare *ChaC_{2b}* complement (CM_{2b}) cell line, which expressed either *LmChaC_{2a}* or *LmChaC_{2b}* protein respectively in comparable amount to CT cells. Finally, pXG-PHLEO/*LmChaC_{2b}* construct was transfected into CM_{2a} cells to develop *ChaC_{2a}* & *ChaC_{2b}* double complemented (CM) leishmanial cell lines, which expressed both *LmChaC_{2a}* and *LmChaC_{2b}* proteins almost same amounts compare to control cells (**Fig.30B**).

3.2.6. Comparative analysis of intracellular GSH and T(SH)₂ content:

Higher expression of GSH degradation enzymes in the cells can consume large amount of intracellular GSH. On the other hand, the amount of GSH as well as T(SH)₂ could be increased in the cells without any glutathione degrading proteins. So we examined at whether the intracellular GSH and T(SH)₂ level in the KO, OE_{2a}, OE_{2b}, CM_{2b} and CM_{2a} cells had changed in comparison to CT and CM cells. By injecting comparable amount of lysate into HPLC, we found that the intracellular GSH content was approximately two fold higher and T(SH)₂ contents was ~4 times greater in the KO cells than the CT cells (**Fig.31**). This result

3.2.5. Variation in *LmChaC2* expression in various cell lines:

By transfecting pXG-B2863/*LmChaC_{2a}* and pXG-B2863/*LmChaC_{2b}* construct in wild type (CT) cell line, *ChaC_{2a}* overexpressed (OE_{2a}) and *ChaC_{2b}* overexpressed (OE_{2b}) cell lines were prepared respectively. Western blotting showed that in comparison to CT cell lines, the OE_{2a} and OE_{2b} cell lines produced more *LmChaC_{2a}*

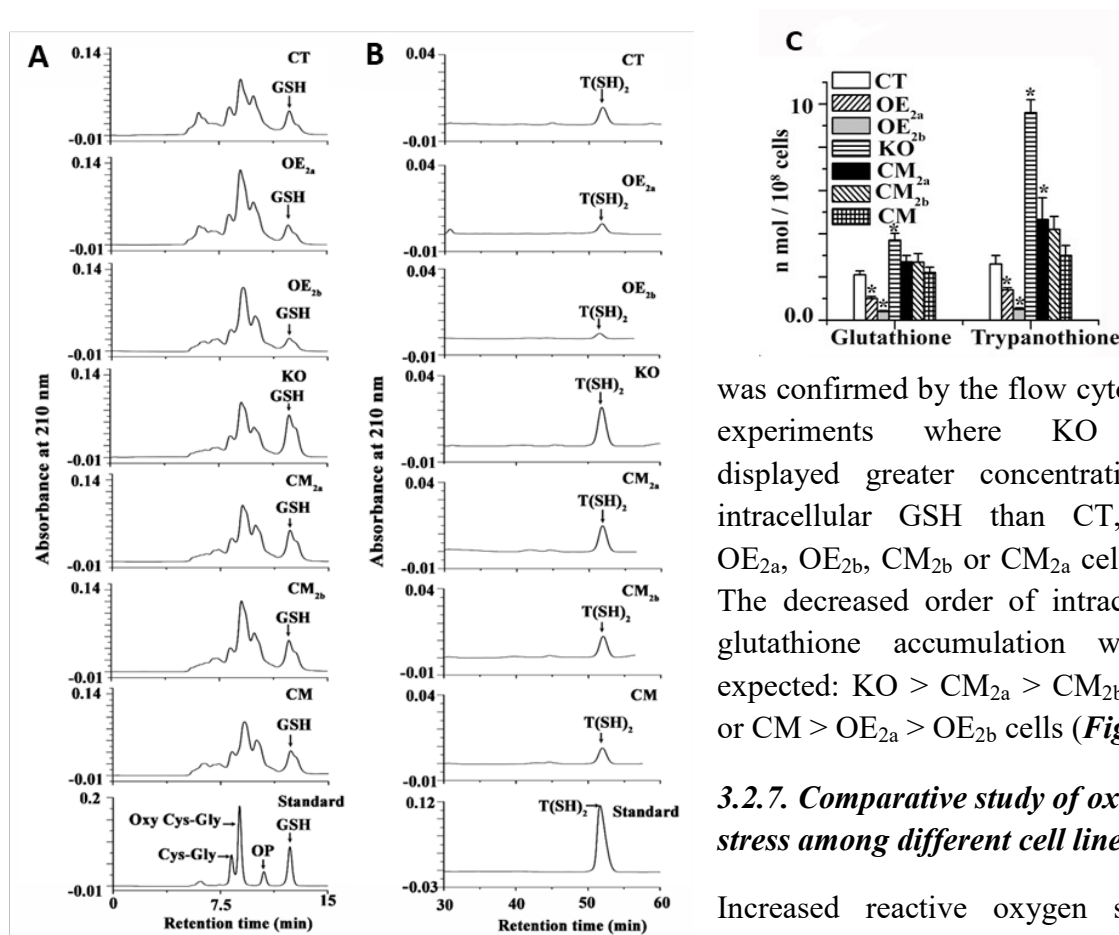


Fig.31: Intracellular GSH and T(SH)₂ quantification by HPLC. (A) HPLC Peaks of GSH in different cell lines, (B) HPLC Peaks of T(SH)₂ in different cell lines, (C) Bar diagram depicts the GSH and T(SH)₂ level in CT, OE_{2a}, OE_{2b}, KO, CM_{2a}, CM_{2b} and CM promastigote cells. 2×10^8 promastigotes were taken for making cell lysate. The lysate was centrifuged at 13000 g for 10 mins at 4°C and then the supernatant was filtered through 0.22µm Millipore filter paper. 40 µl samples were injected to the HPLC system on a SunfireTM C₁₈ column (5 µm 4.6 x 250 mm, Waters) and a mobile phase of 2% (v/v) aqueous perchloric acid at 1.0 ml/min. The concentration of standard Cys-Gly, 5-oxoproline, GSH and T(SH)₂ are 1.0 mM, 1.0 mM, 1.0 mM and 2.77 mM, respectively. All the data are representative of at least three independent experiments. (Adapted from Das et al, J Biol Chem.2022 Sep 17; 298(11):102510)

was confirmed by the flow cytometry experiments where KO cells displayed greater concentration of intracellular GSH than CT, CM, OE_{2a}, OE_{2b}, CM_{2b} or CM_{2a} cell lines. The decreased order of intracellular glutathione accumulation was as expected: KO > CM_{2a} > CM_{2b} > CT or CM > OE_{2a} > OE_{2b} cells (**Fig.32**).

3.2.7. Comparative study of oxidative stress among different cell lines:

Increased reactive oxygen species (ROS) level within the cell are usually triggered by cellular GSH and T(SH)₂ depletion. A chemically reduced derivative of fluorescein known as 2', 7'-dichlorodihydrofluorescein diacetate (H2DCFDA) is employed as a biomarker for reactive oxygen species (ROS) in cells. Therefore, to assess the intracellular oxidative stress in CT, CM, OE_{2a}, OE_{2b}, CM_{2a}, KO and CM_{2b} cell lines at late log phase, H2DCFDA was used. Flow cytometric data indicates that in

comparison to the CT, OE_{2a}, OE_{2b}, CM_{2b}, CM_{2a} and CM cell lines, intracellular ROS level was lower in null mutant population (**Fig.33A**). From these data we can conclude that by accelerating the breakdown of GSH in the *Leishmania* parasite, the LmChaC2 proteins were able to increase endogenous ROS production. The disruption of intracellular Ca²⁺ homeostasis is associated with the production of ROS and it is now widely accepted that intracellular ROS play a crucial role in regulating intracellular Ca²⁺ homeostasis (173). In KO, OE_{2a}, OE_{2b}, CM, CT, CM_{2a} and CM_{2b} cell lines, intracellular Ca²⁺ levels were assessed

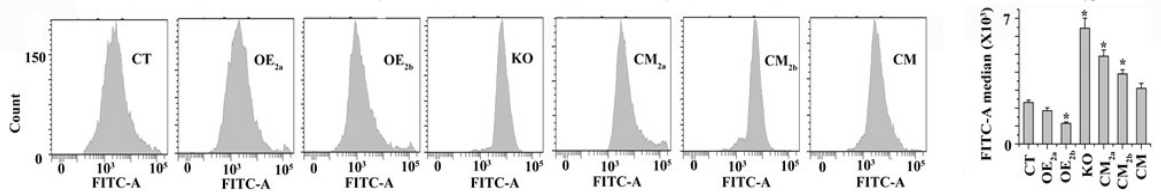


Fig.32: Flow cytometric measurement of intracellular GSH level. Intracellular GSH concentration was measured in CT, OE_{2a}, OE_{2b}, KO, CM_{2a}, CM_{2b} and CM promastigote cells by intracellular GSH Detection Assay Kit (Abcam). 10⁶ CT, OE_{2a}, OE_{2b}, KO, CM_{2a}, CM_{2b} and CM promastigote cells were taken and after washing with 1x PBS spin down at 1500g for 6 minutes. 5 µl of 200X Thiol Green Dye was mixed into 1 ml of cell suspension and incubated at 22°C for 10-15 minutes, then washed the cells at 1000 rpm for 4 mins and re-suspended in 1ml of assay buffer. All data are representative of at least three independent experiments. (Adapted from Das et al, J Biol Chem.2022 Sep 17; 298(11):102510)

using a flow cytometry experiment using the calcium sensing cell permeant fluorescent Fluo4 AM dye which is excited at 494 nm wavelength. The intensity of green fluorescence was estimated by flow cytometry which indicates that KO cells showed almost two fold lower

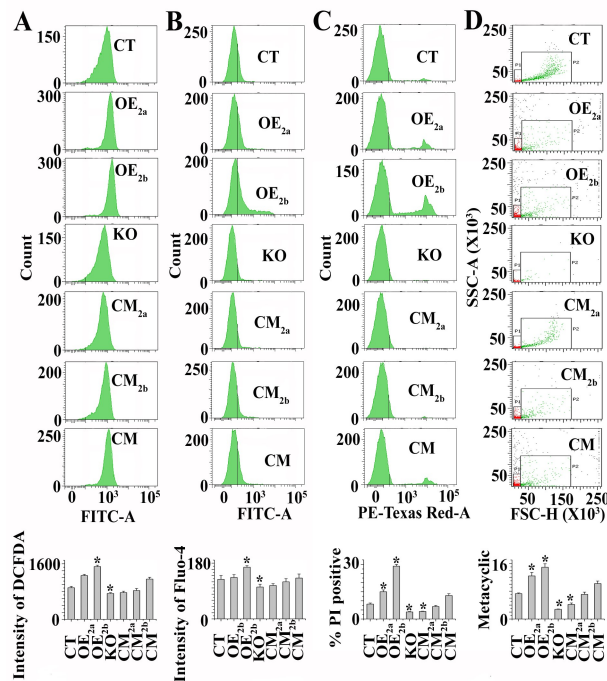


Fig.33: Characteristics of control (CT), ChaC_{2a} overexpressed (OE_{2a}), ChaC_{2b} overexpressed (OE_{2b}), knockout (KO), ChaC_{2a} complement (CM_{2a}), ChaC_{2b} complement (CM_{2b}) and ChaC_{2a} & ChaC_{2b} complement (CM) cells. (A) Flow cytometric measurement of intracellular H₂O₂ level by H₂DCFDA. (B) The intracellular calcium level was quantified by the flow cytometric analysis using Fluo4 AM. (C) Proportion of cell death (PI positive staining) was measured in late log phase population by flow cytometric analysis. (D) Metacyclic (PNA negative) population in late log phase promastigotes was measured by flow cytometry after the isolation using PNA. The gating on the dot-plots corresponds to different cell sizes and forward-angle light scatter (FSC) intensities (FSC_{low} and FSC_{high}). FSC_{low} (denoted by small box area) represents mainly metacyclic (PNA-) population. (Adapted from Das et al, J Biol Chem.2022 Sep 17; 298(11):102510)

intensity compared to CT cells. All of these oxidative stress related experiments indicating that knockout of LmChaC2 genes shielded the cells from oxidative stress induced cytosolic Ca²⁺ elevation. The increased order of cytosolic Ca²⁺ accumulation was KO < CM_{2a} < CM_{2b} < CT or CM < OE_{2a} < OE_{2b} cells (**Fig.33B**).

3.2.8. Cell viability in late log phase cell lines:

ROS homeostasis disruption and a surge in cytosolic Ca²⁺ both can lead to cell death. In order to determine whether the deletion of LmChaC_{2a} and LmChaC_{2b} genes protected the cells against oxidative stress-mediated cell death, we used propidium iodide (PI) (Fluorescent dye for staining nucleic acids of non-lived cells) to compare the proportion of viable parasites (PI negative) among OE_{2b}, OE_{2a}, CM_{2a}, KO, CM_{2b}, CT and CM cell lines. Data from flow cytometry showed that the majority of the population of null mutant parasites was PI

negative. But a greater proportion of PI-positive cells were discovered in the OE population which had lower levels of GSH due to the excess production of LmChaC2 proteins. These results indicated that LmChaC2 gene deletion provided the protection of the cells from cell death during late log phase (**Fig.33C**).

3.2.9. Comparative studies of metacyclogenesis among cell lines:

Alteration of the ROS level can lead to the change in metacyclogenesis process (differentiation of the cells from non-infective procyclic stages to non-dividing infective metacyclic stages). To evaluate whether the absence of LmChaC2 proteins prevented the oxidative stress-induced metacyclogenesis, metacyclic stages of parasites were isolated. We were succeeded to differentiate metacyclic form of promastigotes from CM_{2b}, OE_{2a}, OE_{2b}, CM, CT, CM_{2a}, and KO late log phase cell cultures by the process of negative agglutination response with peanut agglutinin (PNA). Procyclic parasites easily agglutinate but metacyclic promastigote forms do not interact with peanut agglutinin because of developmental alterations in oligosaccharides on the lipophosphoglycan, which is terminally exposed (174). Main surface glycoconjugate and lipophosphoglycan goes through species-specific changes at the time of metacyclogenesis. An increase in repeat units results in an expanded glycocalyx which shields metacyclic parasites from lysis through complement in mammalian hosts. Comparing the KO cell population to OE_{2a}, CM, OE_{2b}, CT, CM_{2a} or CM_{2b} cells, a quantitative flow cytometric study of PNA agglutination suggest that the KO cell population had less number of metacyclic (PNA-) parasites (**Fig.33D**). These findings strongly indicated that LmChaC2 gene deletion prevents procyclic (non-infectious stage) promastigote cells to metacyclic (infectious stage) promastigotes cell differentiation.

3.2.10. Variation in the expression of antioxidant gene LmAPX in different cell lines:

It has been discovered that oxidative stress causes the antioxidant gene, ascorbate peroxidase (LmAPX) to be upregulated in the *Leishmania* parasite (175). We used quantitative RT-PCR

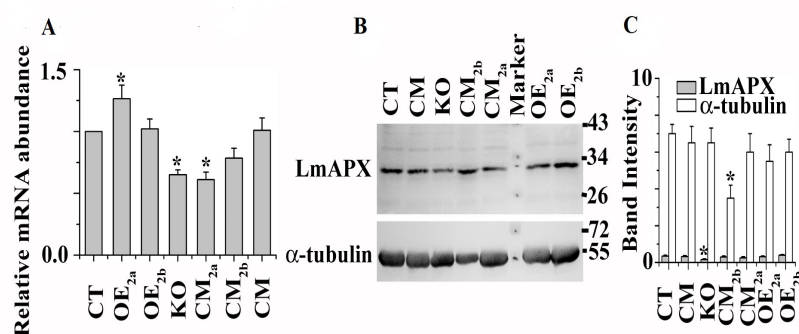


Fig.34: Expression profile of LmAPX in different variants of *L. major*. (A) Comparative studies of LmAPX mRNA abundance among CT, OE_{2a}, OE_{2b}, KO, CM_{2a}, CM_{2b} and CM promastigote cells were measured by qRT PCR. (B) Western blotting analysis was performed by using anti-LmAPX and anti- α -tubulin antibody, where 200 μ g of *L. major* cell lysate were loaded. (C) Bar diagram represents the percentage of band intensities in B. All data are representative of at least three independent experiments. (Adapted from Das et al, J Biol Chem.2022 Sep 17; 298(11):102510)

and Western blotting experiments to detect LmAPX expression profile in CM_{2b}, KO, OE_{2a}, CT, CM_{2a}, CM and OE_{2b} cells due to the possibility that the reductive environment may have reduced the expression of the LmAPX gene in the parasite. Results from qRT-PCR indicated that null mutants exhibit approximate two fold lower levels of LmAPX mRNA expression than CT or CM cells (**Fig.34A**). Ascorbate

peroxidase was expressed in the following order: KO < CM_{2a} < CM_{2b} < CT or CM < OE_{2a} < OE_{2b} cells. These findings were subjected to a Western blot analysis for additional validation and the outcomes were strikingly comparable to the qRT-PCR data (**Fig.34, B and C**). These findings collectively suggested that LmAPX was suppressed in a reducing milieu.

3.2.11. Discussion

In the previous chapter, biophysical function of LmChaC2 proteins in *Leishmania* parasite is well documented. Consistent with the prior findings to know the exact regulatory mechanism of expression inside the parasite, we investigated the expression in promastigote as well as infected mice-derived amastigote parasites. From semi-qRT PCR and Western blotting results, we concluded that both the proteins are expressed in both amastigote and promastigote stages. In addition, LmChaC_{2b} expression was induced almost 3.5 fold in sulfur-limited condition whereas constitutive expression was observed in case of LmChaC_{2a}. Required for T(SH)₂ biosynthesis, GSH is an important thiol small molecule for detoxification of ROS and protection against oxidative stress. At par with this our results show, when GSH degrading enzymes were deleted from the parasite genome, KO cells showed higher intracellular GSH/T(SH)₂ concentration and subsequently lower level of oxidative stress, free intracellular Ca²⁺ ion and decreased cell death during late log phase. In addition, lower proportion of infective metacyclic cells were present in LmChaC2 knock out cell lines compared to CT, CM, CM_{2a}, CM_{2b}, OE_{2a} and OE_{2b} cell lines. From this observation it is clear that deletion of LmChaC2 prevented the cell differentiation from the non-infective procyclic to infective metacyclic stages. Another observation is that the expression level of antioxidant protein (LmAPX) in null mutant is lower than CT or CM cells suggesting that the reducing environment might be repressed the expression of antioxidant gene in parasite. So far we have discussed about the regulation and expression of LmChaC2 proteins as well as comparative studies in metacyclogenesis and cell death in late log phase. In the next chapter, we are going to discuss about the potential biological function of LmChaC2 proteins in GSH homeostasis and disease progression.

CHAPTER 3

**“Role of LmChaC2 proteins in
GSH homeostasis and disease
progression”**

RESULTS (Chapter 3)

“Role of LmChaC2 proteins in GSH homeostasis and disease progression”

<i>3.3.1. Background</i>	62
<i>3.3.2. Growth curve analysis</i>	62
<i>3.3.3. Cell viability in stationary phase cell lines</i>	64
<i>3.3.4. In vitro Leishmania infection</i>	64
<i>3.3.5. In vivo Leishmania infection</i>	65
<i>3.3.6. Discussion</i>	66

3.3.1 Background

The important low molecular mass tripeptide thiol or glutathione (glutamate, cysteine and glycine) serves several functions in the cells. Among those one of the important roles of glutathione is sulfur storage (91). When GSH is getting degraded by GSH degrading enzymes, essential sulfur nutrient will be released in the form of sulfur containing amino acids such as cysteine. Moreover, GSH degradation provides essential amino acids like cysteine, glycine and glutamic acid which are required for the synthesis of protein. GSH plays a central role in redox balance maintenance in higher eukaryotes as well as some prokaryotes. In trypanosomatids, maximum amount of glutathione is converted into a unique low molecular mass dithiol - N1, N8-bis(glutathionyl)spermidine or trypanothione (T(SH)₂) that plays the main role in redox homeostasis instead of GSH in these organisms and trypanothione reductase (TR) keeps this di-thiol in reduced form. T(SH)₂ have more reducing efficiency than GSH although redox potential is comparable of these thiols. The single enzyme that links these parasites' NADPH and thiol-regulated redox systems is called TR (164). It is well known that GSH depletion is a potent marker of apoptosis and excessive as well as lower level of GSH is detrimental for the cell survival (99,100,176). In *Leishmania donovani*, growth is arrested after the treatment of buthionine sulfoximine (BSO). BSO is a potent inhibitor of γ -glutamylcysteine synthetase, which is an essential enzyme for GSH synthesis (177). By supplying extracellular GSH to *L. infantum*, the intracellular thiol concentration were raised (178). Glutamylcysteine synthase was knocked down by RNA interference in *T. brucei* but was rescued by GSH supplementation (72). These observations strongly indicated the presence of GSH transporter in these organisms.

Previous chapter have shown that the LmChaC2 enzyme specifically degrade only GSH and LmChaC2-deleted cells displayed increased intracellular GSH/T(SH)₂ concentrations which resulted in lower levels of oxidative stress, intracellular Ca²⁺ ions, decreased cell death and metacyclogenesis in late log phase. These results strongly indicated that the proteins might have an important role in GSH homeostasis. So the function of LmChaC2 proteins in GSH homeostasis through growth curve analysis among different cell lines in different types of sulfur limited conditions and in vitro as well as in vivo disease development by different LmChaC2 containing cell types will be discussed in this chapter.

3.3.2. Growth curve analysis:

Growth curve analysis was carried out to determine whether the availability or unavailability of exogenous GSH has any impact on the growth of null mutants on sulfur-limited medium. Growth curve were analyzed among different varieties of cell lines in different environmental conditions: a) fully sulfur-deficient media, b) GSH supplemented sulfur limited media, c) NAC supplemented sulfur limited media and d) complete nutrient rich media.

a) Fully sulfur-deficient media:

Sulfur is an essential biomolecule for building sulfur containing amino acids and vitamins (thiamine and biotin). All the cell types were cultured in sulfur limited media with the 10^6 inoculum. As expected, the growth curve data showed that none of the cell types could proliferate in sulfur-limited medium (**Fig.35A**).

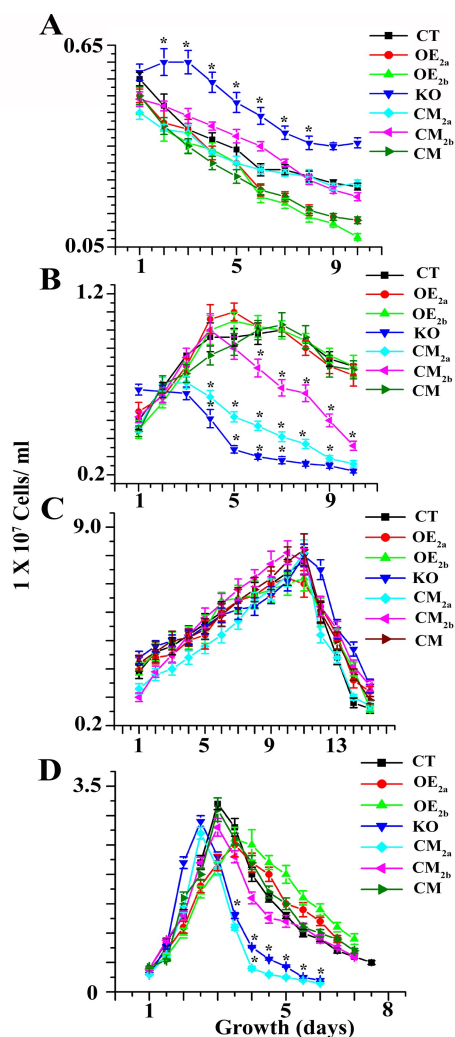


Fig.35: Comparative analysis of the growth profile among CT, OE_{2a}, OE_{2b}, KO, CM_{2a}, CM_{2b} and CM promastigotes. (A) 10^5 mid-log phase promastigote parasites were inoculated in 5ml fully sulfur deficient M199 media (Himedia-AT1076) containing 10% FBS. (B) 10^6 mid-log phase promastigote parasites were seeded in 5ml of GSH supplemented (4 mg/ml) sulfur deficient M199 media containing 10% FBS. (C) 10^6 mid-log phase cells were cultured in 5 ml of N-acetyl cysteine supplemented (25 mg/L) sulfur deficient M199 media containing 10% FBS. (D) 10^6 mid-log phase promastigotes were inoculated in 10 ml normal M199 media containing 10% FBS. *Statistically significant value of less than 0.05. (Adapted from Das et al, J Biol Chem. 2022 Sep 17; 298(11):102510)

b) *GSH supplemented sulfur limited media:*

As GSH degradation supplies sulfur to the cells, next we measured the growth curve in the presence of GSH as a sulfur source. After viable cell counting, growth curve analysis indicates that LmChaC2 expressing cell lines such as CT, OE_{2a}, OE_{2b}, CM_{2b}, CM_{2a} or CM cells successfully grew when extracellular GSH is present. But interestingly null mutant population failed to grow even in the presence of externally provided GSH (**Fig.35B**). These findings imply that leishmanial ChaC protein enables the growth of this parasite in the presence of GSH as solely sulfur source.

c) *NAC supplemented sulfur limited media:*

An acetylated modified cysteine compound, N-acetyl cysteine (NAC) is act as a precursor of amino acid cysteine and GSH. So, next we investigated the growth rates of the null mutants in NAC supplemented sulfur limited media. It was interestingly

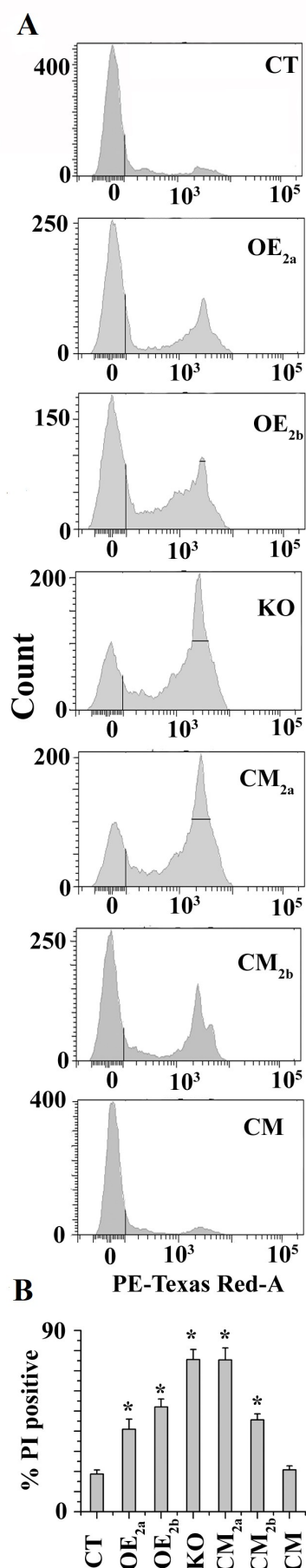


Fig.36: Cell viability in stationary phase cell lines. (A) Flow cytometric measurement of dead cells (PI positive staining cells) percentage was analyzed by flow cytometry at late stationary phase population. (B) Bar diagram represents the percentage dead cells among CT, OE_{2a}, OE_{2b}, KO, CM_{2a}, CM_{2b} and CM promastigote cells. *Statistically significant value of less than 0.05. (Adapted from Das et al, J Biol Chem.2022 Sep 17; [298\(11\):102510](#))

discovered that null mutants could grow like other cell lines in NAC containing sulfur limited media (**Fig.35C**). These finding indicates that when NAC was utilized as the sulphur source, KO cell was able to grow by de novo synthesizing all essential sulfur containing component such as GSH, T(SH)₂ and amino acids.

d) Complete nutrient rich media:

Then to investigate the function of LmChaC2 proteins in *Leishmania* parasite, 10⁶ parasite cells were inoculated and grown in 10 ml of complete nutrient rich M199 media. Growth curve suggested that in comparison to CM, CM_{2b}, OE_{2a}, OE_{2b} or CT promastigote cells, LmChaC2 null mutant cells and CM_{2a} cells had faster growth rates. Although the growth rate of KO cells were higher but they failed to survive for a longer period in the late stages of culture media unlike OE_{2b}, CT, CM_{2b} or CM cell lines (**Fig.35D**). This finding strongly suggests that LmChaC_{2b} protein is important for the parasites to survive for an extended period of time under harsh condition.

3.3.3. Cell viability in stationary phase cell lines:

Consistent with the previous finding from growth analysis by cell counting, next we investigated the cell viability by flow cytometry in stationary culture phase among all variant of cell lines. Flow cytometric studies suggested that KO cells possessed 75% PI positive cells in comparison with 18% in CT and 20% in CM in stationary phase, which is about 4 fold higher dead cells in LmChaC2 null mutant than CT and CM cells. This result clarifies the rapidly declined growth rate of KO cells compared to CM or CT cells (**Fig.36**).

3.3.4. In vitro Leishmania infection:

Leishmania as intracellular obligatory parasite mostly prefers to infect phagocytes as a host cell. Macrophage is one of the

phagocytes, which is readily infected by the *L. major* parasites. We focused on the *Leishmania* promastigotes' infectivity rate to infect macrophages because *L. major* cells

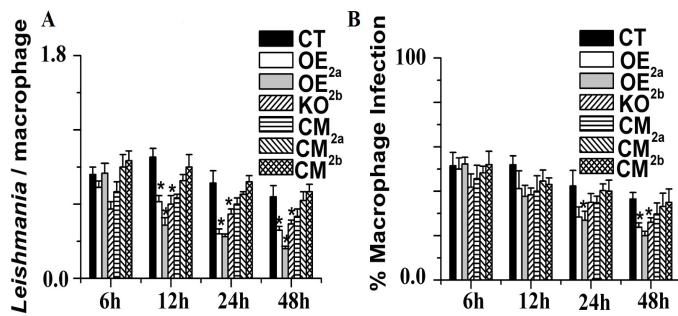


Fig.37: In vitro *Leishmania* infection assay. (A) The number of *Leishmania* inside each infected macrophage was quantified. For each instant, 200 macrophages were taken for counting. (B) The percentage of macrophages that were infected with different LmChaC2 variants of parasites. For each instant and cell type, 200 infected macrophages were quantified. *Statistically significant value of less than 0.05. (Adapted from Das et al, J Biol Chem.2022 Sep 17; 298(11):102510)

multiply in host macrophage cells. We investigated the degree of phagocytosis among CM, OE_{2a}, CT, OE_{2b}, KO, CM_{2a} and CM_{2b} cells. Lower interaction or adhering rates were observed in KO promastigotes in comparison to OE_{2a}, OE_{2b}, CT, CM_{2a}, CM_{2b} or CM cells. After 48 hours of incubation, the number of LmChaC2 null mutant parasites was still lower compared to the control cells in the macrophages. Presence of the lower amount of infective metacyclic promastigotes in KO parasites could be the possible explanation of the reduced infection level (**Fig.37A**). Furthermore, the proportion of macrophages harboring KO mutant parasites was also noticeably lower compared to the CT and CM cell lines (**Fig.37B**).

3.3.5. In vivo *Leishmania* infection:

To identify whether the *Leishmania major* LmChaC2 knock out mutant are capable to develop infections in mice model, we studied in vivo infection assay. 5×10^6 stationary phase promastigotes cells were injected into BALB/c mice in left footpad to investigate the in vivo infection. Here we found that in comparison to LmChaC2 knock out cells, CT and CM promastigotes could cause a severe disease in BALB/c mice. On the other hand, OE_{2a} and

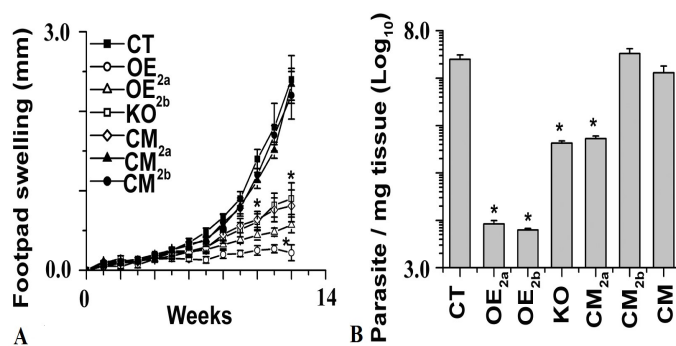


Fig.38: In vivo *Leishmania* infection assay. (A) Infection in BALB/c mice model. Footpad swelling of mice with different LmChaC2 mutants was noticed for three groups (8 mice/group). (B) Parasite burden in left hind footpad of mice was measured after three months post infection. *Statistically significant value of less than 0.05. (Adapted from Das et al, J Biol Chem.2022 Sep 17; 298(11):102510)

OE_{2b} promastigotes displayed very little virulence in an infection model in vivo (**Fig.38A**). This data reveals that the level of intracellular GSH content must be precisely controlled for the leishmanial infection. To further validate the observations, we measured the parasite burden in OE_{2a}, OE_{2b}, CT, KO, CM_{2a}, CM_{2b} and CM after 12 weeks of leishmanial infection. In contrast to the KO and OE cell lines, the higher degree of parasite burden was found in CT and CM cells (**Fig.38B**). Altogether, these results suggested that a fine-tuning of the amount of intracellular GSH content is crucial for *Leishmania* infection.

3.3.6. Discussion

In the previous chapter, the requirement of LmChaC2 proteins in intracellular GSH or T(SH)₂ concentration regulated oxidative stress induced cell death during late log phase and infective metacyclic cell differentiation has been well defined. LmChaC2 null mutant cells has shown less number of dead cells in late log phase, although the fate of the knockout cells in the stationary phase was unknown. Growth curve analysis showed that although the CT cells growth rate was slower than KO parasite, CT promastigotes sustain for the long time in aged media in comparison to KO cells. This observation suggests that under difficult growth conditions, slower growth was necessary for long-term survival. Now the question arises about the connection between slower growth rate and long term survival. One explanation is that the KO promastigotes' high replication rate might use the glycolysis pathway rather than the citric acid cycle to produce more NADPH and partially oxidized intermediates for synthesis of excessive amounts of DNA, RNA or proteins and that would quickly deplete all essential ingredients of the media. In line with the earlier concept, *Leishmania* promastigotes in dividing procyclic stages uses high glucose concentrations, maintaining controlled flux into the citric acid cycle with concurrent generation of NADH by emitting partially oxidized intermediates like acetate, alanine and succinate into the culture media (179). With regard to amastigote stages, scientists had demonstrated through heavy water labeled experiments that the quiescent metabolic state of *Leishmania* in murine lesion may induce a intrinsic defense to various stresses (nutrient, temperature and pH) and is crucial for slow but consistent replication as well as survival of the parasite (57,180). Growth curve analysis in supplemented sulfur deficient media indicates that LmChaC2-expressing cells can easily proliferate in GSH supplemented sulphur depleted media but null mutants failed to survive, suggesting that LmChaC2 plays a pivotal role for cell survival when GSH is used as solely sulphur-source. Again in vivo and in vitro infection analysis suggests that LmChaC2 proteins regulated GSH level plays a crucial role in the infectivity and survivability of the parasite within BALB/c mice. Altogether it is concluded that LmChaC2 proteins aided GSH homeostasis is required for slower growth and long-term viability, which is important for disease progression in mice model.

“Learning gives creativity. Creativity leads to thinking. Thinking provides knowledge. Knowledge makes you great.”

- A.P.J. Abdul Kalam

Conclusion & Perspectives

CONCLUSION & PERSPECTIVE

Although it is widely acknowledged that GSH is necessary for *Leishmania* to survive but it is still unclear whether the GSH homeostasis is required for the survival of the parasites. For the first time, we have demonstrated the importance of LmChaC2-mediated controlled GSH degradation in chronic infection. Here, we explain the following key points: i) we showed that two ChaC proteins (LmChaC_{2a} and LmChaC_{2b}) of different molecular masses can degrade GSH to generate 5-oxoproline and Cys-Gly dipeptide in both promastigote and amastigote phases of the *Leishmania* parasites; ii) LmChaC_{2b} (38 kDa) has a considerably higher catalytic efficiency than the constitutively expressed protein LmChaC_{2a} (28 kDa); iii) under sulphur restriction, the LmChaC_{2b} expression was upregulated; iv) null mutant data suggesting the LmChaC2 proteins regulate the concentration of GSH/T(SH)₂ in the cell as well as intracellular calcium concentration, cell differentiation from noninfective procyclic to infective metacyclic stages and cell death; v) requirement of LmChaC_{2b} protein for the long survival of the parasite in late stationary culture and is crucial for the development of disease. Survival of the parasite in late stationary phase may depend on the LmChaC2 mediated catalysis of GSH to form Cys, Glu, and Gly amino acids. Prior research shows that the overall thiol concentration did not significantly alter throughout the several logarithmic growth phases in the cells but a 6-fold decrease in thiol concentration was noticed after the entry of the parasite into the stationary phase (181). Similar to this, the T(SH)₂ concentration does not change during the various logarithmic growth phases in *T. cruzi*, *L. major* and *L. donovani* but drops quickly during the stationary phase culture (166). Our findings demonstrated that stationary phase culture and sulfur-limited medium induce the production of LmChaC_{2b} protein. Therefore, when the nutrients are depleted during late stationary phase culture, catalytically effective LmChaC_{2b} protein may be responsible for delivering Cys, Glu, and Gly from GSH degradation for critical protein synthesis (**Fig.39**).

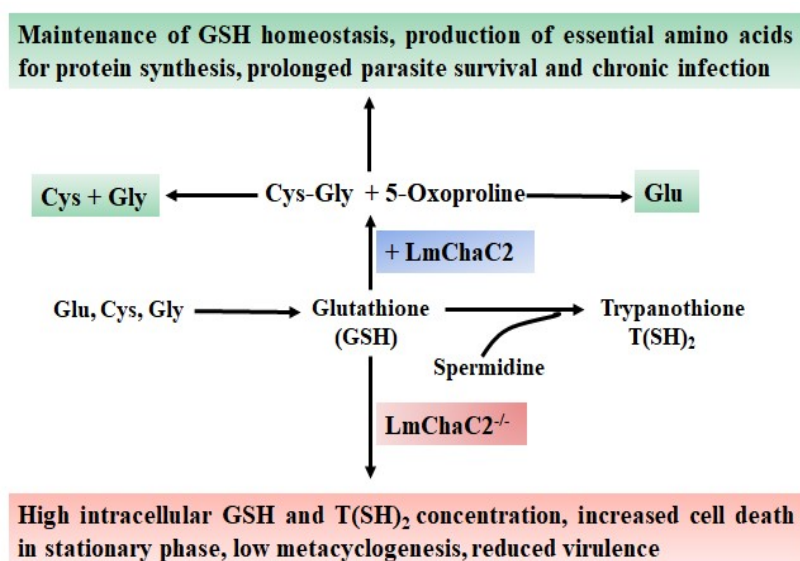


Fig.39: Schematic diagram depicts the importance of LmChaC2 proteins in the parasites. LmChaC2 enzyme is essential for GSH homeostasis maintenance, produces essential amino acids for protein synthesis and long term survival as well as chronic infection.

In the early phases of host-*Leishmania* interactions, the parasite's T(SH)₂ and redox proteins effectively control redox homeostasis to endure the oxidative burst (182). Since CT cells are

substantially more virulent than LmChaC_{2b} overexpressed cell lines which contain very little T(SH)₂, suggesting that T(SH)₂ is crucial for the progression of disease. On the other hand, KO mutants had 4-fold excess T(SH)₂ also displayed less virulent characteristics than CT. This could imply that an excessive amount of T(SH)₂ accumulation could harm the parasite itself. Several previous studies demonstrate the harmful consequences of excess GSH level in unicellular eukaryotes and mammalian cell (176,183). By adding NAC or overexpressing of glutamate cysteine ligase can alter the elevated GSH level mediated redox balance, which induces the reductive stress linked to mitochondrial dysfunction (184). Other studies demonstrated that too much GSH inhibits the growth of the intracellular *Mycobacterium tuberculosis* parasite. However its mutant variant that is defective in excess GSH uptake grew better within the host cell (macrophage) (185,186). From their observations, they strongly proposed that this pathogen is subjected to reductive stress inside the phagocytic host. We demonstrated that KO mutant which is deficient in the breakdown of GSH were unable to display a serious disease manifestation in contrast to CT promastigotes. These results suggest that glutamate/cysteine/glycine generation from glutathione recycling may be important for the parasite and necessary for protein synthesis (187).

In human, ChaC1 shows ~10-20 times more catalytic activity than ChaC2 and here we have shown that LmChaC_{2b} protein exhibit almost 17 times more catalytic efficiency than LmChaC_{2a} in *Leishmania* parasite. It is still unclear which amino acid residues in these proteins are responsible for this variation in catalytic efficiency. Thus further work is needed to identify those specific amino acid residues that will be elucidating this mystery. Furthermore, LmChaC_{2a} is constitutively expressed and LmChaC_{2b} protein is inducibly expressed in sulfur limited media. So extensive molecular study is needed to explore how this sulfur stress induces the expression of LmChaC_{2b} in this particular situation.

Bibliography

1. Perez, J. M. (2009) Parasites, Pests, and Pets in a Global World: New Perspectives and Challenges. *J Exot Pet Med* **18**, 248-253
2. Huntington, M. K., Allison, J., and Nair, D. (2016) Emerging Vector-Borne Diseases. *Am Fam Physician* **94**, 551-557
3. Nii-Trebi, N. I. (2017) Emerging and Neglected Infectious Diseases: Insights, Advances, and Challenges. *Biomed Res Int* **2017**, 5245021
4. Zuma, A. A., Dos Santos Barrias, E., and de Souza, W. (2021) Basic Biology of *Trypanosoma cruzi*. *Curr Pharm Des* **27**, 1671-1732
5. De Lange, T. (1986) The molecular biology of antigenic variation in trypanosomes: gene rearrangements and discontinuous transcription. *Int Rev Cytol* **99**, 85-117
6. El-Sayed, N. M., Myler, P. J., Bartholomeu, D. C., Nilsson, D., Aggarwal, G., Tran, A. N., Ghedin, E., Worthey, E. A., Delcher, A. L., Blandin, G., Westenberger, S. J., Caler, E., Cerqueira, G. C., Branche, C., Haas, B., Anupama, A., Arner, E., Aslund, L., Attipoe, P., Bontempi, E., Bringaud, F., Burton, P., Cadag, E., Campbell, D. A., Carrington, M., Crabtree, J., Darban, H., da Silveira, J. F., de Jong, P., Edwards, K., Englund, P. T., Fazelina, G., Feldblyum, T., Ferella, M., Frasch, A. C., Gull, K., Horn, D., Hou, L., Huang, Y., Kindlund, E., Klingbeil, M., Kluge, S., Koo, H., Lacerda, D., Levin, M. J., Lorenzi, H., Louie, T., Machado, C. R., McCulloch, R., McKenna, A., Mizuno, Y., Mottram, J. C., Nelson, S., Ochaya, S., Osoegawa, K., Pai, G., Parsons, M., Pentony, M., Pettersson, U., Pop, M., Ramirez, J. L., Rinta, J., Robertson, L., Salzberg, S. L., Sanchez, D. O., Seyler, A., Sharma, R., Shetty, J., Simpson, A. J., Sisk, E., Tammi, M. T., Tarleton, R., Teixeira, S., Van Aken, S., Vogt, C., Ward, P. N., Wickstead, B., Wortman, J., White, O., Fraser, C. M., Stuart, K. D., and Andersson, B. (2005) The genome sequence of *Trypanosoma cruzi*, etiologic agent of Chagas disease. *Science* **309**, 409-415
7. Perry, K., and Agabian, N. (1991) mRNA processing in the Trypanosomatidae. *Experientia* **47**, 118-128
8. Levick, M. P., Blackwell, J. M., Connor, V., Coulson, R. M., Miles, A., Smith, H. E., Wan, K. L., and Ajioka, J. W. (1996) An expressed sequence tag analysis of a full-length, spliced-leader cDNA library from *Leishmania major* promastigotes. *Mol Biochem Parasitol* **76**, 345-348
9. Ilgoutz, S. C., Zawadzki, J. L., Ralton, J. E., and McConville, M. J. (1999) Evidence that free GPI glycolipids are essential for growth of *Leishmania mexicana*. *EMBO J* **18**, 2746-2755
10. Parsons, M. (2004) Glycosomes: parasites and the divergence of peroxisomal purpose. *Mol Microbiol* **53**, 717-724
11. Adak, S., and Pal, S. (2013) Ascorbate peroxidase acts as a novel determiner of redox homeostasis in *Leishmania*. *Antioxid Redox Signal* **19**, 746-754
12. Carter, N. S., Yates, P., Arendt, C. S., Boitz, J. M., and Ullman, B. (2008) Purine and pyrimidine metabolism in *Leishmania*. *Adv Exp Med Biol* **625**, 141-154
13. Bates, P. A. (2007) Transmission of *Leishmania* metacyclic promastigotes by phlebotomine sand flies. *Int J Parasitol* **37**, 1097-1106
14. Zink, A. R., Spigelman, M., Schraut, B., Greenblatt, C. L., Nerlich, A. G., and Donoghue, H. D. (2006) Leishmaniasis in ancient Egypt and Upper nubia. *Emerg Infect Dis* **12**, 1616-1617
15. Steverding, D. (2017) The history of leishmaniasis. *Parasit Vectors* **10**, 82
16. Pratlong, F., Dedet, J. P., Marty, P., Portus, M., Deniau, M., Dereure, J., Abranches, P., Reynes, J., Martini, A., Lefebvre, M., and et al. (1995) *Leishmania*-human immunodeficiency virus coinfection in the Mediterranean basin: isoenzymatic

- characterization of 100 isolates of the *Leishmania infantum* complex. *J Infect Dis* **172**, 323-326
17. Poinar, G., Jr., and Poinar, R. (2004) Evidence of vector-borne disease of Early Cretaceous reptiles. *Vector Borne Zoonotic Dis* **4**, 281-284
 18. Poinar, G., Jr., and Poinar, R. (2004) Paleoleishmania proterus n. gen., n. sp., (Trypanosomatidae: Kinetoplastida) from Cretaceous Burmese amber. *Protist* **155**, 305-310
 19. Poinar, G., Jr. (2008) *Leptoconops nosopheris* sp. n. (Diptera: Ceratopogonidae) and *Paleotrypanosoma burmanicus* gen. n., sp. n. (Kinetoplastida: Trypanosomatidae), a biting midge--trypanosome vector association from the Early Cretaceous. *Mem Inst Oswaldo Cruz* **103**, 468-471
 20. Thomaz-Soccol, V., Lanotte, G., Rioux, J. A., Pratlong, F., Martini-Dumas, A., and Serres, E. (1993) Monophyletic origin of the genus *Leishmania* Ross, 1903. *Ann Parasitol Hum Comp* **68**, 107-108
 21. Swaminath, C. S., Shortt, H. E., and Anderson, L. A. (2006) Transmission of Indian kala-azar to man by the bites of *Phlebotomus argentipes*, ann and brun. 1942. *Indian J Med Res* **123**, 473-477
 22. Guerin, P. J., Olliaro, P., Sundar, S., Boelaert, M., Croft, S. L., Desjeux, P., Wasunna, M. K., and Bryceson, A. D. (2002) Visceral leishmaniasis: current status of control, diagnosis, and treatment, and a proposed research and development agenda. *Lancet Infect Dis* **2**, 494-501
 23. Desjeux, P. (2004) Leishmaniasis: current situation and new perspectives. *Comp Immunol Microbiol Infect Dis* **27**, 305-318
 24. Mokni, M. (2019) [Cutaneous leishmaniasis]. *Ann Dermatol Venereol* **146**, 232-246
 25. Weigle, K. A., Santrich, C., Martinez, F., Valderrama, L., and Saravia, N. G. (1993) Epidemiology of cutaneous leishmaniasis in Colombia: a longitudinal study of the natural history, prevalence, and incidence of infection and clinical manifestations. *J Infect Dis* **168**, 699-708
 26. Daneshbod, Y., Oryan, A., Davarmanesh, M., Shirian, S., Negahban, S., Aledavood, A., Davarpanah, M. A., Soleimanpoor, H., and Daneshbod, K. (2011) Clinical, histopathologic, and cytologic diagnosis of mucosal leishmaniasis and literature review. *Arch Pathol Lab Med* **135**, 478-482
 27. Abadias-Granado, I., Diago, A., Cerro, P. A., Palma-Ruiz, A. M., and Gilaberte, Y. (2021) Cutaneous and Mucocutaneous Leishmaniasis. *Actas Dermosifiliogr (Engl Ed)*
 28. Sengupta, R., Chaudhuri, S. J., Moulik, S., Ghosh, M. K., Saha, B., Das, N. K., and Chatterjee, M. (2019) Active surveillance identified a neglected burden of macular cases of Post Kala-azar Dermal Leishmaniasis in West Bengal. *PLoS Negl Trop Dis* **13**, e0007249
 29. Zijlstra, E. E., Alves, F., Rijal, S., Arana, B., and Alvar, J. (2017) Post-kala-azar dermal leishmaniasis in the Indian subcontinent: A threat to the South-East Asia Region Kala-azar Elimination Programme. *PLoS Negl Trop Dis* **11**, e0005877
 30. Killick-Kendrick, R., Molyneux, D. H., Hommel, M., Leaney, A. J., and Robertson, E. S. (1977) *Leishmania* in phlebotomid sandflies. V. The nature and significance of infections of the pylorus and ileum of the sandfly by leishmaniae of the braziliensis complex. *Proc R Soc Lond B Biol Sci* **198**, 191-199
 31. Chang, K. P. (1979) *Leishmania donovani*: promastigote--macrophage surface interactions in vitro. *Exp Parasitol* **48**, 175-189
 32. Basmaciyan, L., Azas, N., and Casanova, M. (2017) Calcein+/PI- as an early apoptotic feature in *Leishmania*. *PLoS One* **12**, e0187756

33. Spotin, A., Rouhani, S., and Parvizi, P. (2014) The associations of *Leishmania major* and *Leishmania tropica* aspects by focusing their morphological and molecular features on clinical appearances in Khuzestan Province, Iran. *Biomed Res Int* **2014**, 913510
34. Araujo, T. F., Calarga, A. P., Zorgi, N. E., Rangel, O., Levy, C. E., and Giorgio, S. (2020) Phenotype evaluation of human and canine isolates of *Leishmania infantum*. *Comp Immunol Microbiol Infect Dis* **73**, 101551
35. Kumar, A. (2019) Transmission of leishmaniasis from human to other vertebrates: a rapid zoonanthropotic evolution. *Int Microbiol* **22**, 399-401
36. Avila-Garcia, M., Mancilla-Ramirez, J., Segura-Cervantes, E., Farfan-Labonne, B., Ramirez-Ramirez, A., and Galindo-Sevilla, N. (2013) Transplacental transmission of cutaneous *Leishmania mexicana* strain in BALB/c mice. *Am J Trop Med Hyg* **89**, 354-358
37. Palatnik-de-Sousa, C. B., Paraguai-de-Souza, E., Gomes, E. M., Soares-Machado, F. C., Luz, K. G., and Borojevic, R. (1996) Transmission of visceral leishmaniasis by blood transfusion in hamsters. *Braz J Med Biol Res* **29**, 1311-1315
38. Turchetti, A. P., Souza, T. D., Paixao, T. A., and Santos, R. L. (2014) Sexual and vertical transmission of visceral leishmaniasis. *J Infect Dev Ctries* **8**, 403-407
39. Quinnell, R. J., and Courtenay, O. (2009) Transmission, reservoir hosts and control of zoonotic visceral leishmaniasis. *Parasitology* **136**, 1915-1934
40. Rittig, M. G., and Bogdan, C. (2000) *Leishmania*-host-cell interaction: complexities and alternative views. *Parasitol Today* **16**, 292-297
41. Lodge, R., Diallo, T. O., and Descoteaux, A. (2006) *Leishmania donovani* lipophosphoglycan blocks NADPH oxidase assembly at the phagosome membrane. *Cell Microbiol* **8**, 1922-1931
42. Seguin, O., and Descoteaux, A. (2016) *Leishmania*, the phagosome, and host responses: The journey of a parasite. *Cell Immunol* **309**, 1-6
43. Akhondi, M., Kuhls, K., Cannet, A., Votypka, J., Marty, P., Delaunay, P., and Sereno, D. (2016) A Historical Overview of the Classification, Evolution, and Dispersion of *Leishmania* Parasites and Sandflies. *PLoS Negl Trop Dis* **10**, e0004349
44. Rogers, M. E., Chance, M. L., and Bates, P. A. (2002) The role of promastigote secretory gel in the origin and transmission of the infective stage of *Leishmania mexicana* by the sandfly *Lutzomyia longipalpis*. *Parasitology* **124**, 495-507
45. Walters, L. L. (1993) *Leishmania* differentiation in natural and unnatural sand fly hosts. *J Eukaryot Microbiol* **40**, 196-206
46. Kamhawi, S. (2006) Phlebotomine sand flies and *Leishmania* parasites: friends or foes? *Trends Parasitol* **22**, 439-445
47. Gossage, S. M., Rogers, M. E., and Bates, P. A. (2003) Two separate growth phases during the development of *Leishmania* in sand flies: implications for understanding the life cycle. *Int J Parasitol* **33**, 1027-1034
48. Sacks, D. L., and Perkins, P. V. (1985) Development of infective stage *Leishmania* promastigotes within phlebotomine sand flies. *Am J Trop Med Hyg* **34**, 456-459
49. Warburg, A., and Schlein, Y. (1986) The effect of post-bloodmeal nutrition of *Phlebotomus papatasi* on the transmission of *Leishmania major*. *Am J Trop Med Hyg* **35**, 926-930
50. van Zandbergen, G., Klinger, M., Mueller, A., Dannenberg, S., Gebert, A., Solbach, W., and Laskay, T. (2004) Cutting edge: neutrophil granulocyte serves as a vector for *Leishmania* entry into macrophages. *J Immunol* **173**, 6521-6525

51. Naderer, T., Vince, J. E., and McConville, M. J. (2004) Surface determinants of Leishmania parasites and their role in infectivity in the mammalian host. *Curr Mol Med* **4**, 649-665
52. McConville, M. J., de Souza, D., Saunders, E., Likic, V. A., and Naderer, T. (2007) Living in a phagolysosome; metabolism of Leishmania amastigotes. *Trends Parasitol* **23**, 368-375
53. Spath, G. F., Epstein, L., Leader, B., Singer, S. M., Avila, H. A., Turco, S. J., and Beverley, S. M. (2000) Lipophosphoglycan is a virulence factor distinct from related glycoconjugates in the protozoan parasite Leishmania major. *Proc Natl Acad Sci U S A* **97**, 9258-9263
54. Antoine, J. C., Prina, E., Lang, T., and Courret, N. (1998) The biogenesis and properties of the parasitophorous vacuoles that harbour Leishmania in murine macrophages. *Trends Microbiol* **6**, 392-401
55. Wilson, J., Huynh, C., Kennedy, K. A., Ward, D. M., Kaplan, J., Aderem, A., and Andrews, N. W. (2008) Control of parasitophorous vacuole expansion by LYST/Beige restricts the intracellular growth of Leishmania amazonensis. *PLoS Pathog* **4**, e1000179
56. Rubin-Bejerano, I., Fraser, I., Grisafi, P., and Fink, G. R. (2003) Phagocytosis by neutrophils induces an amino acid deprivation response in Saccharomyces cerevisiae and Candida albicans. *Proc Natl Acad Sci U S A* **100**, 11007-11012
57. McConville, M. J., Saunders, E. C., Kloehn, J., and Dagley, M. J. (2015) Leishmania carbon metabolism in the macrophage phagolysosome- feast or famine? *F1000Res* **4**, 938
58. Naderer, T., and McConville, M. J. (2008) The Leishmania-macrophage interaction: a metabolic perspective. *Cell Microbiol* **10**, 301-308
59. Alvar, J., Aparicio, P., Aseffa, A., Den Boer, M., Canavate, C., Dedet, J. P., Gradoni, L., Ter Horst, R., Lopez-Velez, R., and Moreno, J. (2008) The relationship between leishmaniasis and AIDS: the second 10 years. *Clin Microbiol Rev* **21**, 334-359, table of contents
60. Bhargava, P., and Singh, R. (2012) Developments in diagnosis and antileishmanial drugs. *Interdiscip Perspect Infect Dis* **2012**, 626838
61. Stager, S., Smith, D. F., and Kaye, P. M. (2000) Immunization with a recombinant stage-regulated surface protein from Leishmania donovani induces protection against visceral leishmaniasis. *J Immunol* **165**, 7064-7071
62. Olobo, J. O., Anjili, C. O., Gicheru, M. M., Mbatia, P. A., Kariuki, T. M., Githure, J. I., Koech, D. K., and McMaster, W. R. (1995) Vaccination of vervet monkeys against cutaneous leishmaniasis using recombinant Leishmania 'major surface glycoprotein' (gp63). *Vet Parasitol* **60**, 199-212
63. Gurunathan, S., Sacks, D. L., Brown, D. R., Reiner, S. L., Charest, H., Glaichenhaus, N., and Seder, R. A. (1997) Vaccination with DNA encoding the immunodominant LACK parasite antigen confers protective immunity to mice infected with Leishmania major. *J Exp Med* **186**, 1137-1147
64. Guha, R., Gupta, D., Rastogi, R., Vikram, R., Krishnamurthy, G., Bimal, S., Roy, S., and Mukhopadhyay, A. (2013) Vaccination with leishmania hemoglobin receptor-encoding DNA protects against visceral leishmaniasis. *Sci Transl Med* **5**, 202ra121
65. Hensley, K., Robinson, K. A., Gabbita, S. P., Salsman, S., and Floyd, R. A. (2000) Reactive oxygen species, cell signaling, and cell injury. *Free Radic Biol Med* **28**, 1456-1462

66. Shelton, M. D., Chock, P. B., and Mieyal, J. J. (2005) Glutaredoxin: role in reversible protein s-glutathionylation and regulation of redox signal transduction and protein translocation. *Antioxid Redox Signal* **7**, 348-366
67. Lillig, C. H., and Holmgren, A. (2007) Thioredoxin and related molecules--from biology to health and disease. *Antioxid Redox Signal* **9**, 25-47
68. Braunshausen, A., and Seebeck, F. P. (2011) Identification and characterization of the first ovothioli biosynthetic enzyme. *J Am Chem Soc* **133**, 1757-1759
69. Ariyanayagam, M. R., and Fairlamb, A. H. (2001) Ovothioli and trypanothione as antioxidants in trypanosomatids. *Mol Biochem Parasitol* **115**, 189-198
70. Fairlamb, A. H., Blackburn, P., Ulrich, P., Chait, B. T., and Cerami, A. (1985) Trypanothione: a novel bis(glutathionyl)spermidine cofactor for glutathione reductase in trypanosomatids. *Science* **227**, 1485-1487
71. Grondin, K., Haimeur, A., Mukhopadhyay, R., Rosen, B. P., and Ouellette, M. (1997) Co-amplification of the gamma-glutamylcysteine synthetase gene *gsh1* and of the ABC transporter gene *pgpA* in arsenite-resistant *Leishmania tarentolae*. *EMBO J* **16**, 3057-3065
72. Huynh, T. T., Huynh, V. T., Harmon, M. A., and Phillips, M. A. (2003) Gene knockdown of gamma-glutamylcysteine synthetase by RNAi in the parasitic protozoa *Trypanosoma brucei* demonstrates that it is an essential enzyme. *J Biol Chem* **278**, 39794-39800
73. Cunningham, M. L., and Fairlamb, A. H. (1995) Trypanothione reductase from *Leishmania donovani*. Purification, characterisation and inhibition by trivalent antimonials. *Eur J Biochem* **230**, 460-468
74. Bocedi, A., Dawood, K. F., Fabrini, R., Federici, G., Gradoni, L., Pedersen, J. Z., and Ricci, G. (2010) Trypanothione efficiently intercepts nitric oxide as a harmless iron complex in trypanosomatid parasites. *FASEB J* **24**, 1035-1042
75. Shames, S. L., Fairlamb, A. H., Cerami, A., and Walsh, C. T. (1986) Purification and characterization of trypanothione reductase from *Crithidia fasciculata*, a newly discovered member of the family of disulfide-containing flavoprotein reductases. *Biochemistry* **25**, 3519-3526
76. Castro, H., Sousa, C., Novais, M., Santos, M., Budde, H., Cordeiro-da-Silva, A., Flohe, L., and Tomas, A. M. (2004) Two linked genes of *Leishmania infantum* encode tryparedoxins localised to cytosol and mitochondrion. *Mol Biochem Parasitol* **136**, 137-147
77. Dormeyer, M., Reckenfelderbaumer, N., Ludemann, H., and Krauth-Siegel, R. L. (2001) Trypanothione-dependent synthesis of deoxyribonucleotides by *Trypanosoma brucei* ribonucleotide reductase. *J Biol Chem* **276**, 10602-10606
78. Onn, I., Milman-Shtepel, N., and Shlomai, J. (2004) Redox potential regulates binding of universal minicircle sequence binding protein at the kinetoplast DNA replication origin. *Eukaryot Cell* **3**, 277-287
79. Nogoceke, E., Gommel, D. U., Kiess, M., Kalisz, H. M., and Flohe, L. (1997) A unique cascade of oxidoreductases catalyses trypanothione-mediated peroxide metabolism in *Crithidia fasciculata*. *Biol Chem* **378**, 827-836
80. Brigelius-Flohe, R., and Flohe, L. (2003) Is there a role of glutathione peroxidases in signaling and differentiation? *Biofactors* **17**, 93-102
81. Herbette, S., Roeckel-Drevet, P., and Drevet, J. R. (2007) Seleno-independent glutathione peroxidases. More than simple antioxidant scavengers. *FEBS J* **274**, 2163-2180

82. Wilkinson, S. R., Meyer, D. J., and Kelly, J. M. (2000) Biochemical characterization of a trypanosome enzyme with glutathione-dependent peroxidase activity. *Biochem J* **352 Pt 3**, 755-761
83. Clark, D., Albrecht, M., and Arevalo, J. (1994) Ascorbate variations and dehydroascorbate reductase activity in *Trypanosoma cruzi* epimastigotes and trypomastigotes. *Mol Biochem Parasitol* **66**, 143-145
84. Raven, E. L. (2003) Understanding functional diversity and substrate specificity in haem peroxidases: what can we learn from ascorbate peroxidase? *Nat Prod Rep* **20**, 367-381
85. Raza, H. (2011) Dual localization of glutathione S-transferase in the cytosol and mitochondria: implications in oxidative stress, toxicity and disease. *FEBS J* **278**, 4243-4251
86. Cairns, N. G., Pasternak, M., Wachter, A., Cobbett, C. S., and Meyer, A. J. (2006) Maturation of arabidopsis seeds is dependent on glutathione biosynthesis within the embryo. *Plant Physiol* **141**, 446-455
87. Dalton, T. P., Dieter, M. Z., Yang, Y., Shertzer, H. G., and Nebert, D. W. (2000) Knockout of the mouse glutamate cysteine ligase catalytic subunit (Gclc) gene: embryonic lethal when homozygous, and proposed model for moderate glutathione deficiency when heterozygous. *Biochem Biophys Res Commun* **279**, 324-329
88. Wu, A. L., and Moye-Rowley, W. S. (1994) GSH1, which encodes gamma-glutamylcysteine synthetase, is a target gene for yAP-1 transcriptional regulation. *Mol Cell Biol* **14**, 5832-5839
89. Bourbouloux, A., Shahi, P., Chakladar, A., Delrot, S., and Bachhawat, A. K. (2000) Hgt1p, a high affinity glutathione transporter from the yeast *Saccharomyces cerevisiae*. *J Biol Chem* **275**, 13259-13265
90. Bachhawat, A. K., and Kaur, A. (2017) Glutathione Degradation. *Antioxid Redox Signal* **27**, 1200-1216
91. Penninckx, M. J., and Elskens, M. T. (1993) Metabolism and functions of glutathione in micro-organisms. *Adv Microb Physiol* **34**, 239-301
92. Meister, A., and Anderson, M. E. (1983) Glutathione. *Annu Rev Biochem* **52**, 711-760
93. Noctor, G., Queval, G., Mhamdi, A., Chaouch, S., and Foyer, C. H. (2011) Glutathione. *Arabidopsis Book* **9**, e0142
94. Panday, S., Talreja, R., and Kavdia, M. (2020) The role of glutathione and glutathione peroxidase in regulating cellular level of reactive oxygen and nitrogen species. *Microvasc Res* **131**, 104010
95. Arthur, J. R. (2000) The glutathione peroxidases. *Cell Mol Life Sci* **57**, 1825-1835
96. Dalle-Donne, I., Rossi, R., Colombo, G., Giustarini, D., and Milzani, A. (2009) Protein S-glutathionylation: a regulatory device from bacteria to humans. *Trends Biochem Sci* **34**, 85-96
97. Peterson, J. D., Herzenberg, L. A., Vasquez, K., and Waltenbaugh, C. (1998) Glutathione levels in antigen-presenting cells modulate Th1 versus Th2 response patterns. *Proc Natl Acad Sci U S A* **95**, 3071-3076
98. Lubos, E., Loscalzo, J., and Handy, D. E. (2011) Glutathione peroxidase-1 in health and disease: from molecular mechanisms to therapeutic opportunities. *Antioxid Redox Signal* **15**, 1957-1997
99. Townsend, D. M., Tew, K. D., and Tapiero, H. (2003) The importance of glutathione in human disease. *Biomed Pharmacother* **57**, 145-155
100. Franco, R., and Cidlowski, J. A. (2009) Apoptosis and glutathione: beyond an antioxidant. *Cell Death Differ* **16**, 1303-1314

101. Forman, H. J., Zhang, H., and Rinna, A. (2009) Glutathione: overview of its protective roles, measurement, and biosynthesis. *Mol Aspects Med* **30**, 1-12
102. Meister, A. (1973) On the enzymology of amino acid transport. *Science* **180**, 33-39
103. Orłowski, M., and Meister, A. (1971) Isolation of highly purified gamma-glutamylcysteine synthetase from rat kidney. *Biochemistry* **10**, 372-380
104. Snoke, J. E. (1955) Isolation and properties of yeast glutathione synthetase. *J Biol Chem* **213**, 813-824
105. Tate, S. S., and Meister, A. (1981) gamma-Glutamyl transpeptidase: catalytic, structural and functional aspects. *Mol Cell Biochem* **39**, 357-368
106. Connell, G. E., and Hanes, C. S. (1956) Enzymic formation of pyrrolidone carboxylic acid from gamma-glutamyl peptides. *Nature* **177**, 377-378
107. Van der Werf, P., Orłowski, M., and Meister, A. (1971) Enzymatic conversion of 5-oxo-L-proline (L-pyrrolidone carboxylate) to L-glutamate coupled with cleavage of adenosine triphosphate to adenosine diphosphate, a reaction in the -glutamyl cycle. *Proc Natl Acad Sci U S A* **68**, 2982-2985
108. Kumar, C., Sharma, R., and Bachhawat, A. K. (2003) Utilization of glutathione as an exogenous sulfur source is independent of gamma-glutamyl transpeptidase in the yeast *Saccharomyces cerevisiae*: evidence for an alternative glutathione degradation pathway. *FEMS Microbiol Lett* **219**, 187-194
109. Ganguli, D., Kumar, C., and Bachhawat, A. K. (2007) The alternative pathway of glutathione degradation is mediated by a novel protein complex involving three new genes in *Saccharomyces cerevisiae*. *Genetics* **175**, 1137-1151
110. Kumar, A., Tikoo, S., Maity, S., Sengupta, S., Sengupta, S., Kaur, A., and Bachhawat, A. K. (2012) Mammalian proapoptotic factor ChaC1 and its homologues function as gamma-glutamyl cyclotransferases acting specifically on glutathione. *EMBO Rep* **13**, 1095-1101
111. Kaur, A., Gautam, R., Srivastava, R., Chandel, A., Kumar, A., Karthikeyan, S., and Bachhawat, A. K. (2017) ChaC2, an Enzyme for Slow Turnover of Cytosolic Glutathione. *J Biol Chem* **292**, 638-651
112. Fujiwara, S., Kawazoe, T., Ohnishi, K., Kitagawa, T., Popa, C., Valls, M., Genin, S., Nakamura, K., Kuramitsu, Y., Tanaka, N., and Tabuchi, M. (2016) RipAY, a Plant Pathogen Effector Protein, Exhibits Robust gamma-Glutamyl Cyclotransferase Activity When Stimulated by Eukaryotic Thioredoxins. *J Biol Chem* **291**, 6813-6830
113. Rajput, R., Verma, V. V., Chaudhary, V., and Gupta, R. (2013) A hydrolytic gamma-glutamyl transpeptidase from thermo-acidophilic archaeon *Picrophilus torridus*: binding pocket mutagenesis and transpeptidation. *Extremophiles* **17**, 29-41
114. Verma, V. V., Gupta, R., and Goel, M. (2015) "Phylogenetic and evolutionary analysis of functional divergence among Gamma glutamyl transpeptidase (GGT) subfamilies". *Biol Direct* **10**, 49
115. Brannigan, J. A., Dodson, G., Duggleby, H. J., Moody, P. C., Smith, J. L., Tomchick, D. R., and Murzin, A. G. (1995) A protein catalytic framework with an N-terminal nucleophile is capable of self-activation. *Nature* **378**, 416-419
116. Inoue, M., Hiratake, J., Suzuki, H., Kumagai, H., and Sakata, K. (2000) Identification of catalytic nucleophile of *Escherichia coli* gamma-glutamyltranspeptidase by gamma-monofluorophosphono derivative of glutamic acid: N-terminal thr-391 in small subunit is the nucleophile. *Biochemistry* **39**, 7764-7771
117. Okada, T., Suzuki, H., Wada, K., Kumagai, H., and Fukuyama, K. (2007) Crystal structure of the gamma-glutamyltranspeptidase precursor protein from *Escherichia coli*. Structural changes upon autocatalytic processing and implications for the maturation mechanism. *J Biol Chem* **282**, 2433-2439

118. Wickham, S., West, M. B., Cook, P. F., and Hanigan, M. H. (2011) Gamma-glutamyl compounds: substrate specificity of gamma-glutamyl transpeptidase enzymes. *Anal Biochem* **414**, 208-214
119. Heisterkamp, N., Groffen, J., Warburton, D., and Sneddon, T. P. (2008) The human gamma-glutamyltransferase gene family. *Hum Genet* **123**, 321-332
120. Jaspers, C. J., and Penninckx, M. J. (1984) Glutathione metabolism in yeast *Saccharomyces cerevisiae*. Evidence that gamma-glutamyltranspeptidase is a vacuolar enzyme. *Biochimie* **66**, 71-74
121. Ohkama-Ohtsu, N., Radwan, S., Peterson, A., Zhao, P., Badr, A. F., Xiang, C., and Oliver, D. J. (2007) Characterization of the extracellular gamma-glutamyl transpeptidases, GGT1 and GGT2, in *Arabidopsis*. *Plant J* **49**, 865-877
122. Ohkama-Ohtsu, N., Zhao, P., Xiang, C., and Oliver, D. J. (2007) Glutathione conjugates in the vacuole are degraded by gamma-glutamyl transpeptidase GGT3 in *Arabidopsis*. *Plant J* **49**, 878-888
123. Grzam, A., Martin, M. N., Hell, R., and Meyer, A. J. (2007) gamma-Glutamyl transpeptidase GGT4 initiates vacuolar degradation of glutathione S-conjugates in *Arabidopsis*. *FEBS Lett* **581**, 3131-3138
124. Curthoys, N. P., and Hughey, R. P. (1979) Characterization and physiological function of rat renal gamma-glutamyltranspeptidase. *Enzyme* **24**, 383-403
125. PetitClerc, C., Shiele, F., Bagrel, D., Mahassen, A., and Siest, G. (1980) Kinetic properties of gamma-glutamyltransferase from human liver. *Clin Chem* **26**, 1688-1693
126. Woodlock, T. J., Brown, R., Mani, M., Pompeo, L., Hoffman, H., Segel, G. B., and Silber, R. (1990) Decreased L system amino acid transport and decreased gamma-glutamyl transpeptidase are independent processes in human chronic lymphocytic leukemia B-lymphocytes. *J Cell Physiol* **145**, 217-221
127. Davis, S. R., Quinlivan, E. P., Stacpoole, P. W., and Gregory, J. F., 3rd. (2006) Plasma glutathione and cystathionine concentrations are elevated but cysteine flux is unchanged by dietary vitamin B-6 restriction in young men and women. *J Nutr* **136**, 373-378
128. Hanigan, M. H., and Frierson, H. F., Jr. (1996) Immunohistochemical detection of gamma-glutamyl transpeptidase in normal human tissue. *J Histochem Cytochem* **44**, 1101-1108
129. Kaur, H., Kumar, C., Junot, C., Toledano, M. B., and Bachhawat, A. K. (2009) Dug1p Is a Cys-Gly peptidase of the gamma-glutamyl cycle of *Saccharomyces cerevisiae* and represents a novel family of Cys-Gly peptidases. *J Biol Chem* **284**, 14493-14502
130. Kaur, H., Ganguli, D., and Bachhawat, A. K. (2012) Glutathione degradation by the alternative pathway (DUG pathway) in *Saccharomyces cerevisiae* is initiated by (Dug2p-Dug3p)₂ complex, a novel glutamine amidotransferase (GATase) enzyme acting on glutathione. *J Biol Chem* **287**, 8920-8931
131. Desai, P. R., Thakur, A., Ganguli, D., Paul, S., Morschhauser, J., and Bachhawat, A. K. (2011) Glutathione utilization by *Candida albicans* requires a functional glutathione degradation (DUG) pathway and OPT7, an unusual member of the oligopeptide transporter family. *J Biol Chem* **286**, 41183-41194
132. Gila, B. C., Moon, H., Antal, K., Hajdu, M., Kovacs, R., Jonas, A. P., Pusztahelyi, T., Yu, J. H., Pocs, I., and Emri, T. (2021) The DUG Pathway Governs Degradation of Intracellular Glutathione in *Aspergillus nidulans*. *Appl Environ Microbiol* **87**
133. Oakley, A. J., Yamada, T., Liu, D., Coggan, M., Clark, A. G., and Board, P. G. (2008) The identification and structural characterization of C7orf24 as gamma-

- glutamyl cyclotransferase. An essential enzyme in the gamma-glutamyl cycle. *J Biol Chem* **283**, 22031-22042
134. Mungrue, I. N., Pagnon, J., Kohannim, O., Gargalovic, P. S., and Lusic, A. J. (2009) CHAC1/MGC4504 is a novel proapoptotic component of the unfolded protein response, downstream of the ATF4-ATF3-CHOP cascade. *J Immunol* **182**, 466-476
135. Chandel, A., Das, K. K., and Bachhawat, A. K. (2016) Glutathione depletion activates the yeast vacuolar transient receptor potential channel, Yvc1p, by reversible glutathionylation of specific cysteines. *Mol Biol Cell* **27**, 3913-3925
136. Tattoli, I., Sorbara, M. T., Vuckovic, D., Ling, A., Soares, F., Carneiro, L. A., Yang, C., Emili, A., Philpott, D. J., and Girardin, S. E. (2012) Amino acid starvation induced by invasive bacterial pathogens triggers an innate host defense program. *Cell Host Microbe* **11**, 563-575
137. Goebel, G., Berger, R., Strasak, A. M., Egle, D., Muller-Holzner, E., Schmidt, S., Rainer, J., Presul, E., Parson, W., Lang, S., Jones, A., Widschwendter, M., and Fiegl, H. (2012) Elevated mRNA expression of CHAC1 splicing variants is associated with poor outcome for breast and ovarian cancer patients. *Br J Cancer* **106**, 189-198
138. Tang, C., Lan, D., Zhang, H., Ma, J., and Yue, H. (2013) Transcriptome analysis of duck liver and identification of differentially expressed transcripts in response to duck hepatitis A virus genotype C infection. *PLoS One* **8**, e71051
139. Zhang, W., Li, H., Cheng, G., Hu, S., Li, Z., and Bi, D. (2008) Avian influenza virus infection induces differential expression of genes in chicken kidney. *Res Vet Sci* **84**, 374-381
140. Chi, Z., Zhang, J., Tokunaga, A., Harraz, M. M., Byrne, S. T., Dolinko, A., Xu, J., Blackshaw, S., Gaiano, N., Dawson, T. M., and Dawson, V. L. (2012) Botch promotes neurogenesis by antagonizing Notch. *Dev Cell* **22**, 707-720
141. Romanoski, C. E., Che, N., Yin, F., Mai, N., Pouldar, D., Civelek, M., Pan, C., Lee, S., Vakili, L., Yang, W. P., Kayne, P., Mungrue, I. N., Araujo, J. A., Berliner, J. A., and Lusic, A. J. (2011) Network for activation of human endothelial cells by oxidized phospholipids: a critical role of heme oxygenase 1. *Circ Res* **109**, e27-41
142. Yasuda, M., Tanaka, Y., Ryu, M., Tsuda, S., and Nakazawa, T. (2014) RNA sequence reveals mouse retinal transcriptome changes early after axonal injury. *PLoS One* **9**, e93258
143. Magne, L., Blanc, E., Legrand, B., Lucas, D., Barouki, R., Rouach, H., and Garlatti, M. (2011) ATF4 and the integrated stress response are induced by ethanol and cytochrome P450 2E1 in human hepatocytes. *J Hepatol* **54**, 729-737
144. Crawford, R. R., Prescott, E. T., Sylvester, C. F., Higdon, A. N., Shan, J., Kilberg, M. S., and Mungrue, I. N. (2015) Human CHAC1 Protein Degrades Glutathione, and mRNA Induction Is Regulated by the Transcription Factors ATF4 and ATF3 and a Bipartite ATF/CRE Regulatory Element. *J Biol Chem* **290**, 15878-15891
145. Chi, Z., Byrne, S. T., Dolinko, A., Harraz, M. M., Kim, M. S., Umanah, G., Zhong, J., Chen, R., Zhang, J., Xu, J., Chen, L., Pandey, A., Dawson, T. M., and Dawson, V. L. (2014) Botch is a gamma-glutamyl cyclotransferase that deglycinates and antagonizes Notch. *Cell Rep* **7**, 681-688
146. Kumar, S., Kaur, A., Chattopadhyay, B., and Bachhawat, A. K. (2015) Defining the cytosolic pathway of glutathione degradation in *Arabidopsis thaliana*: role of the ChaC/GCG family of gamma-glutamyl cyclotransferases as glutathione-degrading enzymes and AtLAP1 as the Cys-Gly peptidase. *Biochem J* **468**, 73-85
147. Paulose, B., Chhikara, S., Coomey, J., Jung, H. I., Vatamaniuk, O., and Dhankher, O. P. (2013) A gamma-glutamyl cyclotransferase protects *Arabidopsis* plants from heavy

- metal toxicity by recycling glutamate to maintain glutathione homeostasis. *Plant Cell* **25**, 4580-4595
148. Hubberten, H. M., Klie, S., Caldana, C., Degenkolbe, T., Willmitzer, L., and Hoefgen, R. (2012) Additional role of O-acetylserine as a sulfur status-independent regulator during plant growth. *Plant J* **70**, 666-677
149. Mhamdi, A., Hager, J., Chaouch, S., Queval, G., Han, Y., Taconnat, L., Saindrenan, P., Gouia, H., Issakidis-Bourguet, E., Renou, J. P., and Noctor, G. (2010) Arabidopsis GLUTATHIONE REDUCTASE1 plays a crucial role in leaf responses to intracellular hydrogen peroxide and in ensuring appropriate gene expression through both salicylic acid and jasmonic acid signaling pathways. *Plant Physiol* **153**, 1144-1160
150. Orłowski, M., and Meister, A. (1973) -Glutamyl cyclotransferase. Distribution, isozymic forms, and specificity. *J Biol Chem* **248**, 2836-2844
151. Oakley, A. J., Coggan, M., and Board, P. G. (2010) Identification and characterization of gamma-glutamylamine cyclotransferase, an enzyme responsible for gamma-glutamyl-epsilon-lysine catabolism. *J Biol Chem* **285**, 9642-9648
152. Abraham, G. N., and Podell, D. N. (1981) Pyroglutamic acid. Non-metabolic formation, function in proteins and peptides, and characteristics of the enzymes effecting its removal. *Mol Cell Biochem* **38 Spec No**, 181-190
153. Dahl, N., Pigg, M., Ristoff, E., Gali, R., Carlsson, B., Mannervik, B., Larsson, A., and Board, P. (1997) Missense mutations in the human glutathione synthetase gene result in severe metabolic acidosis, 5-oxoprolinuria, hemolytic anemia and neurological dysfunction. *Hum Mol Genet* **6**, 1147-1152
154. Ye, G. J., Breslow, E. B., and Meister, A. (1996) The amino acid sequence of rat kidney 5-oxo-L-prolinase determined by cDNA cloning. *J Biol Chem* **271**, 32293-32300
155. Van Der Werf, P., Griffith, O. W., and Meister, A. (1975) 5-Oxo-L-prolinase (L-pyroglutamate hydrolase). Purification and catalytic properties. *J Biol Chem* **250**, 6686-6692
156. Nishimura, A., Ozaki, Y., Oyama, H., Shin, T., and Murao, S. (1999) Purification and characterization of a novel 5-oxoprolinase (without ATP-hydrolyzing activity) from *Alcaligenes faecalis* N-38A. *Appl Environ Microbiol* **65**, 712-717
157. Cappiello, M., Alterio, V., Amodeo, P., Del Corso, A., Scaloni, A., Pedone, C., Moschini, R., De Donatis, G. M., De Simone, G., and Mura, U. (2006) Metal ion substitution in the catalytic site greatly affects the binding of sulfhydryl-containing compounds to leucyl aminopeptidase. *Biochemistry* **45**, 3226-3234
158. Towne, C. F., York, I. A., Neijssen, J., Karow, M. L., Murphy, A. J., Valenzuela, D. M., Yancopoulos, G. D., Neefjes, J. J., and Rock, K. L. (2005) Leucine aminopeptidase is not essential for trimming peptides in the cytosol or generating epitopes for MHC class I antigen presentation. *J Immunol* **175**, 6605-6614
159. Dringen, R., Gutterer, J. M., Gros, C., and Hirrlinger, J. (2001) Aminopeptidase N mediates the utilization of the GSH precursor CysGly by cultured neurons. *J Neurosci Res* **66**, 1003-1008
160. Kozak, E. M., and Tate, S. S. (1982) Glutathione-degrading enzymes of microvillus membranes. *J Biol Chem* **257**, 6322-6327
161. Beneke, T., Madden, R., Makin, L., Valli, J., Sunter, J., and Gluenz, E. (2017) A CRISPR Cas9 high-throughput genome editing toolkit for kinetoplastids. *R Soc Open Sci* **4**, 170095
162. Sollelis, L., Ghorbal, M., MacPherson, C. R., Martins, R. M., Kuk, N., Crobu, L., Bastien, P., Scherf, A., Lopez-Rubio, J. J., and Sterkers, Y. (2015) First efficient

- CRISPR-Cas9-mediated genome editing in *Leishmania* parasites. *Cell Microbiol* **17**, 1405-1412
163. Ivens, A. C., Peacock, C. S., Worthey, E. A., Murphy, L., Aggarwal, G., Berriman, M., Sisk, E., Rajandream, M. A., Adlem, E., Aert, R., Anupama, A., Apostolou, Z., Attipoe, P., Bason, N., Bauser, C., Beck, A., Beverley, S. M., Bianchetin, G., Borzym, K., Bothe, G., Bruschi, C. V., Collins, M., Cadag, E., Ciarloni, L., Clayton, C., Coulson, R. M., Cronin, A., Cruz, A. K., Davies, R. M., De Gaudenzi, J., Dobson, D. E., Duesterhoeft, A., Fazelina, G., Fosker, N., Frasch, A. C., Fraser, A., Fuchs, M., Gabel, C., Goble, A., Goffeau, A., Harris, D., Hertz-Fowler, C., Hilbert, H., Horn, D., Huang, Y., Klages, S., Knights, A., Kube, M., Larke, N., Litvin, L., Lord, A., Louie, T., Marra, M., Masuy, D., Matthews, K., Michaeli, S., Mottram, J. C., Muller-Auer, S., Munden, H., Nelson, S., Norbertczak, H., Oliver, K., O'Neil, S., Pentony, M., Pohl, T. M., Price, C., Purnelle, B., Quail, M. A., Rabbinowitsch, E., Reinhardt, R., Rieger, M., Rinta, J., Robben, J., Robertson, L., Ruiz, J. C., Rutter, S., Saunders, D., Schafer, M., Schein, J., Schwartz, D. C., Seeger, K., Seyler, A., Sharp, S., Shin, H., Sivam, D., Squares, R., Squares, S., Tosato, V., Vogt, C., Volckaert, G., Wambutt, R., Warren, T., Wedler, H., Woodward, J., Zhou, S., Zimmermann, W., Smith, D. F., Blackwell, J. M., Stuart, K. D., Barrell, B., and Myler, P. J. (2005) The genome of the kinetoplastid parasite, *Leishmania major*. *Science* **309**, 436-442
164. Fairlamb, A. H., and Cerami, A. (1992) Metabolism and functions of trypanothione in the Kinetoplastida. *Annu Rev Microbiol* **46**, 695-729
165. Lu, S. C. (2013) Glutathione synthesis. *Biochim Biophys Acta* **1830**, 3143-3153
166. Krauth-Siegel, R. L., and Comini, M. A. (2008) Redox control in trypanosomatids, parasitic protozoa with trypanothione-based thiol metabolism. *Biochim Biophys Acta* **1780**, 1236-1248
167. Orłowski, M., and Meister, A. (1970) The gamma-glutamyl cycle: a possible transport system for amino acids. *Proc Natl Acad Sci U S A* **67**, 1248-1255
168. Manta, B., Comini, M., Medeiros, A., Hugo, M., Trujillo, M., and Radi, R. (2013) Trypanothione: a unique bis-glutathionyl derivative in trypanosomatids. *Biochim Biophys Acta* **1830**, 3199-3216
169. Berriman, M., Ghedin, E., Hertz-Fowler, C., Blandin, G., Renault, H., Bartholomeu, D. C., Lennard, N. J., Caler, E., Hamlin, N. E., Haas, B., Bohme, U., Hannick, L., Aslett, M. A., Shallom, J., Marcello, L., Hou, L., Wickstead, B., Alsmark, U. C., Arrowsmith, C., Atkin, R. J., Barron, A. J., Bringaud, F., Brooks, K., Carrington, M., Cherevach, I., Chillingworth, T. J., Churcher, C., Clark, L. N., Corton, C. H., Cronin, A., Davies, R. M., Doggett, J., Djikeng, A., Feldblyum, T., Field, M. C., Fraser, A., Goodhead, I., Hance, Z., Harper, D., Harris, B. R., Hauser, H., Hostetler, J., Ivens, A., Jagels, K., Johnson, D., Johnson, J., Jones, K., Kerhornou, A. X., Koo, H., Larke, N., Landfear, S., Larkin, C., Leech, V., Line, A., Lord, A., Macleod, A., Mooney, P. J., Moule, S., Martin, D. M., Morgan, G. W., Mungall, K., Norbertczak, H., Ormond, D., Pai, G., Peacock, C. S., Peterson, J., Quail, M. A., Rabbinowitsch, E., Rajandream, M. A., Reitter, C., Salzberg, S. L., Sanders, M., Schobel, S., Sharp, S., Simmonds, M., Simpson, A. J., Tallon, L., Turner, C. M., Tait, A., Tivey, A. R., Van Aken, S., Walker, D., Wanless, D., Wang, S., White, B., White, O., Whitehead, S., Woodward, J., Wortman, J., Adams, M. D., Embley, T. M., Gull, K., Ullu, E., Barry, J. D., Fairlamb, A. H., Opperdoes, F., Barrell, B. G., Donelson, J. E., Hall, N., Fraser, C. M., Melville, S. E., and El-Sayed, N. M. (2005) The genome of the African trypanosome *Trypanosoma brucei*. *Science* **309**, 416-422
170. Sacks, D. L. (1989) Metacyclogenesis in *Leishmania* promastigotes. *Exp Parasitol* **69**, 100-103

171. Sacks, D. L., Brodin, T. N., and Turco, S. J. (1990) Developmental modification of the lipophosphoglycan from *Leishmania major* promastigotes during metacyclogenesis. *Mol Biochem Parasitol* **42**, 225-233
172. McConville, M. J., Turco, S. J., Ferguson, M. A., and Sacks, D. L. (1992) Developmental modification of lipophosphoglycan during the differentiation of *Leishmania major* promastigotes to an infectious stage. *EMBO J* **11**, 3593-3600
173. Deniaud, A., Sharaf el dein, O., Maillier, E., Poncet, D., Kroemer, G., Lemaire, C., and Brenner, C. (2008) Endoplasmic reticulum stress induces calcium-dependent permeability transition, mitochondrial outer membrane permeabilization and apoptosis. *Oncogene* **27**, 285-299
174. Sacks, D. L., and Perkins, P. V. (1984) Identification of an infective stage of *Leishmania* promastigotes. *Science* **223**, 1417-1419
175. Dolai, S., Yadav, R. K., Pal, S., and Adak, S. (2008) *Leishmania major* ascorbate peroxidase overexpression protects cells against reactive oxygen species-mediated cardiolipin oxidation. *Free Radic Biol Med* **45**, 1520-1529
176. Rajasekaran, N. S., Connell, P., Christians, E. S., Yan, L. J., Taylor, R. P., Orosz, A., Zhang, X. Q., Stevenson, T. J., Peshock, R. M., Leopold, J. A., Barry, W. H., Loscalzo, J., Odelberg, S. J., and Benjamin, I. J. (2007) Human alpha B-crystallin mutation causes oxido-reductive stress and protein aggregation cardiomyopathy in mice. *Cell* **130**, 427-439
177. Kapoor, P., Sachdev, M., and Madhubala, R. (2000) Inhibition of glutathione synthesis as a chemotherapeutic strategy for leishmaniasis. *Trop Med Int Health* **5**, 438-442
178. Mukherjee, A., Roy, G., Guimond, C., and Ouellette, M. (2009) The gamma-glutamylcysteine synthetase gene of *Leishmania* is essential and involved in response to oxidants. *Mol Microbiol* **74**, 914-927
179. Saunders, E. C., Ng, W. W., Chambers, J. M., Ng, M., Naderer, T., Kromer, J. O., Likic, V. A., and McConville, M. J. (2011) Isotopomer profiling of *Leishmania mexicana* promastigotes reveals important roles for succinate fermentation and aspartate uptake in tricarboxylic acid cycle (TCA) anaplerosis, glutamate synthesis, and growth. *J Biol Chem* **286**, 27706-27717
180. Kloehn, J., Saunders, E. C., O'Callaghan, S., Dagley, M. J., and McConville, M. J. (2015) Characterization of metabolically quiescent *Leishmania* parasites in murine lesions using heavy water labeling. *PLoS Pathog* **11**, e1004683
181. Weldrick, D. P., Chodacka, B., Vogt, R., and Steenkamp, D. J. (1999) The effect of buthionine sulfoximine on the growth of *Leishmania donovani* in culture. *FEMS Microbiol Lett* **173**, 139-146
182. Dumas, C., Ouellette, M., Tovar, J., Cunningham, M. L., Fairlamb, A. H., Tamar, S., Olivier, M., and Papadopoulou, B. (1997) Disruption of the trypanothione reductase gene of *Leishmania* decreases its ability to survive oxidative stress in macrophages. *EMBO J* **16**, 2590-2598
183. Mavi, P. S., Singh, S., and Kumar, A. (2020) Reductive Stress: New Insights in Physiology and Drug Tolerance of Mycobacterium. *Antioxid Redox Signal* **32**, 1348-1366
184. Zhang, H., Limphong, P., Pieper, J., Liu, Q., Rodesch, C. K., Christians, E., and Benjamin, I. J. (2012) Glutathione-dependent reductive stress triggers mitochondrial oxidation and cytotoxicity. *FASEB J* **26**, 1442-1451
185. Venketaraman, V., Dayaram, Y. K., Talaue, M. T., and Connell, N. D. (2005) Glutathione and nitrosoglutathione in macrophage defense against *Mycobacterium tuberculosis*. *Infect Immun* **73**, 1886-1889

BIBLIOGRAPHY

186. Venketaraman, V., Dayaram, Y. K., Amin, A. G., Ngo, R., Green, R. M., Talaue, M. T., Mann, J., and Connell, N. D. (2003) Role of glutathione in macrophage control of mycobacteria. *Infect Immun* **71**, 1864-1871
187. Das, S., Panja, P., Chowdhury, G., Biswas, S., Dholey, Y., and Adak, S. (2022) The ChaC family of gamma-glutamyl cyclotransferases is required for *Leishmania* to switch to a slow growth state and for long-term survival of the parasite. *J Biol Chem*, 102510

PUBLICATIONS

- ❖ **Das, S., Panja, P., Chowdhury, G., Biswas, S., Dholey, Y., and Adak, S. (2022) The ChaC family of gamma-glutamyl cyclotransferases is required for *Leishmania* to switch to a slow growth state and for long-term survival of the parasite. *J Biol Chem*, 102510**
- ❖ **Biswas, S., Adhikari, A., Mukherjee, A., Das, S., and Adak, S. (2020) Regulation of *Leishmania major* PAS domain-containing phosphoglycerate kinase by cofactor Mg²⁺ ion at neutral pH. *FEBS J.* **287**, 5183–5195**
- ❖ **Adhikari, A., Biswas, S., Mukherjee, A., Das, S., and Adak, S. (2019) PAS domain-containing phosphoglycerate kinase deficiency in *Leishmania major* results in increased autophagosome formation and cell death. *Biochem. J.* **476**, 1303–1321**

CONFERENCES

- ❖ Participated and presented a poster entitled “**Requirement of ChaC family of γ -glutamyl cyclotransferases in *Leishmania* parasite for switching to its slow growth state and long-term survival**” at the 14th Annual Meeting of the Proteomics Society, India and International Conference on Protein & Proteomics (PSI-ICPP 2022) organized by CSIR- Indian Institute of Chemical Biology, Kolkata. (Certificate attached)



The ChaC family of γ -glutamyl cyclotransferases is required for *Leishmania* to switch to a slow growth state and for long-term survival of the parasite

Received for publication, August 5, 2022, and in revised form, September 12, 2022. Published, Papers in Press, September 17, 2022.

<https://doi.org/10.1016/j.jbc.2022.102510>

Sumit Das, Puja Panja, Gaurab Chowdhury, Saroj Biswas, Yuthika Dholey¹, and Subrata Adak*

From the Division of Structural Biology & Bio-informatics, CSIR-Indian Institute of Chemical Biology, Kolkata, India

Edited by Ruma Banerjee

The ChaC family of γ -glutamyl cyclotransferases is conserved throughout all Kingdoms and catalyzes the degradation of GSH. So far, the ChaC family proteins in trypanosomal parasites are missing in the literature. Here, we report two members of the ChaC family of γ -glutamyl cyclotransferases (LmChaC_{2a} and LmChaC_{2b}) in the unicellular pathogen *Leishmania*. Activity measurements suggest that these proteins catalyze degradation of GSH but no other γ -glutamyl peptides. Recombinant LmChaC_{2a} protein shows \sim 17-fold lower catalytic efficiency ($k_{\text{cat}} \sim 0.9 \text{ s}^{-1}$) than LmChaC_{2b} ($k_{\text{cat}} \sim 15 \text{ s}^{-1}$), although they showed comparable K_m values (\sim 1.75 mM for LmChaC_{2a} and \sim 2.0 mM for LmChaC_{2b}) toward GSH. qRT-PCR and Western blot analyses suggest that the LmChaC_{2a} protein was found to be constitutively expressed, whereas LmChaC_{2b} was regulated by sulfur stress. To investigate its precise physiological function in *Leishmania*, we generated overexpressed, knockout, and complement cell lines. Flow cytometric analyses show the presence of a higher intracellular GSH concentration and lower intracellular ROS level, indicative of a more reductive environment in null mutants. We found LmChaC2-expressing cells grow in GSH-containing sulfur-limited media, while the null mutants failed to grow, suggesting that LmChaC2 is crucial for cell growth with GSH as the only sulfur source. Null mutants, although reach the stationary phase rapidly, display impaired long-term survival, indicating that LmChaC2-mediated GSH degradation is necessary for prolonged survival. *In vivo* studies suggest that LmChaC2-dependent controlled GSH degradation promotes chronic infection by the parasite. Altogether, these data indicate that LmChaC2 plays an important role in GSH homeostasis in *Leishmania*.

Generally, GSH displays extreme diverse roles in prokaryotic and eukaryotic cells including mitochondrial iron-sulfur biogenesis (1), elimination of oxidative stress, metal and xenobiotic detoxification, redox buffer, storage and transport of sulfur (2, 3), and its capacity to regulate protein function by glutathionylation (4).

In addition, GSH also regulates immune cell functions, like initiating the Th1 or Th2 immune responses by controlling the antigen-processing machinery in antigen-presenting cells (5).

Furthermore, the depletion of GSH is one of the markers of apoptosis (6) and low GSH concentration, are closely associated with several diseases (7). On the other hand, excessive GSH levels are also detrimental to the cell (8–10). It is well known that GSH synthesis and degradation play a significant role in maintaining GSH homeostasis (11, 12).

Protozoan parasites, trypanosomatids, have several unique features; one of them is trypanothione [T(SH)₂] based redox metabolism. A massive amount of reactive oxygen species (ROS) is produced by activated macrophages as initial line of defense against the parasites (13, 14). Surviving parasite is able to tolerate the ROS during its life cycle by recruiting a number of antioxidant molecules including unique redox proteins and low molecular weight thiols (15). The main ROS detoxification system in trypanosomatids is a chain of reactions where trypanothione reduces 2-Cys-peroxiredoxin and GSH peroxidase-like enzymes sequentially after receiving reducing equivalents from trypanothione (a GSH-spermidine conjugate) (16–18). While the GSH biosynthesis steps of the parasite are common to mammals, the T(SH)₂ biosynthesis pathways are only present in trypanosomatids (19, 20). Both γ -glutamylcysteine synthetase and GSH synthetase in the parasite's GSH biosynthesis pathway are known (21, 22), whereas the breakdown of GSH to amino acids is completely unknown in this parasite.

ChaC (cation transport regulator-like protein) is the third gene of CHA operon in *Escherichia coli* and is supposed to function as a γ -glutamyl cyclotransferase (23). The activity of ChaC protein toward the reduced form of GSH involves the cleavage of γ -glutamyl bond of GSH with subsequent production of 5-oxoproline and Cys-Gly (24). Human ChaC1 protein has been shown to be induced under endoplasmic reticulum (ER) stress condition in the cells (25, 26). Two ChaC homologs, ChaC1 and ChaC2, are found in higher eukaryotes, where constitutively expressed ChaC2 protein displays \sim 10 to 20 times reduced catalytic efficiency compared to inducibly expressed ChaC1 protein (27).

We have found two putative ChaC-like proteins of different molecular weights (237 amino acids and 323 amino acids) in tandem array within *Leishmania major* genome database. Those putative ChaC-like proteins are present in the genome database of all trypanosomal parasites. Although the eukaryotic ChaC1 and ChaC2 are the GSH-degrading enzymes (26, 27), the potential functions of leishmanial

* For correspondence: Subrata Adak, adaks@iicb.res.in.

ChaC2 proteins from *Leishmania major*

putative ChaC proteins have not yet been explored. In this article, we characterize the two ChaC proteins from *L. major* (LmChaC_{2a} and LmChaC_{2b}), which catalyze the γ -glutamyl bond cleavage of the GSH to produce Cys-Gly and 5-oxoproline. Surprisingly, our data revealed that the LmChaC_{2b} (larger protein) showed ~17 fold more catalytic activity compared to the LmChaC_{2a} (smaller protein). Although LmChaC_{2b} protein expression was significantly increased in sulfur-limited media and stationary phase culture, LmChaC_{2a} protein is constitutively expressed. In addition, we demonstrate for the first time that the growth rate of null mutants is very high but they display impaired long-term survival in the aged culture and reduced pathogenicity in macrophage and BALB/c mice.

Results

Sequence analysis of LmChaC_{2a} and LmChaC_{2b} proteins

Two putative LmChaC sequences in tandem array (systematic name: LmjF.22.1190 and LmjF.22.1200) within *L. major* genome database (<https://tritrypdb.org/tritrypdb/app>) have been identified as ORF, comprising of 237 and 323

residues, respectively. Multiple sequence alignment revealed that the shorter version (237 amino acids) and the longer version of putative LmChaC proteins (323 amino acids) bear 32% and 35% identity with the human ChaC1, respectively (Fig. 1). On the other hand, the shorter version and the longer version of putative LmChaC protein have about 40% and 45% identity with the human ChaC2, respectively (Fig. 1). Signature YGSL/I motif and catalytic glutamate residue were present in both genes, confirming that both proteins belong to the ChaC family of γ -glutamyl cyclotransferase proteins. As higher sequence identity is observed with human ChaC2 protein, we have denoted the shorter version (237 amino acids) as LmChaC_{2a} and the longer version (323 amino acids) as LmChaC_{2b}.

Biochemical characteristics of LmChaC_{2a} and LmChaC_{2b} proteins

To identify the biochemical properties of LmChaC_{2a} and LmChaC_{2b} proteins, both the full length proteins were expressed in *E. coli* cells. Purified LmChaC_{2b} and LmChaC_{2a} proteins migrated to positions in the gel as predicted by

```

LmChaC2a -----MSSSS 5
LmChaC2b -----MPKTDTDVSAHHHYGTHQPPTGGSTPASHVAASLPKLLPAQPELPHQH 48
HsChaC1 MGGAQLELPSGARPGVCVRRSFRAHAGDQPRRPPGPIVPG----TMKQESAAPNTPTPS 56
HsChaC2 ----- 0

LmChaC2a ELVTRATHYHEQFGLPSFDDRVFVVFYGSILWKQNFEDAEYEAYIKGYKRVFYQGSRD 65
LmChaC2b STETASTRYHEQFGLPSFDDHVFFVVFYGSILWKQNFEDAEYEAYIKGYKRVFYQGSRH 108
HsChaC1 QS----PTPSAQFPRNDGDPQALWIFGYGSLVWRPDFAYSDSRVGFRGYSRRFWQGDTF 112
HsChaC2 -----MWVFGYGSILWKVDFPYQDKLVGYITNYSRRFWQGSTD 38
          : :*****:*: :* :. . .: :.* * :**

LmChaC2a HRGVPDKPGRVVTLVLLPSEDKEQRVYGKAYQLPADPEKLNRIQALDVRE--KGGYERLFV 123
LmChaC2b HRGVPDKPGRVVTLVLLPSEDKEQRVYGKAYQLPADPEKLNRIQALDVRE---GGYDRVQL 165
HsChaC1 HRGSDKMPGRVVTLV--EDHEGCTWGVAYVQVQGEQVSKA--LKYLNVREAVLGGYDTKEV 168
HsChaC2 HRGVPGKPGRVVTLV--EDPAGCVWGVAYRLPVGKEEEV--KAYLDFRE--KGGYRTTTV 92
          ***      *****: **      .:* **::      .      *:.**      ***      :

LmChaC2a TIYDAHPSFATDGEDRP-----LRLA 144
LmChaC2b TLFNAHPTTGNLTTTTPMLPAPMSKSFKIESSTQYVPPRQNSSDVEAGVAEKVLDIFSHP 225
HsChaC1 TFYPQDAP----- 176
HsChaC2 IFYPKDPT----- 100
          :: .

LmChaC2a DKGTGTPGKAMVCLCYNATEDNADYLGPATMEAMARQILSSTGLSGPNREYLYNLDRALR 204
LmChaC2b NPAVQPRKNVYLYCYIATEQNEGYVGEASMEEMAAEILSCAGVSGSNREYLFLLADCLR 285
HsChaC1 -----DQPLKALAYVATPQNGYLGPAPEEAIATQILACRGFSGHNLEYLLRLADFMQ 229
HsChaC2 -----TKPFSVLLYIGTCNDNPDYLGPALLEDIAEQIFNAAGPSGRNTEYLFELANSIR 153
          : . * * . * : * . * : * * * : * : * : . * * * * * * * * * : :

LmChaC2a DMGA--ADPHVFELAALARQLEVECPAVIC--SEKK-I---- 237
LmChaC2b AMGA--TDPHVFELDAVAKRIILRGREAEEFA--AGAKRVATMA 323
HsChaC1 LCGPQAQDEHLAAIVDAVGTM-----LPCFCPTEQALALV- 264
HsChaC2 NLVPEEAEHLFALEKLVKERLEGKQNLNCI----- 184
          * *: : .
  
```

Figure 1. Sequence analysis of ChaC family of γ -glutamyl cyclotransferases from *Leishmania major*. Amino acid sequence of LmChaC_{2a} and LmChaC_{2b} were aligned with human ChaC1 and ChaC2. *indicates identical residue. Dashes indicate variations in sequence length among aligned proteins. Underline denotes active site residues.

theoretical relative molecular weight of 38 kDa (Fig. 2A, lane 4) and 28 kDa protein (Fig. 2A, lane 9), respectively. Products of the assay mixture were identified by HPLC after the enzymatic reaction of these LmChaC2 family proteins on GSH. When these proteins are present in assay mixture, peaks of GSH disappeared and new peaks for 5-oxoproline and Cys-Gly dipeptide emerged (Fig. 2B). Production of 5-oxoproline from GSH degradation confirmed the γ -glutamyl cyclotransferase activity of the LmChaC family proteins. Both LmChaC_{2a} and LmChaC_{2b} proteins follow standard Michaelis–Menten kinetics with respect to the substrate (GSH) (Figs. 2C and S1). The K_m values for GSH were very similar between LmChaC_{2a} and LmChaC_{2b} proteins: 1.75 ± 0.08 mM for LmChaC_{2a} and 2.0 ± 0.15 mM for LmChaC_{2b}. These K_m values were comparable with human as well as mouse ChaC protein (27). Our experimental K_m value of recombinant LmChaC2 proteins is high with respect to

intracellular concentration of GSH (0.21 mM in promastigotes and 0.39 mM in amastigotes stage (28)). One possible reason is that either the K_m value of natural LmChaC2 within intracellular environment might be lower compared to experimental value of recombinant protein or the previous determinations of intracellular GSH concentrations may not be sufficiently reliable. Although K_m of both proteins are similar but LmChaC_{2a} proteins show ~ 17 -fold lower catalytic efficiency ($k_{cat} = 0.9 \pm 0.1$ s⁻¹) than LmChaC_{2b} ($k_{cat} = 15 \pm 1.8$ s⁻¹). To evaluate the relative activities of the LmChaC2 proteins toward different γ -Glu-dipeptides, T(SH)₂, and GSSG, we estimated their γ -glutamyl cyclotransferase activity by measuring the 5-oxoproline concentration (Figs. 2D and S2). The results showed that both enzymes showed activity toward GSH (Fig. 2B) but no activity toward the other γ -Glu-amino acids as well as GSSG and T(SH)₂ (Figs. 2D and S2). These results suggest that both LmChaC2 proteins serve as γ -glutamyl

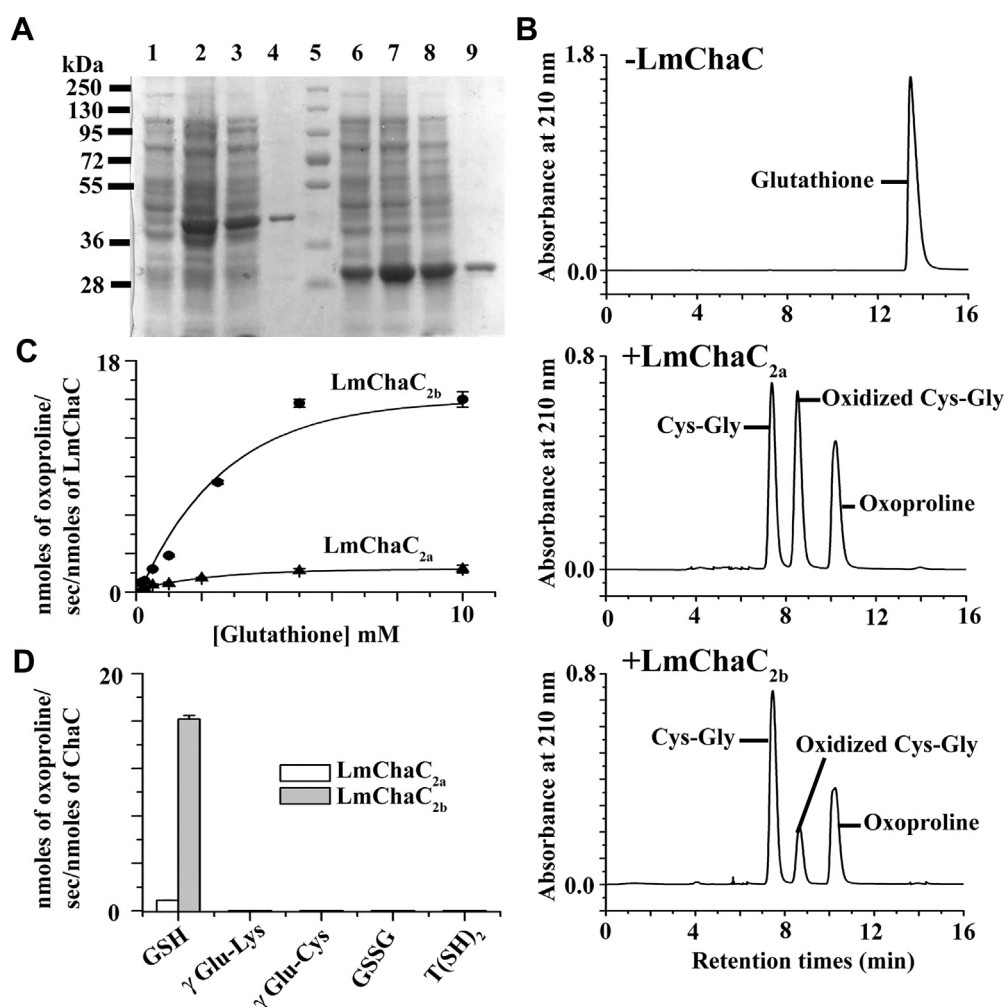


Figure 2. Biochemical characteristics of LmChaC_{2a} and LmChaC_{2b}. A, SDS-PAGE. Lanes: 1, -IPTG (LmChaC_{2b}); 2, +IPTG (LmChaC_{2b}); 3, lysate (LmChaC_{2b}); 4, purified LmChaC_{2b} protein; 5, molecular weight marker; 6, -IPTG (LmChaC_{2a}); 7, +IPTG (LmChaC_{2a}); 8, lysate (LmChaC_{2a}); and 9, purified (LmChaC_{2a}). B, the LmChaC proteins display enzymatic activity specifically toward GSH producing 5-oxoproline and Cys-Gly. Assay mixture was analyzed using HPLC system on a Sunfire C₁₈ column (5 μ m 4.6 \times 250 mm, Waters) and a mobile phase of 2% (v/v) aqueous perchloric acid at 1.0 ml/min flow rate. C, GSH-dependent oxoproline production. All values were derived from time-dependent oxoproline production curve at different concentration of GSH in SI Fig. S1. The initial velocity of LmChaC_{2a} and LmChaC_{2b} was calculated within 5 min and 2 min incubation period, respectively. D, LmChaC activity in the presence of different γ -glutamyl dipeptides, GSSG and T(SH)₂. The concentrations of T(SH)₂, GSSG, γ -Glu-Lys, γ -Glu-Cys, LmChaC_{2a}, and LmChaC_{2b} used were 10 mM, 10 mM, 10 mM, 10 mM, 3.57 μ M, and 0.26 μ M, respectively.

ChaC2 proteins from *Leishmania major*

cyclotransferases acting specifically on GSH degradation but no other γ -glutamyl peptides.

Regulation of LmChaC_{2a} and LmChaC_{2b} proteins in *Leishmania parasite*

Earlier researchers have reported that the human ChaC1 expression was induced by ER stress or sulfur starvation, whereas human ChaC2 was constitutively expressed (25, 27). To identify whether GSH degrading enzymes, LmChaC_{2a} and LmChaC_{2b}, are constitutively or inducibly expressed in the parasite, we performed semi-quantitative real-time PCR (sqRT-PCR) and Western blot analyses. The results suggested that both the LmChaC_{2a} and the LmChaC_{2b} were expressed in the promastigote as well as the amastigote stages (Fig. 3, A and B). qRT-PCR analysis data suggested that LmChaC_{2b} expression does not change significantly during the log phase of growth but increases 1.5 times during stationary phase with or without treatment with acidic pH 5.6 (Fig. 3C). However, treatments with neither tunicamycin (ER stress-inducing agent) nor H₂O₂ (oxidative stress inducer) could significantly influence the expression of either of the proteins (Fig. 3D). The breakdown of GSH also provides sulfur for the cells. Therefore, we used qRT-PCR and Western blot analysis to investigate the effect of sulfur-limited media on the expression of LmChaC_{2a} and LmChaC_{2b} (Fig. 3, E and F). We found that LmChaC_{2b} transcription was significantly increased (3.5-fold) in sulfur-limited media up to 48 h (Fig. 3E), but after 48 h, the level of LmChaC_{2b} started decreasing (data not shown), which might be caused by a decrease in cell viability. On the other hand, there was no significant change in the mRNA levels of LmChaC_{2a}. We also assessed the protein expression levels by using Western blot technique where LmChaC_{2b} expression increased significantly at 48 h incubation in sulfur-limited media but LmChaC_{2a} level remained constant (Fig. 3F). These results indicate that LmChaC_{2a} protein was constitutively expressed, whereas LmChaC_{2b} was controlled by sulfur stress.

Characterization of control (CT), ChaC_{2a} overexpressed (OE_{2a}), ChaC_{2b} overexpressed (OE_{2b}), knockout (KO), ChaC_{2a} complement (CM_{2a}), ChaC_{2b} complement (CM_{2b}), and ChaC_{2a} & ChaC_{2b} double complement (CM) cells

To investigate the LmChaC_{2a} and LmChaC_{2b} function in *L. major*, CRISPR/Cas9 gene editing technique was used (Fig. 4A) to knock the genes out. PCR analysis from genomic DNA (gDNA) and Western blotting confirmed that null mutant cells (KO) no longer expressed LmChaC_{2a} or LmChaC_{2b} gene (Fig. 4, B and C). The OE_{2a} and OE_{2b} cell lines expressed higher amounts of LmChaC_{2a} and LmChaC_{2b} proteins compared to CT cell line, respectively. Western blot analysis demonstrated that the CM_{2a} cell line expressed only LmChaC_{2a} protein, whereas CM_{2b} cell line expressed only LmChaC_{2b} protein. The double complemented (CM) leishmanial cell lines expressed both the proteins in amounts comparable to control cells. Next, we investigated whether the levels of intracellular GSH and T(SH)₂ were changed in the OE_{2a}, OE_{2b}, KO, CM_{2a}, and CM_{2b} cells compared to CT and

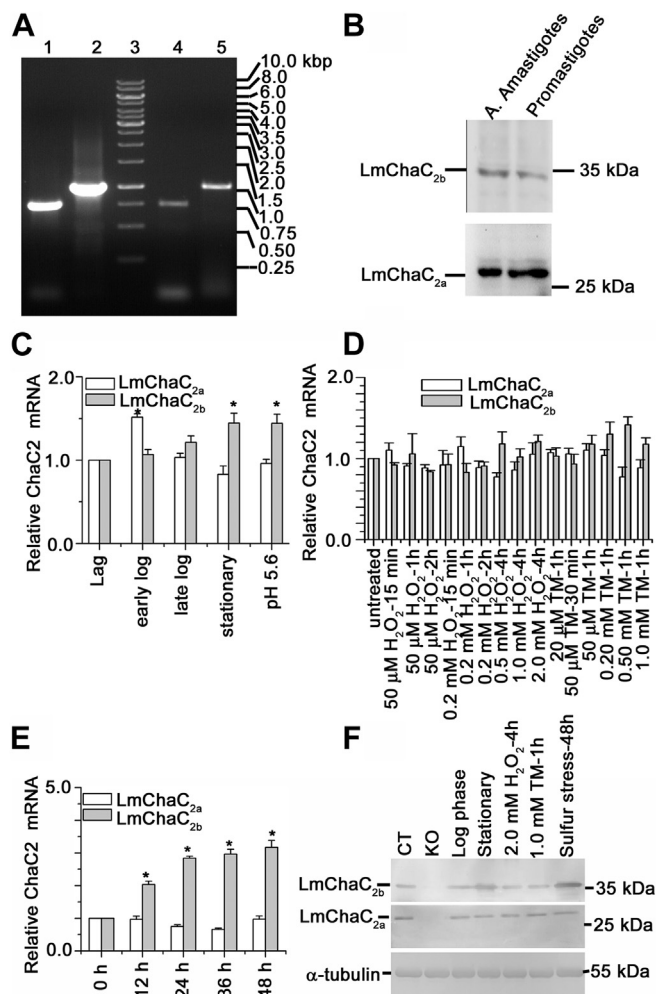


Figure 3. mRNA and protein expression of LmChaC_{2a} as well as LmChaC_{2b} in the promastigote and the amastigote stages of parasite. **A**, agarose gel analysis of PCR-amplified products from cDNA of LmChaC_{2a} and LmChaC_{2b}. Lane 3 shows the molecular mass marker, lanes 1 and 2, correspond to PCR product from cDNA of promastigotes with LmChaC_{2a} and LmChaC_{2b} specific primers, respectively. Lanes 4 and 5, correspond to PCR product from cDNA of purified intracellular amastigotes using LmChaC_{2a} and LmChaC_{2b} specific primers, respectively. **B**, the lysate of promastigotes and the axenic amastigotes (A. Amastigotes) stages of *L. major* was used for Western blotting. Rabbit anti-LmChaC_{2a} and anti-LmChaC_{2b} antibody are used in Western blot analysis. **C**, the measurement of gene transcript abundance was analyzed by using quantitative real-time PCR (qRT-PCR) at different stages during growth of promastigotes. pH 5.6 denoted stationary phase promastigotes those were incubated at acidic pH 5.6 (pH of phagolysosome) for 24 h. **D**, the measurement of mRNA abundance in promastigotes stage of parasite was analyzed by using qRT-PCR in presence of H₂O₂ and ER stress inducer tunicamycin. **E**, the measurement of mRNA transcript in promastigotes stage of parasite, which incubated at sulfur-limited media up to 48 h. **F**, gene expression was analyzed by Western blot in presence of sulfur-limited media (for 48 h), H₂O₂ (2 mM for 4 h), or tunicamycin (1 mM for 1 h). All the data are representative of at least three independent experiments. *Statistically significant value of less than 0.05. cDNA, complementary DNA; ER, endoplasmic reticulum.

CM cells (Figs. 4D and S3). HPLC analysis suggested that KO cells had ~2- and ~4-fold higher intracellular GSH and T(SH)₂ content compared to CT cells, respectively. Flow cytometry results confirmed that KO cells had higher amount of intracellular GSH (Fig. 4E) compared to CT, OE_{2a}, OE_{2b}, CM_{2a}, CM_{2b}, or CM cell lines. As expected, the order of intracellular GSH accumulation was KO > CM_{2a} > CM_{2b} > CT or CM > OE_{2a} > OE_{2b} cells.

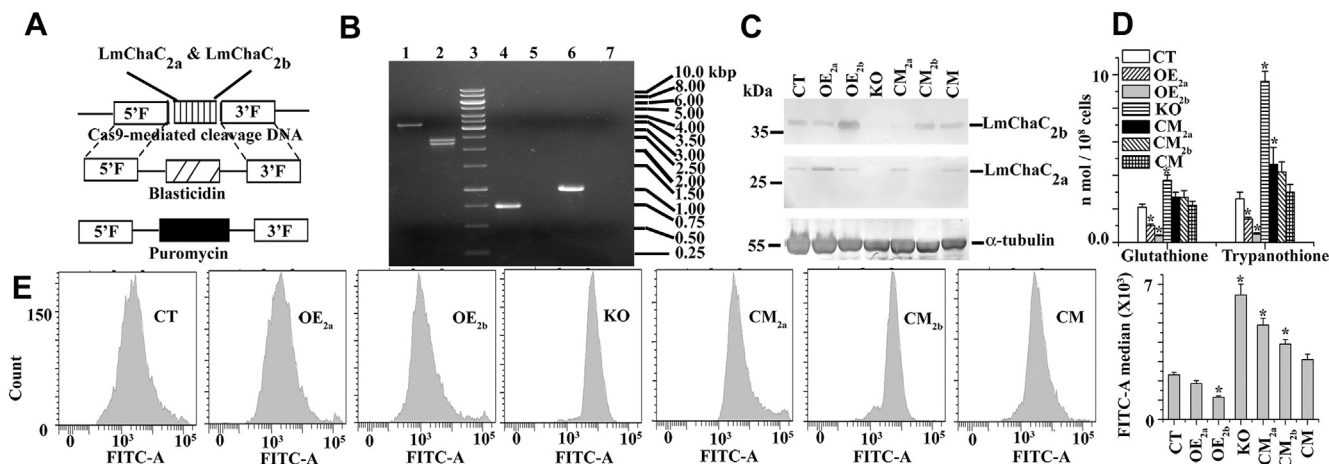


Figure 4. Generation of stable KO strain for both *LmCha2a* and *LmCha2b* alleles by CRISPR/Cas9 based editing. A, schematic representation of the *LmCha2a* and *LmCha2b* locus and the plasmid constructs used for gene replacement. B, agarose gel analysis of PCR amplified products of *LmCha2a* and *LmCha2b* genes. Lanes 1/4/6 and 2/5/7 correspond to PCR with gDNA from WT and KO mutants, respectively, with primers external (5' and 3' flanking region) (lanes 1–2) of both genes, internal of *LmCha2a* gene (lanes 4–5) and internal of *LmCha2b* gene (lanes 6–7). The expected size of the *LmCha2a*-*LmCha2b* genes, PURO, and BLAST gene PCR product are 3.2, 2.4, and 2.3 Kb, respectively. The expected size of the PCR product with internal primers of *LmCha2a* and *LmCha2b* are 0.714 and 0.972 Kb, respectively. C, Western blot analysis was done by using anti-*LmCha2a*, anti-*LmCha2b*, and anti- α -tubulin antibody. 200 μ g of *L. major* lysate were used for Western blotting. D, intracellular GSH and T(SH)₂ measurement by HPLC system. Cell lysate was making from 2×10^8 promastigotes at 4 °C and then the supernatant was filtered through 0.22 μ m Millipore filter paper. Forty microliters sample was injected to the HPLC analysis using C₁₈ HPLC column (Sunfire C₁₈ 5 μ m 4.6 \times 250 mm Column, Waters) with a 2% (v/v) aqueous solution of perchloric acid used as the mobile phase with 1 ml/min flow rate at 210 nm. Peak of GSH and T(SH)₂ were appeared at ~12 and ~52 min, respectively (HPLC chromatogram was shown in SI Fig. S3). GSH and T(SH)₂ were identified with authentic standards. The intracellular concentration of GSH and T(SH)₂ was measured from standard curve. E, flow cytometric determination of intracellular GSH by intracellular GSH Detection Assay Kit (Abcam). All the data are representative of at least three independent experiments. *Statistically significant value of less than 0.05. gDNA, genomic DNA.

Depletion of cellular GSH and T(SH)₂ often leads to an increased level of ROS within the cell. To evaluate the intracellular ROS concentration in CT, OE_{2a}, OE_{2b}, KO, CM_{2a}, CM_{2b}, and CM late log phase cell lines, we used DCFDA (fluorescent probe). The intracellular ROS level in the KO population was lower compared to the CT, OE_{2a}, OE_{2b}, CM_{2a}, CM_{2b}, and CM cells, indicating that the *LmCha2* proteins were able to enhance the endogenous ROS generation by degradation of GSH in the *Leishmania* parasite (Fig. 5A). The importance of intracellular ROS in maintaining intracellular Ca²⁺ homeostasis is now widely acknowledged. We measured intracellular Ca²⁺ levels in OE_{2a}, OE_{2b}, CT, KO, CM_{2a}, CM_{2b}, and CM cell lines by flow cytometry assay using the calcium sensor, Fluo 4AM dye (Fig. 5B). The intensity of the green fluorescence of Fluo 4AM dye for the KO cells was at least two folds lower than that in the CT cells, suggesting that deletion of *LmCha2* genes protected the cells against oxidative stress-mediated increase of cytosolic Ca²⁺ (Fig. 5B). The order of elevation of cytosolic Ca²⁺ accumulation was KO < CM_{2a} < CM_{2b} < CT or CM < OE_{2a} < OE_{2b} cells. Cell death can result from disruption of ROS homeostasis and an increase in cytosolic Ca²⁺. To investigate whether depletion of *LmCha2a* and *LmCha2b* genes shielded against oxidative stress-induced cell death, we compared the percentage of viable (propidium iodide [PI] negative) parasites among OE_{2a}, OE_{2b}, CT, KO, CM_{2a}, CM_{2b}, and CM late log phase cell lines by flow cytometry assay using the PI dye (Fig. 5C). Flow cytometry data revealed that the majority of the null mutant parasite population was PI negative (Fig. 5C), while higher amount of PI positive cells was found in the OE population, where excess amounts of *LmCha2* proteins had resulted in reduced amount of GSH. These results

suggested that deletion of *LmCha2* genes protected cells against cell death at late log phase cell lines. We next tested whether deletion of *LmCha2* proteins inhibits the oxidative stress-induced cell differentiation from procyclic (noninfective stage) to nondividing metacyclic (infective stage) promastigotes. By negative agglutination reaction with peanut agglutinin (PNA), we were able to isolate metacyclic promastigotes from OE_{2a}, OE_{2b}, CT, KO, CM_{2a}, CM_{2b}, and CM late log phase cell cultures (PNA). While procyclic parasites readily agglutinate, metacyclic promastigotes, due to developmental changes in terminally exposed oligosaccharides on the lipophosphoglycan, do not interact with peanut agglutinin (PNA⁻) (29). Interestingly, a quantitative analysis of PNA agglutination by flow cytometry revealed that KO cell population consisted of lower metacyclic (PNA⁻) parasites compared to OE_{2a}, OE_{2b}, CT, CM_{2a}, CM_{2b}, or CM cells (Fig. 5D). These results strongly suggested that deletion of *LmCha2* genes prevent the cell differentiation from procyclic (noninfective stage) to metacyclic (infective stage) promastigote cells.

Deletion of *LmCha2a* and *LmCha2b* alleles leads to decreased expression of the antioxidant gene *LmAPX*

The upregulation of antioxidant gene, ascorbate peroxidase (*LmAPX*), in the *Leishmania* parasite by oxidative stress has been reported (30). To examine the possibility that *LmAPX* gene expression in parasite was downregulated by reductive environment, we performed qRT-PCR and Western blot to measure *LmAPX* in KO, OE_{2a}, OE_{2b}, CT, CM_{2a}, CM_{2b}, and CM cells. qRT-PCR results suggested a lower expression of *LmAPX* (2-fold) mRNA in null mutants compared to CT or

ChaC2 proteins from *Leishmania major*

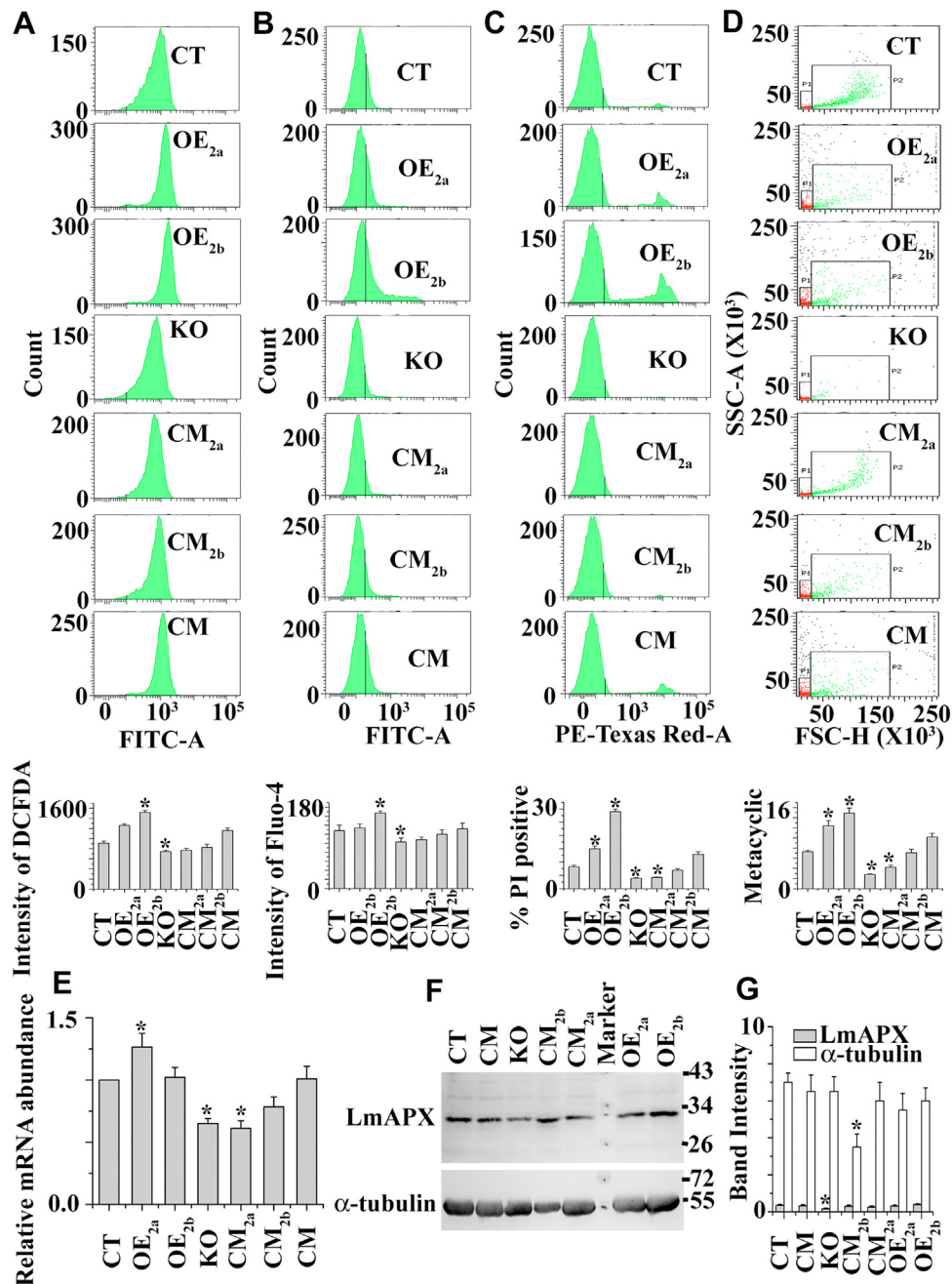


Figure 5. Characteristics of control (CT), ChaC_{2a} overexpressed (OE_{2a}), ChaC_{2b} overexpressed (OE_{2b}), KO, ChaC_{2a} complement (CM_{2a}), ChaC_{2b} complement (CM_{2b}), and ChaC_{2a} & ChaC_{2b} complement (CM) cells. A, flow cytometric determination of intracellular ROS by DCFDA. B, the intracellular Ca²⁺ level was measured by flow cytometric method using Fluo 4AM. C, percentage of death cells (PI positive staining) was measured in the late log phase population by flow cytometric analysis. D, metacyclic (PNA negative) population in the late log phase cells were analyzed by flow cytometry after their purification using PNA. The gating on the dot-plots corresponds to different cell sizes and forward-angle light scatter (FSC) intensities (FSC_{low} and FSC_{high}). FSC_{low} (denoted by small box area) represents mainly the metacyclic (PNA⁻) population. E, comparative studies of mRNA abundance of LmAPX among CT, OE_{2a}, OE_{2b}, KO, CM_{2a}, CM_{2b}, and CM promastigotes were analyzed by using quantitative real-time PCR. F, Western blot analysis was done by using anti-LmAPX and anti-α-tubulin antibody. Two hundred micrograms of *L. major* lysate were used for Western blotting. G, bar diagram depicted as the percentage of band intensities in panel (F). All the data are representative of at least three independent experiments. *Statistically significant value of less than 0.05. PI, propidium iodide; ROS, reactive oxygen species.

CM cells (Fig. 5E). The order of ascorbate peroxidase expression was KO < CM_{2a} < CM_{2b} < CT or CM < OE_{2a} < OE_{2b} cells. Western blot analysis was performed (Fig. 5, F and G) to further validate these data, and the results were remarkably similar to qRT-PCR data. Altogether, these results indicated that LmAPX was repressed under reducing environment.

GSH homeostasis is essential for slow growth and long-term survival of *L. major* promastigotes

The intracellular thiols were increased by providing extracellular GSH in *Leishmania infantum* (31) and GSH supplementation rescued an RNAi knockdown of γ-glutamylcysteine synthetase in *Trypanosoma brucei* (32), indicating that GSH transporter is present in this type of parasite. To investigate

whether growth of null mutants in sulfur-limited media is affected by absence or presence of external GSH, growth curve analysis was performed. As expected, the growth curves showed that none of cell lines could grow in sulfur-limited media (Fig. 6A). While the KO population could not grow in GSH-containing sulfur-limited media, the OE_{2a}, OE_{2b}, CT, CM_{2a}, CM_{2b}, or CM cell line expressing ChaC family proteins grew very efficiently in presence of extracellular GSH (Fig. 6B). These results suggest that ChaC family protein in *Leishmania* helps to grow when GSH was used as the only sulfur source. Next, we examined whether null mutants can grow in N-acetyl cysteine (NAC) containing sulfur-limited media. Interestingly, it was observed that null mutants were able to grow in NAC containing sulfur-limited media (Fig. 6C). These results indicate that the KO cell can synthesize *de novo* GSH, T(SH)₂, and other sulfur containing amino acid when NAC was used as the sulfur source. To investigate the role of ChaC2 proteins in the parasite, *Leishmania* were grown in normal nutrient-rich media. KO and CM_{2a} cells had higher growth rates compared to OE_{2a}, OE_{2b}, CT, CM_{2b}, or CM promastigotes (Fig. 6D). KO cells were grown faster but the parasite could not survive for longer time in the aged culture media compared to OE_{2b}, CT, CM_{2b}, or CM cell lines. These results indicate that LmChaC_{2b} protein is required for long-time survival under unfavorable growth condition. According to flow cytometry (Fig. 6E) studies, KO cells contained 4-fold (75%) more dead cells (PI-positive cells) than CT (18%) or CM (20%) cells at late stationary phase culture. These results provide an explanation why the growth rate of KO cell was declined rapidly compared to CT cells.

LmChaC2 is crucial for disease development

L. major cells, after infection, grow in host macrophage cells; therefore, we concentrated on the infectivity rate of *Leishmania* promastigotes with the macrophages. We examined to what extent OE_{2a}, OE_{2b}, CT, KO, CM_{2a}, CM_{2b}, and CM cells were phagocytosed by the host cells (macrophages). The interaction rates of the KO promastigotes with macrophage were lower compared to those of OE_{2a}, OE_{2b}, CT, CM_{2a}, CM_{2b}, or CM cells (Fig. 7A). Number of KO parasites in the infected macrophages was still lower compared to control cells when checked after 48 h of incubation. The lower level of infection in KO parasites might be due to lower number of infective metacyclic promastigotes. Additionally, the percentage of macrophages infected with null mutants was also significantly low compared to the CT and CM cell lines (Fig. 7B). We discovered that, in contrast to null mutants, CT and CM promastigotes in the BALB/c mice model could develop a severe disease (Fig. 7C). On the other hand, the OE_{2a} and OE_{2b} promastigotes were showing very negligible virulence *in vivo* infection model, revealing a fine tuning of the amount of intracellular GSH content is crucial for *Leishmania* infection. To strengthen the aforementioned results, we measured OE_{2a}, OE_{2b}, CT, KO, CM_{2a}, CM_{2b}, and CM parasite burden at 12 weeks post infection (Fig. 7D). Optimum level of parasite burden was present in CT and CM cells compared to

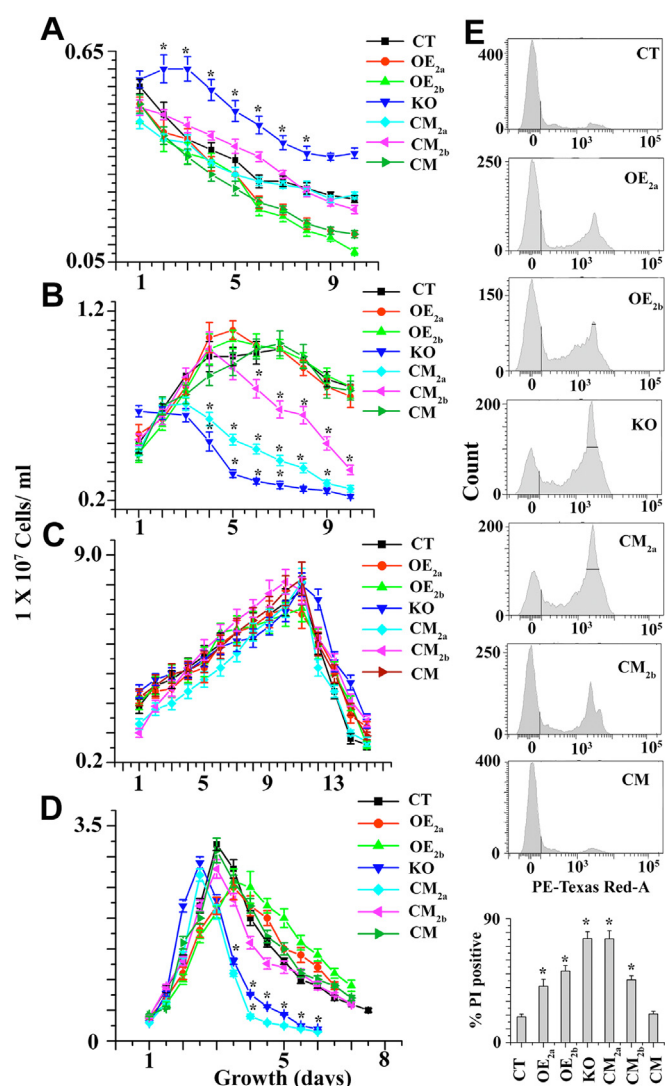


Figure 6. Comparative studies of the growth profile among CT, OE_{2a}, OE_{2b}, KO, CM_{2a}, CM_{2b}, and CM promastigotes. A, 10⁶ mid-log phase promastigotes were seeded in 5 ml sulfur-deficient M199 media (Himedia-AT1076) supplemented with 10% FBS. B, 10⁶ mid-log phase promastigotes were seeded in 5 ml sulfur-deficient M199 media supplemented with 10% FBS in presence of 4 mg/ml GSH. C, 10⁶ mid-log phase cells were inoculated in 5 ml sulfur-deficient M199 media supplemented with 10% FBS (Gibco) in presence of 25 mg/L N-acetyl cysteine. D, 10⁶ mid-log phase promastigotes were seeded in 10 ml normal M199 media supplemented with 10% FBS. E, percentage of death cells (PI positive staining) was measured by flow cytometric analysis during the late stationary phase population. *Statistically significant value of less than 0.05. FBS, fetal bovine serum; PI, propidium iodide.

KO and OE cell lines. These data confirmed the importance of LmChaC2 protein-mediated intracellular GSH homeostasis in parasite infection.

Discussion

It is well known that GSH is essential for *Leishmania* survival, but it is still unknown whether GSH homeostasis in the parasite is required for survival or not. In this article, we have shown for the first time that LmChaC-dependent controlled GSH degradation is crucial for chronic infection. Here, we discuss the following salient points: (a) we demonstrate that

ChaC2 proteins from *Leishmania major*

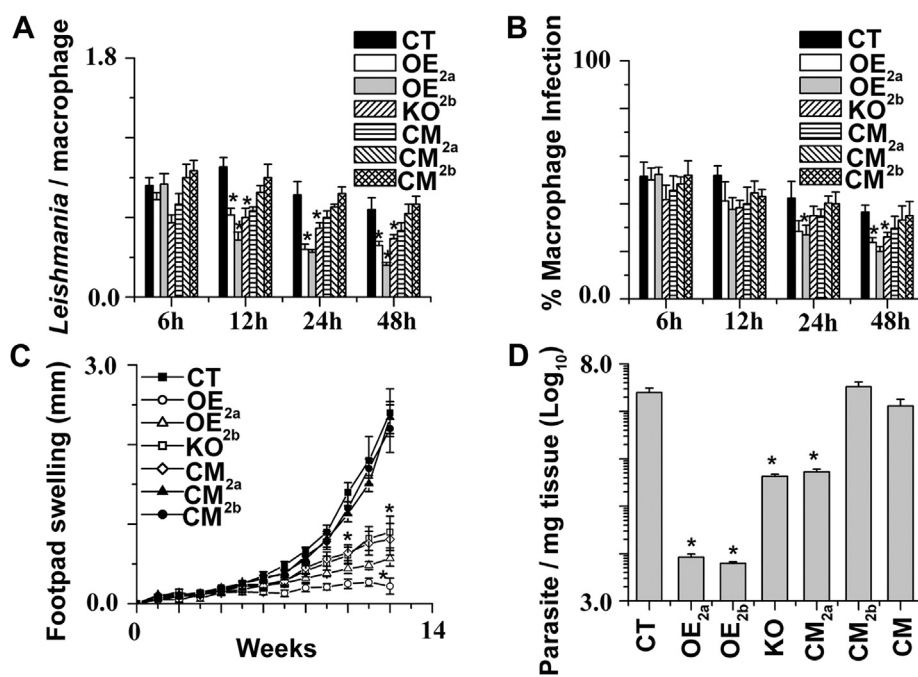


Figure 7. *In vitro* and *in vivo* infection with CT, OE_{2a}, OE_{2b}, KO, CM_{2a}, CM_{2b}, and CM promastigotes. **A**, the number of *Leishmania* within each infected macrophage was counted. For each time point, 200 macrophages were counted. **B**, the percentage of macrophages infected with different LmChaC_{2a} and LmChaC_{2b} variants of parasites. For each time point and cell type, 200 infected macrophages were analyzed. **C**, infection in BALB/c mice. Footpad swelling of different LmChaC_{2a} and LmChaC_{2b} variants was observed for the three groups (8 mice/group). **D**, parasite burden in the footpad after 12 weeks post infection. *Statistically significant value of less than 0.05.

both the promastigote and the amastigote stages of *Leishmania* parasites express two ChaC proteins of different molecular weights (LmChaC_{2a} and LmChaC_{2b}), which can degrade GSH to produce 5-oxoproline and Cys-Gly dipeptide; (b) the constitutively expressed LmChaC_{2a} (28 kDa) protein has a much lower catalytic efficiency than LmChaC_{2b} (38 kDa); (c) the expression of the LmChaC_{2b} gene was induced under sulfur limitation; (d) the results from null mutants suggest that LmChaC2 proteins control intracellular GSH/T(SH)₂ concentration, level of oxidative stress, Ca²⁺ concentration, differentiation from noninfective procyclic stage to nondividing infective metacyclic stage and cell death; (e) LmChaC_{2b} gene is required for the long-term parasite survival during stationary phase culture and plays a key role for disease development. Taken together, our data suggest that GSH homeostasis is pivotal for the long-term parasite survival during stationary phase culture and disease development in mice.

Generally, trypanosomatids lack genes like GSH reductase (GR) as well as thioredoxin reductase (TrxR) (33–35), which are essential for maintaining the intracellular thiol redox homeostasis through the GSH/GR and thioredoxin/TrxR systems in most eukaryotic organisms. On the other hand, trypanosomatids possess a unique pathway of redox metabolism that is based on the low molecular mass dithiol trypanothione [bis(glutathionyl) spermidine], T(SH)₂ (18) and T(SH)₂ reductase (36). Therefore, the three main functions of GSH in *Leishmania* parasite are (a) being an essential component in T(SH)₂ biosynthesis, (b) S-glutathionylation of protein and drugs, and (c) providing cysteine, glycine, and glutamate by degradation. In the GSH cycle of host and parasite, the first two steps for the

biosynthesis of GSH from Glu, Cys, and Gly are common in both the organisms. In this article, we showed that the GSH can be degraded by the GSH-specific ChaC-family of γ -GCT (γ -glutamyl cyclotransferase) enzymes to produce cysteinyl-glycine and 5-oxoproline. Like host genes, the *Leishmania* genome sequence have putative 5-oxoprolinase (LmjF.18.1040) and putative M20/M25/M40 family dipeptidase (LmjF.33.1610) genes. The GSH degradation products 5-oxoproline and cysteinyl-glycine are cleaved by 5-oxoprolinase and dipeptidases, respectively, to yield Glu, Cys, and Gly. In contrast to host, parasite's genome lacks γ -glutamyl transpeptidase (GGT) gene, which has a transpeptidation activity and is involved in the process by which γ -glutamyl group is transferred to the amino acid to produce γ -glutamyl amino acid and cysteinyl-glycine (37). In addition, γ -GCT (C7orf24) and γ -glutamyl amine cyclotransferase (GGACT) are found in mammalian cells; the former enzyme reacts with various γ -glutamyl amino acids to produce 5-oxoproline and amino acids (38) and the latter reacts with γ -glutamyl amine to produce 5-oxoproline and amine (39). However, two parasite specific unique enzymes, glutathionyl-spermidine synthetase and T(SH)₂ synthetase can consume GSH in presence of spermidine and produce T(SH)₂, which controls the intracellular redox environment in parasite.

Required for T(SH)₂ biosynthesis, GSH is an important thiol small molecule for detoxification of ROS and protection against oxidative stress. At par with this, our results show, when GSH degrading enzymes were deleted from the parasite genome, KO cells showed higher intracellular GSH/T(SH)₂ concentration and subsequently lower level of oxidative stress,

free intracellular Ca^{2+} ion and cell death during late log phase. Albeit CT cells had lower growth rate compared to KO promastigotes in nutrient enriched normal media (Fig. 6D), CT parasite survive for longer time in the aged culture media compared to KO cell lines, indicating that slower growth was required for long-term survival under unfavorable growth condition. This raises the question as to why slower growth rate was required for long-term survival. One possible explanation is a high rate of replication, as observed in the KO promastigotes, might exploit glycolysis pathway rather than tricarboxylic acid cycle and generate more NADPH and partially oxidized intermediates for the synthesis of excessive amount of DNA, RNA, and proteins and consequently deplete rapidly all essential nutrients from media. Consistent with previous concept, procyclic dividing stage of *Leishmania* promastigotes uses high glucose concentrations, at the same time maintaining controlled flux into the tricarboxylic acid cycle with concomitant production of NADH by secreting partially oxidized intermediates, such as acetate, succinate, and alanine into the culture medium (40). In case of intracellular amastigote stage, a group of researchers had shown from their heavy water labeling experiments that metabolically quiescent state in *Leishmania* parasites in murine lesions may underlie the intrinsic resistance to many stresses (temperature, pH, and nutrient) and is important for slow but constant replication and persistence of the parasite (41, 42). We report here a beneficial role of LmChaC2 proteins in promastigote stage of parasites; LmChaC2-dependent degradation of GSH to Cys, Glu, and Gly may be required for survival in stationary phase culture. Earlier work reports no significant change in the total intracellular thiol concentration during various logarithmic growth phases, but a 6-fold decrease in thiol level is observed as the parasites enter the stationary phase (43). Similarly, the T(SH)₂ concentration (1–2 mM) remains unaltered during the different logarithmic growth phases of the insect stages of *Trypanosoma cruzi*, *L. major*, and *Leishmania donovani* but decreases rapidly during the stationary phase culture (28). Our results showed that LmChaC_{2b} protein was induced during stationary phase culture and sulfur-limited media (Fig. 3, C, E, and F). Thus, catalytically efficient LmChaC_{2b} protein might be responsible for supplying Cys, Glu, and Gly from GSH that could be utilized for essential protein synthesis during stationary phase, when those nutrients become limited.

T(SH)₂ and redox proteins of the parasite regulate efficiently the redox homeostasis and withstand the oxidative burst during the early stages of host-*Leishmania* interactions (44). The virulence of LmChaC_{2b} overexpressed cell lines (having negligible amount of T(SH)₂) is much lower compared to CT cells, indicating that T(SH)₂ plays an important role in disease development. On the other hand, KO mutants (4-fold excess T(SH)₂) too have shown lower virulent property than CT. This may suggest that excessive T(SH)₂ production might as well be harmful to parasite itself. Several other reports have shown deleterious effects of excessive GSH in both mammalian cells and unicellular eukaryotes (8, 9). Increasing GSH concentration by using either addition of NAC or genetic manipulation study (*i.e.*, overexpression of glutamate cysteine ligase catalytic

subunit (GCLC)/glutamate cysteine ligase modifier subunit (GCLM)) affects the redox status that promotes reductive stress associated with mitochondrial dysfunction (10). Other reports showed that excess GSH is inhibitory to the growth of intracellular human pathogen *Mycobacterium tuberculosis* (45) while its mutant, defective in the uptake of excess GSH, had grown better inside the macrophages (46). They strongly suggested from their observations that this pathogen is exposed to reductive stress within the phagocytic host. In this article, we show that KO mutants defective in the degradation of GSH could not manifest a severe disease, compared to CT promastigotes (Fig. 7C). These findings suggest that the generation of cysteine/glutamate/glycine from the recycling of GSH could be vital for protein synthesis and is of significance to the parasite.

Experimental procedures

Materials

Leishmania strain bank of our Institute provides *L. major* (strain 5ASKH) cells. All chemicals were procured from Sigma or sources reported previously (47–50).

Ethics statement

Our institutional animal facility provided all BALB/c mice and rabbits and was taking care of all animals. The research project was approved by the IICB Animal Ethical Committee (Registration No.147/1999, CPCSEA). Our institutional animal facility was registered with the Committee for the Purpose of Control and Supervision on Experiments on Animals (CPCSEA), Government of India. The BALB/c mice and rabbits were handled according to their guidelines.

Cloning of LmChaC_{2a} and LmChaC_{2b}

By using QIAamp DNA mini kit, gDNA from promastigotes stage of *L. major* was purified. Primer 1 and primer 2 (Table S1) were used to amplify 714-bp containing LmChaC_{2a} ORF fragment by PCR. The PCR product was digested and cloned using NdeI/BamHI restriction enzymes in the pET28a vector. DNA sequencing was carried out to confirm the ORF. The entire LmChaC_{2b} ORF was similarly amplified by PCR using primer 3 and primer 4 (Table S1) to generate a 972 bp fragment that was digested and cloned into the pET16b vector between NdeI/BamHI restriction sites and confirmed the ORF by DNA sequencing.

Expression and purification of LmChaC_{2a} and LmChaC_{2b}

Recombinant pET28a/LmChaC_{2a} and pET16b/LmChaC_{2b} construct were transformed into *E. coli* BL21 (DE3) and *E. coli* C41 (DE3) cells to express LmChaC_{2a} and LmChaC_{2b} proteins, respectively. Recombinant pET28a/LmChaC_{2a} and pET16b/LmChaC_{2b} transformed cells were inoculated in separate 50 ml LB broth for overnight at 37 °C in the presence of kanamycin (50 µg/ml) and ampicillin (200 µg/ml), respectively. Following overnight growth, cultures were transferred separately into the 500 ml of terrific broth in the presence of respective drug and

ChaC2 proteins from *Leishmania major*

incubated at 37 °C. About 0.5 mM IPTG was added after attaining the absorbance 0.5 to 0.8 at 600 nm and bacteria were induced for 16 h at 16 °C. Then, the induced cells were harvested by centrifuging at 6000 rpm for 7 min and after washing the pellet with PBS, pellet was resuspended in lysis buffer containing 50 mM potassium phosphate buffer (pH 6.0), 100 mM sodium chloride, glycerol (10%), β -mercaptoethanol, lysozyme (1 mg/ml), imidazole (20 mM), protease inhibitor cocktail without EDTA (Thermo Scientific), and PMSF (1 mM). The complete cell lysis was performed by frequent vortexing, followed by sonication for 20 s pulse and 40 s gap, repeated for 18 times in ice (Ultrasonic homogenizer, model-U250, Takashi). The whole lysate was centrifuged at 14,000 rpm for 1 h and supernatant was loaded into a pre-equilibrated Ni²⁺-NTA column. To obtain the protein from the column, elution buffer was used that contains 250 mM imidazole. Dialysis was performed thrice for removing maximum amount of imidazole from the protein for further analysis. The 10% SDS-PAGE was run to confirm the purity and molecular weight of the proteins.

Activity measurement by HPLC

Ten micrograms of LmChaC_{2a} or 1.0 μ g of LmChaC_{2b} were incubated with 10 mM γ -Glu-Cys, γ -Glu- ϵ -Lys, GSSG, T(SH)₂, or GSH in 100 μ l of reaction mix containing 50 mM Tris-HCl buffer (pH 8) to examine the γ -GCT activity of the LmChaC proteins. Up to 60 min of incubation at 37 °C, reactions were terminated by heat denaturation at 95 °C for 5 min. Then, denatured proteins were removed by centrifugation at 14,000 rpm for 30 min before injection of the sample in HPLC (Waters). Twenty microliters of the reaction mixture were injected to analyze the reaction products in HPLC using reverse phase C₁₈ HPLC column (SunfireTM C₁₈ 5 μ m 4.6 \times 250 mm column, Waters) and 2% perchloric acid as mobile phase (flow rate 1 ml/min, wavelength 210 nm). Authentic standards were used to identify the substrate and all of the products (Cys-Gly, GSH, and 5-oxoproline). Reaction product peaks are appeared at 7.1 min, 8.2 min, and 9.9 min, those are identified as Cys-Gly, oxidized Cys-Gly, and 5-oxoproline, respectively. The concentration of GSH degradation with time was measured by the production of 5-oxoproline from standard curve. Initial velocity of LmChaC proteins was measured at different concentrations of GSH to determine the K_m value for GSH. In case of time-dependent enzymatic reaction, 100 μ g of LmChaC_{2a} or 10.0 μ g of LmChaC_{2b} were incubated in 1.0 ml of 50 mM Tris-HCl buffer (pH 8) at 37 °C with different concentration of GSH. Hundred microliter aliquots were withdrawn from the reaction mixture at different time intervals. Withdrawal sample was quickly terminated by heat denaturation at 95 °C for 5 min. The enzyme-catalyzed reactions in LmChaC proteins exhibited saturation kinetics. Michaelis-Menten constant (K_m) and the turnover number (k_{cat}) values were calculated by using Michaelis-Menten enzyme kinetics in scientific statistics software (analysis of nonlinear regression) GRAPHPAD PRISM 6, GraphPad Software, Inc.

Generation of genetically modified T7/Cas9 positive *L. major*

Genetically modified T7/Cas9 positive *L. major* was prepared by transfecting the cells with PacI digested linear pTB007 (Flag::NLS::Cas9::NLSNLS::T7 RNAP) plasmid (51, 52). Cells were serially passaged and maintained in M199 media (Gibco) with 10% fetal bovine serum (FBS) (Gibco) and hygromycin B (100 μ g/ml) (Roche). PacI digested linear pTB007 was integrated in the β -tubulin locus of *L. major* for T7 RNA polymerase and Cas9 proteins stable expression. Genetically modified *L. major* was identified by PCR method using Cas9 gene specific primer 5 and 6 (Table S1).

Generation of stable KO strain (LmChaC_{2a} + LmChaC_{2b})^{-/-} for both LmChaC_{2a} and LmChaC_{2b} alleles by CRISPR/Cas9-based editing

CRISPR-Cas9-based editing was performed for KO of both LmChaC_{2a} and LmChaC_{2b} genes in genetically modified *L. major* (strain 5ASKH) promastigote cells (containing T7 polymerase and Cas9). Primer sequences were designed for KO of both LmChaC_{2a} and LmChaC_{2b} (LmjF.22.1190 and LmjF.22.1200) genes by using LeishGEdit server (<http://leishgedit.net/>). Two repair cassettes bearing the puromycin and the blasticidin-resistance genes were amplified from pTPuro_v1 and pTblast_v1 vectors, respectively, by using 15 ng pT plasmids, 0.2 mM dNTPs, 3% (v/v) dimethyl sulfoxide, 2 μ M of primers 7 and 8 (Table S1), 1 unit platinum Taq DNA polymerase high fidelity (Invitrogen) and 1 \times high fidelity reaction buffer in 40 μ l reaction mixture. PCR steps were initial denaturation at 95 °C for 5 min, then 40 cycles comprise of 30 s at 98 °C, 30 s at 65 °C, and 2 min 15 s at 72 °C, and lastly a final extension of 7 min at 72 °C. Two single-guide RNA (sgRNA) cassettes targeting the 5' end of LmChaC_{2a} and the 3' end of LmChaC_{2b} (5' and 3' sgRNA templates) were amplified by using 0.2 mM dNTPs, 2 μ M of primer 9 (primer G00, sgRNA scaffold), 2 μ M of primer 10 (LmChaC_{2a} 5' sgRNA primers) or primer 11 (LmChaC_{2b} 3' sgRNA primers) (Table S1), and 1 unit platinum Taq DNA polymerase high fidelity (Invitrogen). PCR steps were initial denaturation for 30 s at 98 °C, followed by 35 cycles of 10 s at 98 °C, 30 s at 60 °C, and 15 s at 72 °C and a final extension step of 10 min at 72 °C. The 1% agarose gel was run to confirm the molecular weight and purity of the PCR products. Two PCR purified drug cassettes, 5' sgRNA template, and 3' sgRNA template were cotransfected into log phase T7/Cas9 positive *L. major* cells by electroporation. Electroporation was performed in Bio-Rad Gene Pulsar apparatus using 450 V and 500 μ F capacitance. The transfected cells were revived for 24 h in Schneider's *Drosophila* insect media (Gibco) at 22 °C. After revival at Schneider's *Drosophila* insect media, cells were transferred in M199 media (Gibco) supplemented with 15% FBS, 100 μ g/ml hygromycin B, 20 μ g/ml puromycin dihydrochloride (Sigma-Aldrich), and 5 μ g/ml blasticidin (Invitrogen) at 22 °C.

Construction of overexpression system in *L. major* (OE_{2a} and OE_{2b})

To amplify LmChaC_{2a} ORF, we used primers 12 and 13 (Table S1). Using primers 14 and 15 (Table S1), entire ORF of

LmChaC_{2b} was amplified by PCR. The amplified products were separately inserted into pXG-B2863 vector between SmaI and BamHI sites to construct recombinant pXG-B2863/LmChaC_{2a} and pXG-B2863/LmChaC_{2b}. Recombinant pXG-B2863 vector containing LmChaC_{2a} or LmChaC_{2b} was transfected in *L. major* by electroporation using 450 V and 500 μ F capacitances with a Bio-Rad Gene Pulsar apparatus. Finally, 200 μ g/ml of neomycin was used to maintain all the transfected cells. Western blot analysis was used to confirm over-expressed cell lines with a rabbit anti-LmChaC_{2a} or rabbit anti-LmChaC_{2b} antibody (1:100).

Complementation of LmChaC_{2a} gene in KO mutant (CM_{2a})

Recombinant pXG-B2863 vector containing LmChaC_{2a} was transfected into the KO cells. Finally, antibiotics neomycin (200 μ g/ml), puromycin (20 μ g/ml), and blasticidin (5 μ g/ml) was used to maintain the transfected CM_{2a} promastigotes at 22 °C. LmChaC_{2a} expression was confirmed by Western blot with rabbit anti-LmChaC_{2a} antibody (1:100).

Complementation of LmChaC_{2b} in KO mutant (CM_{2b})

The ORF of LmChaC_{2b} was amplified using primer 18 and 19 (Table S1). BamHI site of pXG-PHLEO vector was used to generate recombinant pXG-PHLEO/LmChaC_{2b}, which was transfected into the KO cells. Phleomycin (10 μ g/ml), puromycin (20 μ g/ml), and blasticidin (5 μ g/ml) antibiotics was used to maintain transfected cell lines at 22 °C. LmChaC_{2b} expression was measured by Western blot using rabbit anti-LmChaC_{2b} antibody (1:100).

Complementation of both LmChaC_{2a} and LmChaC_{2b} genes in KO mutant (CM)

LmChaC_{2b}/pXG-PHLEO plasmids were transfected into CM_{2a} cells. Antibiotics neomycin, phleomycin, puromycin, and blasticidin (as earlier concentration) was used to maintain the transfected CM cell lines. Expression of both LmChaC_{2a} and LmChaC_{2b} proteins were confirmed by Western blot analysis.

Production of polyclonal antibodies against LmChaC_{2a} and LmChaC_{2b} proteins

Polyclonal antibodies were generated against the pure recombinant LmChaC_{2a} or LmChaC_{2b} by injecting LmChaC_{2a} or LmChaC_{2b} (20 mg) protein subcutaneously along with Freund's complete adjuvant (Sigma) to a 6-month-old female rabbit, respectively. Next three booster doses of LmChaC_{2a} or LmChaC_{2b} protein (15 mg) along with incomplete adjuvant (Sigma) were administered to respective female rabbit at the interval of 15 days. Two weeks after the last injection, blood was collected from both the ear of rabbits and serum was isolated from the blood by centrifugation at 3000 rpm (20 min) for Western blot analysis.

Western blot analysis

Protein samples were loaded on 10% SDS-PAGE for separation on the basis of molecular weight and then transferred on 0.45 μ m nitrocellulose membrane (Merck-Millipore) by wet transfer for 1 h at 90V with TE series transphor electrophoresis unit (Hoefer) at 4 °C. The 5% bovine serum albumin solution was used to block the membrane for 3 h at 37 °C, after that polyclonal anti-rabbit LmChaC_{2a} or LmChaC_{2b} antibody was applied for overnight incubation at 4 °C. Then membrane was washed thrice with 1 \times Tris-buffered saline with Tween-20 at 5 min interval and membrane was incubated for 2 h with AP-conjugated anti-rabbit secondary antibody (1:16,000) (Sigma) or horseradish peroxidase (HRP) conjugate secondary antibody (1:16,000) (Merck). Anti- α -tubulin antibody (Merck) and AP or HRP-conjugated antimouse secondary antibody (1:15,000) (Sigma) was used to detect α -tubulin, which was measured as a loading control. Clarity Max TM Western ECL substrate (Bio-rad) and NBT-BCIP (Roche) was applied to develop the band for HRP conjugate antibody and AP conjugated antibody, respectively.

ROS measurement by CM-H₂DCFDA

ROS production was measured with CM-H₂DCFDA (Invitrogen) by flow cytometer. Control, overexpressed, KO, and complement cells (1 \times 10⁷ promastigotes/ml) were washed two times with 1 \times PBS at 4000 rpm (4 °C) for 6 min. Then 6 μ M CM-H₂DCFDA was applied to the cells for 30 min incubation at 26 °C in dark with gentle shaking and fluorescent intensity was measured in the flow cytometer (BD LSR Fortessa) (Ex λ -493 nm; Em λ -527 nm for CM-H₂DCFDA).

Intracellular calcium (Ca²⁺) measurement

Cell permeant calcium indicator Fluo-4/AM (Invitrogen) was used to measure intracellular Ca²⁺ concentrations. About 1 \times 10⁷ control, overexpressed, KO, and complement cells were pelleted and washed twice at 4000 rpm for 6 min with chilled 1 \times PBS. Then, all the cells were incubated separately with 6 μ M Fluo-4/AM along with 5 μ M pluronic acid F127 for 60 min at room temperature (RT). After that cells were washed twice with fresh media and measured the fluorescence with flow cytometer (BD LSR Fortessa) (Ex λ -494 nm; Em λ -506 nm).

Cell death measurement by flow cytometry

DNA intercalating fluorescence dye PI, only permeable to nonliving cells, was used to determine cell death. About 10⁷ control, overexpressed, KO, and complement cells were pelleted down and washed two times with PBS and resuspended in 1 \times PBS containing PI (5 μ g/ml) (Calbiochem) and kept at RT for 15 to 20 min in dark. Fluorescence from the cells was measured by flow cytometer (BD FACS LSR Fortessa) (Ex λ -488 nm; Em λ -617 nm).

Growth curve measurement

To investigate the growth profile of different type of cells, 10⁶ mid-log phase control, overexpressed, KO, and

ChaC2 proteins from *Leishmania major*

complement cells were inoculated in M199 media (10 ml) (Gibco) supplemented with 10% FBS (Gibco). The growth rates of promastigotes were measured by counting cells in Neubauer chamber (hemocytometer) at 24 h interval up to 15 days. To investigate the growth profile of different types of cells in sulfur deficient M199 media, 1×10^6 mid-log phase promastigotes were seeded in 5 ml sulfur-deficient M199 media (Himedia-AT1076) supplemented with 10% FBS in the presence or absence of 4 mg/ml reduced GSH or 25 mg/L NAC (Sigma).

Intracellular GSH measurement by flow cytometer

Intracellular level of GSH was measured by intracellular GSH Detection Assay Kit (Abcam). About 10^6 control, over-expressed, KO, and complement cells were taken and washed the cells with twice with $1 \times$ PBS at 1500g for 6 min. Five microliters of 200 \times Thiol Green Dye was mixed into 1 ml of cell suspension and incubated at 22 °C for 15 min, then washed the cells at 1000 rpm for 4 min and resuspended in 1 ml of assay buffer. Fluorescence intensity was measured by flow cytometer (BD FACS LSR Fortessa) (Ex_{λ} -490 nm; Em_{λ} -525 nm).

Intracellular GSH and T(SH)₂ measurement by HPLC

About 2×10^8 promastigotes were taken and washed with $1 \times$ Dulbecco's PBS (Sigma) for two times. Then, the cells were resuspended in 200 μ l extraction buffer containing 0.1 M HCl and 1 mM EDTA and sonicated for 5 min with vortexing at every 30 s and freeze thaw cycle for two times to ensure cell lysis. Supernatant was collected after centrifuging the samples at 14,000 rpm for 15 min at 4 °C and 40 μ l filtered supernatant was injected for HPLC analysis using reverse phase C₁₈ HPLC column (Waters) with 2% aqueous solution of perchlorate used as mobile phase (flow rate 1 ml/min, wavelength 210 nm). Peak of GSH and T(SH)₂ were appeared at 12 min and 52 min, respectively (Fig. S1). GSH and T(SH)₂ peaks were identified with authentic standards. The intracellular concentration of GSH and T(SH)₂ was measured from standard curve.

Macrophage infection

Murine macrophage cell line RAW 264.7 was adhered on the coverslips (2×10^6 macrophages/coverslip) and infected with different LmChaC variant promastigotes cell lines in 0.5 ml of RPMI 1640/10% FBS at 10:1 ratio of parasite to cell in a condition of 5% CO₂ and 37 °C. Parasite entry was determined after 2 h of infection and intracellular parasite entry was calculated up to 48 h of post infection. After each time-point, unphagocytosed cells were removed by PBS wash and immediately fixed with 100% methanol. Finally, cells were stained with PI and Olympus IX81 microscope was used to visualize and quantify the parasite entry.

Mice infection

For comparative study of cutaneous infection in mice, 5×10^6 stationary phase promastigotes of different LmChaC variant cells were injected subcutaneously in left hind footpads

of 4 to 6 weeks old female BALB/c mice. Daily measurements of footpad swelling with a slide caliper were used to monitor the disease's progression.

Parasite loads in footpad of mice

Limiting dilution assay was performed to determine the parasite loads in footpad of mice infected with different LmChaC variants. Section of the footpad tissues were homogenized in M199 medium and tissue debris were removed by centrifugation at 500 rpm for 10 min. Then, the supernatant was centrifuged at 4000 rpm for 10 min to pellet down the cells. Pellet was resuspended and serially diluted in M199/10% FBS in a sterile 96-well tissue culture plate. The highest dilution at which the growth of promastigotes could be appeared after 10 to 15 days of incubation at 22 °C was used to calculate the number of visible parasites/mg of tissue.

Measurement of LmChaC_{2a} and LmChaC_{2b} mRNA expression in promastigotes as well as amastigotes

Semiquantitative reverse transcriptase PCR was performed to measure LmChaC_{2a} and LmChaC_{2b} in promastigote and amastigotes *L. major* cells. RNAqueous-4PCR Kit (Ambion) was used to extract total RNA from different leishmanial cell lines according to manufacturer's protocol. Complementary DNA (cDNA) was then synthesized from the RNA using Primerscript first cDNA synthesis kit (Takara). Primers 1 and 2 was used to amplify LmChaC_{2a}, whereas LmChaC_{2b} was amplified using primer 3 and primer 4 to get 714 bp and 972 bp fragment, respectively.

qRT-PCR for measuring LmChaC_{2a} and LmChaC_{2b} mRNA level in presence of H₂O₂, tunicamycin, and sulfur-limited media

Real-time PCR was performed to measure LmChaC_{2a} and LmChaC_{2b} in promastigote after treatment of H₂O₂, tunicamycin, and sulfur-limited media. Isolation of total RNA and cDNA synthesis were performed using RNAqueous-4PCR Kit (Ambion) and Primerscript first cDNA synthesis kit (Takara), respectively. Faststart Universal SYBR Green Master (Roche) was used to perform real-time quantitative PCR on StepOne Real-Time PCR system (Applied Biosystems) with respective primers. Using 18S rRNA as the endogenous control, the mRNA quantification was performed by the comparative CT method.

Statistical analysis

The mean \pm SD of at least three independent experiments was used to express all results. The Student's *t* test or ANOVA were used to calculate the statistical analysis for the parametric data using Origin 6.0 software (Microcal software, Inc). The difference between individual groups was evaluated using post hoc analysis (multiple comparison *t* test) after the ANOVA. A *p* value of less than 0.05 was accepted statistically significant.

Data availability

All data generated and analyzed during this study are contained within the article

Supporting information—This article contains supporting information.

Acknowledgments—We thank Dr S. M. Beverley (Washington University, St Louis, MO) for providing pXG-B2863 and pXG-phleo vector as a gift; Dr Jeremy C. Mottram for pTB007, pTPuro_v1 and pTBlast_v1 vector as a gift; Dr Swati Pal for LmAPX antibody.

Author contributions—S. A. conceptualization; S. D., P. P., G. C., S. B., Y. D., and S. A. methodology; S. D., P. P., G. C., S. B., Y. D., and S. A. formal analysis; S. D., P. P., G. C., S. B., Y. D., and S. A. investigation; S. A. resources; S. D., P. P., G. C., S. B., Y. D., and S. A. data curation; S. A. writing—original draft; S. D. visualization; S. A. supervision; S. A. project administration; S. A. funding acquisition.

Funding and additional information—This work was supported by Council of Scientific and Industrial Research (CSIR) NCP Project MLP-136, Department of Science and Technology, (project no CRG/2021/000421), UGC fellowships (to S. D, P. P. and Y. D.) and CSIR fellowships (to S. B. and G. C.).

Conflict of interest—The authors declare that they have no conflicts of interest with the contents of this article.

Abbreviations—The abbreviations used are: cDNA, complementary DNA; ER, endoplasmic reticulum; FBS, fetal bovine serum; gDNA, genomic DNA; HRP, horseradish peroxidase; NAC, N-acetyl cysteine; PI, propidium iodide; ROS, reactive oxygen species; qRT-PCR, quantitative real-time PCR; sgRNA, single-guide RNA.

References


1. Meister, A., and Anderson, M. E. (1983) Glutathione. *Annu. Rev. Biochem.* **52**, 711–760
2. Penninckx, M. J., and Elskens, M. T. (1993) Metabolism and functions of glutathione in micro-organisms. *Adv. Microb. Physiol.* **34**, 239–301
3. Arthur, J. R. (2000) The glutathione peroxidases. *Cell Mol. Life Sci.* **57**, 1825–1835
4. Dalle-Donne, I., Rossi, R., Colombo, G., Giustarini, D., and Milzani, A. (2009) Protein S-glutathionylation: a regulatory device from bacteria to humans. *Trends Biochem. Sci.* **34**, 85–96
5. Peterson, J. D., Herzenberg, L. A., Vasquez, K., and Waltenbaugh, C. (1998) Glutathione levels in antigen-presenting cells modulate Th1 versus Th2 response patterns. *Proc. Natl. Acad. Sci. U. S. A.* **95**, 3071–3076
6. Franco, R., and Cidlowski, J. A. (2009) Apoptosis and glutathione: beyond an antioxidant. *Cell Death Differ.* **16**, 1303–1314
7. Townsend, D. M., Tew, K. D., and Tapiero, H. (2003) The importance of glutathione in human disease. *Biomed. Pharmacother. Biomed. Pharmacother.* **57**, 145–155
8. Rajasekaran, N. S., Connell, P., Christians, E. S., Yan, L.-J., Taylor, R. P., Orosz, A., et al. (2007) Human alpha B-crystallin mutation causes oxido-reductive stress and protein aggregation cardiomyopathy in mice. *Cell* **130**, 427–439
9. Mavi, P. S., Singh, S., and Kumar, A. (2020) Reductive stress: new insights in physiology and drug tolerance of Mycobacterium. *Antioxid. Redox Signal.* **32**, 1348–1366
10. Zhang, H., Limphong, P., Pieper, J., Liu, Q., Rodesch, C. K., Christians, E., et al. (2012) Glutathione-dependent reductive stress triggers mitochondrial oxidation and cytotoxicity. *FASEB J. Off. Publ. Fed. Am. Soc. Exp. Biol.* **26**, 1442–1451

11. Baudouin-Cornu, P., Lagniel, G., Kumar, C., Huang, M.-E., and Labarre, J. (2012) Glutathione degradation is a key determinant of glutathione homeostasis. *J. Biol. Chem.* **287**, 4552–4561
12. Bachhawat, A. K., and Yadav, S. (2018) The glutathione cycle: glutathione metabolism beyond the γ -glutamyl cycle. *IUBMB Life* **70**, 585–592
13. Nathan, C., and Shiloh, M. U. (2000) Reactive oxygen and nitrogen intermediates in the relationship between mammalian hosts and microbial pathogens. *Proc. Natl. Acad. Sci. U. S. A.* **97**, 8841–8848
14. Sacks, D., and Sher, A. (2002) Evasion of innate immunity by parasitic protozoa. *Nat. Immunol.* **3**, 1041–1047
15. Irigoien, F., Cibils, L., Comini, M. A., Wilkinson, S. R., Flohé, L., and Radi, R. (2008) Insights into the redox biology of Trypanosoma cruzi: trypanothione metabolism and oxidant detoxification. *Free Radic. Biol. Med.* **45**, 733–742
16. Nogoceke, E., Gommel, D. U., Kiess, M., Kalisz, H. M., and Flohé, L. (1997) A unique cascade of oxidoreductases catalyses trypanothione-mediated peroxide metabolism in Crithidia fasciculata. *Biol. Chem.* **378**, 827–836
17. Trujillo, M., Budde, H., Piñeyro, M. D., Stehr, M., Robello, C., Flohé, L., et al. (2004) Trypanosoma brucei and Trypanosoma cruzi trypanothione peroxidases catalytically detoxify peroxynitrite via oxidation of fast reacting thiols. *J. Biol. Chem.* **279**, 34175–34182
18. Fairlamb, A. H., Blackburn, P., Ulrich, P., Chait, B. T., and Cerami, A. (1985) Trypanothione: a novel bis(glutathionyl)spermidine cofactor for glutathione reductase in trypanosomatids. *Science* **227**, 1485–1487
19. Tetaud, E., Manai, F., Barrett, M. P., Nadeau, K., Walsh, C. T., and Fairlamb, A. H. (1998) Cloning and characterization of the two enzymes responsible for trypanothione biosynthesis in Crithidia fasciculata. *J. Biol. Chem.* **273**, 19383–19390
20. Oza, S. L., Shaw, M. P., Wyllie, S., and Fairlamb, A. H. (2005) Trypanothione biosynthesis in Leishmania major. *Mol. Biochem. Parasitol.* **139**, 107–116
21. Abbott, J. J., Ford, J. L., and Phillips, M. A. (2002) Substrate binding determinants of Trypanosoma brucei gamma-glutamylcysteine synthetase. *Biochemistry* **41**, 2741–2750
22. Arrick, B. A., Griffith, O. W., and Cerami, A. (1981) Inhibition of glutathione synthesis as a chemotherapeutic strategy for trypanosomiasis. *J. Exp. Med.* **153**, 720–725
23. Kumar, A., Tikoo, S., Maity, S., Sengupta, S., Sengupta, S., Kaur, A., et al. (2012) Mammalian proapoptotic factor ChaC1 and its homologues function as γ -glutamyl cyclotransferases acting specifically on glutathione. *EMBO Rep.* **13**, 1095–1101
24. Kumar, C., Igarria, A., D’Autreaux, B., Planson, A.-G., Junot, C., Godat, E., et al. (2011) Glutathione revisited: a vital function in iron metabolism and ancillary role in thiol-redox control. *EMBO J.* **30**, 2044–2056
25. Mungro, I. N., Pagnon, J., Kohannim, O., Gargalovic, P. S., and Lusic, A. J. (2009) CHAC1/MGC4504 is a novel proapoptotic component of the unfolded protein response, downstream of the ATF4-ATF3-CHOP cascade. *J. Immunol.* **182**, 466–476
26. Crawford, R. R., Prescott, E. T., Sylvester, C. F., Higdon, A. N., Shan, J., Kilberg, M. S., et al. (2015) Human CHAC1 protein degrades glutathione, and mRNA induction is regulated by the transcription factors ATF4 and ATF3 and a bipartite ATF/CRE regulatory element. *J. Biol. Chem.* **290**, 15878–15891
27. Kaur, A., Gautam, R., Srivastava, R., Chandel, A., Kumar, A., Karthikeyan, S., et al. (2017) ChaC2, an enzyme for slow turnover of cytosolic glutathione. *J. Biol. Chem.* **292**, 638–651
28. Krauth-Siegel, R. L., and Comini, M. A. (2008) Redox control in trypanosomatids, parasitic protozoa with trypanothione-based thiol metabolism. *Biochim. Biophys. Acta* **1780**, 1236–1248
29. Sacks, D. L., and Perkins, P. V. (1984) Identification of an infective stage of Leishmania promastigotes. *Science* **223**, 1417–1419
30. Dolai, S., Yadav, R. K., Pal, S., and Adak, S. (2008) Leishmania major ascorbate peroxidase overexpression protects cells against reactive oxygen species-mediated cardiolipin oxidation. *Free Radic. Biol. Med.* **45**, 1520–1529
31. Mukherjee, A., Roy, G., Guimond, C., and Ouellette, M. (2009) The gamma-glutamylcysteine synthetase gene of Leishmania is essential and involved in response to oxidants. *Mol. Microbiol.* **74**, 914–927

ChaC2 proteins from *Leishmania major*

32. Huynh, T. T., Huynh, V. T., Harmon, M. A., and Phillips, M. A. (2003) Gene knockdown of gamma-glutamylcysteine synthetase by RNAi in the parasitic protozoa *Trypanosoma brucei* demonstrates that it is an essential enzyme. *J. Biol. Chem.* **278**, 39794–39800
33. Berriman, M., Ghedin, E., Hertz-Fowler, C., Blandin, G., Renauld, H., Bartholomeu, D. C., *et al.* (2005) The genome of the African trypanosome *Trypanosoma brucei*. *Science* **309**, 416–422
34. El-Sayed, N. M., Myler, P. J., Bartholomeu, D. C., Nilsson, D., Aggarwal, G., Tran, A.-N., *et al.* (2005) The genome sequence of *Trypanosoma cruzi*, etiologic agent of Chagas disease. *Science* **309**, 409–415
35. Ivens, A. C., Peacock, C. S., Worthey, E. A., Murphy, L., Aggarwal, G., Berriman, M., *et al.* (2005) The genome of the kinetoplastid parasite, *Leishmania major*. *Science* **309**, 436–442
36. Fairlamb, A. H., and Cerami, A. (1992) Metabolism and functions of trypanothione in the Kinetoplastida. *Annu. Rev. Microbiol.* **46**, 695–729
37. Orłowski, M., and Meister, A. (1970) The gamma-glutamyl cycle: a possible transport system for amino acids. *Proc. Natl. Acad. Sci. U. S. A.* **67**, 1248–1255
38. Oakley, A. J., Yamada, T., Liu, D., Coggan, M., Clark, A. G., and Board, P. G. (2008) The identification and structural characterization of C7orf24 as gamma-glutamyl cyclotransferase. An essential enzyme in the gamma-glutamyl cycle. *J. Biol. Chem.* **283**, 22031–22042
39. Oakley, A. J., Coggan, M., and Board, P. G. (2010) Identification and characterization of gamma-glutamylamine cyclotransferase, an enzyme responsible for gamma-glutamyl-epsilon-lysine catabolism. *J. Biol. Chem.* **285**, 9642–9648
40. Saunders, E. C., Ng, W. W., Chambers, J. M., Ng, M., Naderer, T., Krömer, J. O., *et al.* (2011) Isotopomer profiling of *Leishmania mexicana* promastigotes reveals important roles for succinate fermentation and aspartate uptake in tricarboxylic acid cycle (TCA) anaplerosis, glutamate synthesis, and growth. *J. Biol. Chem.* **286**, 27706–27717
41. McConville, M. J., Saunders, E. C., Kloehn, J., and Dagley, M. J. (2015) *Leishmania* carbon metabolism in the macrophage phagolysosome—feast or famine? *F1000Res.* **4**, 938
42. Kloehn, J., Saunders, E. C., O’Callaghan, S., Dagley, M. J., and McConville, M. J. (2015) Characterization of metabolically quiescent *Leishmania* parasites in murine lesions using heavy water labeling. *PLoS Pathog.* **11**, e1004683
43. Weldrick, D. P., Chodacka, B., Vogt, R., and Steenkamp, D. J. (1999) The effect of buthionine sulfoximine on the growth of *Leishmania donovani* in culture. *FEMS Microbiol. Lett.* **173**, 139–146
44. Dumas, C., Ouellette, M., Tovar, J., Cunningham, M. L., Fairlamb, A. H., Tamar, S., *et al.* (1997) Disruption of the trypanothione reductase gene of *Leishmania* decreases its ability to survive oxidative stress in macrophages. *EMBO J.* **16**, 2590–2598
45. Venketaraman, V., Dayaram, Y. K., Talae, M. T., and Connell, N. D. (2005) Glutathione and nitrosoglutathione in macrophage defense against *Mycobacterium tuberculosis*. *Infect. Immun.* **73**, 1886–1889
46. Venketaraman, V., Dayaram, Y. K., Amin, A. G., Ngo, R., Green, R. M., Talae, M. T., *et al.* (2003) Role of glutathione in macrophage control of mycobacteria. *Infect. Immun.* **71**, 1864–1871
47. Das, P., Mukherjee, A., and Adak, S. (2021) Glyceraldehyde-3-phosphate dehydrogenase present in extracellular vesicles from *Leishmania major* suppresses host TNF-alpha expression. *J. Biol. Chem.* **297**, 101198
48. Adhikari, A., Biswas, S., Mukherjee, A., Das, S., and Adak, S. (2019) PAS domain-containing phosphoglycerate kinase deficiency in *Leishmania major* results in increased autophagosome formation and cell death. *Biochem. J.* **476**, 1303–1321
49. Biswas, S., Adhikari, A., Mukherjee, A., Das, S., and Adak, S. (2020) Regulation of *Leishmania major* PAS domain-containing phosphoglycerate kinase by cofactor Mg²⁺ ion at neutral pH. *FEBS J.* **287**, 5183–5195
50. Pal, S., Dolai, S., Yadav, R. K., and Adak, S. (2010) Ascorbate peroxidase from *Leishmania major* controls the virulence of infective stage of promastigotes by regulating oxidative stress. *PLoS One* **5**, e11271
51. Beneke, T., Madden, R., Makin, L., Valli, J., Sunter, J., and Gluenz, E. (2017) A CRISPR Cas9 high-throughput genome editing toolkit for kinetoplastids. *R. Soc. Open Sci.* **4**, 170095
52. Sollelis, L., Ghorbal, M., MacPherson, C. R., Martins, R. M., Kuk, N., Crobu, L., *et al.* (2015) First efficient CRISPR-Cas9-mediated genome editing in *Leishmania* parasites. *Cell. Microbiol.* **17**, 1405–1412

Regulation of *Leishmania major* PAS domain-containing phosphoglycerate kinase by cofactor Mg^{2+} ion at neutral pH

Saroj Biswas, Ayan Adhikari, Aditi Mukherjee, Sumit Das and Subrata Adak 

Division of Structural Biology & Bio-informatics, CSIR-Indian Institute of Chemical Biology, Kolkata, India

Keywords

divalent metal binding; *Leishmania*; mutation; PAS domain; phosphoglycerate kinase

Correspondence

S. Adak, Division of Structural Biology & Bio-informatics, CSIR-Indian Institute of Chemical Biology, 4, Raja S.C. Mullick Road, Kolkata – 700 032, India
 Tel: +91 33 2473-6793
 E-mail: adaks@iicb.res.in

(Received 4 December 2019, revised 12 February 2020, accepted 18 March 2020)

doi:10.1111/febs.15305

Recently, we described the PAS domain-containing phosphoglycerate kinase (PGK) from *Leishmania major* (LmPAS-PGK) that shows acidic pH (5.5)-dependent optimum catalytic activity. The PAS domain of LmPAS-PGK is expected to regulate PGK activity during catalysis, but the mechanism of regulation by PAS domain at the molecular level is uncharacterized. In this work, we have utilized the full-length, PAS domain-deleted, and mutant enzymes to measure the enzymatic activity in the presence of divalent cation at various pH values. Catalytic activity measurement indicates that Mg^{2+} binding through PAS domain inhibits the PGK activity at pH 7.5, and this inhibition is withdrawn at pH 5.5. To identify the Mg^{2+} binding residues of the PAS domain, we exploited a systematic mutational analysis of all (four) His residues in the PAS domain for potential divalent cation binding. Replacement of His-57 with alanine resulted in depression in the presence of Mg^{2+} at pH 7.5, but H71A, H89A, and H111A showed similar characteristics with respect to the wild-type protein. Fluorescence and isothermal titration calorimetry studies revealed that H57 is responsible for Mg^{2+} binding in the absence of substrates. Thus, the protonated form of His57 at acidic pH 5.5 destabilizes the Mg^{2+} binding in the PAS domain, which is an essential requirement in the wild-type LmPAS-PGK for a conformational alteration in the sensor domain that, sequentially, activates the PGK domain, resulting in the synthesis of higher amounts of ATP.

Introduction

PAS or Per-Arnt-Sim is an abbreviation of *Drosophila* period clock protein, vertebrate aryl hydrocarbon receptor nuclear translocator, and *Drosophila* single-minded protein. PAS domain (roughly 100 amino acids long) is mainly attached to a wide range of effector domains that have diverse functions in cellular signaling systems [1]. The roles of this domain within sensory proteins are protein/protein interaction [2-4],

signal transfer [5], and sensing stimuli [6]. PAS domain is able to bind small molecules or ions, which can either serve as a direct signal [7-9] or provide a cofactor that allows understanding of signals such as visible light [10-12], redox potential [13-16], or dissolved gases [17,18].

Phosphoglycerate kinase (PGK) catalyzes the reversible transfer of the 1-phosphoryl group from 1,3-

Abbreviations

LmPAS-PGK, PAS domain-containing phosphoglycerate kinase from *Leishmania major*; PAS, Per (*Drosophila* period clock protein)-Arnt (vertebrate aryl hydrocarbon receptor nuclear translocator)-Sim (*Drosophila* single-minded protein); PAS-deleted LmPAS-PGK, 115 amino acid deleted from N-terminal of LmPAS-PGK; PGA, phosphoglycerate; PGK, phosphoglycerate kinase; PhoQ, a transmembrane histidine kinase sensor protein controls the phosphate (Pho) regulon.

bisphosphoglycerate to ADP, to produce ATP and 3-phosphoglycerate (3-PGA) in the first ATP-generating step of glycolysis. Besides functioning in glycolysis, PGK shows moonlighting functions such as elevating plasma level of angiostatin [19], DNA replication, and repair [20]. Sequence alignment studies, mutational analysis, and X-ray crystal structures of various PGKs reveal that the active-site residues are highly conserved [21–25]. This enzyme has two equally sized domains of Rossmann fold topology and an interdomain region. The first half of PGK domain is responsible for 3-phosphoglycerate/1,3-bisphosphoglycerate binding, and the second half of PGK domain is responsible for nucleotide (ADP/ATP) binding. The interdomain region contains helices 7, 13, 14, and 15 (residues 169–185 and 351–394) [25]. After binding of both substrates, the two domains come in close proximity, thus transiting from an open (without substrate) to substrate-bound closed conformation for catalysis. This type of mechanism is proposed from the ternary complex of *Trypanosoma brucei* PGKC with 3-PGA and MgADP bound [25], and the ternary complex of *Thermotoga maritima* PGK with 3-PGA and MgAMP-PNP bound [24]. The substrate-bound domain closure required for catalysis is still not fully understood.

Three isoforms of PGK (PAS-PGK, PGKB, and PGKC) are found in human pathogen *Leishmania* spp [26–29]. PGKB and PGKC enzymes are localized in the cytosol and the glycosome (single-membrane peroxisome-like organelle), respectively. They are expressed in both the amastigote and the promastigote forms [26]. On the other hand, PAS-PGK contains an N-terminal regulatory PAS domain that is connected to a C-terminal catalytic PGK domain and is present in the glycosome as well as the lysosome [28]. PAS-PGK is a monomeric 59-kDa enzyme. Comparative studies among overexpression, gene knockout, and complement cell line suggest that PAS domain-containing PGK from *Leishmania major* (LmPAS-PGK) plays an important role in cell survival through autophagy. Although the optimum activities of human PGK, yeast PGK, and leishmanial PGK (B and C) are at neutral pH, the optimum activity of LmPAS-PGK is at pH 5.5. Surprisingly, the comparative study between full-length and PAS domain-deleted enzymes revealed that the PAS domain of LmPAS-PGK primarily regulates the PGK catalytic activity with respect to pH changes.

The PAS domain of a transmembrane histidine kinase sensor protein (PhoQ) has been reported to bind divalent cations through aspartic and glutamic acid residues in an acidic patch, forming bridges with inner membrane phospholipids to maintain PhoQ

repression [7,30]. NMR experiments demonstrate that the repression of PhoQ can be withdrawn by displacement of divalent cations from this acidic region by acidic pH [31]. It is still unclear whether cofactor Mg^{2+} or Mn^{2+} of LmPAS-PGK binds at PAS domain involving the same mechanism for repression at neutral pH. In the present study, we specifically used PAS domain-deleted protein and several His mutants within the PAS domain to investigate the putative regulatory role of these histidines in catalysis. Our data show that the PAS domain-deleted protein as well as the H57A mutant protein resulted in almost complete loss of Mg^{2+} - or Mn^{2+} -dependent repression of the enzyme at neutral pH, and suggest important mechanistic roles of His-57 in the divalent cation binding of the PAS domain. Based on these results, a concerted reaction mechanism for LmPAS-PGK is proposed.

Results

Higher concentration of ATP and ADP acts as inhibitor

Trypanosoma brucei hexokinase activity is highly sensitive to the substrate ATP or ADP at acidic pH of the assay, and glycerol 3-P or glycerol 2-P protects the enzyme from the inactivation by the substrate ATP or ADP at acidic pH [32]. To investigate whether the PAS domain of LmPAS-PGK protects the PGK activity from the inactivation by the substrate ATP or ADP at acidic pH, we have compared the substrate (ATP) or the product (ADP)-dependent PGK activity between full-length and PAS domain-deleted (truncated) enzymes at various pH values (Fig. 1). At both pH 7.5 and 5.5, full-length enzyme showed saturation kinetics up to 1 mM ATP and very high concentrations of ATP inhibited the PGK activity (Fig. 1A). Similarly, the truncated enzyme displayed optimal activity at 1 mM ATP and inhibition at higher concentration (Fig. 1B) at both pH 7.5 and pH 5.5. Activity change during low or high concentration of substrate ATP was fitted by a substrate inhibition equation [$Y = V_{max} * X / (K_m + X * (1 + X / K_i))$] in PRISM 6 software (GraphPad Software, San Diego, CA, USA), generating V_{max} (maximum enzyme velocity), K_m (Michaelis–Menten constant), and K_i (dissociation constant for substrate binding in such a way that two substrates can bind to an enzyme) values of both full-length and PAS domain-deleted (truncated) enzymes at various pH values. V_{max} , K_m , and K_i values of both full-length and truncated enzymes at various pH values are listed in Table 1. The K_i values were 0.26 mM for full-length enzyme and 0.44 mM for truncated enzyme

at pH 5.5, indicating that the K_i values for ATP in both enzymes were similar in acidic pH. On the other hand, the K_i values were 1.3 mM for full-length enzyme and 0.1 mM for truncated enzyme at pH 7.5, suggesting that the K_i value for ATP in the full-length enzyme was ~13 times higher than truncated enzyme at neutral pH. The theoretical values of V_{max} and K_m from fitting curves (Table 1) were ~2- to 5-fold higher than experimental values from saturation curve fitting data up to 1 mM ATP; those were reported earlier [28]. One possibility for this discrepancy is that the theoretical values of V_{max} and K_m from the equation of substrate inhibition model are considered where the substrate does not inhibit enzyme activity. In case of product inhibition study, we used different concentrations of ADP (in the presence of 1 mM ATP) in the assay mixture at pH 7.5 as well as pH 5.5. Both full-length (Fig. 1C) and truncated enzymes (Fig. 1D) were inhibited with increasing concentration of ADP. All data were fitted by using a hyperbolic decay equation using ORIGIN 6.0 software (Microcal Software, Northampton, MA, USA) and listed in Table 1. Half-maximal inhibitory concentration values (IC_{50}) were 1.1 mM for full-length enzyme and 1.3 mM for truncated enzyme at pH 5.5, indicating that the IC_{50} value for ADP in both enzymes was comparable at acidic pH. The IC_{50} value of full-length enzyme (0.5 mM) for ADP was in similar range compared to truncated enzyme (0.9 mM) at pH 7.5. Altogether, these results suggest that the inhibition constant (K_i) for substrate (ATP) is significantly changed in PAS domain-containing enzyme compared to truncated enzyme at pH 7.5, whereas the inhibition constant (IC_{50}) for product (ADP) is unaltered.

Cofactor Mg^{2+} acts as an inhibitor of the full-length LmPAS-PGK

In order to sense the environment, the PAS domains in numerous sensory proteins are known to bind small molecules including divalent cations. Several groups of workers reported that the *Salmonellae* PhoQ sensor kinase is directly inhibited when the PAS domain is bound to cofactor Mg^{2+} at neutral pH 7.5 [31]. To determine whether LmPAS-PGK is directly inhibited when exposed to cofactor Mg^{2+} at neutral pH 7.5, we compared PGK activity among full-length protein, PAS-deleted protein, and yeast PGK (lacking PAS domain) at various pH values (Fig. 2A–C). As observed in the Mg^{2+} -dependent PGK activity curve at pH 7.5, the catalytic activity of full-length LmPAS-PGK was decreased with increasing concentration of Mg^{2+} (Fig. 2A). In contrast, the PGK activity of the full-length LmPAS-PGK protein was increased with increasing

concentration of Mg^{2+} ions at acidic pH 5.5. On the other hand, both the PAS domain-deleted LmPAS-PGK (Fig. 2B) and the yeast PGK (Fig. 2C) showed that the catalytic activity of enzyme is directly proportional to Mg^{2+} ion at both neutral pH 7.5 and acidic pH 5.5. Together, these results indicate that Mg^{2+} ions might be released from PAS domain at acidic pH 5.5 and, subsequently, the Mg^{2+} -induced autoinhibitory role of PAS domain is repressed in the full-length LmPAS-PGK at acidic pH 5.5. The Mg^{2+} cation is generally not transformed during catalysis, so we can measure a dissociation constant value (K_D) instead of K_m from half-saturation kinetics curve (Fig. 2A–C). In case of full-length LmPAS-PGK protein, we were unable to measure the accurate K_D value of Mg^{2+} ion for catalytic site due to very low value (< 0.01 mM) at pH 7.5, whereas we can measure the K_D value (0.21 mM) of Mg^{2+} ion for regulatory site from inhibition kinetics at pH 7.5. The K_D values for truncated enzyme and yeast PGK at pH 7.5 were 0.10 mM and 0.13 mM, respectively. These data indicated that the dissociation constant for Mg^{2+} binding in the catalytic site of full-length enzyme was lower compared to both truncated enzymes and yeast PGK at neutral pH. On the other hand, the K_D values for full-length LmPAS-PGK, truncated PAS-PGK, and yeast PGK at pH 5.5 were 0.6, 0.17, and 0.7 mM, respectively, suggesting that the dissociation constant for Mg^{2+} cation in the catalytic site of all PGKs was of similar order at acidic pH.

Role of other divalent cation in LmPAS-PGK

To identify the other divalent cation ligand for PAS domain, we measured the PGK activity in the presence of several well-known divalent cations including Ca^{2+} and Mn^{2+} (Fig. 2D–F). At pH 7.5, very low concentration of Mg^{2+} (0.01 mM) and very high concentration of Ca^{2+} (2 mM) supported PGK activity in full-length LmPAS-PGK, with a negative consequence on activity only at higher concentration of Mg^{2+} (2 mM) or Mn^{2+} (2 mM; Fig. 2D). Inhibition by higher concentration of Mg^{2+} (2 mM) or Mn^{2+} (2 mM) at neutral pH was not observed in both PAS domain-deleted protein and yeast PGK (Fig. 2E,F). These results suggest that the activity of LmPAS-PGK was insensitive to Ca^{2+} ion due to PAS domain that may not be able to bind Ca^{2+} ion, whereas Mn^{2+} ion (like Mg^{2+} ion) can bind to PAS domain and inhibits the catalytic PGK activity at pH 7.5.

Histidine 57 is important for the repression of PAS domain-mediated catalytic PGK domain

Our earlier report suggested that the maximal activity of LmPAS-PGK was at around pH 5.5, close to the

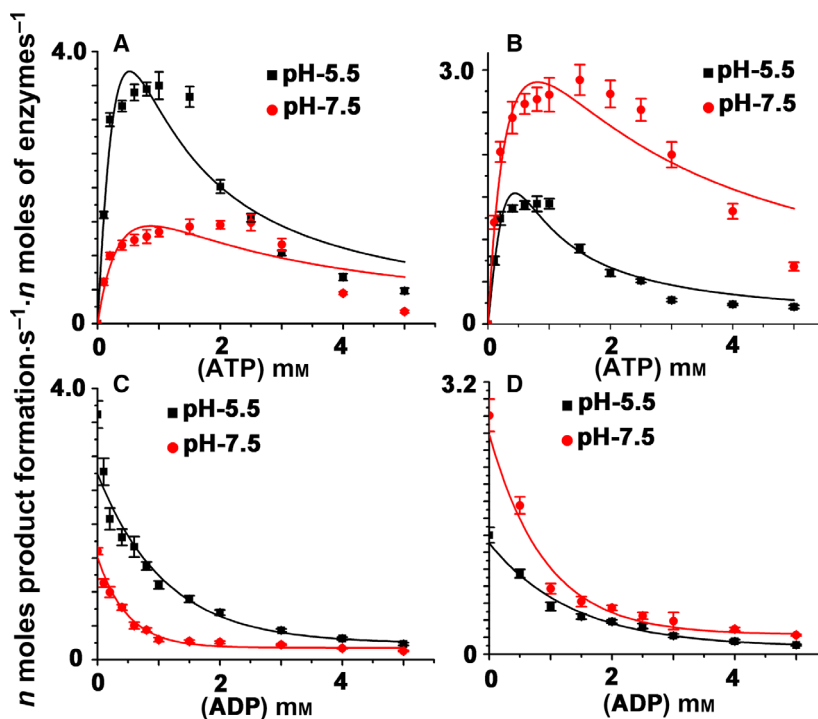


Fig. 1. Comparative studies of ATP- and ADP-dependent PGK activity between full-length and PAS domain-deleted LmPAS-PGK. Panels A and B show ATP-dependent PGK activity of wild-type and truncated enzymes, respectively. Panels C and D show ADP-dependent PGK activity of wild-type and truncated enzymes, respectively. The assay mixture was composed of 50 mM Tris/HCl buffer (pH 7.5) or acetate buffer (pH 5.5), 0.15 mM NADH, 50 µg enzyme, 0.8 mM Mg²⁺, 2.5 mM 3-PGA, various concentrations of ATP or ADP, and 0.04U of rabbit muscle glyceraldehyde 3-phosphate dehydrogenase. Supplementing the low concentration of ATP (1 mM) was initially added to the reaction mixture for fueling the PGK activity in ADP-dependent inhibition assay mixture. Data were plotted as means ± SD from three independent experiments for each assessment. The substrate (ATP) inhibition was fitted by using the following equation $Y = V_{max} * X / (K_m + X * (1 + X/K_i))$ in Prism 6 software; where K_i is the dissociation constant for substrate binding in such a way that two substrates can bind to an enzyme. In case of product inhibition (ADP), all data were fitted by using a hyperbolic decay equation using ORIGIN 6.0 software.

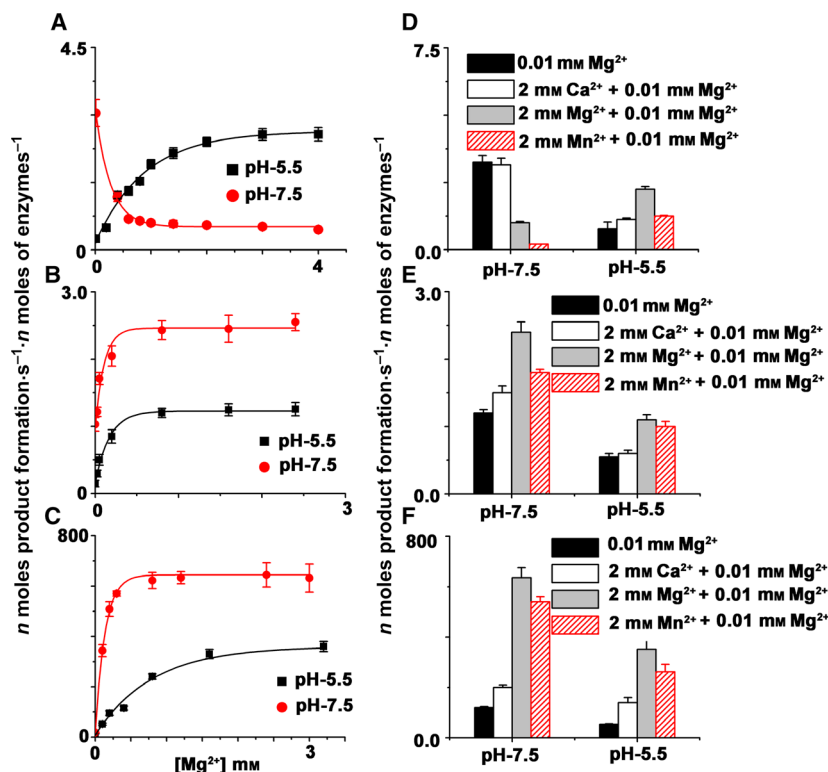
Table 1. Apparent rate constant values of both full-length and PAS domain-deleted enzymes at various pH values (5.5 and 7.5). All rate constant values are extracted from Fig. 1. V_{max} , K_m , K_i , and IC_{50} values were generated from fitting curves. The values represent the mean and standard deviation for three measurements each.

	Apparent rate constants from substrate and product inhibition models							
	pH 5.5				pH 7.5			
	ATP			ADP	ATP			ADP
LmPAS-PGK	V_{max} (s ⁻¹)	K_m (mM)	K_i (mM)	IC_{50} (mM)	V_{max} (s ⁻¹)	K_m (mM)	K_i (mM)	IC_{50} (mM)
Full length	18 ± 5	1.0 ± 0.4	0.26 ± 0.16	1.1 ± 0.06	3.2 ± 1	0.54 ± 0.2	1.3 ± 0.7	0.5 ± 0.02
Truncated (Δ 115)	5.8 ± 1.0	0.41 ± 0.1	0.44 ± 0.2	1.3 ± 0.1	14 ± 6	2 ± 0.9	0.1 ± 0.04	0.9 ± 0.05

pH value at which histidine residues (pK_a of histidine is ~ 6.0) get protonated [28]. Thus, on the basis of these results we hypothesized that the protonation of a histidine residue in a critical region of the PAS domain might act as the conformational switch associated with the activation. In the primary structure of PAS domain of LmPAS-PGK, four histidine residues are

present at position 57, 71, 89, and 111. To investigate the possibility that protonation of one or more of the histidine residues is responsible for pH-mediated catalytic PGK domain activation, all four His residues are changed to Ala and tested all four mutant proteins for divalent metal ion-dependent PGK activity at various pH values. Figure 3 shows that wild-type and all

Fig. 2. Comparative studies of divalent cation-dependent PGK activity among full-length proteins (Panels A and D), PAS-deleted proteins (Panels B and E), and yeast PGK (lacking PAS domain; Panels C and F) at various pH values (7.5 and 5.5). The assay mixture was composed of 50 mM Tris/HCl buffer (pH 7.5) or acetate buffer (pH 5.5), 0.15 mM NADH, 10 μ g LmPAS-PGK proteins or 1.0 μ g yeast PGK, 1.0 mM ATP, 2.5 mM 3-phosphoglyceric acid, different concentrations of divalent cation, and 0.04 U of rabbit muscle glyceraldehyde 3-phosphate dehydrogenase. Data were plotted as means \pm SD from three independent experiments for each assessment.



His mutant proteins follow standard Michaelis–Menten kinetics with respect to both of its substrates (3-PGA and 1.0 mM ATP). The K_m and k_{cat} values of wild-type and all four His mutants were compared in Table 2 for both pH 7.5 and pH 5.5. The K_m values for ATP of the wild-type protein at pH 7.5 (152 μ M) were very similar to all His mutant proteins (156 μ M for H57A, 122 μ M for H71A, 139 μ M for H89A, and 163 μ M for H111A). Similarly, the K_m values for ATP of the wild-type protein at pH 5.5 (118 μ M) were unaltered after Ala mutation at all His residues (134 μ M for H57A, 102 μ M for H71A, 125 μ M for H89A, and 128 μ M for H111A). The K_m values for 3PGA of the wild-type protein at pH 7.5 (530 μ M) were comparable with all His mutant proteins (511 μ M for H57A, 490 μ M for H71A, 517 μ M for H89A, and 480 μ M for H111A). Similarly, the K_m values for 3PGA of the wild-type protein at acidic pH 5.5 (661 μ M) were unchanged with all His mutant proteins (610 μ M for H57A, 680 μ M for H71A, 630 μ M for H89A, and 638 μ M for H111A). These results demonstrated that substitution of His residue by Ala in all four positions did not affect the K_m values of both the substrates at both pH 7.5 and 5.5.

The enzymatic activity (k_{cat}) of the wild-type protein at acidic pH 5.5 (3.5 s^{-1}) was similar to all His mutant

proteins (3.8 s^{-1} for H57A, 3.3 s^{-1} for H71A, 3.2 s^{-1} for H89A, and 3.6 s^{-1} for H111A; Table 2). Although the enzymatic activity of the wild-type at neutral pH 7.5 (1.4 s^{-1}) was similar to H71A (1.28 s^{-1}), H89A (1.35 s^{-1}), and H111A (1.3 s^{-1}) mutant proteins, the H57A protein (4.5 s^{-1}) showed threefold higher enzymatic activity compared to wild-type protein (Table 2 and Fig. 3). These results suggest that the H57 residue in the PAS domain is not directly involved in substrate binding, yet it is responsible for the repression of PGK activity at neutral pH 7.5.

Unlike wild-type LmPAS-PGK protein, the PGK activity of the H57A out of four His mutants was increased with increasing concentration of Mg^{2+} ions at neutral pH 7.5 (Fig. 4). Thus, the H57A mutations tested are derepressed at pH 7.5 compared to wild-type and other His mutants (H71A, H89A, and H111A) in the presence of 2.0 mM Mg^{2+} or Mn^{2+} . The loss of the imidazole side chain at position His57 by alanine destabilizes specifically the repressed state. Thus, the presence of a histidine at position 57 is required to maintain wild type repression of LmPAS-PGK through cofactor Mg^{2+} binding in PAS domain. Taken together, these data indicate that activation by acidic pH is a result of protonation of His57 not H71, H89, and H111 residue.

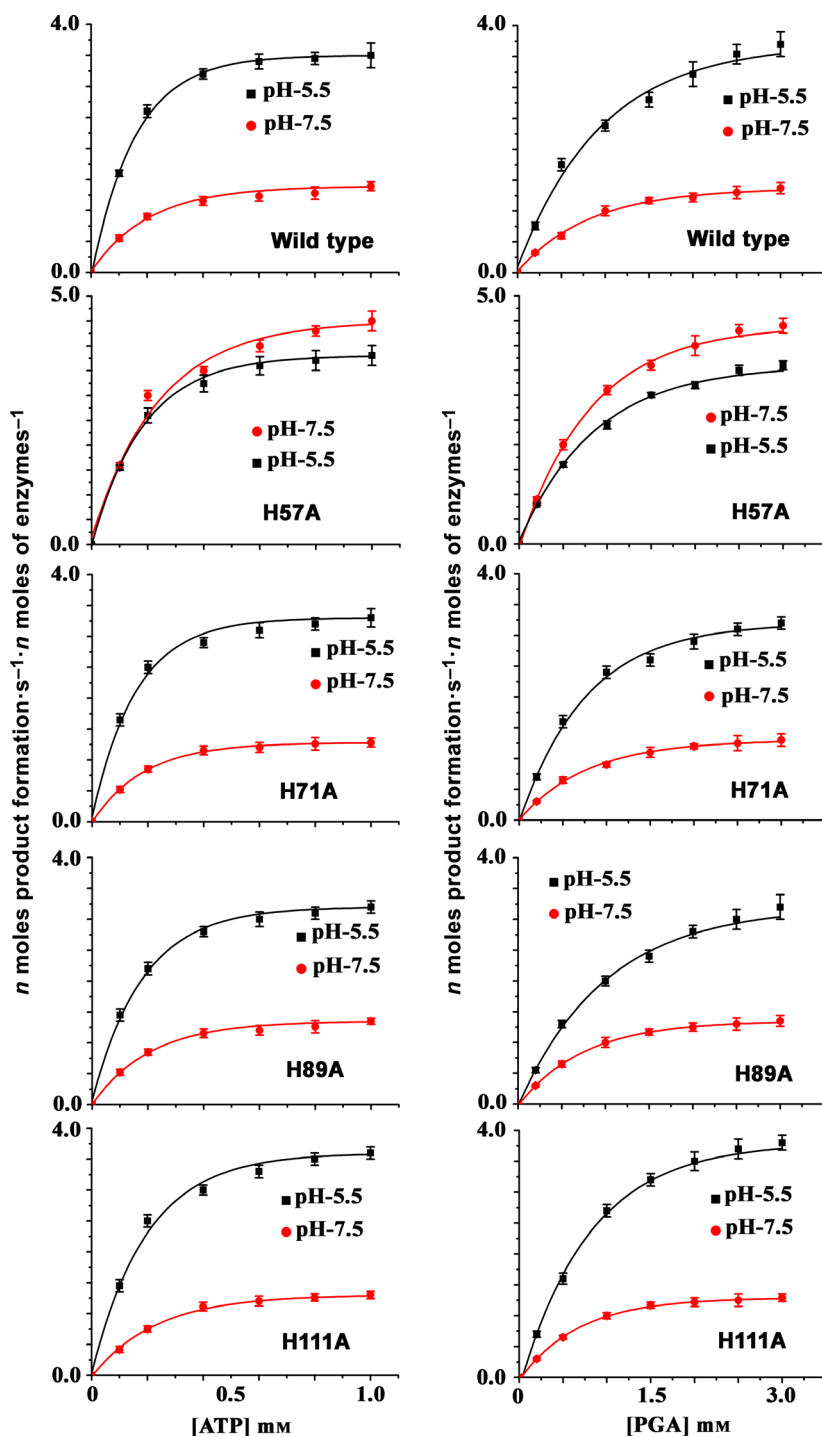


Fig. 3. Velocity of wild-type, H57A, H71A, H89A, and H111A proteins with varying concentrations of ATP or 3-PGA. All data are fitted to a hyperbolic curve. The K_m and k_{cat} values from the fitting curve are listed in Table 2. Data were plotted as means \pm SD from three independent experiments for each assessment.

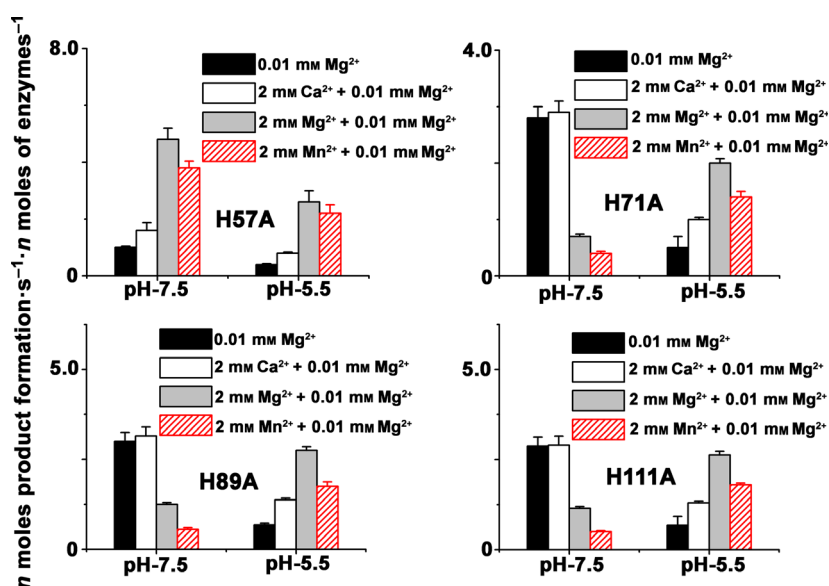
LmPAS-PGK-Mg²⁺ interactions determined by tryptophan fluorescence spectroscopy and isothermal titration calorimetry

The primary sequence of LmPAS-PGK contains three tryptophan residues: two in the PAS domain (Trp40 and Trp95) and one in the PGK catalytic domain

(Trp445). The maximum tryptophan fluorescence of LmPAS-PGK occurred at 331 nm (Fig. 5A). As binding of Mg²⁺ ion is a prerequisite for inhibition, the interaction of Mg²⁺ ion with both wild-type and H57A LmPAS-PGK was studied by tryptophan fluorescence spectroscopy. At pH 7.5, titration of enzyme with

Table 2. Catalytic activities of wild-type and mutant LmPAS-PGK proteins at both pH 5.5 and 7.5. The catalytic activities were determined at 25 °C as described under 'Materials and methods'. The values represent the mean and standard deviation for three measurements each.

LmPAS-PGK	Catalytic activity parameters							
	pH 7.5				pH 5.5			
	K_m (μM)		k_{cat} (s^{-1})		K_m (μM)		k_{cat} (s^{-1})	
	ATP	3PGA	ATP	3PGA	ATP	3PGA	ATP	3PGA
Wild-type	152 ± 4	530 ± 25	1.4 ± 0.10	1.37 ± 0.12	118 ± 4	661 ± 19	3.5 ± 0.13	3.7 ± 0.2
H57A	156 ± 8	511 ± 34	4.5 ± 0.2	4.4 ± 0.3	134 ± 8	610 ± 24	3.8 ± 0.2	3.6 ± 0.16
H71A	122 ± 5	490 ± 41	1.28 ± 0.05	1.3 ± 0.05	102 ± 5	680 ± 50	3.3 ± 0.3	3.2 ± 0.1
H89A	139 ± 10	517 ± 45	1.35 ± 0.09	1.35 ± 0.08	125 ± 4	630 ± 38	3.2 ± 0.15	3.2 ± 0.3
H111A	163 ± 14	480 ± 29	1.3 ± 0.10	1.29 ± 0.1	128 ± 9	638 ± 29	3.6 ± 0.23	3.8 ± 0.18

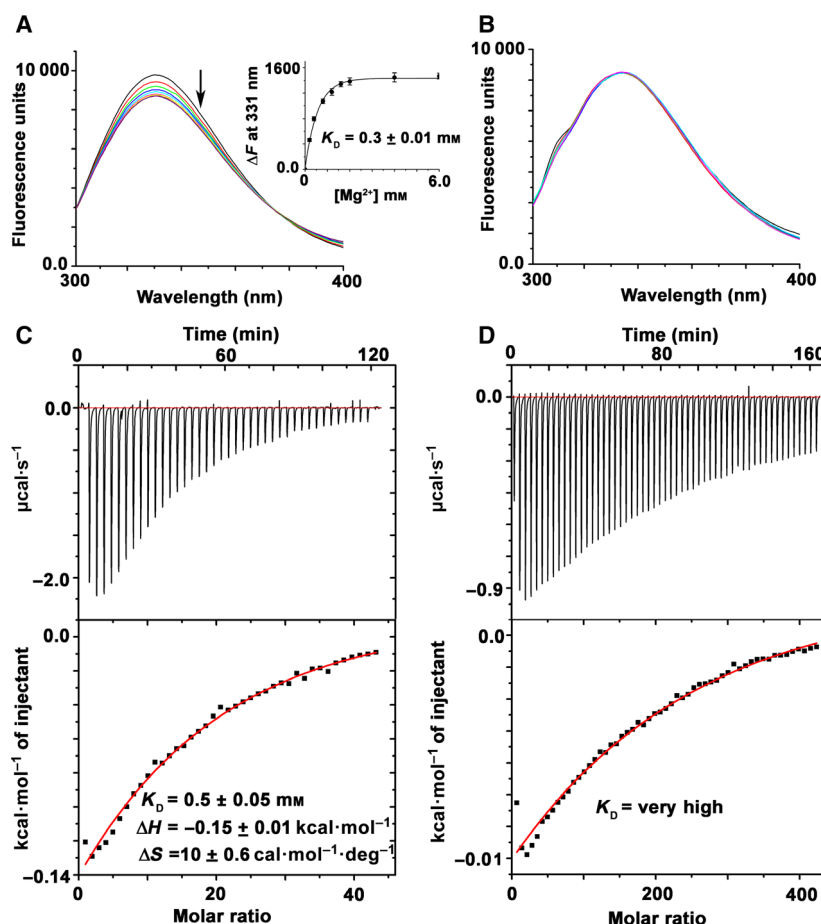
Fig. 4. Comparative studies of divalent cation-dependent PGK activity among H57A, H71A, H89A, and H111A at various pH values (7.5 and 5.5). The assay mixture was composed of 50 mM Tris/HCl buffer (pH 7.5) or acetate buffer (pH 5.5), 0.15 mM NADH, 10 μg enzyme, 1.0 mM ATP, 2.5 mM 3-phosphoglyceric acid, and 0.04U of rabbit muscle glyceraldehyde 3-phosphate dehydrogenase. Data were plotted as means \pm SD from three independent experiments for each assessment.

Mg^{2+} ion (Fig. 5A) resulted in quenching of the tryptophan fluorescence emission maxima in a Mg^{2+} ion concentration-dependent manner (Fig. 5A). Such quenching of fluorescence emission maxima, known to result from the Trp becoming more opened up from the hydrophobic environment, is indication of changes to the local environment around the Trp residue. Once the changes of buffer control titrations ran in parallel were subtracted, the maximum ligand binding-induced changes of the intrinsic fluorescence intensity were 1500 units for Mg^{2+} . Changes of the tryptophan fluorescence in response to titration of the enzyme- Mg^{2+} complexes vs Mg^{2+} concentration were plotted (Fig. 5A, inset), and the apparent equilibrium dissociation constant (K_D) for Mg^{2+} was 0.3 ± 0.01 mM. The tryptophan fluorescence of the H57A changed by the addition of MgCl_2 was a very small reduction of

fluorescence intensity due to buffer dilution (Fig. 5B). This provides further support for the involvement of H57 residue in Mg^{2+} ion binding in the PAS domain of LmPAS-PGK.

To compare the binding characteristics obtained by tryptophan fluorescence spectroscopy, the interactions of enzyme with Mg^{2+} were also assessed by isothermal titration calorimetry (ITC) at pH 7.5. The ITC titration traces fitted well into a single-site binding model for Mg^{2+} ion binding (Fig. 5C). The apparent equilibrium dissociation constant (K_D) for Mg^{2+} was 0.5 ± 0.05 mM (Fig. 5C). Mg^{2+} binding to H57A mutant was too weak to be reliably determined by ITC (Fig. 5D). The K_D values of the binding of Mg^{2+} ion to LmPAS-PGK revealed here by ITC are in good agreement with the dissociation constants obtained by tryptophan fluorescence spectroscopy. Further analyses

Fig. 5. Determination of wild-type and H57A LmPAS-PGK-Mg²⁺ interactions by tryptophan fluorescence spectroscopy and ITC at pH 7.5. The fluorescence intensity of 20 μM of wild-type (Panel A) and H57A LmPAS-PGK (Panel B) was recorded by fluorescence spectroscopy with increasing concentrations (0–6 mM) of Mg²⁺ ion. Inset shows changes in fluorescence intensity vs ligand concentrations at 331 nm. Data were plotted, and the binding affinities (K_D) for Mg²⁺ ion were determined. The values represent the mean and standard deviation for three measurements each. The changing of fluorescence intensity of H57A LmPAS-PGK with increasing concentration (0–6 mM) of Mg²⁺ ion is negligible (looks like buffer control titrations). Heat changes for titration of wild-type (Panel C) and H57 LmPAS-PGK (Panel D; 50 μM) with 10 mM MgCl₂ for wild-type and 100 mM MgCl₂ for H57A were recorded by ITC (upper panels) with data fit to one-set-of-sites interaction model (bottom panels). The affinity of H57A LmPAS-PGK to Mg²⁺ is too weak to be reliably determined. The data are representative of three independent experiments, and the error value reflects the standard deviations.



of the thermodynamics of wild-type protein and the Mg²⁺ ion interaction reveal that Mg²⁺ ion binding to wild-type protein is enthalpically driven, with a high negative enthalpy (ΔH) of $-0.15 \text{ kcal}\cdot\text{mol}^{-1}$ (Fig. 5C), whereas the metal binding to H57A protein is less favorable binding enthalpy (ΔH) of $-0.01 \text{ kcal}\cdot\text{mol}^{-1}$ (Fig. 5D).

Discussion

Most of the PGKs show optimal activity at neutral pH 7.5 but the optimal activity of the unusual LmPAS-PGK at acidic pH 5.5 makes it unique, and we are trying to understand the relevance of PAS domain mechanistically in the LmPAS-PGK for this unique behavior. Here, some salient points of this work are as follows: (a) We demonstrate that the LmPAS-PGK can be directly activated by acidic pH, (b) we have found that a change in pH does not impact on the response of LmPAS-PGK to product (ADP) inhibition, (c) the catalytic activity of LmPAS-PGK protein is decreased with increasing concentration of cofactor Mg²⁺ or Mn²⁺ at neutral pH 7.5,

(d) inhibition by higher concentration of Mg²⁺ or Mn²⁺ (2 mM) at neutral pH is insensitive to both PAS domain-deleted protein and yeast PGK (lacking PAS domain), (e) His57 in PAS domain plays crucial role for the Mg²⁺- or Mn²⁺-dependent repression of catalytic PGK domain, and (f) tryptophan fluorescence spectroscopy and ITC experiments indicate that His57 in PAS domain is essential for the Mg²⁺ ion binding. Taken together, a central finding coming from above salient points is that the network of interaction that includes H57 is essential for divalent cation-mediated repression and is also associated with pH-mediated activation. Similar type of divalent cation binding has been previously observed in PAS domains of other proteins, such as PhoQ from *Salmonella typhimurium* and WalK from *Streptococcus aureus*, which senses the cations Ca²⁺, Mg²⁺, Zn²⁺, etc. [31,33].

Generally, Mg²⁺ ion is an essential cofactor for the kinase activity. Although very low concentration of Mg²⁺ ions shows optimum activity at neutral pH 7.5, in the presence of Mg²⁺ chelator, EDTA, LmPAS-PGK does not show any PGK activity (data not

shown), indicating that Mg^{2+} ion is an essential cofactor for the PGK activity in this enzyme. The essential role of magnesium is consistent with PAS domain-deleted LmPAS-PGK data and has been observed in H57A LmPAS-PGK. The ^{31}P NMR analysis of a RhATP-PGA-PGK complex [34] and the closed form of PGK crystal structure [25] suggest that in the presence of the substrate 1,3-bisphosphoglycerate, the divalent Mg^{2+} ion switches from coordinating the α - and β -phosphates of ADP to bridging the β -phosphate of ADP and the 1-phosphate of 1,3-bisphosphoglycerate. Taken together, LmPAS-PGK has two binding sites for Mg^{2+} ions; one is in the active site of PGK domain (through ADP binding), and other is in the regulatory site of PAS domain (through His57 residue). One of the possible roles of H57 in divalent cation-mediated repression as well as acidic pH-mediated activation is that either H57 is required for divalent cation binding, which forms bridge between regulatory PAS domain and catalytic PGK domain, or the H57 indirectly controls divalent cation binding, which regulates pH-dependent PGK activation.

The immediate question that comes is what physiological implications of the observed inhibition are apparently involved in the parasite survival. Gene knockout studies suggest that LmPAS-PGK has a protecting role at longer durations of culture media where unfavorable growth conditions are occurred like nutrient stress, acidic pH, or toxic metabolite [28]. Normally, the concentration of cytosolic Mg^{2+} ion is ~ 1 mM, which is enough for optimum ATP generation by the standard kinase enzyme in the parasite, but Mg^{2+} or Mn^{2+} deficiency leads to the lowering of ATP generation for slowing down the cell growth. The Mg^{2+} - or Mn^{2+} -sensitive LmPAS-PGK may supply ATP under metal ion stress and thus can help in the survivability of these intracellular pathogens.

Due to the lack of X-ray crystal structure of PAS domain-containing PGK protein from any other organisms in the literature, we have shown a modeled structure of LmPAS-PGK (see Fig. 6). His57 is located on the long $\alpha 5$ -helix of the regulatory PAS domain of LmPAS-PGK, which locates near hinge region of the catalytic PGK domain. This $\alpha 5$ -helix contains the acidic patch Asp60 and Asp63 where divalent cation might be bound in LmPAS-PGK. The Mg^{2+} ions are hypothesized to form bridges between the PAS domain and the PGK domain. Our experimental data indicate that PGK domain can be activated at neutral pH by displacement of Mg^{2+} cations from the PAS domain in H57A mutant. It is plausible that this type of structural

alteration could destabilize the Mg^{2+} cation bridge that functions to maintain repression of the PGK activity. The H57 interaction network might be required for maintaining divalent cation repression, presumably via structural rigidity that holds the hinge region of the PGK domain, because despite the Mg^{2+} cation bridge, the substrate-induced domain closer to PGK domain might be freely occurred during catalysis. The X-ray crystal structure of divalent cation-bound PAS-PGK protein will be helpful in elucidating the complete network interaction of metal binding site in LmPAS-PGK in the near future.

Materials and methods

Materials

Ni^{2+} -nitrilotriacetate resin and imidazole were obtained from Sigma-Aldrich (St. Louis, MO, USA). Other reagents sources were described in previous papers [28,35,36].

Mutagenesis

Site-directed mutagenesis of full length of LmPAS-PGK in the pTrcHisA was performed using the QuikChange site-directed mutagenesis kit from Agilent (Santa Clara, CA, USA). Mutations (underlined) and their corresponding oligonucleotides were as follows: H57A-sense: 5'-CGTCCCCACTGCCCCGCTGGATGTACAGG-3'; and H57A-antisense: 5'-CCTGTACATCCAGCGGGGCAGTGGGACG-3'; H71A-sense: 5'-CCTTATGGCAGCCCTTGCCAAC-3'; and H71A-antisense: 5'-GTTGGCAAGGGCTGCCATAAGG-3'; H89A-sense: 5'-CCGCGACCCCCGCCGCAACAGTGG 3'; and H89A-antisense: 5'-CCACTGTTGCGGCGGGGTCGCGG-3'; H111A-sense: 5'-GTTCCGGGTGGCCATCAACATCCG-3'; and H111A-antisense: 5'-CGGATGTTGATGGCCACCCCGA AC-3'. The confirmation of mutations was carried out at the molecular biology core facility of the Indian Institute of Chemical Biology.

Protein expression and purification

Full-length, PAS domain-deleted, and mutant proteins were overexpressed in *Escherichia coli* BL21 DE3 and purified using Ni^{2+} -nitrilotriacetate affinity chromatography as reported earlier [28]. After loading the crude extract, the column was washed with 10 column volumes of washing buffer containing 50 mM Tris/HCl buffer (pH 7.5), 250 mM NaCl, 10% glycerol, and 1 mM PMSF. Finally, bound enzymes were washed by the same buffer containing 50 mM imidazole and eluted with equilibrium buffer containing 200 mM imidazole, and then, the proteins were dialyzed three times with 20 mM Tris buffer (pH 7.5) having 10%

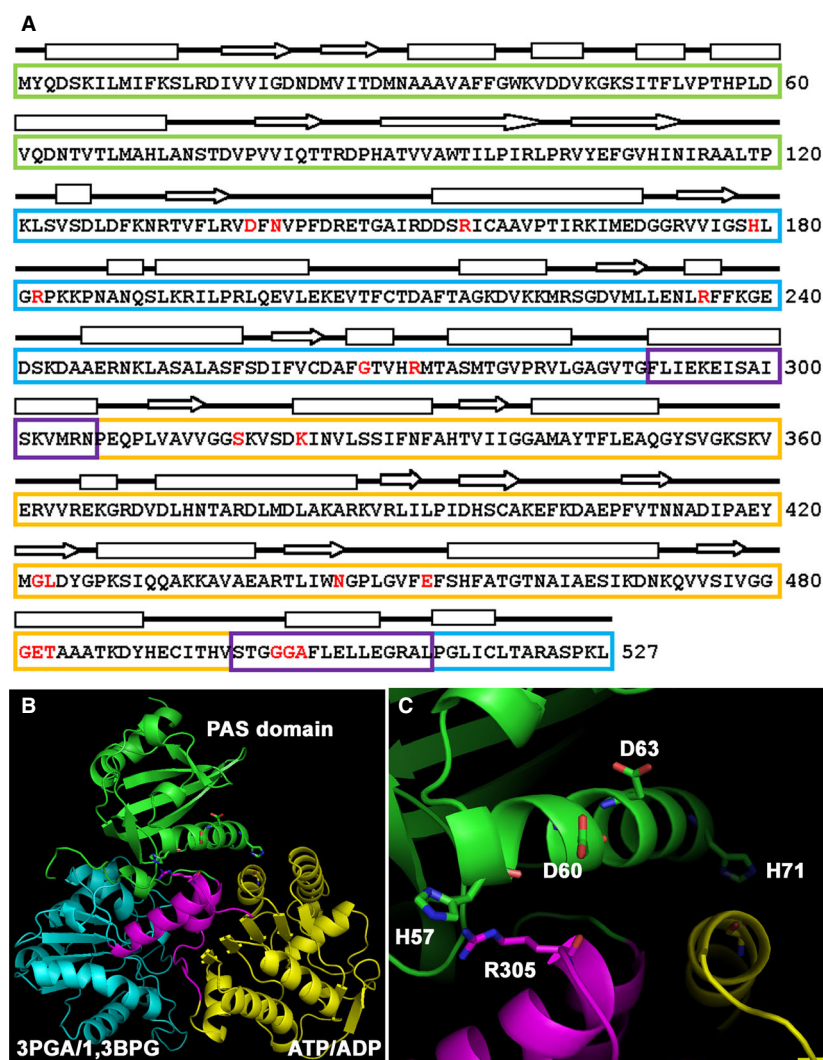


Fig. 6. Model illustrating the potential interaction site between regulatory PAS domain and catalytic PGK domain. Secondary structure with active-site residues (red color) (A) and ribbon representation (B) of LmPAS-PGK model structure determined from the X-ray structure of closed form of *Trypanosoma brucei* phosphoglycerate kinase (PDB ID: 13PK) as well as the crystal structure of PAS domain of *Streptococcus aureus* Walk protein (PDB ID: 4MN5). Above, black arrows show β -strands, and empty boxes show α -helices. The PAS domain is green (residues 1–120), the N-terminal of PGK domain (residues 121–290 and 513–527) is cyan, the C-terminal of PGK domain (residues 307–497) is yellow, and the hinge region (residues 291–306 and 497–512) is purple. The hinge regions are critical for conformational change and catalysis. This model structure was done by knowledge-based homology modeling using the Modeller [38] and PyMOL software [39]. (C) is the same as (B) after magnification.

glycerol. The purified proteins were concentrated and stored at -80°C . Molecular weight and purity of the proteins were confirmed by 12% SDS/PAGE. The concentrations of the proteins were determined by using Bio-Rad Reagent with BSA as the standard.

Enzyme assay using UV–visible spectroscopy

All kinetic studies of full-length, truncated ($\Delta 115$), and mutant LmPAS-PGK were performed at 25°C on Shimadzu UV-2550 spectrophotometer (Shimadzu Corporation, Kyoto, Japan) using quartz cuvette of 1.0 cm path length. The assay mixture was composed of 50 mM Tris/HCl buffer (pH 7.5; Amresco, Radnor, PA, USA), 0.15 mM NADH (Merck, Kenilworth, NJ, USA), 0.8 mM MgSO_4 (Sigma), 1 mM ATP (Sigma), 2.5 mM 3-phosphoglyceric acid (Sigma), and 0.04 U of rabbit muscle glyceraldehyde 3-phosphate dehydrogenase (GAPDH; Sigma). After incubating in a spectrophotometer at 25°C for 5 min

to achieve temperature equilibrium, the reaction was initiated with the addition of purified enzyme. Absorbance was recorded at 340 nm from 0 to 5 min. NADH oxidation was measured as loss of the absorbance at 340 nm. The molar extinction coefficient of NADH was $6.2 \times 10^3 \text{ M}^{-1}\text{cm}^{-1}$ at 340 nm.

For the determination of K_m value for ATP, we measured initial velocity of full-length and mutant proteins at different concentrations of ATP at a fixed concentration of 3-PGA (2.5 mM). In case of 3-PGA, we measured initial velocity of full-length and mutant proteins at different concentrations of 3-PGA at fixed concentration of ATP (1 mM). The enzyme-catalyzed reactions in LmPAS-PGK displayed saturation kinetics up to 1 mM of ATP concentration. The turnover number (k_{cat}) and the Michaelis–Menten constant (K_m) values were determined by using Michaelis–Menten enzyme kinetics in scientific statistics software (analysis of nonlinear regression) GRAPHPAD PRISM 6, GraphPad Software, Inc. CA, USA.

Determination of the pH-dependent enzyme activity

To determine the pH optimum of full-length and mutant LmPAS-PGK, kinetic studies of all the proteins were done using the following buffers (50 mM): acetate (pH 3.5–5.5), MES and phosphate buffers (pH 5.5–6.5), Tris/HCl (pH 6.8–8.8), and TEA-HCl (pH 7.5) under standard conditions.

Mg²⁺ binding by fluorescence quenching

The tryptophan fluorescence spectroscopy experiments were performed using F-7000 FL Spectrophotometer, Hitachi (Chiyoda, Tokyo, Japan), and a 1-mL quartz cuvette. The excitation wavelength was fixed to 295 nm, and emission spectra were collected between 300 and 400 nm with a slit width of 5 nm. To measure enzyme–metal ion interactions, recombinant wild-type and H57A LmPAS-PGK enzyme at 20 μM were allowed to equilibrate in 50 mM Tris/HCl buffer (pH 7.5) for 20 min before being titrated with divalent cation solutions. Wild-type and mutant were tested with increasing concentrations of MgCl₂ from 0 to 6 mM. The background fluorescence quenching caused by the dilution with the buffer was monitored by running parallel buffer control titrations. Data from three independent experiments were analyzed using nonlinear regression with ‘One Site-Specific Binding’ model ($Y = B_{\max} * X / (K_D + X)$ where Y is the fluorescence intensity, B_{\max} is the maximum specific binding, X is the ligand concentration, and K_D is the apparent equilibrium dissociation constant) in GRAPHPAD PRISM 6.0.

Mg²⁺ binding by ITC

To determine the divalent metal binding parameters of the LmPAS-PGK enzyme, experiments using ITC were performed, and titration experiments were conducted using a MicroCal VP-ITC Microcalorimeter (Presently Malvern instrument, Malvern, UK) [37]. The experiments were performed at 25 °C, and all samples were thoroughly degassed under vacuum for 30 min before loading. Solutions of MgCl₂ and the LmPAS-PGK were prepared in 50 mM Tris/HCl buffer at pH 7.5. The sample cell was loaded with 50 μM LmPAS-PGK solution, and the syringe was filled with a 10 mM (for wild-type) or 100 mM (for H57A) solution of the appropriate magnesium chloride in the same buffer. The MgCl₂ solution was added sequentially by multiple injections of a 7 μL (for wild-type) or 5 μL (for H57A) volume, at 180-s intervals with a stirring speed of 307 r.p.m. This experiment allows the determination of metal's heat of dilution in a buffer solution, which permits the correct determination of the heat exchange profile. ORIGIN 7.0 software (Northampton, MA, USA) was used for data acquisition and analysis. ITC data provided K , the

binding constant; ΔH , enthalpy change; and ΔS , the entropy change values. Each experiment was repeated thrice, and the error value reflects the standard deviations.

Molecular modeling

Molecular modeling was used to build a structural model from the LmPAS-PGK sequence. BLASTp using PDB allowed the selection of the ternary complex of PGK from *T. brucei* (PDB ID: 13PK) and the PAS domain of *S. aureus* WalK protein (PDB ID: 4MN5) as the template for molecular modeling. Sequence alignment with two templates helped to get the full-length model structure. MODELLER 9.1 [38] produced five models, from which the best model, with the lowest energy, was selected.

Acknowledgements

This work was supported by Department of Science and Technology (EMR/2016/001415), CSIR Fellowships (to SB and AM), and University Grants Commission Fellowships to AA and SD.

Conflict of interests

The authors declare no conflict of interest.

Author contributions

SA and SB designed the research; SB, AA, SD, and AM performed the research; and SA analyzed the data and wrote the paper.

References

- Henry JT & Crosson S (2011) Ligand-binding PAS domains in a genomic, cellular, and structural context. *Annu Rev Microbiol* **65**, 261–286.
- Lee J, Tomchick DR, Brautigam CA, Machius M, Kort R, Hellingwerf KJ & Gardner KH (2008) Changes at the KinA PAS-A dimerization interface influence histidine kinase function. *Biochemistry* **47**, 4051–4064.
- Ma X, Sayed N, Baskaran P, Beuve A & van den Akker F (2008) PAS-mediated dimerization of soluble guanylyl cyclase revealed by signal transduction histidine kinase domain crystal structure. *J Biol Chem* **283**, 1167–1178.
- Neiditch MB, Federle MJ, Pompeani AJ, Kelly RC, Swem DL, Jeffrey PD, Bassler BL & Hughson FM (2006) Ligand-induced asymmetry in histidine sensor kinase complex regulates quorum sensing. *Cell* **126**, 1095–1108.
- Oka Y, Matsushita T, Mochizuki N, Quail PH & Nagatani A (2008) Mutant screen distinguishes between

- residues necessary for light-signal perception and signal transfer by phytochrome B. *PLoS Genet* **4**, e1000158.
- 6 Taylor BL & Zhulin IB (1999) PAS domains: internal sensors of oxygen, redox potential, and light. *Microbiol Mol Biol Rev* **63**, 479–506.
 - 7 Cho US, Bader MW, Amaya MF, Daley ME, Klevit RE, Miller SI & Xu W (2006) Metal bridges between the PhoQ sensor domain and the membrane regulate transmembrane signaling. *J Mol Biol* **356**, 1193–1206.
 - 8 Reinelt S, Hofmann E, Gerharz T, Bott M & Madden DR (2003) The structure of the periplasmic ligand binding domain of the sensor kinase CitA reveals the first extracellular PAS domain. *J Biol Chem* **278**, 39189–39196.
 - 9 Vescovi EG, Ayala YM, Di Cera E & Groisman EA (1997) Characterization of the bacterial sensor protein PhoQ. Evidence for distinct binding sites for Mg²⁺ and Ca²⁺. *J Biol Chem* **272**, 1440–1443.
 - 10 Christie JM, Salomon M, Nozue K, Wada M & Briggs WR (1999) LOV (light, oxygen, or voltage) domains of the blue-light photoreceptor phototropin (nph1): binding sites for the chromophore flavin mononucleotide. *Proc Natl Acad Sci USA* **96**, 8779–8783.
 - 11 Purcell EB, Siegal-Gaskins D, Rawling DC, Fiebig A & Crosson S (2007) A photosensory two-component system regulates bacterial cell attachment. *Proc Natl Acad Sci USA* **104**, 18241–18246.
 - 12 Swartz TE, Tseng T-S, Frederickson MA, Paris G, Commerci DJ, Rajashekara G, Kim J-G, Mudgett MB, Splitter GA, Ugalde RA *et al.* (2007) Blue-light-activated histidine kinases: two-component sensors in bacteria. *Science* **317**, 1090–1093.
 - 13 Purcell EB, McDonald CA, Palfey BA & Crosson S (2010) An analysis of the solution structure and signaling mechanism of LovK, a sensor histidine kinase integrating light and redox signals. *Biochemistry* **49**, 6761–6770.
 - 14 Qi Y, Rao F, Luo Z & Liang Z-X (2009) A flavin cofactor-binding PAS domain regulates c-di-GMP synthesis in *AxDGC2* from *Acetobacter xylinum*. *Biochemistry* **48**, 10275–10285.
 - 15 Soderback E, Reyes-Ramirez F, Eydmann T, Austin S, Hill S & Dixon R (1998) The redox- and fixed nitrogen-responsive regulatory protein NIFL from *Azotobacter vinelandii* comprises discrete flavin and nucleotide-binding domains. *Mol Microbiol* **28**, 179–192.
 - 16 Ukaegbu UE, Henery S & Rosenzweig AC (2006) Biochemical characterization of MmoS, a sensor protein involved in copper-dependent regulation of soluble methane monooxygenase. *Biochemistry* **45**, 10191–10198.
 - 17 Gilles-Gonzalez MA, Gonzalez G, Perutz MF, Kiger L, Marden MC & Poyart C (1994) Heme-based sensors, exemplified by the kinase FixL, are a new class of heme protein with distinctive ligand binding and autoxidation. *Biochemistry* **33**, 8067–8073.
 - 18 Tuckerman JR, Gonzalez G, Sousa EH, Wan X, Saito JA, Alam M & Gilles-Gonzalez MA (2009) An oxygen-sensing diguanylate cyclase and phosphodiesterase couple for c-di-GMP control. *Biochemistry* **48**, 9764–9774.
 - 19 Lay AJ, Jiang X-M, Kisker O, Flynn E, Underwood A, Condron R & Hogg PJ (2000) Phosphoglycerate kinase acts in tumour angiogenesis as a disulphide reductase. *Nature* **408**, 869–873.
 - 20 Popanda O, Fox G & Thielmann HW (1998) Modulation of DNA polymerases alpha, delta and epsilon by lactate dehydrogenase and 3-phosphoglycerate kinase. *Biochim Biophys Acta* **1397**, 102–101.
 - 21 Cliff MJ, Bowler MW, Varga A, Marston JP, Szabo J, Hounslow AM, Baxter NJ, Blackburn GM, Vas M & Waltho JP (2010) Transition state analogue structures of human phosphoglycerate kinase establish the importance of charge balance in catalysis. *J Am Chem Soc* **132**, 6507–6516.
 - 22 Szilagy AN, Ghosh M, Garman E & Vas M (2001) A 1.8 °Å resolution structure of pig muscle 3-phosphoglycerate kinase with bound MgADP and 3-phosphoglycerate in open conformation: new insight into the role of the nucleotide in domain closure. *J Mol Biol* **306**, 499–511.
 - 23 Watson HC, Walker NP, Shaw PJ, Bryant TN, Wendell PL, Fothergill LA, Perkins RE, Conroy SC, Dobson MJ & Tuite MF (1982) Sequence and structure of yeast phosphoglycerate kinase. *EMBO J* **1**, 1635–1840.
 - 24 Auerbach G, Huber R, Grättinger M, Zaiss K, Schurig H, Jaenicke R & Jacob U (1997) Closed structure of phosphoglycerate kinase from *Thermotoga maritima* reveals the catalytic mechanism and determinants of thermal stability. *Structure* **5**, 1475–1483.
 - 25 Bernstein BE, Michels PA & Hol WG (1997) Synergistic effects of substrate-induced conformational changes in phosphoglycerate kinase activation. *Nature* **385**, 275–278.
 - 26 Adje CA, Opperdoes FR & Michels PA (1997) Organization, sequence and stage-specific expression of the phosphoglycerate kinase genes of *Leishmania mexicana mexicana*. *Mol Biochem Parasitol* **90**, 155–168.
 - 27 Kaushik S, Krishnarjuna B, Raghothama S, Aggarwal S, Raghunathan V & Ganjiwale A (2012) Theoretical and in vitro studies of a C-terminal peptide from PGKC of *Leishmania mexicana mexicana*. *Mol Biochem Parasitol* **185**, 27–35.
 - 28 Adhikari A, Biswas S, Mukherjee A, Das S & Adak S (2019) PAS domain-containing phosphoglycerate kinase deficiency in *Leishmania major* results in increased autophagosome formation and cell death. *Biochem J* **476**, 1303–1321.

- 29 McCoy G, Badal M, Prescott Q, Lux H & Hart DT (1997) Characterisation of phosphoglycerate kinase genes in *Leishmania major* and evidence for the absence of a third closely related gene or isoenzyme. *Mol Biochem Parasitol* **90**, 169–181.
- 30 Cheung J, Bingman CA, Reingold M, Hendrickson WA & Waldburger CD (2008) Crystal structure of a functional dimer of the PhoQ sensor domain. *J Biol Chem* **283**, 13762–13770.
- 31 Prost LR, Daley ME, Le Sage V, Bader MW, Le Moual H, Klevit RE & Miller SI (2007) Activation of the bacterial sensor kinase PhoQ by acidic pH. *Mol Cell* **26**, 165–174.
- 32 Dodson HC, Morris MT & Morris JC (2011) Glycerol 3-phosphate alters *Trypanosoma brucei* hexokinase activity in response to environmental change. *J Biol Chem* **286**, 33150–33157.
- 33 Monk IR, Shaikh N, Begg SL, Gajdiss M, Sharkey LKR, Lee JYH, Pidot SJ, Seemann T, Kuiper M, Winnen B *et al.* (2019) Zinc-binding to the cytoplasmic PAS domain regulates the essential WalK histidine kinase of *Staphylococcus aureus*. *Nat Commun* **10**, 3067.
- 34 Pappu KM, Gregory JD & Serpersu EH (1994) Substrate activity of Rh(III)ATP with phosphoglycerate kinase and the role of the metal ion in catalysis. *Arch Biochem Biophys* **311**, 503–508.
- 35 Roy J, Sen Santara S, Adhikari A, Mukherjee A, & Adak S (2015) Control of catalysis in globin coupled adenylate cyclase by a globin-B domain. *Arch Biochem Biophys* **579**, 85–90.
- 36 Roy J, Sen Santara S, Bose M, Mukherjee S, Saha R & Adak S (2014) The ferrous-dioxy complex of *Leishmania major* globin coupled heme containing adenylate cyclase: the role of proximal histidine on its stability. *Biochim Biophys Acta* **1844**, 615–622.
- 37 Doyle ML (1997) Characterization of binding interactions by isothermal titration calorimetry. *Curr Opin Biotechnol* **8**, 31–35.
- 38 Fiser A & Sali A (2003) Modeller: generation and refinement of homology-based protein structure models. *Methods Enzymol* **374**, 461–491.
- 39 DeLano WL (2002) The PyMOL molecular graphics system. <http://www.pymol.org/>

Research Article

PAS domain-containing phosphoglycerate kinase deficiency in *Leishmania major* results in increased autophagosome formation and cell death

Ayan Adhikari, Saroj Biswas, Aditi Mukherjee, Sumit Das and  Subrata Adak

Division of Structural Biology & Bio-informatics, CSIR-Indian Institute of Chemical Biology, 4, Raja S.C. Mullick Road, Kolkata - 700 032, India

Correspondence: Subrata Adak (adaks@iicb.res.in)

Per-Arnt-Sim (PAS) domains are structurally conserved and present in numerous proteins throughout all branches of the phylogenetic tree. Although PAS domain-containing proteins are major players for the adaptation to environmental stimuli in both prokaryotic and eukaryotic organisms, these types of proteins are still uncharacterized in the trypanosomatid parasites, *Trypanosoma* and *Leishmania*. In addition, PAS-containing phosphoglycerate kinase (PGK) protein is uncharacterized in the literature. Here, we report a PAS domain-containing PGK (LmPAS-PGK) in the unicellular pathogen *Leishmania*. The modeled structure of N-terminal of this protein exhibits four antiparallel β sheets centrally flanked by α helices, which is similar to the characteristic signature of PAS domain. Activity measurements suggest that acidic pH can directly stimulate PGK activity. Localization studies demonstrate that the protein is highly enriched in the glycosome and its presence can also be seen in the lysosome. Gene knockout, overexpression and complement studies suggest that LmPAS-PGK plays a fundamental role in cell survival through autophagy. Furthermore, the knockout cells display a marked decrease in virulence when host macrophage and BALB/c mice were infected with them. Our work begins to clarify how acidic pH-dependent ATP generation by PGK is likely to function in cellular adaptability of *Leishmania*.

Introduction

Human pathogen *Leishmania* are digenetic parasites, whose life cycle involves two hosts: the vertebrate macrophage and the sand fly vector. The transformation of the parasite from its promastigote stage (inside the midgut of the sand fly) to the amastigote stage (inside the vertebrate macrophage) requires several significant cellular remodeling, which in turn are heavily dependent on the environmental cues [1]. One of the key cellular remodeling processes during this transformation is the modulation of the glycosome [2], wherein the activity and the type of different glycosomal enzymes change considerably. Even, the number of glycosomes per cell changes and this is regulated by a co-ordinated process called pexophagy (autophagy of glycosomes) [3]. Usually, the number of glycosomes in a promastigote is more than that of in an amastigote and this turn-over of the glycosome has been implicated to play a very important role in cellular differentiation [2].

Per-Arnt-Sim (PAS) domains are widely present in proteins of all kingdoms of life. The PAS domains are usually made up of 100–120 amino acids and are bound to a wide range of enzymatic and nonenzymatic regulatory modules, which participate in various cellular signaling pathways [4]. PAS domains carry out diverse functions within sensory proteins by transferring signals [5] or facilitating protein/protein interaction [6] as well as by directly sensing environmental stimuli [7]. Depending on the structure, small molecules/ions can bind to the PAS domain can either serve as a direct signal [8] or can bind to a cofactor that allows the perception of signals like dissolved gases [9], redox potential [10,11] and visible light [12]. On the basis of genome studies, recently a

Received: 21 January 2019
Revised: 8 April 2019
Accepted: 12 April 2019

Accepted Manuscript online:
15 April 2019
Version of Record published:
30 April 2019

comprehensive review on PAS domains in kinetoplastids has been published in the literature [13]. Despite the diverse function of PAS domains in both Prokarya and Eukarya, no PAS domain-containing protein has been characterized from the Kinetoplastida group.

Phosphoglycerate kinase (PGK) catalyzes the reversible conversion of ADP and 1,3-bisphosphoglycerate to ATP and 3-phosphoglycerate. Besides, it is considered as a moonlighting protein. A group of biologists have already reported that *Leishmania* contains two PGKs, one localized in the cytosol (PGKB) and the other localized in the glycosome (PGKC) and they are expressed in both the amastigote and the promastigote forms [14]. The cytosolic and glycosomal PGK are expressed as 80% and 20% of the total PGK activity, respectively [14,15]. PGKC has a 62 residue C-terminal extension with a peroxisomal targeting signal (PTS), which is responsible for importing this isoenzyme to the glycosomes [16].

In this manuscript, we have characterized a novel PAS domain-containing PGK protein from *Leishmania major* (LmPAS-PGK), which contains an N-terminal regulatory PAS domain that is linked to a C-terminal catalytic PGK domain. To understand the biochemical function of this protein, we cloned, expressed, and characterized the LmPAS-PGK protein. Surprisingly, our data revealed that the PAS domain of LmPAS-PGK primarily regulates the PGK activity with respect to pH changes. Experimental results provide evidence for the existence of the LmPAS-PGK, which can catalyze optimal ATP synthesis at an acidic pH 5.5 and it is localized in both the glycosome and the lysosome. In addition, we present, for the first time, LmPAS-PGK null mutants have more autophagosomes and they have less infectious property with respect to macrophage infection as well as cutaneous lesions in BALB/c mice.

Experimental procedures

Parasite culture

Leishmania major wild-type parasites (strain 5ASKH) were cultured at 22°C in M199 medium (Invitrogen) supplemented with 40 mM HEPES, 200 µM adenine, 1% penicillin–streptomycin (Invitrogen) (v/v), 50 µg/ml gentamicin (Abbott), and 10% heat-inactivated fetal bovine serum (FBS, Invitrogen).

Animal ethics statement

All BALB/c mice were obtained from and maintained in our institutional animal facility (Kolkata, India). The studies were approved by CSIR-IICB Animal Ethical Committee (Registration no. 147/1999, CPCSEA), registered with Committee for the purpose of Control and Supervision on Experiments on Animals (CPCSEA), Govt. of India, and BALB/c mice were handled according to their guidelines.

Cloning of *L. major* PAS-PGK

Genomic DNA from *L. major* promastigotes was isolated by a genomic DNA isolation kit (Qiagen). The PCR amplification was carried out by using primers 1 and 2 (Supplementary Table S1) for cloning of full-length proteins and primers 3 and 4 (Supplementary Table S1) for cloning of Δ115 PAS-PGK. The PCR products from two separate reactions were purified and cloned into the BamHI and HindIII sites of pTrcHisA (Invitrogen) for full-length LmPAS-PGK and the BamHI and HindIII sites of pET28a (Novagen) for Δ115 LmPAS-PGK.

Overexpression of LmPAS-PGK with or without N-terminal RFP tag

LmPAS-PGK ORF was amplified using primers 5 and 6 (Supplementary Table S1) and cloned into the SmaI- and BamHI digested pXG-B2863 vector. The primers 7 and 8 (Supplementary Table S1) were used for making PCR product in PAS-PGK-RFP-fused overexpression construct and cloned into the BglII/NotI site of pNUS-mRFPnD vector. Transformation of the LmPAS-PGK-containing vectors in *Leishmania* cells was performed by electroporation as described earlier [17]. Overexpressed cells with or without RFP were maintained at 100 µg/ml blasticidin (Invitrogen) or 200 µg/ml neomycin (Roche), respectively.

Generation of stable knockout strain for LmPAS-PGK alleles

Modified pXG-Neo and pXG-Hyg vectors were used to generate the knockout constructs of LmPAS-PGK gene. Primers 9 and 10 (Supplementary Table S1) were used for amplifying 1.0 kbp 5'-flank, and primers 11 and 12 (Supplementary Table S1) were used for amplifying 1.0 kbp 3'-flank of the gene. Both 5'-flank and 3'-flank DNA fragments were cloned on either side (HindIII/SalI and SmaI/BamHI) of neomycin and hygromycin gene

of pXG-Neo and pXG-Hyg vectors, respectively [18]. Both constructs were then digested with HindIII and BamHI to get linear fragments of the gene deletion constructs LmPAS-PGK::NEO and LmPAS-PGK::HYG, which were transfected into *L. major* sequentially. Knockout cells were maintained in 50 µg/ml neomycin (Roche) and 100 µg/ml hygromycin drug (Roche).

Gene knockouts were confirmed by PCR using primers 13 and 14 (Supplementary Table S1) as internal to the gene. Primers 15 and 16 (Supplementary Table S1) were used as external to the gene. KO cells were further confirmed by Western blotting.

Complementation of LmPAS-PGK in null mutants

To restore LmPAS-PGK in the knockout parasites, LmPAS-PGK ORF was amplified by PCR using the primers 17 and 18 (Supplementary Table S1). The amplified product was cloned at the same site of pXG-PHLEO vector and the plasmid DNA was transfected into the knockout promastigotes. Transfected promastigotes were finally maintained in the presence of 60 µg/ml neomycin, 100 µg/ml hygromycin and 10 µg/ml phleomycin drug. Complimentary clones were confirmed by measuring LmPAS-PGK expression by Western blot analysis with rabbit anti-LmPAS-PGK antibody (1:50).

N-terminal RFP-fused cysteine peptidase B (RFP/CPB) overexpression system was constructed for use in *Leishmania*

Primers 19 and 20 (Supplementary Table S1) were used to amplify the ORF of *L. major* CPB (LmjF.08.1010) by PCR. The amplified portion was cloned into the BglII/NotI sites of pNUS-mRFPnD vector. The DNA was then transfected in *L. major* by electroporation. Overexpressed cells were maintained at 100 µg/ml blasticidin (Invitrogen).

N-terminal FLAG-fused vacuolar proton pyrophosphatase 1 (FLAG/VP1) overexpression system was constructed for use in *Leishmania*

Primers 21 and 22 (Supplementary Table S1) were used to amplify the ORF of *L. major* vacuolar proton pyrophosphatase 1 (LmjF.31.1220) by PCR. The amplicon was cloned into the SmaI/BamHI sites of pXG-B2863 vector. The DNA was then electroporated into the *L. major* cells. Overexpressing cells were maintained at 100 µg/ml neomycin (Roche).

RFP/CPB and FLAG/VP1-fused overexpression system were constructed for use in *Leishmania*

The FLAG tag VP1-containing pXG-B2863 vector was transfected into the RFP/CPB-fused overexpression system in *Leishmania* promastigotes. Transfected promastigotes were finally maintained in the presence of 100 µg/ml neomycin and 100 µg/ml blasticidin drug.

RFP/ATG8-fused overexpression system was constructed for use in *Leishmania*

Primers 23 and 24 (Supplementary Table S1) were used to amplify the ORF of *L. major* ATG8 gene (LmjF.19.1630) by PCR. The amplified portion was cloned into the BglII/NotI site of pNUS-mRFPnD vector generating an N-terminal RFP-fused ATG8. The DNA was then transfected in CT, OE, KO and CM cell type separately by the electroporation. Both RFP/ATG8 overexpressing CT and OE cells were maintained at 100 µg/ml neomycin (Roche) and 100 µg/ml blasticidin (Invitrogen). The RFP/ATG8 overexpressing KO cells were cultured in the presence of neomycin (50 µg/ml), hygromycin (100 µg/ml) and blasticidin (100 µg/ml). RFP/ATG8-overexpressing CM cells were maintained in the presence of 60 µg/ml neomycin, 100 µg/ml hygromycin, blasticidin (100 µg/ml) and 10 µg/ml phleomycin drug.

Expression and purification of protein

Recombinant LmPAS-PGK were transformed into *Escherichia coli* BL21 (DE3) and were grown overnight in 50 ml of Luria–Bertani broth containing 200 µg/ml ampicillin (Sigma) at 37°C. The overnight grown culture was then inoculated in 500 ml of terrific broth. When the culture reached an absorbance of around 0.6–0.8 at 600 nm, 0.5 mM isopropyl β-D-1-thiogalactopyranoside (IPTG) was added and bacteria were further grown at 25°C for ~18 h. Cells were then harvested by centrifugation at 8000×g for 10 min and washed two times with

1× PBS. The pellet of a 500 ml culture was resuspended in 5 ml of 50 mM Tris buffer (pH 7.5) containing 250 mM NaCl, 10% glycerol, a protein inhibitor mixture tablet without EDTA (Roche) and PMSF (Sigma). The resuspended solution was kept in ice for ~45–60 min and the cells were freeze-thawed in liquid nitrogen followed by a 20-sec pulse sonicator with 40-sec rest on ice in-between. Then the lysate was centrifuged at 14 000×g for 60 min at 4°C. The cell-free supernatant, also called the crude extract was loaded onto a Ni²⁺-NTA column. The column was washed with equilibrium buffer containing 50 mM Tris buffer, pH 7.5 containing 250 mM NaCl, 10% glycerol, followed by the same buffer containing 50 mM imidazole and eluted with equilibrium buffer containing 250 mM imidazole and dialyzed three times against 20 mM Tris buffer (pH 7.5) having 10% glycerol.

The purification of Δ 115LmPAS-PGK was carried out in the same way as above except recombinant Δ 115 LmPAS-PGK after transformation into *Escherichia coli* BL21 (DE3) were grown in Luria–Bertani broth containing 50 µg/ml kanamycin (SRL) and after induction with IPTG, it was further grown at 16°C for ~18 h. Molecular weight and purity of both the proteins were confirmed by 13% SDS–PAGE.

Size-exclusion chromatography

LmPAS-PGK was studied by gel exclusion chromatography at 28°C using a column namely Biosuite™ 250 (Waters) in an HPLC system preequilibrated with 50 mM potassium phosphate buffer pH 7.5 containing 150 mM NaCl, with a flow rate 0.8 ml/min at A₂₈₀. Column calibration was done using standard protein mixture of glutamate dehydrogenase (290 kDa), lactate dehydrogenase (142 kDa), enolase (67 kDa), myokinase (32 kDa) and cytochrome c (12 kDa).

Enzyme assay using UV-visible spectroscopy

All kinetic studies of both LmPAS-PGK and Δ 115LmPAS-PGK were performed at 25°C on Shimadzu UV-2550 spectrophotometer using quartz cuvette of 1.0-cm path length. The assay mixture was composed of 40 mM TEA-HCl buffer (pH 7.5) (Amresco), 0.15 mM NADH (Merck), 0.8 mM MgSO₄, 1 mM ATP (Sigma), 2.5 mM 3-phosphoglyceric acid (Sigma) and 0.04U of rabbit muscle glyceraldehyde 3-phosphate dehydrogenase (GAPDH, Sigma). After incubating in a spectrophotometer at 25°C for 5 min to achieve temperature equilibrium, the reaction was initiated with the addition of pure enzyme. Absorbance from 0 to 5 min was recorded. NADH oxidation was measured as loss of the absorbance at 340 nm. The concentration of NADH was determined from $\epsilon_{340} = 6.2 \times 10^3 \text{ M}^{-1} \text{ cm}^{-1}$.

The different PAS domain ligands were added in the assay mixture individually in their effective concentration.

Determination of the pH-dependent enzyme activity

To determine the pH-optimum of LmPAS-PGK and Δ 115LmPAS-PGK, kinetic studies of both the proteins were done using the following buffers (50 mM): acetate (pH 3.5–5.5), MES and phosphate buffers (pH 5.5–6.5), Tris–HCl (pH 6.8–8.8), TEA-HCl (pH 7.5) under standard conditions. The pH was adjusted at room temperature. Shimadzu UV-2550 spectrophotometer with quartz cuvette of 1.0-cm path length was used.

Fluorescence quenching

To determine the folding properties of full-length LmPAS-PGK under different pH conditions, fluorescence quenching of tryptophan residue was observed. A scan from 320 nm to 380 nm was taken after exciting the protein at 295 nm using buffers of different pH. The buffers used were acetate buffer (pH 3.5–5.5), phosphate buffer (pH 6.0–7.0), TEA-HCl (pH 7.5), Tris–HCl (pH 8.0–9.0). F-7000 FL Spectrophotometer, Hitachi was used with 1.0 cm path length cuvette.

Production of polyclonal antibodies against LmPAS-PGK

Polyclonal antibodies against the purified recombinant PAS-PGK (20 µg) was raised by subcutaneous injection in 6-month-old female rabbit using Freund's complete adjuvant (Sigma). This was followed by three booster doses of recombinant PAS-PGK (15 µg) with incomplete adjuvant (Sigma) at 2-week intervals. The rabbit was bled 2 weeks after the last booster and sera were collected and used for western blot analysis.

Western blot analysis

Proteins were resolved on 13% SDS-PAGE and then transferred on nitrocellulose membrane (GE Healthcare) by Bio-Rad semidry apparatus. After 1 h of blocking in 5% BSA, the membrane was incubated overnight with antiserum against recombinant LmPAS-PGK protein at a dilution of 1:50 at 4°C. The membrane was washed with 1× TBS containing 0.1% Tween20 (TBS-T) and then incubated in alkaline phosphatase (AP)-conjugated anti-rabbit secondary antibody (1:15 000) of Sigma. NBT/BCIP solution from Roche was used for band detection. α -Tubulin was used as endogenous control and AP-conjugated anti-mouse secondary antibody (1:15 000) was used against α -tubulin.

In case of determining RFP/ATG8 and RFP/ATG8-PE, the proteins were resolved on 10% SDS-PAGE containing 6 M urea and then transferred on PVDF membrane (Merck Millipore) by Bio-Rad semidry apparatus. The membrane was blocked by 5% BSA for 30 min and incubated overnight with anti-rabbit RFP antibody (Thermo Scientific) at a dilution of 1:1000 at 4°C. The membrane was washed with 1× TBS containing 0.1% Tween 20 (TBS-T) and then incubated with AP-conjugated anti-rabbit secondary antibody (1:15 000) of Sigma. NBT/BCIP solution (Roche) was used for band detection. Wortmannin (Sigma) and bafilomycin A1 (Sigma) were used as controls at concentrations of 10 μ M and 50 nM, respectively.

Co-localization of the protein expressed from the recombinant gene pNUS/PGK-RFP with the acidic compartments

10^7 mid-log phase pNUS/PGK-RFP overexpressing *L. major* cells were washed twice with PBS and then resuspended with 1 ml PBS. 3 μ M of lysotracker green (Molecular Probe, Invitrogen) was added and incubated for 30 min at 28°C. Then the cells were washed with PBS and fixed on the poly-L-lysine-coated slides. Finally, they were stained with DAPI and mounted with antifade mounting media, and observed under a confocal microscope (Leica). The wavelength used were DAPI ($Ex_\lambda = 350$ nm, $Em_\lambda = 470$ nm), RFP ($Ex_\lambda = 535$ nm, $Em_\lambda = 615$ nm), lysotracker green ($Ex_\lambda = 504$, $Em_\lambda = 511$ nm).

Co-localization of the protein expressed from the recombinant gene pNUS/PGK-RFP with glycosome

10^7 mid-log pNUS/PGK-RFP overexpressing *L. major* cells were washed thrice with 1× PBS and then fixed on poly-L-lysine-coated slides. The slides were dipped in a solution containing 1% Triton X-100 and 50 μ g/ml RNase A (Calbiochem). Following the blocking with 1.5% BSA for 2 h, the slides were incubated with anti-rabbit GAPDH antibody (1:800) for overnight at 4°C. The next day, the slides were washed with 1× PBS and incubated with Alexa Fluor 488-conjugated anti-rabbit secondary antibody (Thermo Scientific) at a dilution of 1:2000 for 2 h. Finally, they were stained with DAPI and mounted on a poly-L-lysine-coated slide with antifade mounting media (Invitrogen). The wavelength used for Alexa Fluor 488 secondary antibody were $Ex_\lambda = 488$ nm and $Em_\lambda = 522$ nm.

Co-localization of LmPAS-PGK in the lysosome

10^7 mid-log pNUS/CBP-RFP overexpressing *L. major* cells were washed with 1× PBS and then fixed on poly-L-lysine-coated slides. The slides were dipped in a solution containing 1% Triton X-100 and 50 μ g/ml RNase A. Following the blocking with 1.5% BSA for 2 h the slides were incubated with anti-rabbit PAS-PGK antibody (1:800) for overnight at 4°C. The next day, the slides were washed with 1× PBS and incubated with Alexa Fluor 488 goat anti-rabbit secondary antibody at a dilution of 1:2000 for 1 h. Finally, they were mounted with antifade mounting media (with DAPI).

Co-localization of LmPAS-PGK in the acidocalcisome

The co-localization of LmPAS-PGK with the acidocalcisomal marker VP1 was determined by double immunofluorescence. 10^7 mid-log pXG/FLAG-VP1 overexpressing *L. major* cells were washed with 1× PBS and then fixed on poly-L-lysine-coated slides. The slides were dipped in a solution containing 1% Triton X-100 and 50 μ g/ml RNase A. Following the blocking with 1.5% BSA for 2 h, the slides were incubated with a mixture of anti-rabbit PAS-PGK antibody (1:800) and anti-mice FLAG antibody (Sigma) for overnight at 4°C. The next day, the slides were washed with 1× PBS and incubated with both anti-mice Alexa Fluor 546 (Thermo Scientific) and anti-rabbit Alexa Fluor 488-conjugated secondary antibody at a dilution of 1:2000 for 2 h.

Finally, they were mounted with antifade with DAPI. The wavelength used for Alexa Fluor 546-conjugated secondary antibody were $Ex_{\lambda} = 546$ nm and $Em_{\lambda} = 575$ nm.

Co-localization of LmPAS-PGK with mitochondria

10^7 mid-log phase pNUS/PGK-mRFP overexpressing *L. major* cells were washed twice with PBS and then resuspended with 1.0 ml PBS. 500 nM of MitoTracker green (Molecular Probe, Invitrogen) was added and incubated for 30 min at 28°C. Then the cells were washed with PBS and fixed on the poly-L-lysine-coated slides. Finally, they were mounted with antifade with DAPI. The wavelength used for MitoTracker green were $Ex_{\lambda} = 490$ and $Ex_{\lambda} = 516$ nm.

Isolation of mitochondrial and cytosolic fractions

Isolation of mitochondrial and cytosolic fractions was performed from *L. major* promastigotes by hypotonic lysis followed by Percoll gradient centrifugation at 4°C [17]. The purity of each fraction was checked by Western blot analysis with organelle-specific marker rabbit anti-*(L. major)* ascorbate peroxidase (APX, 1:50) antibodies for the mitochondria and rabbit anti-*(L. donovani)*-adenosine kinase (ADK, 1:50) for the cytosol. The AP-conjugated anti-rabbit secondary antibody (Sigma) was used at a dilution 1:15 000.

Isolation of lysosomal fractions

Lysosome was isolated following the method described by Jinn et al. [19] with slight modifications. Briefly, *L. major* cells were centrifuged $500\times g$ for 5 min to obtain cell pellets. After the removal of media, pellets were washed with PBS and centrifuged again. The obtained pellets were resuspended in sucrose homogenization buffer (0.25 M sucrose, 20 mM HEPES) containing protease inhibitor (Roche), and lysed by Dounce homogenizer and cell lysis was confirmed under a light microscope. Homogenates were centrifuged again at $500\times g$ for 5 min to eliminate the cell debris. The supernatant was centrifuged at $7000\times g$ for 10 min to eliminate the mitochondrial fraction. The resulting supernatant was centrifuged again at $20\,000\times g$ for 60 min to yield the crude lysosomal fraction (CLF) as a pellet. The CLF was washed again with 10 mM $CaCl_2$ and centrifuged at $7000\times g$ for 15 min. The supernatant contains purified lysosome. The purity of lysosomal fraction was checked by Western blot analysis with organelle-specific marker RFP tag CPB. The primary antibody used was anti-rabbit RFP antibody.

Isolation of acidocalcisomal fractions

Acidocalcisome was isolated using the method described by Salto et al. [20] with certain modifications. *L. major* cells were centrifuged at $500\times g$ for 10 min to obtain cell pellets. The pellets were then washed with PBS and centrifuged. The resultant pellet was resuspended in the lysis buffer comprising of 125 mM sucrose, 50 mM KCl, 4 mM $MgCl_2$, 0.5 mM EDTA, 20 mM K-HEPES, 5 mM dithiothreitol and protease inhibitor cocktail. The cells were completely homogenized by syringe (needle gauge 0.30×12.5 mm). The lysate at first was centrifuged at $150\times g$ for 5 min and then at $325\times g$ for 10 min. The supernatant fractions were taken together and centrifuged for 30 min at $11\,000\times g$. The pellet was resuspended in lysis buffer and applied to the 34% step of the discontinuous (20–40% (v/v)) gradient of iodixanol, with gradients of 20, 25, 30, 34, 37, and 40% iodixanol, diluted in lysis buffer. The gradient was centrifuged at $50\,000\times g$ for 60 min. The acidocalcisome fraction pelleted on the bottom of the tube and was resuspended in lysis buffer. The purity of acidocalcisomal fraction was checked by Western blot analysis with organelle-specific marker FLAG-tagged vacuolar proton pyrophosphatase 1. The primary antibody used was anti-mice FLAG antibody.

Isolation of glycosomal fractions

Glycosome was isolated following the method described by Colasante et al. [21] with minor modifications. *L. major* promastigotes were harvested by centrifugation for 10 min at $2000\times g$, and were washed once in 10 ml of wash buffer (25 mM Tris, 1 mM EDTA, 1 mM DTT, 250 mM sucrose, pH 7.8). After centrifugation, the cell pellet was resuspended in 2 ml homogenization medium (250 mM sucrose, 1 mM EDTA, 0.1% (v/v) ethanol, 5 mM MOPS, pH 7.2) containing protease inhibitor (complete EDTA-free, Roche Applied Science) and was lysed using syringe (needle gauge: -0.30×12.5 mm). Cell lysis was confirmed by light microscopy. The cell lysate was centrifuged sequentially for 5 min each at $100\times g$ and $3000\times g$ to remove cell debris and cell nuclei. The resulting supernatant was centrifuged at $17\,000\times g$ for 15 min to obtain a glycosomal enriched pellet. This pellet was resuspended in 1.0 ml homogenizing buffer and was loaded on top of a 24 ml linear 20–40% (v/v)

optiprep gradient (Sigma), mounted on 50% 2.5 ml optiprep cushion and centrifuged at 170 000×g for 1 h. Nine fractions (1.0 ml each) were collected from the bottom of the tube. They were centrifuged at 30 000×g to obtain the pellet. The pellet was resuspended in homogenizing buffer and again centrifuged at 30 000×g to obtain the purified glycosomal pellet. The purity of the fraction was checked by western blotting using the glycosome-specific GAPDH. The primary antibody used was rabbit anti-*(L. major)* GAPDH antibody (1:100).

Measurement of pyrophosphatase activity in purified acidocalcisome

Around 58 mg/ml protein equivalent of purified acidocalcisome with and without 0.5% Triton X was incubated in a solution containing 50 mM Tris-HCl (pH 7.5), 10 mM sodium pyrophosphate and 10 mM magnesium chloride for 10 min [22,23]. After 10 min, the detection reagent containing 10% ammonium molybdate in 10 N H₂SO₄ and 5% ferrous sulfate was added. The resulting solution was incubated again for 10 min at 25°C. Then 500 μl aliquots from each sample is transferred to spectrophotometer cuvette and the absorbance was recorded at 660 nm. Inorganic phosphates were used as standards. A standard curve was prepared by plotting the ΔA_{660 nm} versus concentration of phosphate.

Measurement of peroxidase activity in purified mitochondria

3 mg/ml protein equivalent of purified mitochondria with and without 0.5% Triton X was incubated in a solution containing 50 μM ferrocytochrome c, 50 mM phosphate buffer (pH 7.5), at a final volume of 1.0 ml. The reaction was started by the addition of 0.3 mM H₂O₂. Ferrocytochrome c oxidation was measured as loss of absorbance at 550 nm. The concentration of oxidized cytochrome c was determined from ε₅₅₀ = 2.1 × 10⁴ M⁻¹ cm⁻¹.

Measurement of ATP

10⁷ cells were lysed by 0.5% Triton X in the presence of 50 μM of ARL 67156 trisodium salt hydrate (Sigma) at 95°C for 1 min. ATP content in the lysate was measured by a luciferin-luciferase bioluminescence assay using the ATP determination kit (Molecular Probes) according to the manufacturer's protocol. Briefly, the samples were added to the reaction mixture containing reaction buffer, D-luciferin, DTT and the enzyme firefly luciferase and the luminescence was measured by a luminometer (Glomax, Promega). ATP concentrations were calculated from the ATP standard curve.

Measurement of glycolytic flux

The glycolytic flux of the CT, OE, CM and KO cell lines was measured by using the Glycolysis Cell-Based Assay Kit (Cayman Chemicals) following the manufacturer's protocol. Briefly, CT, OE, CM and KO cells were grown in M199 media with and without 50 mM inhibitor of glycolysis (2-deoxy D-glucose). 10⁷ cells from each cell type were centrifuged at 3500 rpm for 5 min and the supernatant was collected. 10 μl of supernatant was added to 190 μl of reaction solution containing assay buffer, glycolysis assay enzyme mixture, glycolysis assay cofactor and glycolysis assay substrate. The resulting mixture was carefully loaded onto 96-well plate using a multichannel pipette. After 30 min of incubation, the absorbance was measured at 490 nm using a plate reader. The lactate provided by the manufacturer was used as standard.

Determination of autophagic flux by flow cytometry

10⁷ log phase CT, OE, CM and KO cells from control and starved conditions were washed twice and resuspended in 1× assay buffer containing 2.0 μl of the provided green detection reagent (autophagy detection kit dye, Abcam) and incubated for 30 min at 37°C. The samples were then sorted by flow cytometry (BD FACS LSRFortessa) using the FITC filter (Ex_λ = 488 nm, Em_λ = 517 nm). 10 000 events were measured for every sample. The nutrient starvation was achieved by incubating the cells in 1× PBS at 28°C for 2 h.

Determination of autophagic flux by fluorescence microscopy

10⁷ log phase CT, OE, CM and KO control and nutrient-starved promastigotes were washed twice and resuspended in 1× assay buffer containing 2 μl of the provided green detection reagent (autophagy detection kit dye) and incubated for 30 min at 37°C. The cells were then fixed on poly-L-lysine-coated slides. Finally, they were mounted with antifade mounting media (with DAPI) and observed under a fluorescence microscope (Olympus). The wavelength used were-DAPI (Ex_λ = 350 nm, Em_λ = 470 nm) and autophagy detection kit dye

($Ex_{\lambda} = 488$ nm, $Em_{\lambda} = 517$ nm). The nutrient starvation was achieved by incubating the cells in 1× PBS at 28°C for 2 h.

Determination of the formation of ATG8 puncta

10^7 mid-log phase CT, OE, CM and KO cells overexpressing RFP/ATG8 from the normal and stressed conditions were washed twice with 1× PBS and fixed on poly-L-lysine-coated slides. They were mounted with anti-fade mounting media with DAPI and observed under a fluorescence microscope. The wavelength used were-DAPI ($Ex_{\lambda} = 350$ nm, $Em_{\lambda} = 470$ nm) and RFP/ATG8 ($Ex_{\lambda} = 535$ nm and $Em_{\lambda} = 615$ nm). The nutrient starvation was achieved by incubating the cells in 1× PBS at 28°C for 2 h.

Infection in mice

Disease progression was monitored by daily caliper measurement of footpad swelling. Parasite loads in footpad tissue of mice containing CT, OE, CM and KO parasites were determined by limiting dilution assay with slight modifications. Briefly, 1 mg of footpad tissue were sequentially immersed in 70% ethanol, and sterile H₂O before homogenization of weighed tissue in M199 media supplemented with gentamicin and penicillin–streptomycin containing 10% heat-inactivated FBS. Each tissue homogenate was serially diluted in the same medium in a 96-well flat-bottom tissue culture plate. The number of viable parasites per milligram of tissue was determined from the highest dilution at which promastigotes could be grown out after up to 10–15 days' incubation at 22°C.

In vitro promastigote growth profile analysis

10^6 mid-log phase cells were inoculated in 10 ml of M199 media supplemented with 10% FBS. Growth rates were measured at a 24-h interval by counting cell number in an improved Neubauer chamber (hemocytometer) for 8 consecutive days. Experiments were done in triplicate for each cell type.

Determination of cell viability by flow cytometry

Cell viability was determined by propidium iodide exclusion assay. Briefly, 10^7 promastigotes from the various duration of incubated culture were washed and resuspended in PBS containing 5 µg/ml of propidium iodide (Calbiochem) and incubated at room temperature for 15 min in the dark. The stained cells were subjected to FACS (BD FACS LSRFortessa) analysis ($Ex_{\lambda} = 488$ nm; $Em_{\lambda} = 617$ nm). 10 000 events were analyzed.

Statistical analysis

All data were expressed as the means ± SD from at least three independent experiments. Statistical analyses for all data were calculated using analysis of variance wherever applicable using Origin 6.0 software (Microcal Software). *P* value of less than 0.05 was considered statistically significant.

Results and discussion

Primary structure of LmPAS-PGK protein

A sequence (systematic name: LmjF.30.3380) in the *L. major* genome database (<http://www.genedb.org/genedb/leish/>) has been identified as an ORF, comprising 527 amino acid residues. It exhibits two striking features: first, its N-terminus (residues 1–115) displays limited homology to PAS domain (Figure 1) and second, the C-terminus (residues 116–527) bears ~50% identity with PGK (Figure 1). A common PAS domain usually comprises of four/five-strand of antiparallel β-sheet and three/four flanking α-helices [7,24]. SWISS-MODEL protein modeling predicts that four antiparallel β-sheet and four flanking α-helices are conserved in this protein (Figure 2A). The C-terminus of this gene contains PGK like conserved active site residues as well as the tertiary structure (Figures 1 and 2B). These features suggested that this protein is a PAS domain-containing PGK protein (LmPAS-PGK).

Biochemical characteristics of LmPAS-PGK

To identify the biochemical characteristics of LmPAS-PGK, both the full-length protein and PAS domain deleted catalytic domain (Δ115 LmPAS-PGK, 115 amino acid deleted from the N-terminus of wild-type full-length LmPAS-PGK protein) were expressed in *E. coli*. Purified LmPAS-PGK and Δ115 LmPAS-PGK migrated to positions as expected from the theoretical relative molecular mass of 62 kDa (Figure 2C, lane 4) and 47 kDa

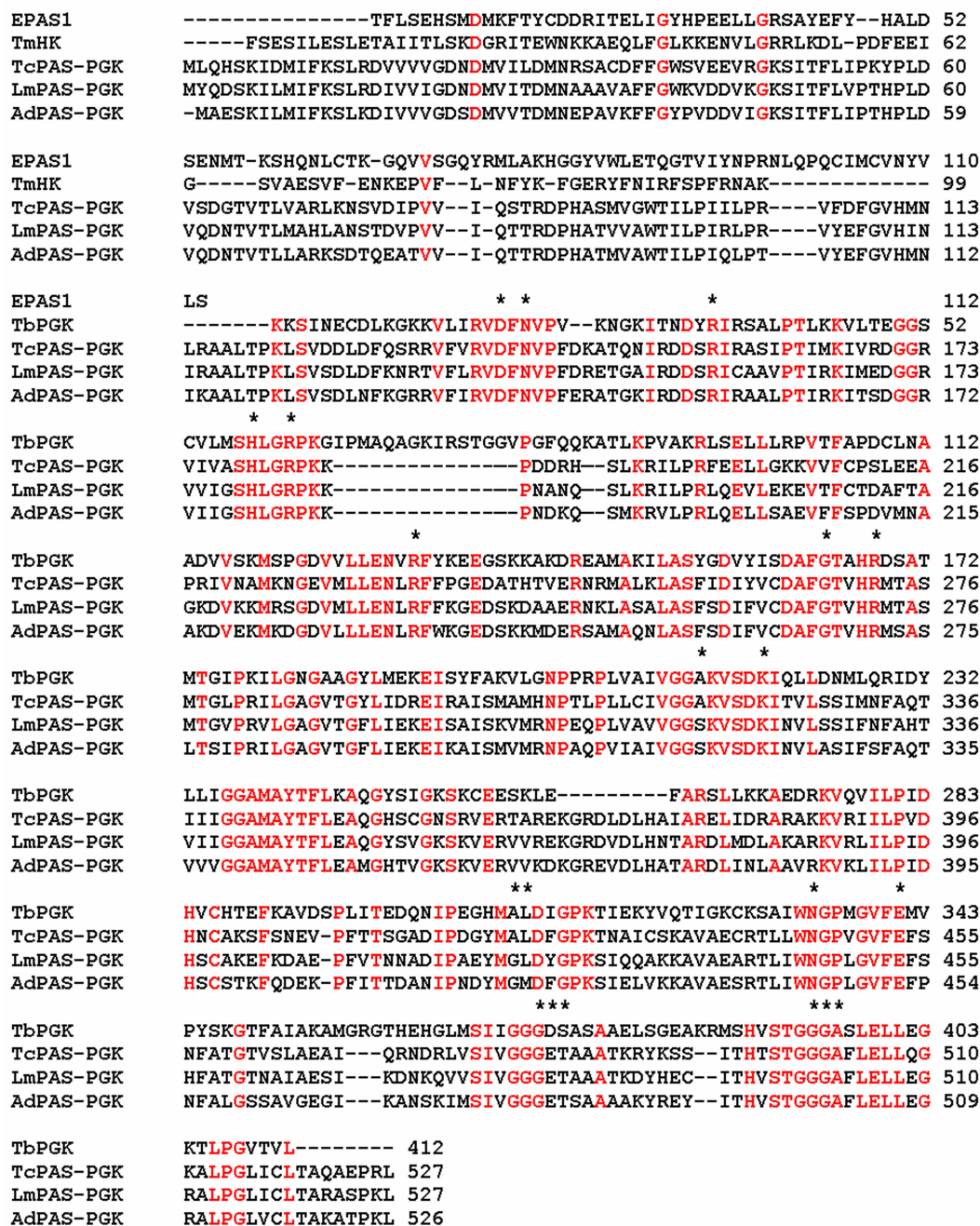


Figure 1. Sequence alignment of LmPAS-PGK.

The sequence of LmPAS-PGK was aligned with the PAS domain of human Endothelial PAS domain-containing protein 1, also known as HIF-2 α (EPAS1, accession number NP_001421), PAS domain of *Thermotoga maritima* histidine kinase (TmHK, accession number 3A0R_A), *T. cruzi* PAS domain-containing phosphoglycerate kinase (TcPAS-PGK, accession number ESS69068), *T. brucei* phosphoglycerate kinase (TbPGK, accession number AAA32120), *A. deanei* PAS domain-containing phosphoglycerate kinase (AdPAS-PGK, accession number EPY28995). * and red color denote active site and identical residue, respectively.

protein (Figure 2C, lane 9), respectively. Figure 2D showed that both full-length and Δ 115 LmPAS-PGK proteins were monomeric. For sensing environment, many of the PAS domains in sensory proteins are known to bind small molecules including heme [25–27], FAD [28], FMN [29], 4-hydroxycinnamic acid [30], fatty

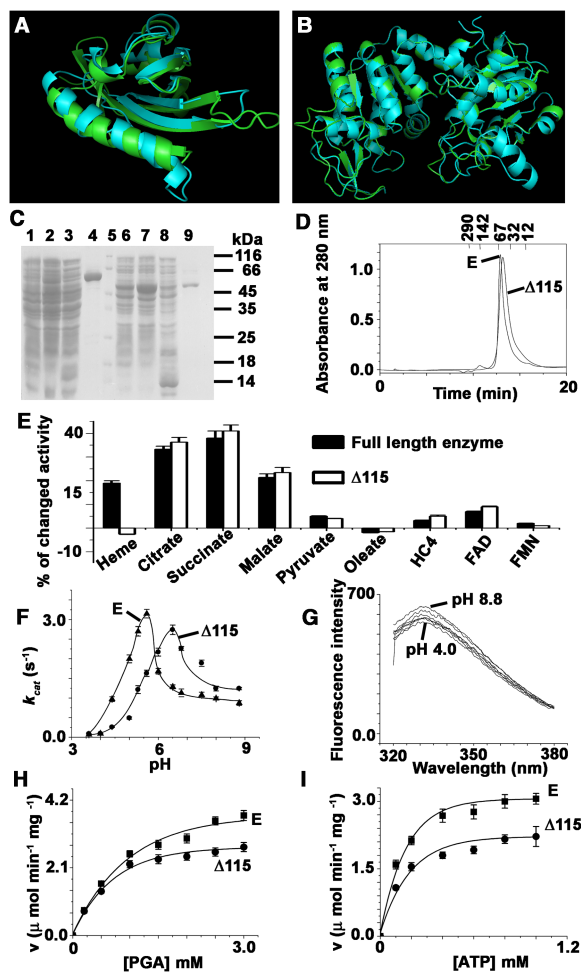


Figure 2. Biochemical characteristics of LmPAS-PGK.

(A) Based on the published X-ray crystallographic structures of the PAS domain of EPAS1 (cyan color) [54] (PDB entry code: 4xt2.2), we constructed a three-dimensional model of the PAS domain of LmPAS-PGK (green color) by knowledge-based homology modeling using the SWISS-MODEL [55] and PyMOL software [56]. (B) The ribbon structural model of the PGK domain of LmPAS-PGK was made on basis of the published X-ray crystallographic structures *T. brucei* PGK (PDB entry code: 13PK.1) [37]. (C) SDS–PAGE lanes: 1, lysate without IPTG (full length) 2, lysate with IPTG (full length); 3, lysate unbound flow through (full length); 4, purified full-length protein; 5, molecular weight marker; 6, (–) IPTG ($\Delta 115$); 7, (+) IPTG ($\Delta 115$); 8, flow through ($\Delta 115$); and 9, purified $\Delta 115$ protein. (D) Size-exclusion chromatography of full-length and $\Delta 115$ proteins after purification by using a Biosuite™ 250 HPLC column. (E) Change in activity of LmPAS-PGK and $\Delta 115$ LmPAS-PGK in the presence of different PAS binding ligands. (F) Activity of the LmPAS-PGK and $\Delta 115$ LmPAS-PGK in the presence of different pH values. (G) Tryptophan quenching of LmPAS-PGK under different pH conditions. (H) Velocity of LmPAS-PGK (pH 5.5) and $\Delta 115$ LmPAS-PGK (pH 7.5) with varying concentration of 3-PGA. (I) Velocity of LmPAS-PGK (pH 5.5) and $\Delta 115$ LmPAS-PGK (pH 7.5) with varying concentration of ATP.

acids [31], malate, succinate and citrate [32–34]. The UV-visible spectra of LmPAS-PGK did not have any band at visible region (Supplementary Figure S1) indicating that chromophoric prosthetic groups such as heme, FAD and FMN are unlikely to function as PAS ligands in LmPAS-PGK. To identify the ligand for PAS domain, we measured the PGK activity in the presence of several well-known PAS ligands (Figure 2E). Our results suggest that the activity of LmPAS-PGK was insensitive to FAD, FMN, 4-hydroxycinnamic acid and fatty acid ligands. Although the purified enzyme did not have any heme yet its activity was stimulated by almost ~20% in the presence of heme, indicating that the capability of heme binding to PAS domain is very weak. Although PAS-PGK sequence has no heme regulatory motif, usually containing a CP (Cys-Pro) motif [35], yet the PGK

Table 1 Catalytic activities of full-length and Δ 115 LmPAS-PGK proteins

The catalytic activities were determined at 25°C as described under 'Materials and Methods'. The values represent the mean and standard deviation for three measurements each.

Enzyme	Catalytic activity parameters							
	pH 5.5				pH 7.5			
	K_M (μ M)		k_{cat} (s^{-1})		K_M (μ M)		k_{cat} (s^{-1})	
	ATP	3PGA	ATP	3PGA	ATP	3PGA	ATP	3PGA
LmPAS-PGK	118 \pm 4	661 \pm 19	3.5 \pm 0.09	3.7 \pm 0.2	150 \pm 5	540 \pm 29	1.3 \pm 0.05	1.33 \pm 0.1
Δ 115 LmPAS-PGK	110 \pm 7	630 \pm 22	1.4 \pm 0.1	1.5 \pm 0.2	137 \pm 7	520 \pm 22	2.7 \pm 0.09	2.8 \pm 0.16

activity of the full-length enzyme was significantly enhanced by the addition of heme indicating that the association/dissociation of heme in PAS domain might regulate the catalytic activity of this enzyme.

Other PAS ligands like malate/succinate and citrate stimulated the PGK activity in both full-length and PAS-deleted proteins (Δ 115 LmPAS-PGK) suggesting that this stimulation is independent of the PAS domain and is a characteristic of the PGK domain itself. It is well known that the *Salmonellae* PhoQ sensor kinase is directly activated when the PAS domain is exposed to pH 5.5 [36]. To determine whether LmPAS-PGK is directly activated when exposed to acidic pH, we measured PGK activity of both full-length and PAS-deleted proteins in various pH (Figure 2F). As observed in the pH curve, the activation of the full-length PGK was maximal at pH 5.5 and gradually decreased at neutral pH 7.5. On the other hand, the PGK activity of Δ 115 LmPAS-PGK proteins was higher than the full-length proteins at neutral pH 7.5. Together, these results suggest that the acidic pH 5.5 relieved the autoinhibitory PAS domain from PGK catalytic domain in LmPAS-PGK. These results indicate that the PAS domain appears to have an autoinhibitory role at neutral pH 7.5 in LmPAS-PGK catalysis. The optimum activity of PAS-PGK is at around pH 5.5, close to the pH value at which histidine residues get protonated. Thus, the protonation of a histidine residue in a critical region of the PAS domain might act as the conformational switch associated with the activation. The pH-dependent fluorescence quenching (Figure 2G) suggests that acidic pH presumably triggers a conformational change in LmPAS-PGK that stimulates the catalytic activity of the PGK domain. Full-length proteins at pH 5.5 and Δ 115 LmPAS-PGK proteins at pH 7.5 showed that both proteins follow standard Michaelis–Menten kinetics with respect to both of its substrates (3PGA and ATP) (Figure 2H,I). The K_M and k_{cat} values of full-length as well as Δ 115 protein at both pH 5.5 and 7.5 were compared in Table 1. The K_M values for ATP of the full-length protein (118 μ M at pH 5.5 and 150 μ M at pH 7.5) were very similar to Δ 115 LmPAS-PGK proteins (110 μ M at pH 5.5 and 137 μ M at pH 7.5). The K_M values for 3PGA of the full-length proteins (661 μ M at pH 5.5 and 540 μ M at pH 7.5) were comparable with Δ 115 LmPAS-PGK proteins (630 μ M at pH 5.5 and 520 μ M at pH 7.5). These results demonstrated that its PAS domain did not affect the K_M values of both the substrates. The acidic pH 5.5 significantly enhances catalysis of the full-length enzyme (3.5 s^{-1}) compared with the PAS domain deleted enzyme (1.4 s^{-1}), whereas the neutral pH 7.5 significantly inhibits the enzymatic activity of the full-length protein (1.3 s^{-1}) compared with the PAS domain deleted protein (2.7 s^{-1}). These results suggest that the N-terminal PAS domain is not directly involved in substrate binding yet it is responsible for pH-dependent activation. In the aspect of molecular mechanism of the catalysis, the enzymatic reaction of PGK briefly consists of the following events [37]. PGK exists in an 'open' conformation in the absence of both substrates (1,3-bisphosphoglycerate/3-phosphoglycerate and ADP/ATP). Upon binding of both the substrates, an extensive hinge-bending motion occurs, and this leads to closure of the two domains of PGK. Then, the β -phosphate of ADP initiates a nucleophilic attack on the 1-phosphate of 1,3-BPG by the help of Lys 219 (TbPGK) during the forward glycolytic reaction. The autoinhibiting PAS domain at neutral pH 7.5 may interfere with the substrate-induced domain closing, which can be the possible reason behind of lower catalytic activity.

Subcellular localization of LmPAS-PGK

Since the PGK activity of LmPAS-PGK is optimum at acidic pH, it raises the question of whether the mature proteins localize in acidic organelles of cells. It is well established that glycolytic enzymes are targeted to the

mitochondrial matrix [38], peroxisomes [39], lysosomes [40], and flagella (or cilia) [39,41,42]. To find out the localization of the mature LmPAS-PGK protein, homogenates of RFP/CPB (N-terminal RFP tag-CPB) and FLAG-VP1 (N-terminal FLAG tag-vacuolar proton pyrophosphatase 1) overexpressing *L. major* cells were fractionated by differential centrifugation. Different subcellular fractions were examined by Western blotting with anti-LmPAS-PGK antibody (Figure 3A). Western blot results showed that the LmPAS-PGK protein band was recovered from both glycosomal and lysosomal fractions, where the glycosomal LmGAPDH and lysosomal CPB (as a marker protein) were concentrated (Figure 3A), suggesting that the enzyme is localized in both the glycosome and the lysosome of *Leishmania*. On the other hand, the LmPAS-PGK protein band was absent from the cytosol, mitochondria and acidocalcisome fractions, where the cytosolic ADK, mitochondrial APX and acidocalcisomal vacuolar proton pyrophosphatase 1 (VP1) (as a marker protein) were concentrated (Figure 3A). To confirm this observation, the full-length RFP tag LmPAS-PGK fusion in *L. major* promastigotes were costained with rabbit anti-LmGAPDH (glycosome-specific protein) as primary antibody and Alexa

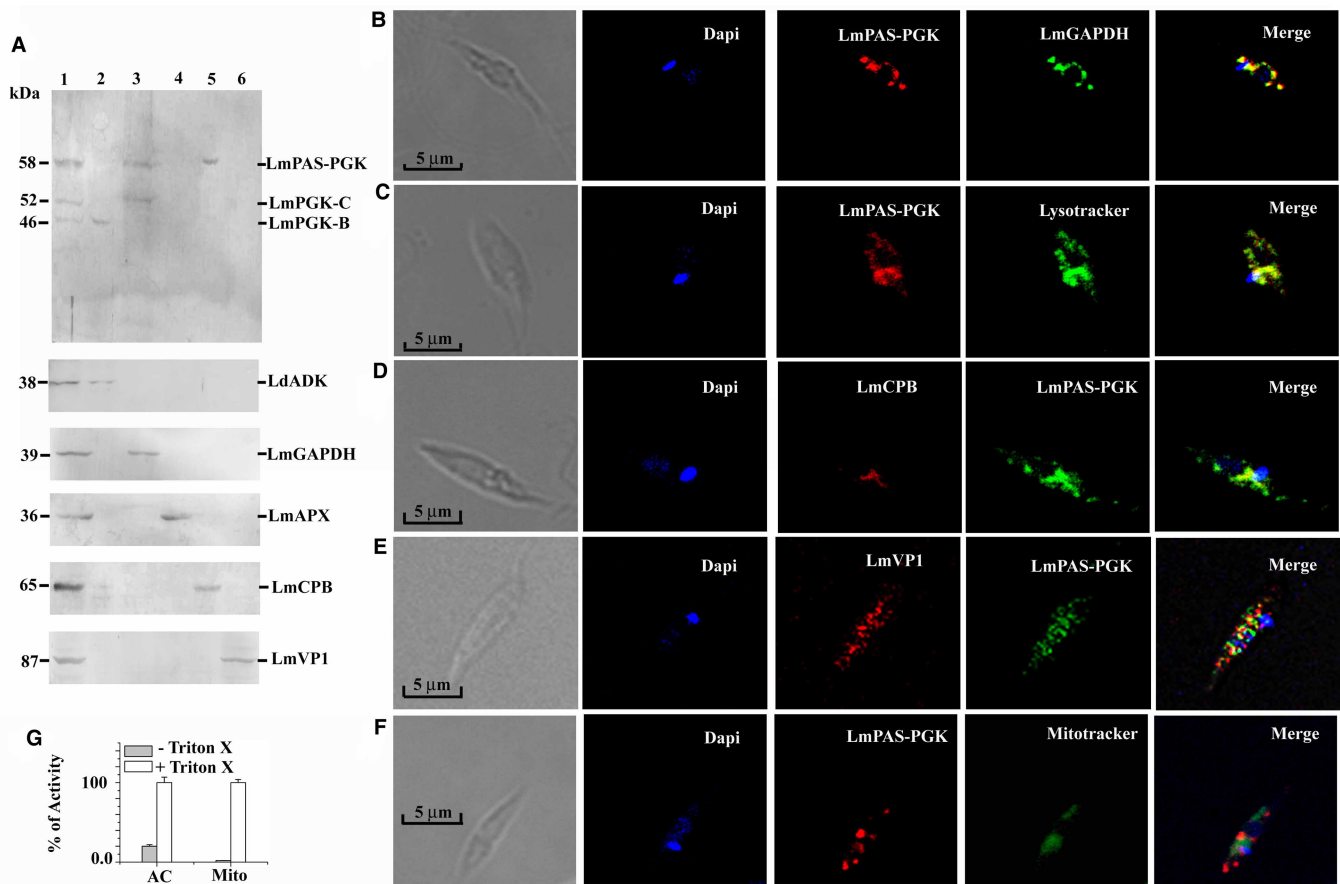


Figure 3. Localization by Western blotting and immunofluorescence.

(A) Subcellular localization was performed using RFP/CPB and FLAG-VP1 overexpression cells. Lanes: 1, cell lysate; 2, cytosolic; 3, glycosomal; 4, mitochondrial; 5, lysosomal and 6, acidocalcisomal fraction. ADK, GAPDH, APX, CPB/RFP (anti-RFP antibody used) and vacuolar proton pyrophosphatase 1/FLAG (VP1) (anti-FLAG antibody used) were used in the subcellular fractions as cytosolic, glycosomal, mitochondrial, lysosomal and acidocalcisomal markers, respectively. (B) LmPAS-PGK-RFP overexpressed promastigotes were colocalized with *L. major* GAPDH (Alexa Fluor 488 secondary antibody) (glycosomal marker). (C) LmPAS-PGK-RFP overexpressed promastigotes were colocalized with lysotracker green (acidic organelles-specific dye). (D) RFP/LmCPB (lysosomal marker) overexpressed promastigotes were colocalized with LmPAS-PGK (Alexa Fluor 488 secondary antibody). (E) FLAG/LmVP1 (Alexa Fluor 546 secondary antibody) (acidocalcisomal marker) overexpressed promastigotes were not colocalized with LmPAS-PGK (Alexa Fluor 488 secondary antibody). (F) LmPAS-PGK-RFP overexpressed promastigotes were colocalized with MitoTracker green (mitochondria-specific dye). (G) Measurement of the activity of marker proteins in the acidocalcisomal (AC) and mitochondrial (Mito) fractions. Pyrophosphatase and APX were used as acidocalcisomal and mitochondrial markers, respectively. Triton X was used as a membrane solubilizing agent. The activity data are representative of three independent experiments.

Fluor 488-conjugated anti-rabbit secondary antibody (Figure 3B). When the images were superimposed (Figure 3B), the co-localization of LmPAS-PGK with the glycosome-specific protein was observed in *L. major* cells. To further investigate the consequence of association of glycosomes with the acidic compartments, *L. major* cells were costained with DAPI (DNA-specific fluorescence dye) and LysoTracker (acidic organelle-specific fluorescence dye) and fixed on the slide (Figure 3C). When the images were superimposed (as shown in Figure 3C), the co-localization with LysoTracker was observed in *L. major* cells (Figure 3C). There are two acidic compartments in a *Leishmania* cell namely the lysosome and the acidocalcisome. Thus, it may localize in one of them or both the organelles. To examine the LmPAS-PGK localization in the lysosome, the full-length RFP tag LmCPB (lysosome-specific protein) fusion in *L. major* promastigotes were costained with rabbit anti-LmPAS-PGK as primary antibody and Alexa Fluor 488-conjugated goat anti-rabbit antibody as secondary antibody (Figure 3D). When the images were superimposed (Figure 3D), the co-localization of LmPAS-PGK with the lysosome-specific protein was observed in *L. major* cells. To investigate LmPAS-PGK localization in the acidocalcisome, the full-length FLAG tag LmVP1 (acidocalcisome-specific protein) fusion in *L. major* promastigotes were costained with a mixture of anti-rabbit PAS-PGK antibody and anti-mice FLAG antibody as primary antibody, and a mixture of Alexa Fluor 488-conjugated goat anti-rabbit antibody and Alexa Fluor 546-conjugated goat anti-mice antibody as secondary antibody (Figure 3E). When the images were superimposed (Figure 3E), the co-localization of LmPAS-PGK with the acidocalcisome-specific protein was not observed in *L. major* cells indicating that LmPAS-PGK is absent from the acidocalcisome. To investigate LmPAS-PGK localization in the mitochondria, *L. major* cells were costained with DAPI and MitoTracker green (mitochondria-specific fluorescence dye) and fixed on the slide (Figure 3F). When the images were superimposed (as shown in Figure 3F), the co-localization with MitoTracker was not observed in *L. major* cells (Figure 3F). Since the LmPAS-PGK is absent from the acidocalcisome as well as in the mitochondria, it raises the question of whether purified organelles were intact during their isolation. To verify that we measured the organelles-specific enzymatic activity with and without 0.5% Triton X-treated purified acidocalcisome and mitochondria (Figure 3G). The enzymatic activity of Triton X-treated organelles was higher than Triton X-untreated organelles. Thus, the absence of PAS-PGK in the acidocalcisome as well as in the mitochondria is not due to breakage and release of luminal contents. Although LmPAS-PGK contains the predicted C-terminal glycosomal tri-peptide (PKL) signal sequence, yet the enzyme is present in the lysosome as well as in the glycosome. The question immediately arises as to how this protein is translocated to the lysosome. One possibility is that it may be trafficked to the lysosome from glycosome via pexophagy (fusion of glycosomes with acidic lysosomes). However, towards the C-terminal end of the PAS-PGK (before glycosomal sorting signal), there is one post-Golgi-sorting motif ⁵⁰⁴FLELL⁵⁰⁸ (Figure 1) (two reminiscent overlapping amino acid sequences: a classical dileucine base motif and tyrosine-based motif). Several groups of researcher have already shown that these types of motif in proteins are required for lysosomal translocation [43–45]. Therefore, the other possibility is that this post-Golgi-sorting motif ⁵⁰⁴FLELL⁵⁰⁸ might be responsible for lysosomal localization.

Characteristics of OE, CT, CM and KO cells

To investigate the LmPAS-PGK function in *L. major*, a gene replacement technique was used (Figure 4). PCR analysis with genomic DNA and Western blotting confirmed that the resulting cells no longer expressed LmPAS-PGK (Figure 4B–D). To investigate whether the growth rate of null mutants is similar to that of CT, CM or OE cells, microscopic viable cell counting analysis was performed (Figure 5A). The growth curve showed that the KO population had a slower growth rate compared with CT, CM or OE promastigotes. Flow cytometry (Figure 5B) studies suggest that KO cells had 5-fold (~22.1%) more dead cells (PI-positive cells) than the CT (4.3%), CM (5.1%) and OE (4.0%) cells within 4 days of incubation period. These results explain why the growth rate of CT, CM or OE cells is higher than that of the KO cells. When the percentage of dead cells among KO, CT, CM and OE cells were measured at various durations of culture media, a significant amount of dead cells found in KO culture compared with CT, CM or OE cells at longer durations of culture media (Figure 5C). These results indicate that PAS-PGK may have a protecting role under unfavorable growth conditions (like nutrient stress, acidic pH or toxic metabolite). Scientists have shown that glucose starvation leads to the lowering of glycosomal pH to around pH 6.6 in *T. brucei* [46,47]. This slightly acidic pH may be necessary to inactivate certain proteins in glycosome for slowing down the cell growth and activate some of the essential proteins required for survival under starvation. The acidic pH sensitive LmPAS-PGK may supply ATP required by these beneficial pathways under glucose starvation and thus can help in the survivability of *Leishmania*. Hence, LmPAS-PGK can synthesize ATP in the glycosome as well in the acidic lysosome. To test

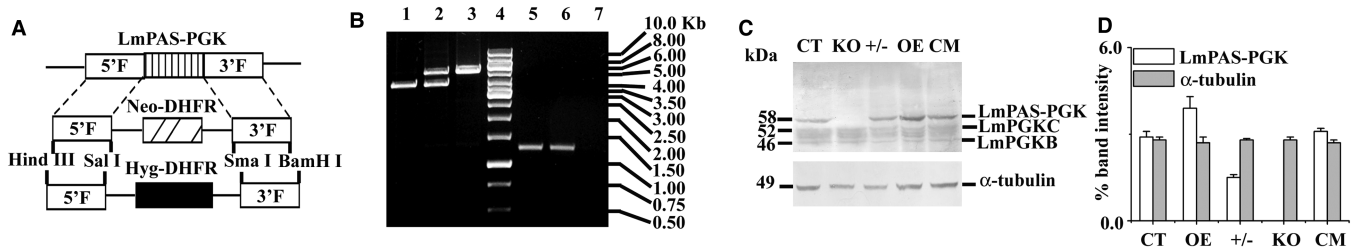


Figure 4. Targeted gene replacement of LmPAS-PGK alleles.

(A) Schematic representation of the LmPAS-PGK locus and the plasmid constructs used for gene replacement. DHFR denotes dihydrofolate reductase. (B) Agarose gel analysis of PCR-amplified products of LmPAS-PGK gene. Lane 4 shows the molecular mass marker, lanes 1 and 2 and 6, and 3 and 7 correspond to PCR with genomic DNA from CT, +/- heterozygous mutants, and KO mutants, respectively, with primers external (lanes 1–3) and internal (lanes 5–7) to the LmPAS-PGK gene. The expected size of the LmPAS-PGK, NEO, and HYG gene PCR product are 3.58, 5.3 and 5.7 kb, respectively. Internal forward and reverse primers were generated from positions 345 and 1584 bp of the gene, respectively. The expected size of the PCR product is 1239 bp. (C) *L. major* lysate was used for Western blotting. Western blot results using rabbit anti-LmPAS-PGK and mouse anti-tubulin antibody are shown. (D) Bar diagram depicting the percentage of band intensities in the Western blot. Band intensity was quantified by ImageJ software (NIH). CM denotes complement cell lines.

this hypothesis, we measured the ATP concentration in cell lysate. Like LmPAS-PGK expression, the order of ATP accumulation was OE > CT = CM > KO cells (Figure 5D). Due to the impermeability of ATP in the glycosome, the ATP molecules that are consumed by hexokinase and phosphofructokinase in the upstream of the glycolytic pathway are to be regenerated inside the glycosomes through the activities of different glycosomal kinases in the downstream of the pathway. The *L. major* genome has six ATP producing glycosomal kinases inside the organelle i.e. PGK isoform C (LmjF.20.0100), isoform PAS-PGK (LmjF.30.3380), phosphoenolpyruvate carboxykinase (LmjF.27.1805 and LmjF.27.1810), glycerol kinase (LmjF.35.3080) and pyruvate phosphate

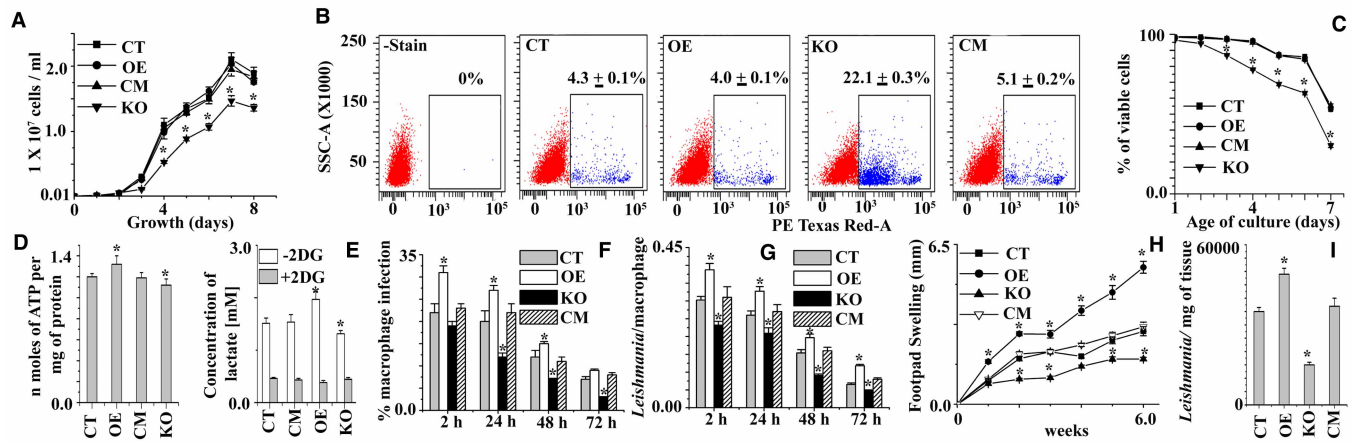


Figure 5. Functional characterization of LmPAS-PGK.

(A) The growth curves of CT, OE, CM (complement cell) and KO cells. (B) Cell viability of CT, OE, CM and KO cells after 4 days of incubation period as measured by flow cytometry using propidium iodide ($Ex_{\lambda} = 488$ nm, $Em_{\lambda} = 617$ nm). (C) % of cell death among CT, OE, CM and KO cells at various time of incubation period. (D) Comparative studies of ATP content among CT, OE, CM and KO cells lysate. (E) Comparative studies of free lactate (end product of glycolysis) among CT, OE, CM and KO cells media. 2-deoxy D-glucose (2DG) used as inhibitor of glycolysis. All assays were done in three independent experiments and data represent mean \pm SD. (F) The percentage of macrophages infected with CT, OE, CM and KO parasites. For each time point, 200 macrophages were counted. (G) The number of *Leishmania* within each infected macrophage was counted. For each time point and cell type, 200 infected macrophages were analyzed. (H) Infection in BALB/c mice. Footpad swelling of CT, OE, CM and KO were observed for the three groups (15 mice/group). (I) Parasite burden in the footpad after 6 weeks of post-infection in CT, OE, CM and KO cells. * denotes $P < 0.05$.

dikinase (LmjF.11.1000). These kinase activities are essential in trypanosomes because compartmentalization of glycolysis inside the glycosomes is essential for preventing a lethal turbo-explosion of glycolysis [48–50]. Our knockout studies suggest that PAS-PGK participates ~7% of total ATP (Figure 5D). The question immediately arises as to why 93% ATP synthesis is not affected in KO cells. The possibility is that another PGK isoform C and other kinases may play an important role in glycosomal ATP synthesis in the absence of LmPAS-PGK. Next, we have measured glycolytic flux in KO cell line and compared with CT, CM and OE cell lines (Figure 5E). Since glycolytic flux is directly proportional to lactate production from glucose we have measured the concentration of lactate (the end product of glycolysis) released into the culture medium in the presence or absence of 2-deoxy D-glucose. OE cells show 20% higher lactate production than CT or CM cell lines but KO cells produce 15% lower lactate than CT or CM cell lines (Figure 5E). These data suggested that the PAS-PGK might have an important role in glycolytic flux.

Macrophages are the host cells for *L. major* promastigotes, therefore, we focused on the interaction of promastigotes with the macrophages. We investigated to what extent KO, CT, CM and OE cells were phagocytosed by the macrophages. The internalization rates of the KO promastigotes were similar to CT, CM and OE cells (Figure 5F). However, after phagocytosing the KO promastigotes, most of the infected macrophages did not have the KO parasites after 72 h of incubation. These data from the KO parasites suggested that the parasites were killed more easily inside the macrophages. In addition, the percentage of macrophages infected with OE increased significantly (Figure 5G). Similarly, we found that KO cells could not develop a severe disease, with an earlier onset of footpad necrosis, compared with CT or CM promastigotes (Figure 5H). These data were confirmed by the OE promastigotes, showing increased virulence *in vivo* infection model. The result of parasite burden during 6-week post-infection indicated that KO parasites, compared with CT or CM, had about 2-fold less parasite burden (Figure 5I) in 1 mg of footpad tissue. These findings indicated that the gene in parasites has some role in disease development in macrophages or mice.

The immediate question that comes is what mechanism is apparently involved in the disease development during infection. Recently, a group of researcher showed that human PGK1 has two additional functions other than ATP generation in cancer. One is the mitochondria-translocated PGK1 activates pyruvate dehydrogenase kinase 1 and inhibits mitochondrial pyruvate utilization to increase glycolytic production [51]. The other function is the phosphorylation of Beclin1 by PGK1 to induce autophagy [52]. Neither *Leishmania* gene database has Beclin1 gene nor the PAS-PGK translocates to the mitochondria. It is well known that the lysosomal dysfunction results in impaired autophagy [53]. The glycosomal and lysosomal localization of LmPAS-PGK, the regulation of glycolytic flux by this protein and protecting the role of this enzyme against old aged culture raise the question of whether this protein has any important function in autophagy. To find out the role of PAS-PGK in the induction of autophagy, we measured the degree of autophagosome formation (autophagic vacuoles) in OE, CT, CM and KO cell lines under normal and nutrient stress conditions by autophagy detection kit, RFP/ATG8 distribution, and ATG8-PE generation as the marker of autophagosome. Bright green fluorescence in the FITC filter is observed when the novel dye supplied with the autophagy detection kit (Abcam) selectively labels the autophagic vacuoles. Flow cytometry (Figure 6A) and microscopic (Figure 6B,C) studies demonstrated that the number of autophagosomes increased in KO cells compared with CT, CM or OE cells (Figure 6A–C) under both normal and nutrient stress conditions. These data were supported by RFP/ATG8 overexpression system, where the expression of N-terminally RFP-fused ATG8 in *L. major* facilitated the monitoring of autophagy by using fluorescence microscopy to detect the presence of RFP-labelled puncta (a marker for tracking autophagosome formation). KO cells showed that the percentage of parasites with puncta and the number of puncta per cell increased with respect to CT, CM or OE cells in mid-logarithmic phase of growth (Figure 6D,E). Autophagosomes of *L. major* cells are frequently quantified by the amount of conversion of ATG8 to membrane-bound ATG8-PE. Conversion of RFP/ATG8 to membrane-bound RFP/ATG8-PE in KO cells was confirmed through immunoblot with anti-RFP antibody. The expression of RFP-/ATG8-PE in KO cells was ~3-fold higher than CT or CM cells whereas OE parasites showed lower expression of ATG8-PE when compared with CT or CM parasites (Figure 6F). Bafilomycin A1 and wortmannin, two well-known inhibitors of autophagy, were used as control while studying the distribution of RFP/ATG-PE. Bafilomycin A1 inhibits the fusion of autophagosome and lysosome leading to the accumulation of autophagosomes whereas wortmannin prevents the autophagosome formation. Similarly, bafilomycin A1-treated cells showed higher amount of RFP/ATG-PE expression whereas wortmannin prevents the RFP/ATG-PE expression in all type of cell lines. Altogether, these data suggest that the LmPAS-PGK can regulate autophagosome formation in *Leishmania* promastigotes.

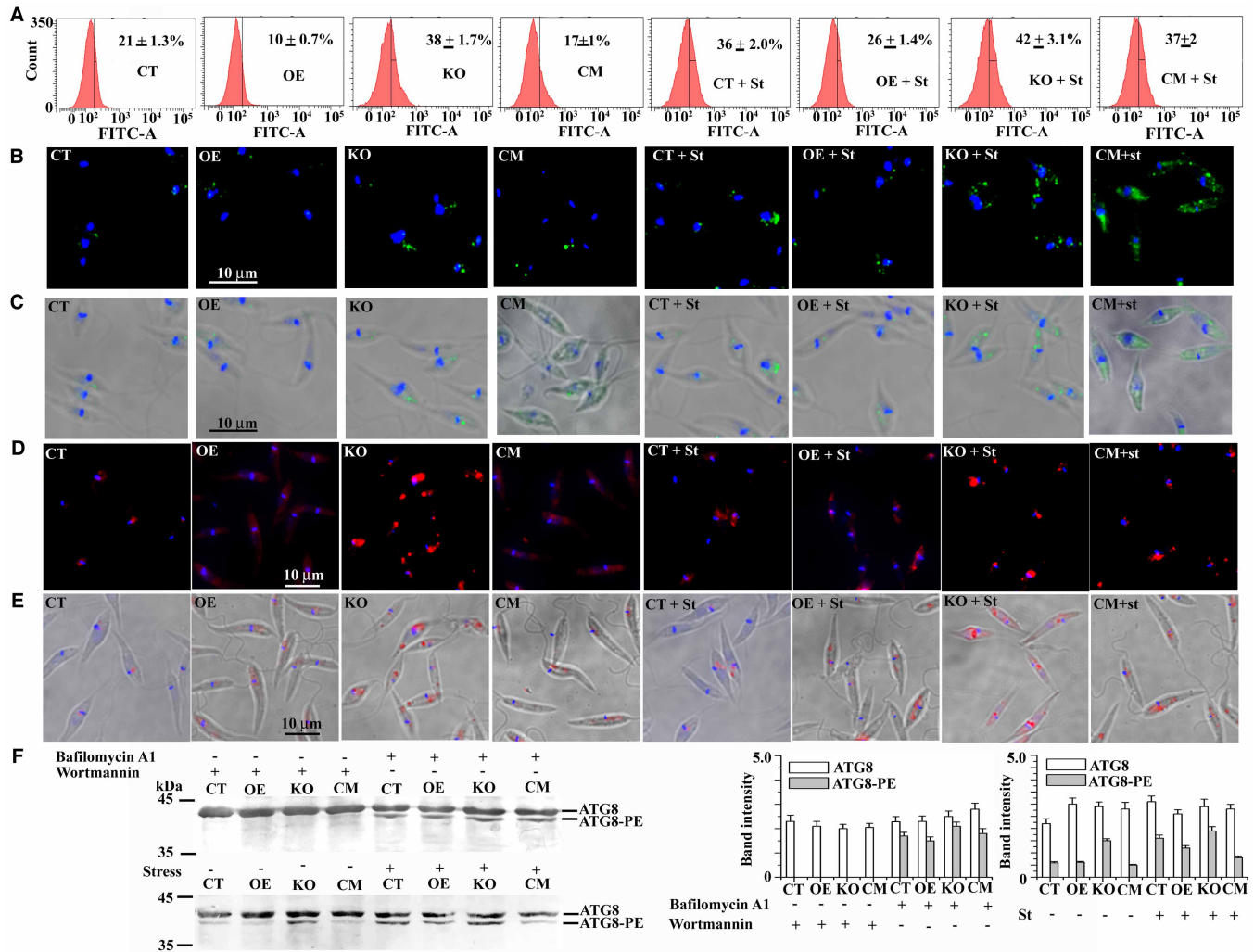


Figure 6. Role of LmPAS-PGK in autophagy.

(A) Autophagic flux measurement of the CT, OE, CM and KO cells under normal and stressed conditions by flow cytometry using autophagy detection kit ($Ex_{\lambda} = 488$ nm, $Em_{\lambda} = 517$ nm). St denotes stressed conditions (glucose starvation). (B) The same samples as (A) were visualized by fluorescence microscopy. (C) The same images as (B) in brightfield background. (D) Formation of RFP/ATG8 puncta in CT, OE, CM and KO cells under normal and stressed conditions using fluorescence microscope. (E) The same images as (D) observed in brightfield background. (F) Western blot analysis of RFP/ATG8 using anti-RFP antibody detecting both RFP/ATG8 and RFP/ATG8-PE. Wortmannin and bafilomycin A1 were used as controls. Bafilomycin A1 (inhibitor of the late phase of autophagy) and glucose starvation induced autophagosome formation in parasites was also confirmed by the increased expression of the ATG8-PE. Inhibitor of early phase of autophagy, wortmannin, was found to inhibit the autophagosome formation in KO parasites.

Conclusion

These data unequivocally demonstrate that PAS-PGK act as an acidic PGK. On the basis of physiological function, PAS-PGK proteins constitute a previously unknown class of PAS-containing protein that differ significantly from the known PAS-containing protein sensors like histidine and serine/threonine kinases, chemoreceptors and photoreceptors, clock proteins, voltage-activated ion channels, cyclic nucleotide phosphodiesterases, regulators of hypoxia responses, and modulators of embryological development, etc. [7]. Our results suggest that the N-terminal domains of PAS-PGK act as a regulator for showing optimum PGK activity at acidic pH. The acidic pH presumably triggers a conformational change that relieves the PAS domain induced inhibition from the C-terminal catalytic PGK domain, resulting in the synthesis of the optimum level of ATP,

which then associates with the lysosomal function and cell survival. The unusual presence of the PAS domain on the N-terminal of the LmPAS-PGK makes it unique from all the other known PGKs.

Abbreviations

ADK, adenosine kinase; AP, alkaline phosphatase; APX, ascorbate peroxidase; CLF, crude lysosomal fraction; CM, complement cell; CPB, cysteine peptidase B; CT, control cell; GAPDH, glyceraldehyde 3 phosphate dehydrogenase; IPTG, isopropyl β -D-1-thiogalactopyranoside; KO, LmPAS-PGK knockout cell; LmPAS-PGK, PAS domain-containing phosphoglycerate kinase from *Leishmania major*; OE, LmPAS-PGK overexpressing cell; PAS, Per (Drosophila period clock protein)-Arnt (vertebrate aryl hydrocarbon receptor nuclear translocator)-Sim (Drosophila single-minded protein); PGK, phosphoglycerate kinase.

Author Contribution

S.A. and A.A. designed research; A.A., S.B., S.D. and A.M. performed research; S.A. analyzed data and wrote the paper.

Funding

This work was supported by Department of Science and Technology (EMR/2016/001415), CSIR fellowships (to A.M. and S.B.), and University Grants Commission fellowships (to A.A. and S.D.).

Acknowledgements

We thank Dr. S. M. Beverley for providing pXG-B2863, pXG-Neo, and pXG-Hyg vectors; Prof. Emmanuel Tetaud (Université de Bordeaux) for providing pNUS-mRFPnD vector; and Dr. A. K. Datta for *Leishmania donovani* adenosine kinase antibody.

Competing Interests

The Authors declare that there are no competing interests associated with the manuscript.

References

- Alexander, J., Satoskar, A.R. and Russell, D.G. (1999) *Leishmania* species: models of intracellular parasitism. *J. Cell Sci.* **112**, 2993–3002 PMID:10462516
- Cull, B., Prado Godinho, J.L., Fernandes Rodrigues, J.C., Frank, B., Schurigt, U., Williams, R.A. et al. (2014) Glycosome turnover in *Leishmania major* is mediated by autophagy. *Autophagy* **10**, 2143–2157 <https://doi.org/10.4161/autophagy.36438>
- Herman, M., Pérez-Morga, D., Schtickzelle, N. and Michels, P.A. (2008) Turnover of glycosomes during life-cycle differentiation of *Trypanosoma brucei*. *Autophagy* **4**, 294–308 <https://doi.org/10.4161/autophagy.5443>
- Henry, J.T. and Crosson, S. (2011) Ligand-binding PAS domains in a genomic, cellular, and structural context. *Annu. Rev. Microbiol.* **65**, 261–286 <https://doi.org/10.1146/annurev-micro-121809-151631>
- Oka, Y., Matsushita, T., Mochizuki, N., Quail, P.H. and Nagatani, A. (2008) Mutant screen distinguishes between residues necessary for light-signal perception and signal transfer by phytochrome B. *PLoS Genet.* **4**, e1000158 <https://doi.org/10.1371/journal.pgen.1000158>
- Lee, J., Tomchick, D.R., Brautigam, C.A., Machius, M., Kort, R., Hellingwerf, K.J. et al. (2008) Changes at the KinA PAS-A dimerization interface influence histidine kinase function. *Biochemistry* **47**, 4051–4064 <https://doi.org/10.1021/bi7021156>
- Taylor, B.L. and Zhulin, I.B. (1999) PAS domains: internal sensors of oxygen, redox potential, and light. *Microbiol. Mol. Biol. Rev.* **63**, 479–506 PMID: 10357859
- Cho, U.S., Bader, M.W., Amaya, M.F., Daley, M.E., Klevit, R.E., Miller, S.I. et al. (2006) Metal bridges between the PhoQ sensor domain and the membrane regulate transmembrane signaling. *J. Mol. Biol.* **356**, 1193–1206 <https://doi.org/10.1016/j.jmb.2005.12.032>
- Gilles-Gonzalez, M.A., Gonzalez, G., Perutz, M.F., Kiger, L., Marden, M.C. and Poyart, C. (1994) Heme-based sensors, exemplified by the kinase FixL, are a new class of heme protein with distinctive ligand binding and autoxidation. *Biochemistry* **33**, 8067–8073 <https://doi.org/10.1021/bi00192a011>
- Söderback, E., Reyes-Ramirez, F., Eydmann, T., Austin, S., Hill, S. and Dixon, R. (1998) The redox- and fixed nitrogen-responsive regulatory protein NIFL from *Azotobacter vinelandii* comprises discrete flavin and nucleotide-binding domains. *Mol. Microbiol.* **28**, 179–192 <https://doi.org/10.1046/j.1365-2958.1998.00788.x>
- Ukaegbu, U.E., Henery, S. and Rosenzweig, A.C. (2006) Biochemical characterization of MmoS, a sensor protein involved in copper-dependent regulation of soluble methane monooxygenase. *Biochemistry* **45**, 10191–10198 <https://doi.org/10.1021/bi060693h>
- Christie, J.M., Salomon, M., Nozue, K., Wada, M. and Briggs, W.R. (1999) LOV (light, oxygen, or voltage) domains of the blue-light photoreceptor phototropin (nph1): binding sites for the chromophore flavin mononucleotide. *Proc. Natl Acad. Sci. U.S.A.* **96**, 8779–8783 <https://doi.org/10.1073/pnas.96.15.8779>
- Rojas-Pirela, M., Rigden, D.J., Michels, P.A., Cáceres, A.J., Concepción, J.L. and Quiñones, W. (2018) Structure and function of Per-ARNT-Sim domains and their possible role in the life-cycle biology of *Trypanosoma cruzi*. *Mol. Biochem. Parasitol.* **219**, 52–66 <https://doi.org/10.1016/j.molbiopara.2017.11.002>
- Adjé, C.A., Opperdoes, F.R. and Michels, P.A. (1997) Organization, sequence and stage-specific expression of the phosphoglycerate kinase genes of *Leishmania mexicana mexicana*. *Mol. Biochem. Parasitol.* **90**, 155–168 [https://doi.org/10.1016/S0166-6851\(97\)00152-7](https://doi.org/10.1016/S0166-6851(97)00152-7)

- 15 McKoy, G., Badal, M., Prescott, Q., Lux, H. and Hart, D.T. (1997) Characterisation of phosphoglycerate kinase genes in *Leishmania major* and evidence for the absence of a third closely related gene or isoenzyme. *Mol. Biochem. Parasitol.* **90**, 169–181 [https://doi.org/10.1016/S0166-6851\(97\)00172-2](https://doi.org/10.1016/S0166-6851(97)00172-2)
- 16 Kaushik, S., Krishnarajuna, B., Raghothama, S., Aggarwal, S., Raghunathan, V. and Ganjiwale, A. (2012) Theoretical and in vitro studies of a C-terminal peptide from PGKC of *Leishmania mexicana mexicana*. *Mol. Biochem. Parasitol.* **185**, 27–35 <https://doi.org/10.1016/j.molbiopara.2012.06.004>
- 17 Dolai, S., Yadav, R.K., Pal, S. and Adak, S. (2008) *Leishmania major* ascorbate peroxidase overexpression protects cells against reactive oxygen species-mediated cardiolipin oxidation. *Free Radic. Biol. Med.* **45**, 1520–1529 <https://doi.org/10.1016/j.freeradbiomed.2008.08.029>
- 18 Pal, S., Dolai, S., Yadav, R.K. and Adak, S. (2010) Ascorbate peroxidase from *Leishmania major* controls the virulence of infective stage of promastigotes by regulating oxidative stress. *PLoS ONE* **5**, e11271 <https://doi.org/10.1371/journal.pone.0011271>
- 19 Jinn, S., Drolet, R.E., Cramer, P.E., Wong, A.H., Toolan, D.M., Gretzula, C.A. et al. (2017) TMEM175 deficiency impairs lysosomal and mitochondrial function and increases α -synuclein aggregation. *Proc. Natl Acad. Sci. U.S.A.* **114**, 2389–2394 <https://doi.org/10.1073/pnas.1616332114>
- 20 Salto, M.L., Kuhlenschmidt, T., Kuhlenschmidt, M., de Lederkremer, R.M. and Roberto, D. (2008) Phospholipid and glycolipid composition of acidocalcisomes of *Trypanosoma cruzi*. *Mol. Biochem. Parasitol.* **158**, 120–130 <https://doi.org/10.1016/j.molbiopara.2007.12.001>
- 21 Colasante, C., Voncken, F., Manful, T., Ruppert, T., Tielens, A.G.M., van Hellemond, J.J. et al. (2013) Proteins and lipids of glycosomal membranes from *Leishmania tarentolae* and *Trypanosoma brucei*. *F1000 Res.* **2**, 27 <https://doi.org/10.12688/f1000research.2-27.v1>
- 22 Shatton, J.B., Ward, C., Williams, A. and Weinhouse, S. (1983) A microcolorimetric assay of inorganic pyrophosphatase. *Anal. Biochem.* **130**, 114–119 [https://doi.org/10.1016/0003-2697\(83\)90657-7](https://doi.org/10.1016/0003-2697(83)90657-7)
- 23 Lemerrier, G., Espiau, B., Ruiz, F.A., Vieira, M., Luo, S., Baltz, T. et al. (2004) A pyrophosphatase regulating polyphosphate metabolism in acidocalcisomes is essential for *Trypanosoma brucei* virulence in mice. *J. Biol. Chem.* **279**, 3420–3425 <https://doi.org/10.1074/jbc.M309974200>
- 24 Möglich, A., Ayers, R.A. and Moffat, K. (2009) Structure and signaling mechanism of Per-ARNT-Sim domains. *Structure* **17**, 1282–1294 <https://doi.org/10.1016/j.str.2009.08.011>
- 25 Gong, W., Hao, B., Mansy, S.S., Gonzalez, G., Gilles-Gonzalez, M.A. and Chan, M.K. (1998) Structure of a biological oxygen sensor: a new mechanism for heme-driven signal transduction. *Proc. Natl Acad. Sci. U.S.A.* **95**, 15177–15182 <https://doi.org/10.1073/pnas.95.26.15177>
- 26 Kurokawa, H., Lee, D.S., Watanabe, M., Sagami, I., Mikami, B., Raman, C.S. et al. (2004) A redox-controlled molecular switch revealed by the crystal structure of a bacterial heme PAS sensor. *J. Biol. Chem.* **279**, 20186–20193 <https://doi.org/10.1074/jbc.M314199200>
- 27 Yoshioka, S., Kobayashi, K., Yoshimura, H., Uchida, T., Kitagawa, T. and Aono, S. (2005) Biophysical properties of a c-type heme in chemotaxis signal transducer protein DcrA. *Biochemistry* **44**, 15406–15413 <https://doi.org/10.1021/bi0513352>
- 28 Taylor, B.L., Zhulin, I.B. and Johnson, M.S. (1999) Aerotaxis and other energy-sensing behavior in bacteria. *Annu. Rev. Microbiol.* **53**, 103–128 <https://doi.org/10.1146/annurev.micro.53.1.103>
- 29 Christie, J.M., Raymond, P., Powell, G.K., Bernasconi, P., Raibekas, A.A., Liscum, E. et al. (1998) Arabidopsis NPH1: a flavoprotein with the properties of a photoreceptor for phototropism. *Science* **282**, 1698–1701 <https://doi.org/10.1126/science.282.5394.1698>
- 30 Baca, M., Borgstahl, G.E., Boissinot, M., Burke, P.M., Williams, D.R., Slater, K.A. et al. (1994) Complete chemical structure of photoactive yellow protein: novel thioester-linked 4-hydroxycinnamyl chromophore and photocycle chemistry. *Biochemistry* **33**, 14369–14377 <https://doi.org/10.1021/bi00252a001>
- 31 King-Scott, J., Konarev, P.V., Panjikar, S., Jordanova, R., Svergun, D.I. and Tucker, P.A. (2011) Structural characterization of the multidomain regulatory protein Rv1364c from *Mycobacterium tuberculosis*. *Structure* **19**, 56–69 <https://doi.org/10.1016/j.str.2010.11.010>
- 32 Kramer, J., Fischer, J.D., Zientz, E., Vijayan, V., Griesinger, C., Lupas, A. et al. (2007) Citrate sensing by the C4-dicarboxylate/citrate sensor kinase DcuS of *Escherichia coli*: binding site and conversion of DcuS to a C4-dicarboxylate- or citrate-specific sensor. *J. Bacteriol.* **189**, 4290–4298 <https://doi.org/10.1128/JB.00168-07>
- 33 Pappalardo, L., Janausch, I.G., Vijayan, V., Zientz, E., Junker, J., Peti, W. et al. (2003) The NMR structure of the sensory domain of the membranous two-component fumarate sensor (histidine protein kinase) DcuS of *Escherichia coli*. *J. Biol. Chem.* **278**, 39185–39188 <https://doi.org/10.1074/jbc.C300344200>
- 34 Zhou, Y.F., Nan, B., Nan, J., Ma, Q., Panjikar, S., Liang, Y.H. et al. (2008) C4-dicarboxylates sensing mechanism revealed by the crystal structures of DctB sensor domain. *J. Mol. Biol.* **383**, 49–61 <https://doi.org/10.1016/j.jmb.2008.08.010>
- 35 Girvan, H.M. and Munro, A.W. (2013) Heme sensor proteins. *J. Biol. Chem.* **288**, 13194–13203 <https://doi.org/10.1074/jbc.R112.422642>
- 36 Prost, L.R., Daley, M.E., Le Sage, V., Bader, M.W., Le Moual, H., Klevit, R.E. et al. (2007) Activation of the bacterial sensor kinase PhoQ by acidic pH. *Mol. Cell* **26**, 165–174 <https://doi.org/10.1016/j.molcel.2007.03.008>
- 37 Bernstein, B.E., Michels, P.A. and Hol, W.G. (1997) Synergistic effects of substrate-induced conformational changes in phosphoglycerate kinase activation. *Nature* **385**, 275–278 <https://doi.org/10.1038/385275a0>
- 38 Saito, T., Nishi, M., Lim, M.I., Wu, B., Maeda, T., Hashimoto, H. et al. (2008) A novel GDP-dependent pyruvate kinase isozyme from *Toxoplasma gondii* localizes to both the apicoplast and the mitochondrion. *J. Biol. Chem.* **283**, 14041–14052 <https://doi.org/10.1074/jbc.M709015200>
- 39 Opperdoes, F.R. and Borst, P. (1977) Localization of nine glycolytic enzymes in a microbody-like organelle in *Trypanosoma brucei*: the glycosome. *FEBS Lett.* **80**, 360–364 [https://doi.org/10.1016/0014-5793\(77\)80476-6](https://doi.org/10.1016/0014-5793(77)80476-6)
- 40 Dodson, H.C., Morris, M.T. and Morris, J.C. (2011) Glycerol 3-phosphate alters *Trypanosoma brucei* hexokinase activity in response to environmental change. *J. Biol. Chem.* **286**, 33150–33157 <https://doi.org/10.1074/jbc.M111.235705>
- 41 Pazour, G.J., Agrin, N., Leszyk, J. and Witman, G.B. (2005) Proteomic analysis of a eukaryotic cilium. *J. Cell Biol.* **170**, 103–113 <https://doi.org/10.1083/jcb.200504008>
- 42 Brown, R.W., Collingridge, P.W., Gull, K., Rigden, D.J. and Ginger, M.L. (2014) Evidence for loss of a partial flagellar glycolytic pathway during trypanosomatid evolution. *PLoS ONE* **9**, e103026 <https://doi.org/10.1371/journal.pone.0103026>
- 43 Sheiner, L., Dowse, T.J. and Soldati-Favre, D. (2008) Identification of trafficking determinants for polytopic rhomboid proteases in *Toxoplasma gondii*. *Traffic* **9**, 665–677 <https://doi.org/10.1111/j.1600-0854.2008.00736.x>
- 44 Letourneur, F. and Klausner, R.D. (1992) A novel di-leucine motif and a tyrosine-based motif independently mediate lysosomal targeting and endocytosis of CD3 chains. *Cell* **69**, 1143–1157 [https://doi.org/10.1016/0092-8674\(92\)90636-0](https://doi.org/10.1016/0092-8674(92)90636-0)
- 45 Bonifacino, J.S. and Traub, L.M. (2003) Signals for sorting of transmembrane proteins to endosomes and lysosomes. *Annu. Rev. Biochem.* **72**, 395–447 <https://doi.org/10.1146/annurev.biochem.72.121801.161800>

- 46 Lin, S., Voyton, C., Morris, M.T., Ackroyd, P.C., Morris, J.C. and Christensen, K.A. (2017) Ph regulation in glycosomes of procyclic form *Trypanosoma brucei*. *J. Biol. Chem.* **292**, 7795–7805 <https://doi.org/10.1074/jbc.M117.784173>
- 47 Lin, S., Morris, M.T., Ackroyd, P.C., Morris, J.C. and Christensen, K.A. (2013) Peptide targeted delivery of pH sensor for quantitative measurements of intraglycosomal pH in live *Trypanosoma brucei*. *Biochemistry* **52**, 3629–3637 <https://doi.org/10.1021/bi400029m>
- 48 Furuya, T., Kessler, P., Jardim, A., Schnauffer, A., Crudder, C. and Parsons, M. (2002) Glucose is toxic to glycosome-deficient trypanosomes. *Proc. Natl Acad. Sci. U.S.A.* **99**, 14177–14182 <https://doi.org/10.1073/pnas.222454899>
- 49 Haanstra, J.R., van Tuijl, A., Kessler, P., Reijnders, W., Michels, P.A., Westerhoff, H.V. et al. (2008) Compartmentation prevents a lethal turbo-explosion of glycolysis in trypanosomes. *Proc. Natl Acad. Sci. U.S.A.* **105**, 17718–17723 <https://doi.org/10.1073/pnas.0806664105>
- 50 Blattner, J., Helfert, S., Michels, P. and Clayton, C. (1998) Compartmentation of phosphoglycerate kinase in *Trypanosoma brucei* plays a critical role in parasite energy metabolism. *Proc. Natl Acad. Sci. U.S.A.* **95**, 11596–11600 <https://doi.org/10.1073/pnas.95.20.11596>
- 51 Li, X., Jiang, Y., Meisenhelder, J., Yang, W., Hawke, D.H., Zheng, Y. et al. (2016) Mitochondria-translocated PGK1 functions as a protein kinase to coordinate glycolysis and the TCA cycle in tumorigenesis. *Mol. Cell* **61**, 705–719 <https://doi.org/10.1016/j.molcel.2016.02.009>
- 52 Qian, X., Li, X., Cai, Q., Zhang, C., Yu, Q., Jiang, Y. et al. (2017) Phosphoglycerate kinase 1 phosphorylates beclin1 to induce autophagy. *Mol. Cell* **65**, 917–931 <https://doi.org/10.1016/j.molcel.2017.01.027>
- 53 Williams, R.A., Tetley, L., Mottram, J.C. and Coombs, G.H. (2006) Cysteine peptidases CPA and CPB are vital for autophagy and differentiation in *Leishmania mexicana*. *Mol. Microbiol.* **61**, 655–674 <https://doi.org/10.1111/j.1365-2958.2006.05274.x>
- 54 Scheuermann, T.H., Stroud, D., Sleet, C.E., Bayeh, L., Shokri, C., Wang, H. et al. (2015) Isoform-selective and stereoselective inhibition of hypoxia inducible factor-2. *J. Med. Chem.* **58**, 5930–5941 <https://doi.org/10.1021/acs.jmedchem.5b00529>
- 55 Schwede, T., Kopp, J., Guex, N. and Peitsch, M.C. (2003) SWISS-MODEL: an automated protein homology-modeling server. *Nucleic Acids Res.* **31**, 3381–3385 <https://doi.org/10.1093/nar/gkg520>
- 56 DeLano, W.L. (2002) The PyMOL molecular graphics system, <http://www.pymol.org/>



CSIR-IICB

PSI-ICPP 2022

CSIR-IICB Kolkata



PSI

CERTIFICATE

Awarded to

Sumit Das

For Poster Presentation
at the

**14th Annual Meeting of the Proteomics Society,
India and International Conference on Proteins &
Proteomics (PSI-ICPP 2022)**

**CSIR-Indian Institute of Chemical Biology, Kolkata
November 03-05, 2022**

Dr. Nakul Chandra Maiti
Organizing Secretary, PSI-ICPP 2022

Dr. Arun Bandyopadhyay
President, PSI-ICPP 2022



KOLKATA



GUWAHATI
1975

NIPER, Kolkata NIPER, Hajipur IASST, Guwahati



Enrolment No. : PhD CW / 2017/43

CSIR - Indian Institute of Chemical Biology

(An autonomous body, under the Ministry of Science & Technology, Government of India)

Certificate

(Courses offered as per UGC guidelines, July 2009)

This is to certify that Mr./Ms. Sumit Das
has successfully completed the Ph.D Course Work conducted by CSIR-IICB for the session
2017

Uday Bandyopadhyay

Uday Bandyopadhyay
Chairperson, Academic Affairs Committee

Samit Chatterjee

Samit Chatterjee
Director



Certificate

Presented to

SUMIT DAS

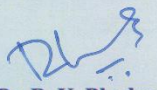
for participation in the

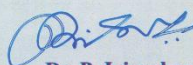
**Training Programme On Laboratory Safety :
Biosafety, Chemical Safety, Radiation Safety
& Fire Safety.**

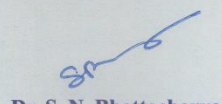
Organized by

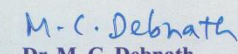
**CSIR-Indian Institute of Chemical Biology,
Kolkata**

30th January 2017


Dr. R. K. Bhadra
Chief Scientist
Head ESU


Dr. P. Jaisankar
Chief Scientist
Chairman


Dr. S. N. Bhattacharya
Principal Scientist
Chairman


M. C. Debnath
Dr. M. C. Debnath
Organizing Secretary


Prof. Samit Chattopadhyay
Director



JADAVPUR UNIVERSITY

KOLKATA-700 032

MARK SHEET

NO.: CW/16052/ 000242


(For Ph.D/M. Phil. Course Work)


Results of the	PH.D. COURSE WORK EXAMINATION, 2017
In	SCIENCE held in DECEMBER, 2017
Name	SUMIT DAS Class Roll No. 201720502007
Examination Roll No.	PHDLSBT17207 Registration No. 27/17/LIFESCIENCE/2517-18

Subject Code / Name	Credit Hr.(c)	Marks
COMPULSORY UNITS:: EX/LSBT/PHD/A & B RESEARCH METHODOLOGY & REVIEW OF LITERATURE	4	68
ELECTIVE UNITS :: EX/LSBT/PHD/1.2A :: TISSUE CULTURE TECHNIQUES EX/LSBT/PHD/1.2B :: MICROBIOLOGY EX/LSBT/PHD/1.2C :: INTRODUCTION TO MOLECULAR BIOLOGY TECHNIQUES	4	77


Total Marks : 145 (out of 200)

Remarks: P

Prepared by : 

Checked by : 

Date of issue : 10-05-2018


Controller of Examinations